

The Physics of Hadronic Tau Decays

Michel Davier,* Andreas Höcker,† and Zhiqing Zhang‡

Laboratoire de l'Accélérateur Linéaire, IN2P3/CNRS and Université de Paris-Sud, BP34, F-91898 Orsay, France

Hadronic τ decays represent a clean laboratory for the precise study of quantum chromodynamics (QCD). Observables (sum rules) based on the spectral functions of hadronic τ decays can be related to QCD quark-level calculations to determine fundamental quantities like the strong coupling constant, parameters of the chiral Lagrangian, $|V_{us}|$, the mass of the strange quark, and to simultaneously test the concept of quark-hadron duality. Using the best available measurements and a revisited analysis of the theoretical framework, the value $\alpha_S(m_\tau^2) = 0.345 \pm 0.004_{\text{exp}} \pm 0.009_{\text{th}}$ is obtained. Taken together with the determination of $\alpha_S(M_Z^2)$ from the global electroweak fit, this result leads to the most accurate test of asymptotic freedom: the value of the logarithmic slope of $\alpha_s^{-1}(s)$ is found to agree with QCD at a precision of 4%. In another approach, the τ spectral functions can be used to determine hadronic quantities that, due to the nonperturbative nature of long-distance QCD, cannot be computed from first principles. An example for this is the contribution from hadronic vacuum polarization to loop-dominated processes like the anomalous magnetic moment of the muon. This article reviews the measurements of nonstrange and strange τ spectral functions and their phenomenological applications.

Contents

I. INTRODUCTION	3
II. THE EXPERIMENTAL STAGE	3
A. Experimental conditions	3
B. Investigating the τ hadronic structure	4
III. TAU BRANCHING FRACTIONS	5
A. The measurement of branching fractions	5
B. Leptonic branching fractions	7
C. Decay modes with kaons	9
D. Nonstrange hadronic branching fractions	11
E. Separation of vector and axial-vector contributions	13
IV. TAU HADRONIC SPECTRAL FUNCTIONS	16
A. Definitions	17
B. The physical mass spectra	18
C. Systematic uncertainties	19
D. Inclusive nonstrange spectral functions	19
1. Vector and axial-vector spectral functions	19
2. Inclusive $V \pm A$ spectral functions	21
E. Strange spectral functions	21
V. COMPARING TAU SPECTRAL FUNCTIONS WITH ELECTRON-POSITRON ANNIHILATION DATA VIA THE CONSERVED VECTOR CURRENT	23
A. Isospin breaking and radiative corrections	23
B. Tau spectral functions and e^+e^- data	24
C. Comparing τ with e^+e^- data	25
1. The 2π spectral function	25
2. The 4π spectral functions	25
3. Branching fractions in τ decays and CVC	27
D. Fits to the $\pi\pi$ spectral function	28
1. Fit to τ data	30
2. Combined fit to τ and e^+e^- data	30

*Electronic address: davier@lal.in2p3.fr

†Electronic address: hoecker@lal.in2p3.fr

‡Electronic address: zhangzq@lal.in2p3.fr

VI. TAU DECAYS AND HADRONIC VACUUM POLARIZATION	31
A. Muon magnetic anomaly	32
B. Input data and their treatment	35
C. Special cases	35
1. The threshold region	35
2. QCD for the high energy contributions	36
D. Results for the lowest order hadronic vacuum polarization	36
E. Hadronic three-loop effects	38
F. Comparing a_μ between theory and experiment	38
G. New physics contributions	40
H. Conclusions and perspectives	40
VII. HADRONIC TAU DECAYS AND QCD	41
A. Renormalization group equations	42
B. Theoretical prediction of R_τ	44
1. The Adler function	45
2. Fixed-order perturbation theory (FOPT)	47
3. Contour-improved fixed-order perturbation theory (CIPT)	47
4. Effective charge perturbation theory (ECPT)	48
5. Estimating unknown higher order perturbative coefficients	49
6. Infrared behavior of the effective charge	51
7. The large- β_0 expansion	52
8. Comparison of the perturbative methods	55
9. Quark-mass and nonperturbative contributions	56
C. Results	58
1. The ALEPH determination of $\alpha_S(m_\tau^2)$ and nonperturbative contributions	59
2. The OPAL results	62
3. Running of $\alpha_S(s)$ below m_τ^2	62
4. Final assessment on the $\alpha_S(m_\tau^2)$ determination	63
5. Evolution to M_Z^2	64
6. Comparison with other determinations of $\alpha_S(M_Z^2)$	65
7. A measure of asymptotic freedom between m_τ^2 and M_Z^2	67
VIII. SPECTRAL FUNCTIONS OF TAU FINAL STATES WITH STRANGENESS	68
A. Strange spectral functions	68
B. Theoretical analysis of $R_{\tau,S}$	70
1. Evidence for the effect of a massive strange quark	71
2. Convergence of the perturbative series	71
3. Phenomenological analysis	72
C. Several approaches	72
1. Summing up the full known terms	73
2. Optimal truncation of the series	73
3. Removing the longitudinal parts	73
The kaon pole and other spin-0 components	73
Other spin-0 components: phenomenological parameterizations	74
D. Results and discussion	74
1. Results with the truncation method	74
2. Verifying the stability of the results	75
3. Comparison between the different analyses	75
E. Sensitivity to $ V_{us} $ and concluding remarks on the m_s determinations	78
IX. CHIRAL SYMMETRY AND QCD SUM RULES	80
A. Chiral sum rules with τ spectral functions	82
B. Operator product expansion	84
C. Borel and pinched weight sum rules	86
D. Inverse moments sum rules and chiral perturbation theory	88
X. CONCLUSIONS AND PERSPECTIVES	90
Acknowledgments	94
References	94

I. INTRODUCTION

Because of its relatively large mass and the simplicity of its decay mechanism, the τ lepton offers many interesting, and sometimes unique, possibilities for testing and improving the Standard Model (SM). These studies involve the leptonic and hadronic sectors and encompass a large range of topics, from the measurement of the leptonic couplings in the weak charged current and the search for lepton flavor violation, providing precise universality tests, to a complete investigation of hadronic production from the Quantum Chromodynamics (QCD) vacuum. For the latter case, the τ decay results have proven to be complementary to those from e^+e^- data, allowing us to perform detailed studies at the fundamental level through the determination of the *spectral functions*, which embody both the rich hadronic structure seen at low energy, and the quark behavior relevant in the higher energy regime. The spectral functions play an important role in the understanding of hadronic dynamics in the intermediate energy range. They represent the basic input for QCD studies and for evaluating low-energy contributions from hadronic vacuum polarization. This is required for the calculation of the muon anomalous magnetic moment and the running of the electromagnetic coupling constant. The topics of interest also include: testing the isospin invariance between the weak charged and electromagnetic hadronic currents, evaluation of chiral sum rules making use of the separate determination of vector and axial-vector components, and a global QCD analysis including perturbative and nonperturbative contributions, offering the possibility for a precise extraction of the strong coupling at a relatively low energy scale, and hence providing a sensitive test of the running when compared to the value obtained at the M_Z scale. The spectral functions into strange ($|\Delta S| = 1$) final states, though Cabibbo-suppressed, can be used to determine the s -quark mass and the CKM element $|V_{us}|$.

This article reviews the measurements of nonstrange and strange τ spectral functions and their phenomenological applications. It is organized as follows. We begin in Section II with an overview on the experimental conditions leading to the measurement of the τ branching fractions (Section III) and hadronic spectral functions (Section IV) by the ALEPH and OPAL experiments at LEP as well as CLEO at CESR. Using isospin symmetry, the τ vector spectral functions are compared to the corresponding e^+e^- annihilation data in Section V. We discuss in this context isospin-breaking and radiative corrections. The use of spectral functions in dispersion relations to compute hadronic vacuum polarization is reviewed in Section VI. A comprehensive QCD analysis of hadronic τ decays is presented in Sections VII and VIII. The main topics here are the determinations of the strong coupling constant and the mass of the strange quark at the scale of the τ mass together with $|V_{us}|$. We discuss nonperturbative contributions to the τ hadronic width and present results from chiral QCD sum rules.

In all analyses we critically examine experimental and theoretical limitations, and provide detailed comparisons between experiments as well as perspectives for the future.

II. THE EXPERIMENTAL STAGE

A. Experimental conditions

Tau physics in the nineties has been dominated by two rather different and in many views complementary experimental facilities: on one hand the LEP experiments ALEPH, DELPHI, L3 and OPAL, operating at the Z resonance at center-of-mass (CM) energies of 91.2 GeV, and on the other hand CLEO at CESR running at the $\Upsilon(4S)$ resonance (10.6 GeV). The τ pair production and decay characteristics at LEP were:

- a mean τ flight length of 2.2 mm.
- a strong boost of the produced τ 's leading to a collimated back-to-back event topology; hence tracks and photon clusters overlap in the detector, requiring excellent double hit resolution in the tracking system and a highly granular electromagnetic calorimeter.
- a large track reconstruction efficiency and low nuclear interactions and multiple scattering due to the high energetic particles in the final state.
- since hadronic background from Z decays occurs with significantly larger particle multiplicity, the selection of τ pairs is almost background free ($< 1 - 2\%$), and the efficiency is large (up to 96% at ALEPH, depending on the final state).

- limited statistics: up to 1.6×10^5 τ pairs have been recorded by each of the LEP experiments between 1990 and 1995.

For CLEO, one has

- a mean τ flight length of 0.25 mm.
- well separated τ decay products in the detector.
- significant hadronic background from $e^+e^- \rightarrow q\bar{q}$ continuum events due to the relatively low average multiplicity in the final state of these events. This requires τ tagging, *i.e.*, one τ is reconstructed (“tagged”) in a leptonic decay, or a hadronic mode with less than three hadrons in the final state. The recoil side of the tagged event is then used as an unbiased sample for physics studies.
- large statistics: for example, the $\tau^- \rightarrow \pi^-\pi^0\nu_\tau$ spectral function analysis (CLEO Coll., 2000d) uses a data sample that contains 3.2×10^6 produced τ pairs.

Due to its superior statistics, CLEO discovered a number of rare modes, and performed studies of their hadronic substructures. Examples for these are $\tau^- \rightarrow \eta K^-\nu_\tau$ (CLEO Coll., 1996) and $\tau^- \rightarrow \eta\pi^-\pi^0\nu_\tau$ (CLEO Coll., 1992), the latter one proceeding through a vector current that is due to the Wess-Zumino chiral anomaly (Decker and Mirkes, 1993; Pich, 1987). The anomaly violates the rule that the weak vector and axial-vector currents produce an even and odd number of pseudoscalars, respectively. The $\tau^- \rightarrow \eta\pi^-\nu_\tau$ mode is a G -parity suppressed *second-class current*, which has not been observed yet.

For the τ decays with a branching fraction greater than 0.1%, the cleaner LEP events provided the more precise branching fraction measurements, many of them with a sub-percent relative accuracy, which are a crucial ingredient to the QCD study of hadronic τ decays. The Cabibbo-suppressed τ decays with $|\Delta S| = 1$ have been studied by all experiments, albeit with limited success due to the restricted particle identification capabilities (except for DELPHI and CLEO III). Much progress is expected in this area from the B -Factory experiments *BABAR* and *Belle*, which have dedicated particle identification equipment using characteristic Cherenkov light emission.

B. Investigating the τ hadronic structure

Most of this review will be concerned with the interplay between measurements involving hadronic (or more precisely semileptonic) τ decays and QCD. This may appear a bit paradoxical in view of the relatively low energy scale of τ physics. Indeed, τ decays to hadrons ($+\nu_\tau$) reveal a rich structure of resonances, the study of which opens an interesting field of research on meson dynamics. The leptonic environment provides a significant advantage for isolating clean hadronic systems and measuring their parameters. Many τ decay modes have been investigated for their resonance structure. The phenomenologically important $\pi^-\pi^0$ vector state is analyzed in detail in Section V.

Taking advantage of its large statistics sample, the CLEO Collaboration was able to perform partial-wave analyses of multi-hadron final states. In particular, the $(3\pi)^-\pi^0$ mode is expected to proceed through the vector current dominated by ρ , $\rho(1450)$, $\rho(1700)$ isovector mesons. Resonances are also produced in two-body decays, such as $\omega\pi$, $\eta\pi$, $a_1\pi$. CLEO measured (CLEO Coll., 2000c) the $\omega\pi$ contribution, which they successfully modeled with interfering ρ , $\rho(1450)$, $\rho(1700)$ resonances as shown in Fig. 1. At least the first two contributions are needed to reproduce the experimental mass spectrum. The helicity angle distribution in the $\omega\pi^-$ center-of-mass is found to be consistent with the expected $l = 1$ wave (Fig. 1), whereas a wrong G -parity contribution arising from a weak second-class current, such as $\tau \rightarrow b_1^-\nu_\tau$, $b_1^- \rightarrow \omega\pi^-$, would lead to an even l value. Such a contribution has been bound to be less than 5.4% of the $\omega\pi^-$ rate. Besides $\omega\pi^-$, the total $(3\pi)^-\pi^0$ mode is shown to be dominated by $\rho\pi\pi$, consistent with originating from $a_1\pi$, $a_1 \rightarrow \rho\pi$.

The decay $\tau \rightarrow \nu_\tau(3\pi)^-$ is the cleanest mode to study axial-vector resonance structure. The spectrum is dominated by the $J^P = 1^+$ a_1 state, known to decay essentially through $\rho\pi$. The hadronic structure of this decay has been studied in a model-independent analysis by the OPAL collaboration, where no evidence for vector or scalar currents has been found (OPAL Coll., 1995a, 1997). A comprehensive analysis of the $\pi^-\pi^0$ channel has been presented by CLEO. First, a model-independent determination of the hadronic structure functions gave no evidence for non-axial-vector contributions (< 17% at 90% CL) (CLEO Coll., 2000b). Second, a partial-wave amplitude analysis was performed (CLEO Coll., 2000a): while the dominant $\rho\pi$ mode has been confirmed, it came as a surprise that an important contribution ($\sim 20\%$) from scalars (σ , $f_0(1470)$,

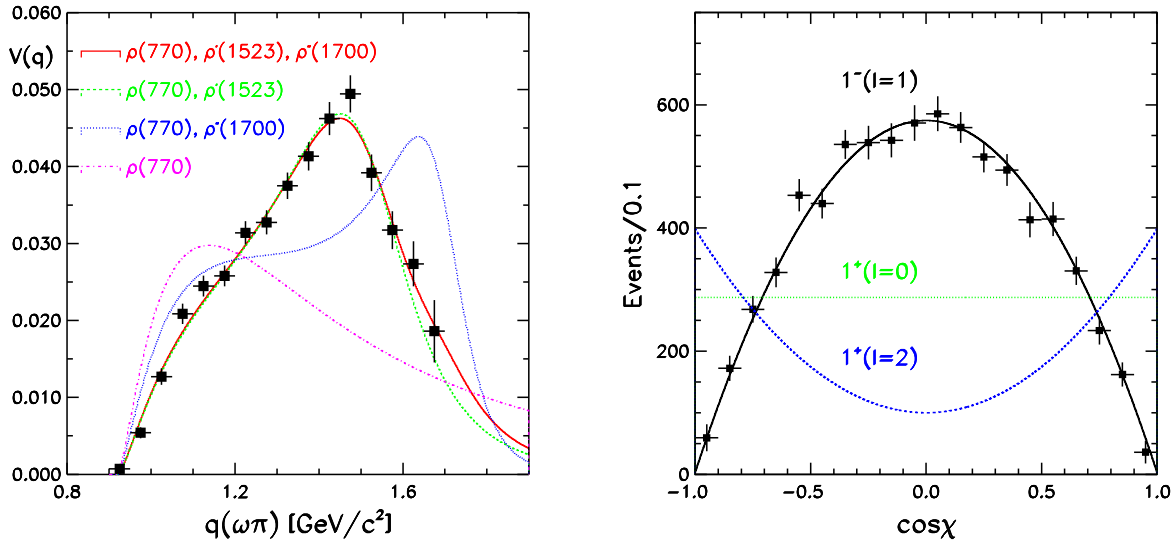


FIG. 1 Left: the spectral function (see Section IV for the definition) for the decay $\tau^- \rightarrow \omega\pi^-\nu_\tau$ vs. the hadronic mass from the CLEO analysis (CLEO Coll., 2000c). The curves are the results of fits to various combinations of ρ , $\rho(1450)$, $\rho(1700)$ resonance contributions. Right: the angular distribution in the $\omega\pi$ center-of-mass frame compared to predictions for different (l) partial waves. Second-class currents would reveal themselves as $l = 0, 2$ waves.

$f_2(1270)$) was found in the 2π subsystem. The precisely determined $a_1^- \rightarrow \pi^- 2\pi^0$ line shape (Fig. 2) shows the opening of the K^*K decay channel. Some interference with a higher mass state (a'_1) was advocated in (DELPHI Coll., 1998). However, no conclusive evidence was found in the CLEO analysis, with a sensitivity about tenfold higher.

Evidence for the decay $\tau \rightarrow f_1(1285)\pi^-\nu_\tau$ has been obtained, with f_1 decay into $\eta\pi^+\pi^-$ and $\eta\pi^0\pi^0$ (CLEO Coll., 1997a), and recently into $2\pi^+ 2\pi^-$ (BABAR Coll., 2005b), the latter decay mode being consistent with $\rho^0\pi^+\pi^-$. Thus many spectroscopy issues can be tackled with τ leptons in a clean environment for single resonance studies.

III. TAU BRANCHING FRACTIONS

Tau hadronic spectral functions (Section IV) are obtained from the measured vector and axial-vector invariant mass spectra, normalized to the corresponding inclusive branching fractions. These are derived from the sum of exclusive branching fractions. Before discussing the spectral functions, we shall thus briefly review the measurement of the τ branching fractions.

A. The measurement of branching fractions

In principle, the measurement of the branching fractions of exclusive τ decays relies on the identification of the corresponding final state and the knowledge of the number of the produced τ leptons in the sample under study. The latter number can be derived from the production cross section, known to high precision in e^+e^- annihilation, and the measured luminosity. The measurement of the final state however requires excellence in many aspects of detector technology and analysis techniques: charged particle tracking and identification for $e/\mu/\pi/K$ separation, photon detection and π^0 (η) reconstruction.

Since very clean and high-efficiency $\tau^+\tau^-$ samples have been produced at LEP, another approach can be considered where all decay channels are simultaneously measured. This global method was pioneered by CELLO at PETRA (CELLO Coll., 1990) with much smaller statistics and less favorable conditions than those encountered at LEP. The detector performance achieved by ALEPH, in particular the excellent granularity of its electromagnetic calorimeter, made it possible to implement this method and take full advantage of the LEP conditions on the Z peak (ALEPH Coll., 1992, 1996a,b, 2005).

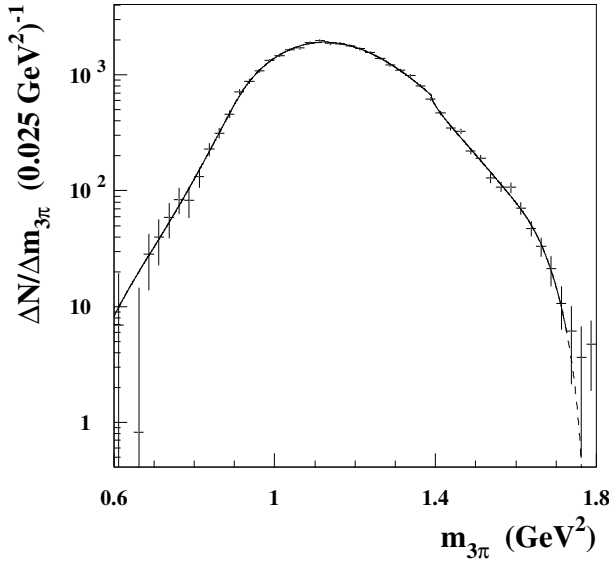


FIG. 2 Hadronic mass distribution for the decay $\tau^- \rightarrow \pi^-\pi^0\pi^0\nu_\tau$ from CLEO (CLEO Coll., 2000a). The curve shows the a_1^- resonance model used in the CLEO analysis, including the opening of the $K^{*0}K^-$ channel near 1.4 GeV. The mass distribution has been corrected for the detector resolution and acceptance.

The ALEPH global analysis of τ branching fractions proceeds from the selection of the $\tau^+\tau^-$ sample, based on the rejection of non- τ backgrounds: Z decays into e^+e^- , $\mu^+\mu^-$ and $q\bar{q}$ pairs, $\gamma\gamma$ -induced processes $e^+e^- \rightarrow e^+e^- X$ (where X can be any fermion-antifermion pair), and cosmic-ray events. The kinematic properties of these backgrounds and their characteristic detector response permit to achieve a high $\tau^+\tau^-$ selection efficiency of 78.9% (91.7% when the $\tau^+\tau^-$ direction points into the active area of the detector) and a low background fraction of 1.2%. Each τ decay is classified on the basis of charged particle and photon/ π^0 multiplicities, and the nature of the charged particles. Charged particle identification is achieved through the response of electromagnetic and hadronic calorimeters, and the ionization loss measurement. Photons need to be identified among the neutral electromagnetic clusters, some of which are induced by charged hadron interactions or by spatial fluctuations of nearby showers (fake photons). Fourteen classes are thus defined in (ALEPH Coll., 2005) for reconstructed decays, where the last one collects the fraction (3.6%) of rejected candidates corresponding to the cases where particle identification is not reliable. The first 13 classes correspond to the following final states produced with ν_τ : $e^-\bar{\nu}_e$, $\mu^-\bar{\nu}_\mu$, h^- , $h^-\pi^0$, $h^-2\pi^0$, $h^-3\pi^0$, $h^-4\pi^0$, $2h^-h^+$, $2h^-h^+\pi^0$, $2h^-h^+2\pi^0$, $2h^-h^+3\pi^0$, $3h^-2h^+$, $3h^-2h^+\pi^0$, where h stands for a pion or kaon.

The branching fractions are determined using

$$n_i^{\text{obs}} - n_i^{\text{bkg}} = \sum_j \varepsilon_{ji} N_j^{\text{prod}}, \quad (1)$$

$$\mathcal{B}_j = \frac{N_j^{\text{prod}}}{\sum_j N_j^{\text{prod}}}, \quad (2)$$

where $n_i^{\text{obs}}(n_i^{\text{bkg}})$ is the number of observed τ candidates (the non- τ background events) that are reconstructed in class i , ε_{ji} the cross-talk efficiency of events that are produced in class j and reconstructed in class i , and N_j^{prod} the number of produced events in class j . The efficiency matrix ε_{ji} is determined from Monte Carlo simulation, based on the event generator KORALZ07 (Jadach *et al.*, 1994) and including the full detector response. The simulation has been calibrated using data for a large number of observables. Among these are particle identification efficiencies, $\tau^+\tau^-$ selection efficiency and the number of fake photon candidates. The selection efficiency remains constant within $\pm \sim 5\%$ for all 13 topologies considered. The linear system of equations (1) is solved for the N_j^{prod} unknown, hence the branching fractions \mathcal{B}_j .

Extensive systematic studies are performed to assess possible biases in the decay assignment. These studies are conducted on data samples in order not to rely on the detector simulation, however detailed it can be.

They include: event selection, non- τ background, particle identification, photon detection efficiency, converted photons, photon identification, fake photons, π^0 reconstruction, bremsstrahlung and radiative photons, π^0 Dalitz decays, secondary nuclear interactions, tracking of charged particles, dynamics in the Monte Carlo generator. The dominant systematic uncertainties for the hadronic modes stem from the photon/ π^0 treatment and secondary interactions.

While measurements of branching fractions larger than 0.1% are more precise at LEP because of its small systematic uncertainties, the larger statistics accumulated by CLEO makes it more competitive for smaller branching fractions. The different experimental conditions also provide complementary information and valuable cross checks.

The ALEPH global analysis assumes a standard τ decay description. However, unknown decay modes not included in the simulation may exist. Since large detection efficiencies are achieved in the $\tau^-\tau^+$ selection, which is therefore robust, these decays would be difficult to pass unnoticed. An independent measurement of the branching fraction for undetected decay modes, *i.e.*, modes not passing the selection cuts, using a direct search with a one-sided τ tag, was done by ALEPH (Snow, 1993), limiting this branching fraction to less than 0.11% at 95% CL. This result justifies the assumption that the sum of the branching fractions for visible τ decays is equal to one. The consistency between the results and the τ decay description in the simulation can be investigated further by verifying that the “branching fraction” for a 14th class in the decay classification, which collects rejected events, turns out to be zero within the measurement errors. The result, $\mathcal{B}_{14} = (0.066 \pm (0.042)\%)$, provides a nontrivial test of the overall procedure at the 0.1% level for branching fractions.

The global method at LEP reaches its limit for decay modes with small branching fractions, which compete with leading channels with fractions that could be more than two orders of magnitude larger. This limit is also determined by the overall τ statistics. It turns out that the two factors contribute at about the same level. Thus final states with more than five hadrons are poorly determined at LEP, whereas CLEO can use its larger statistics to apply stricter cuts for these higher-multiplicity decays with low branching ratios.

A final check of the global analysis can be performed by comparing the sums of the relevant exclusive decay fractions to the topological branching fractions \mathcal{B}_i , where i refers to the charged particle multiplicity in the decay. Even though the latter branching fractions have only limited direct physics implications, their determination represents a valuable cross check as the measurement depends only on selection efficiency, tracking, handling of secondary interactions and electron identification for photon conversions, but not on the explicit photon reconstruction in a calorimeter. Assuming a negligible contribution from charged-particle multiplicities larger than five, in agreement with the 90% CL limit achieved by CLEO ($\mathcal{B}_7 < 2.4 \times 10^{-6}$ (CLEO Coll., 1997c)), ALEPH finds:

$$\mathcal{B}_3 = (14.652 \pm 0.067 \pm 0.086)\% , \quad (3)$$

$$\mathcal{B}_5 = (0.093 \pm 0.009 \pm 0.012)\% , \quad (4)$$

in agreement with the values from a dedicated topological analysis performed by DELPHI (DELPHI Coll., 2001),

$$\mathcal{B}_3^{\text{top}} = (14.569 \pm 0.093 \pm 0.048)\% , \quad (5)$$

$$\mathcal{B}_5^{\text{top}} = (0.115 \pm 0.013 \pm 0.006)\% . \quad (6)$$

B. Leptonic branching fractions

The measurement of the two leptonic decay modes of the τ is of great importance in our context, since they are complementary to the hadronic modes, the fraction of which can be determined by a simple difference. The leptonic branching ratios also turn out to be the most precisely determined τ decay fractions, not affected by systematic uncertainties that are specific to the presence of hadrons in the detector.

Before examining the experimental situation, we shall recall the theoretical expectations within the standard $V - A$ theory with leptonic coupling g_ℓ at the $W\ell\bar{\nu}_\ell$ vertex. The $L = \mu, \tau$ leptonic ($\ell = e, \mu$) partial widths can be computed, including radiative corrections (Marciano and Sirlin, 1988) and safely neglecting neutrino masses:

$$\Gamma(L \rightarrow \nu_L \ell \bar{\nu}_\ell(\gamma)) = \frac{G_L G_\ell m_L^5}{192\pi^3} f\left(\frac{m_\ell^2}{m_L^2}\right) \delta_W^L \delta_\gamma^L , \quad (7)$$

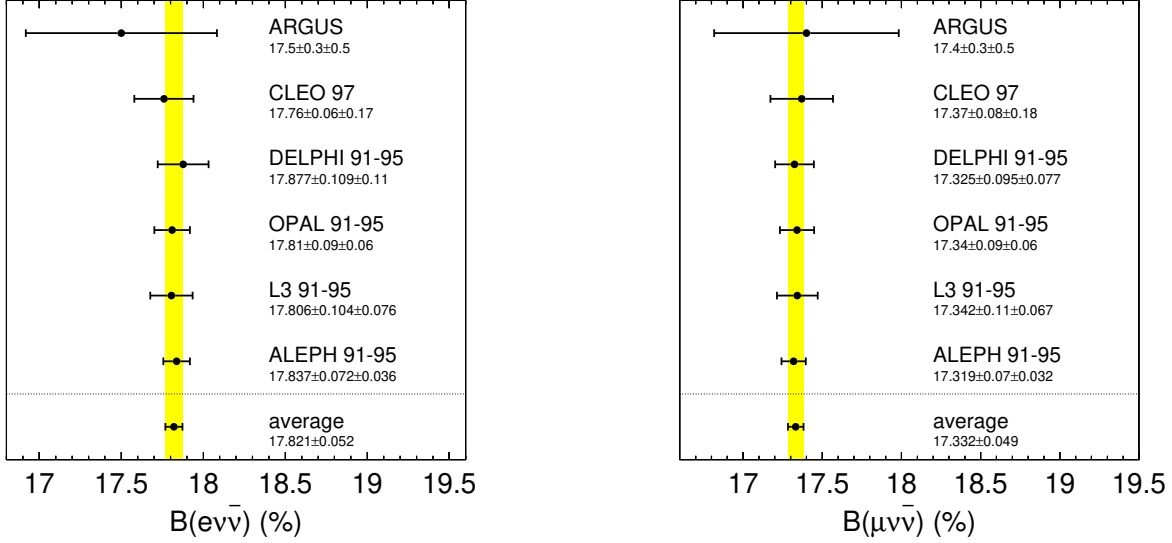


FIG. 3 Measurements of the branching fraction for $\tau^- \rightarrow e^- \bar{\nu}_e \nu_\tau$ (left) and $\tau^- \rightarrow \mu^- \bar{\nu}_\mu \nu_\tau$ (right). References for experiments are (ALEPH Coll., 2005; ARGUS Coll., 1993; CLEO Coll., 1997b; DELPHI Coll., 1999; L3 Coll., 2001; OPAL Coll., 1999a, 2003).

where

$$\begin{aligned}
 G_\ell &= \frac{g_\ell^2}{4\sqrt{2}M_W^2} \\
 \delta_W^L &= 1 + \frac{3}{5} \frac{m_L^2}{M_W^2} \\
 \delta_\gamma^L &= 1 + \frac{\alpha(m_L)}{2\pi} \left(\frac{25}{4} - \pi^2 \right) \\
 f(x) &= 1 - 8x + 8x^3 - x^4 - 12x^2 \ln x
 \end{aligned} \tag{8}$$

Numerically, the radiative and W propagator corrections are small: $\delta_W^\tau = 1 + 2.9 \times 10^{-4}$, $\delta_\gamma^\tau = 1 - 43.2 \times 10^{-4}$, $\delta_W^\mu = 1 + 1.0 \times 10^{-6}$, and $\delta_\gamma^\mu = 1 - 42.4 \times 10^{-4}$.

The experimental situation on the electronic and muonic branching fractions, \mathcal{B}_e and \mathcal{B}_μ , is given in Fig. 3. The results for their average are

$$\mathcal{B}_e = (17.821 \pm 0.052)\%, \tag{9}$$

$$\mathcal{B}_\mu = (17.332 \pm 0.049)\%, \tag{10}$$

with a relative precision of 0.3%. The values for \mathcal{B}_e and \mathcal{B}_μ agree with $e\mu$ universality ($g_e = g_\mu$). Their ratio

$$\frac{\mathcal{B}_\mu}{\mathcal{B}_e} = 0.9726 \pm 0.0041 \tag{11}$$

is consistent with the predicted value equal to $f(m_\mu^2/m_\tau^2)/f(m_e^2/m_\tau^2) = 0.972565 \pm 0.000009$, using lepton masses from (Particle Data Group, 2004). The uncertainty arises essentially from the τ mass determination, $m_\tau = (1777.03^{+0.30}_{-0.26})$ MeV (dominated by the BES result (BES Coll., 2002)).

The result for \mathcal{B}_e can also be compared with the value obtained from the τ and μ masses and lifetimes $\tau_{\tau,\mu}$, under the assumption of $\tau\mu$ universality, according to

$$\begin{aligned}
 \mathcal{B}_e &= \frac{\tau_\tau}{\tau_\mu} \left(\frac{m_\tau}{m_\mu} \right)^5 \frac{f(m_e^2/m_\tau^2)}{f(m_e^2/m_\mu^2)} \frac{\delta_W^\tau \delta_\gamma^\tau}{\delta_W^\mu \delta_\gamma^\mu} \\
 &= \frac{\tau_\tau}{(1631.9 \pm 1.4) \text{ fs}}
 \end{aligned} \tag{12}$$

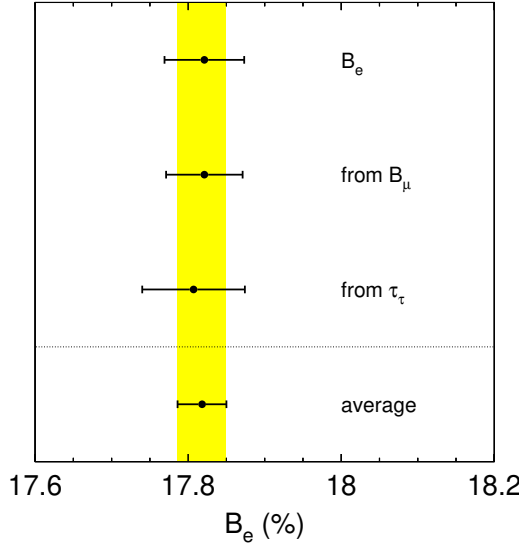


FIG. 4 Comparison of the direct measurement of \mathcal{B}_e with the indirect determinations derived from \mathcal{B}_μ and τ_τ assuming lepton universality in the weak charged current (all values are world averages).

Using the τ lifetime (Particle Data Group, 2004), $\tau_\tau = (290.6 \pm 1.1)$ fs, as well as the μ lifetime, one obtains $\mathcal{B}_e = (17.807 \pm 0.067)\%$, in excellent agreement with the direct measurements.

The consistency of the direct value for \mathcal{B}_e and the two derived values from \mathcal{B}_μ and τ_τ can be inspected on Fig. 4. While the agreement may appear somewhat surprising on statistical grounds, it does provide a consistent and precise combined result for the electronic branching fraction,

$$\mathcal{B}_e^{\text{uni}} = (17.818 \pm 0.032)\%. \quad (13)$$

Hence we find for the branching fraction of $\tau \rightarrow \nu_\tau$ hadrons, \mathcal{B}_{had} , assuming lepton universality and unitarity

$$\mathcal{B}_{\text{had}} = 1 - 1.97257 \mathcal{B}_e^{\text{uni}} = (64.853 \pm 0.063)\%. \quad (14)$$

C. Decay modes with kaons

Measurements of τ decay modes with kaons in the final state are important on at least two counts: (i) to determine the Cabibbo-suppressed component of the hadronic decay width, leading to interesting physics applications (see Section VIII), and (ii) to perform the necessary corrections to the measured topological branching fractions, based on charged particles and π^0 multiplicities and dominated by the nonstrange component. This latter step is made necessary by the difficulty separating charged pions and kaons, and identifying K_L^0 's at the level of an event. The subtraction of strange final states is then performed on a statistical basis.

The most complete measurements of τ branching fractions involving kaons are from ALEPH (ALEPH Coll., 1997a, 1998a,b, 1999a,b). The diversity of the final states can be appreciated from the results that are summarized in Table I. From these results a comprehensive study of the strange sector has been performed, as well as some aspects of the dynamics in the final states with a $K\bar{K}$ pair. The experimental difficulty resides in the fact that both charged and neutral kaons have to be identified into multi-particle final states. The analyses involve the detection of charged kaons through the measurement of specific ionization losses and neutral kaons through either their decay into $\pi^+\pi^-$ (K_S^0) or their interactions in a calorimeter (K_L^0). Assuming CP invariance the K_S^0 and K_L^0 branching fractions can be averaged. The higher efficiency achieved for K_L^0 detection leads to smaller statistical uncertainties. The average results are given in the right-hand column of Table I. Although the strange final states are Cabibbo-suppressed, the precision achieved in these measurements is sufficient for various significant tests, ranging from $\tau - \mu$ lepton universality to hadron dynamics, resonance production, QCD analyses, and the measurement of the Cabibbo angle. In addition, the

TABLE I Summary of branching fractions for τ decays involving kaons from (ALEPH Coll., 1999b). Channels with neutral kaons are measured using either their K_L^0 and K_S^0 components. Modes are split into the strange ($S = -1$) and nonstrange ($S = 0$) sectors of τ decays. The last column presents the average of the results obtained through the detection of K_S^0 and K_L^0 for final states with \bar{K}^0 and K^-K^0 , and the sum of all components for final states with $K^0\bar{K}^0$.

Decay	K^0 detected	S	$\mathcal{B} (10^{-3})$	$\mathcal{B}(K_L^0 + K_S^0) (10^{-3})$
$\tau^- \rightarrow K^-\nu_\tau$	—		6.96 ± 0.29	—
$\tau^- \rightarrow K^-\pi^0\nu_\tau$	—		4.44 ± 0.35	—
$\tau^- \rightarrow \bar{K}^0\pi^-\nu_\tau$	K_L^0		9.28 ± 0.56	
$\tau^- \rightarrow \bar{K}^0\pi^-\nu_\tau$	K_S^0		8.55 ± 1.34	9.17 ± 0.52
$\tau^- \rightarrow \bar{K}^0\pi^-\pi^0\nu_\tau$	K_L^0		3.47 ± 0.65	
$\tau^- \rightarrow \bar{K}^0\pi^-\pi^0\nu_\tau$	K_S^0		2.94 ± 0.82	3.27 ± 0.51
$\tau^- \rightarrow K^-\pi^+\pi^-\nu_\tau$	—	—1	2.14 ± 0.47	—
$\tau^- \rightarrow K^-\pi^0\pi^0\nu_\tau$	—		0.56 ± 0.25	—
$\tau^- \rightarrow \bar{K}^0\pi^-\pi^0\pi^0\nu_\tau$	K_L^0		< 0.66 (95% CL)	
$\tau^- \rightarrow \bar{K}^0\pi^-\pi^0\pi^0\nu_\tau$	K_S^0		0.58 ± 0.36	0.26 ± 0.24
$\tau^- \rightarrow K^-\pi^0\pi^0\nu_\tau$	—		0.37 ± 0.24 (excl. η)	—
$\tau^- \rightarrow K^-\pi^+\pi^-\pi^0\nu_\tau$	—		0.54 ± 0.43 (excl. η)	—
$\tau^- \rightarrow K^-\eta\nu_\tau$	—		$0.29^{+0.15}_{-0.14}$	—
$\tau^- \rightarrow K^-K^+K^-\nu_\tau$	—		< 0.19 (95% CL)	—
$\tau^- \rightarrow K^-K^0\nu_\tau$	K_L^0		1.62 ± 0.24	
$\tau^- \rightarrow K^-K^0\nu_\tau$	K_S^0		1.58 ± 0.45	1.61 ± 0.21
$\tau^- \rightarrow K^-K^0\pi^0\nu_\tau$	K_L^0		1.43 ± 0.32	
$\tau^- \rightarrow K^-K^0\pi^0\nu_\tau$	K_S^0		1.52 ± 0.79	1.45 ± 0.30
$\tau^- \rightarrow K^-K^0\pi^0\pi^0\nu_\tau$	K_L^0		< 0.18 (95% CL)	
$\tau^- \rightarrow K^-K^0\pi^0\pi^0\nu_\tau$	K_S^0	0	< 0.39 (95% CL)	< 0.16 (95% CL)
$\tau^- \rightarrow K_S^0K_L^0\pi^-\nu_\tau$	—		1.01 ± 0.26	
$\tau^- \rightarrow K_S^0K_S^0\pi^-\nu_\tau$	—		0.26 ± 0.12	1.53 ± 0.35
$\tau^- \rightarrow K_S^0K_L^0\pi^-\pi^0\nu_\tau$	—		0.31 ± 0.12	
$\tau^- \rightarrow K_S^0K_S^0\pi^-\pi^0\nu_\tau$	—		< 0.20 (95% CL)	0.31 ± 0.23
$\tau^- \rightarrow K^-K^+\pi^-\nu_\tau$	—		1.63 ± 0.27	—
$\tau^- \rightarrow K^-K^+\pi^-\pi^0\nu_\tau$	—		0.75 ± 0.33	—
$\tau^- \rightarrow K^0h^-h^+h^-\nu_\tau$	K_S^0	mixed	0.23 ± 0.20	0.23 ± 0.20

consistency of the results is checked through the verification of isospin relations between the rates observed for different charge configurations of the same final states.

New experimental results have been released by CLEO (CLEO Coll., 1999a,b, 2003, 2005) and OPAL (OPAL Coll., 2004) achieving significant progress in the $\bar{K}\pi\pi$ modes. The new measurements tend to favor larger branching fractions. In particular, the branching fraction for the $K^-\pi^+\pi^-$ mode, $(2.14 \pm 0.47) \times 10^{-3}$ for ALEPH, becomes in the average $(3.30 \pm 0.28) \times 10^{-3}$ with a χ^2 of 9.6 for 2 DF (about 1% probability). Also, the branching fraction for $\bar{K}^0\pi^-\pi^0$, $(3.27 \pm 0.51) \times 10^{-3}$ for ALEPH, becomes $(3.60 \pm 0.40) \times 10^{-3}$ in the average. A compilation of the world average $S = 1$ branching fractions is given in Table II.

The branching fraction for the decay $\tau^- \rightarrow K^-\nu$, \mathcal{B}_K ,

$$\mathcal{B}_K = (0.681 \pm 0.023)\%, \quad (15)$$

can be compared to the theoretical prediction assuming $\tau\mu$ universality in the charged weak current, $\mathcal{B}_K^{\text{uni}}$, using the values (Particle Data Group, 2004) for the τ and K lifetimes and masses, the $K^- \rightarrow \mu^-\bar{\nu}_\mu$ branching

TABLE II World average branching fractions (10^{-3}) for τ decays into strange final states and ν_τ from (ALEPH Coll., 1999b; CLEO Coll., 2003, 2005; OPAL Coll., 2004; Particle Data Group, 2004). The value for the $(\bar{K}3\pi)^-$ branching fraction takes into account measurements from ALEPH and CLEO, as well as estimates for unseen final states using isospin relations. The estimate for the very small $(\bar{K}4\pi)^-$ fraction, in addition to the measured $K^*-\eta$ rate (CLEO Coll., 1999a), is obtained from an empirical observation of pionic modes and Cabibbo suppression.

Mode	$\mathcal{B}(10^{-3})$
K^-	6.81 ± 0.23
$K^-\pi^0$	4.54 ± 0.30
$\bar{K}^0\pi^-$	8.78 ± 0.38
$K^-\pi^0\pi^0$	0.58 ± 0.24
$\bar{K}^0\pi^-\pi^0$	3.60 ± 0.40
$K^-\pi^+\pi^-$	3.30 ± 0.28
$K^-\eta$	0.27 ± 0.06
$(\bar{K}3\pi)^-$ (estimated)	0.74 ± 0.30
$K_1(1270)^- \rightarrow K^-\omega$	0.67 ± 0.21
$(\bar{K}4\pi)^-$ (estimated) and $K^*-\eta$	0.40 ± 0.12
Sum	29.69 ± 0.86

fraction, and a small radiative correction (Decker and Finkemeier, 1993), $\delta_{\tau/K} = 1.0090 \pm 0.0022$,

$$\begin{aligned} \mathcal{B}_K^{\text{uni}} &= \frac{\tau_\tau B_{K \rightarrow \mu\nu}}{\tau_K} \frac{m_\tau^3}{2m_K m_\mu^2} \left(\frac{1 - m_K^2/m_\tau^2}{1 - m_\mu^2/m_K^2} \right)^2 \delta_{\tau/K} \\ &= \frac{\tau_\tau}{(40\,636 \pm 162) \text{ fs}} = (0.715 \pm 0.003)\%. \end{aligned} \quad (16)$$

D. Nonstrange hadronic branching fractions

Nonstrange hadronic branching fractions represent the largest part of τ decays and the physics goals require the achievement of small systematic uncertainties. The main experimental difficulty for this task is the photon/ π^0 reconstruction. The high collimation of τ decays at LEP energies makes this task quite often difficult, since these photons are close to one another or close to the showers generated by charged hadrons. Of particular relevance is the rejection of fake photons, which are due to hadronic interactions, fluctuations of electromagnetic showers, or an overlap of several showers. These problems reach a tolerable level in ALEPH thanks to the fine granularity of its electromagnetic calorimeter, comprising about 70,000 cells covering the detector angular acceptance, each cell being segmented threefold along the photon direction in order to discriminate between hadronic and electromagnetic showers. Even then, proper and reliable reconstruction methods had to be developed to correctly identify photon candidates. In the ALEPH analysis, a likelihood method is used for discriminating between genuine and fake photons, taking advantage of the detailed calorimeter information for each detected cluster of energy not associated to a charged track. Photons converted in the detector material are also included. Then π^0 's are reconstructed: resolved π^0 's from two-photon pairing, unresolved high-energy π^0 's from merged clusters, and residual π^0 's from the remaining single photons after removing radiative, bremsstrahlung and fake photons with a likelihood method.

The 13 τ decay classes defined in Section III.A are not fully exclusive as they contain contributions from final states involving kaons. They are coming from charged kaons included in the class definition using hadrons (h) and from neutral kaons not taken into account in the classification. These contributions are subtracted on a statistical basis using the branching fractions measured separately (Section III.C).

The τ decays involving η or ω mesons also require special attention because of their electromagnetic decay modes. Indeed the final state classification relies in part on the π^0 multiplicity, thereby assuming that all photons—except those specifically identified as bremsstrahlung or radiative—originate from π^0 decays. Therefore the non- π^0 photons from η and ω decays are treated as π^0 candidates in the ALEPH analysis

TABLE III Results (ALEPH Coll., 2005) on exclusive hadronic branching fractions for modes without kaons. The contributions from channels with η and ω are given separately, the latter one only for the electromagnetic ω decays. The measured branching ratio for $2\pi^-\pi^+3\pi^0$ is consistent with zero and the value listed in the table has been estimated with the help of CLEO results (CLEO Coll., 1993c).

Mode	$\mathcal{B} \pm \sigma_{\text{stat}} \pm \sigma_{\text{syst}}$ (in %)
π^-	$10.828 \pm 0.070 \pm 0.078$
$\pi^-\pi^0$	$25.471 \pm 0.097 \pm 0.085$
$\pi^-2\pi^0$	$9.239 \pm 0.086 \pm 0.090$
$\pi^-3\pi^0$	$0.977 \pm 0.069 \pm 0.058$
$\pi^-4\pi^0$	$0.112 \pm 0.037 \pm 0.035$
$\pi^-\pi^-\pi^+$	$9.041 \pm 0.060 \pm 0.076$
$\pi^-\pi^-\pi^+\pi^0$	$4.590 \pm 0.057 \pm 0.064$
$2\pi^-\pi^+2\pi^0$	$0.392 \pm 0.030 \pm 0.035$
$2\pi^-\pi^+3\pi^0$	$0.013 \pm 0.000 \pm 0.010$
$3\pi^-2\pi^+$	$0.072 \pm 0.009 \pm 0.012$
$3\pi^-2\pi^+\pi^0$	$0.014 \pm 0.007 \pm 0.006$
$\pi^-\pi^0\eta$	$0.180 \pm 0.040 \pm 0.020$
$\pi^-2\pi^0\eta$	$0.015 \pm 0.004 \pm 0.003$
$\pi^-\pi^-\pi^+\eta$	$0.024 \pm 0.003 \pm 0.004$
$a_1^- (\rightarrow \pi^-\gamma)$	$0.040 \pm 0.000 \pm 0.020$
$\pi^-\omega (\rightarrow \pi^0\gamma, \pi^+\pi^-)$	$0.253 \pm 0.005 \pm 0.017$
$\pi^-\pi^0\omega (\rightarrow \pi^0\gamma, \pi^+\pi^-)$	$0.048 \pm 0.006 \pm 0.007$
$\pi^-2\pi^0\omega (\rightarrow \pi^0\gamma, \pi^+\pi^-)$	$0.002 \pm 0.001 \pm 0.001$
$\pi^-\pi^-\pi^+\omega (\rightarrow \pi^0\gamma, \pi^+\pi^-)$	$0.001 \pm 0.001 \pm 0.001$
	estimate
	(ALEPH Coll., 1997a)
	(CLEO Coll., 1997a; Weinstein, 2001)
	(CLEO Coll., 1997a; Weinstein, 2001)
	estimate
	(ALEPH Coll., 1997a)
	(ALEPH Coll., 1997a; CLEO Coll., 1993b)
	(CLEO Coll., 1997a; Weinstein, 2001)
	(CLEO Coll., 1997a; Weinstein, 2001)

and the systematic bias introduced by this effect must be evaluated. The corrections are based on specific measurements by ALEPH of τ decay modes containing those mesons (ALEPH Coll., 1997a). Hence the final results correspond to exclusive branching fractions obtained from the values measured in the topological classification, corrected by the contributions from K , η and ω modes measured separately, taking into account through the simulation their specific selection and reconstruction efficiencies. This delicate bookkeeping takes into account all the major decay modes of the considered mesons (Particle Data Group, 2004), including the isospin-violating $\omega \rightarrow \pi^+\pi^-$ decay mode. The main decay modes considered are $\pi^-\omega$, $\pi^-\pi^0\omega$ and $\pi^-\pi^0\eta$ with branching fractions of $(2.26 \pm 0.18) \times 10^{-2}$, $(4.3 \pm 0.5) \times 10^{-3}$, and $(1.80 \pm 0.45) \times 10^{-3}$ (ALEPH Coll., 1997a), respectively. The first two values are derived from the branching fractions for the $2\pi^-\pi^+\pi^0$ and $2\pi^-\pi^+2\pi^0$ modes obtained in the global analysis and the measured ω fractions of 0.431 ± 0.033 from (ALEPH Coll., 1997a) and the average value, 0.78 ± 0.06 , from (ALEPH Coll., 1997a) and (CLEO Coll., 1993b), respectively.

Small contributions with η and ω have been identified and measured in (CLEO Coll., 1997a; Weinstein, 2001) with the decay modes $\tau^- \rightarrow \nu_\tau\eta\pi^-\pi^+\pi^-$ (2.4 ± 0.5), $\tau^- \rightarrow \nu_\tau\eta\pi^-\pi^0$ (1.5 ± 0.5), $\tau^- \rightarrow \nu_\tau\omega\pi^-\pi^+\pi^-$ (1.2 ± 0.2), and $\tau^- \rightarrow \nu_\tau\omega\pi^-\pi^0$ (1.5 ± 0.5), where the branching fractions are given in units of 10^{-4} . For the sake of completeness these modes have been included. Another small correction has been applied to take into account the a_1^- radiative decay into $\pi\gamma$ with a branching fraction of $(2.1 \pm 0.8) \times 10^{-3}$ (Zielinski, 1984).

The final ALEPH results on the hadronic branching fractions for τ decay modes not including kaons are given in Table III. The branching fractions obtained for the different channels are correlated with each other. On one hand the statistical fluctuations in the data and the Monte Carlo samples are driven by the multinomial distribution of the corresponding events, producing well-understood correlations. On the other hand the systematic effects also induce significant correlations between the different channels. All the systematic studies were done keeping track of the correlated variations in the final branching fraction results, thus allowing a proper propagation of errors. The full covariance matrices from statistical and systematic origins are given in (ALEPH Coll., 2005).

The branching fraction \mathcal{B}_π for the $\pi^- \nu$ decay mode,

$$\mathcal{B}_\pi = (10.83 \pm 0.11)\% , \quad (17)$$

agrees well with a theoretical prediction only depending on the assumption of τ - μ universality, $\mathcal{B}_\pi^{\text{uni}}$, using the values (Particle Data Group, 2004) for the τ and π lifetimes and masses, the $\pi^- \rightarrow \mu^- \bar{\nu}_\mu$ branching fraction, and a small radiative correction (Decker and Finkemeier, 1993), $\delta_{\tau/\pi} = 1.0016 \pm 0.0014$,

$$\begin{aligned} \mathcal{B}_\pi^{\text{uni}} &= \frac{\tau_\tau B_{\pi \rightarrow \mu \nu}}{\tau_\pi} \frac{m_\tau^3}{2m_\pi m_\mu^2} \left(\frac{1 - m_\pi^2/m_\tau^2}{1 - m_\mu^2/m_\pi^2} \right)^2 \delta_{\tau/\pi} \\ &= \frac{\tau_\tau}{(2663.7 \pm 4.0) \text{ fs}} = (10.910 \pm 0.044)\% , \end{aligned} \quad (18)$$

where the error in the denominator of the prediction is dominated by the uncertainty on the structure-dependent radiative correction.

Concerning the $(3\pi)^- \nu$ decay mode, which is dominated by the a_1 resonance, it is interesting to compare the rates in the $2\pi^- \pi^+$ and $\pi^- 2\pi^0$ channels. Dominance of the $\rho\pi$ intermediate state in the a_1 decay predicts equal rates, but (small) isospin-breaking effects are expected from different charged and neutral π (and possibly ρ) masses, slightly favoring the $\pi^- 2\pi^0$ channel. However, a partial-wave analysis of the $\pi^- 2\pi^0$ final state performed by CLEO (CLEO Coll., 2000a) (*cf.* Section II.B) revealed that this decay is in fact rather complicated involving many intermediate states, in particular isoscalars, which amount to about 20% of the total rate and produce strong interference effects. A good description of the a_1 decays was achieved in this study, which can be applied to the $(3\pi)^-$ final state. Including known isospin-breaking effects from the pion masses, it predicts a ratio of the $2\pi^- \pi^+$ to the $\pi^- 2\pi^0$ rate of 0.985. This value is in agreement with the ALEPH measurement (ALEPH Coll., 2005)

$$\frac{\mathcal{B}_{2\pi^- \pi^+}}{\mathcal{B}_{\pi^- 2\pi^0}} = 0.979 \pm 0.018 , \quad (19)$$

supporting the expected trend.

A comparison of recent measurements of the dominant hadronic branching fractions is provided in Figs. 5 and 6. To compare with other experiments, results are given there without charged hadron identification, *i.e.*, the branching fractions correspond to the sum of all branching fractions of the same charged particle topology, whether pions or kaons.

E. Separation of vector and axial-vector contributions

From the complete analysis of the τ branching fractions presented in (ALEPH Coll., 2005) it is possible to determine the nonstrange vector (V) and axial-vector (A) contributions to the total τ hadronic width. It is conveniently expressed in terms of their ratios to the leptonic width, denoted $R_{\tau,V}$ and $R_{\tau,A}$, respectively, while the inclusive strange counterpart is denoted $R_{\tau,S}$. Only limited attempts to separate vector and axial-vector $|\Delta S| = 1$ currents have been performed by the experiments so far (ALEPH Coll., 1999b).

The ratio R_τ for the total hadronic width is calculated from the leptonic branching fractions alone, and eventually from the (massless) electronic branching fraction only¹,

$$R_\tau = \frac{1 - \mathcal{B}_e - \mathcal{B}_\mu}{\mathcal{B}_e} = \frac{1}{\mathcal{B}_e^{\text{uni}}} - 1.9726 = 3.642 \pm 0.012 , \quad (20)$$

for ALEPH, assuming universality in the leptonic weak current. All R values given below are rescaled so that the sum of the hadronic and the leptonic branching fractions, the latter one computed using the “universal” value $\mathcal{B}_e^{\text{uni}}$ (ALEPH), add up to one. The deviations introduced in this way are small, less than 10% of the experimental error, but this procedure guarantees the consistency of all values. Using the ALEPH

¹ The branching ratios $\mathcal{B}_e^{\text{uni}}$ (ALEPH) = $(17.810 \pm 0.039)\%$ and \mathcal{B}_S (ALEPH) = $(2.85 \pm 0.11)\%$ used in this section are from the ALEPH analysis only (ALEPH Coll., 2005) and differ slightly from the world average values given in Sections III.B and III.C.

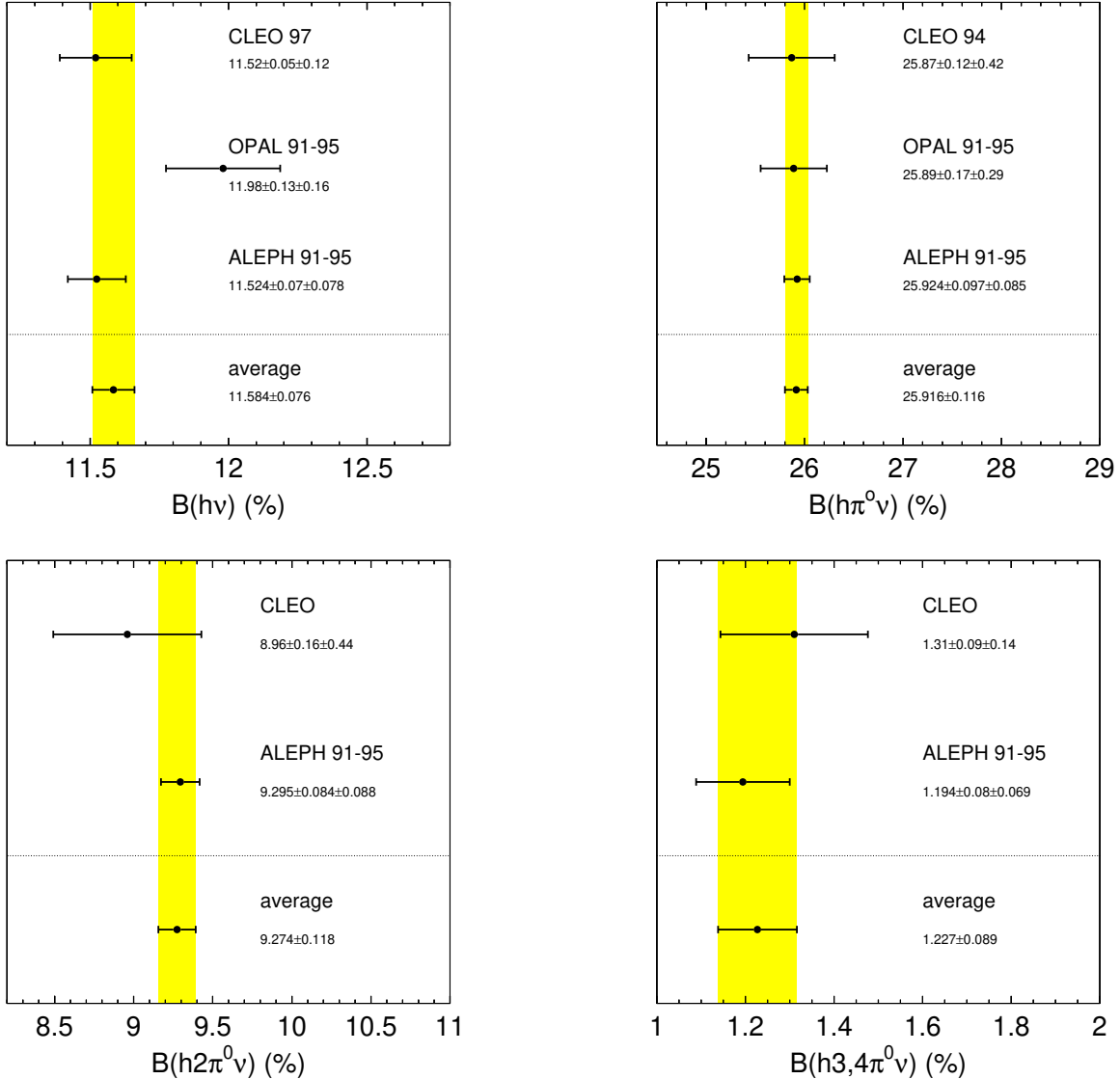


FIG. 5 Comparison of results on the branching fractions for $\tau^- \rightarrow h^- \nu_\tau$, $h^- \pi^0 \nu_\tau$, $h^- 2\pi^0 \nu_\tau$ and the inclusive $h^- 3(4)\pi^0 \nu$ (ALEPH Coll., 2005; CLEO Coll., 1993a, 1994a, 1997b; OPAL Coll., 1998). The world averages are indicated by the shaded vertical bands.

measurement of the strange branching fractions (ALEPH Coll., 1999b), supplemented by a (small) contribution from the $K^{*-} \eta$ channel measured by CLEO (CLEO Coll., 1999a), one finds (see Footnote 1)

$$\begin{aligned} \mathcal{B}_S &= (2.85 \pm 0.11)\% , \\ R_{\tau,S} &= 0.1603 \pm 0.0064 , \end{aligned} \quad (21)$$

and consequently

$$\begin{aligned} \mathcal{B}_{V+A} &= (62.01 \pm 0.14)\% , \\ R_{\tau,V+A} &= 3.482 \pm 0.014 , \end{aligned} \quad (22)$$

for the nonstrange component.

Separation of V and A components in hadronic final states with only pions is straightforward. Even number of pions has $G = 1$ corresponding to vector states, while an odd number of pions has $G = -1$, which tags

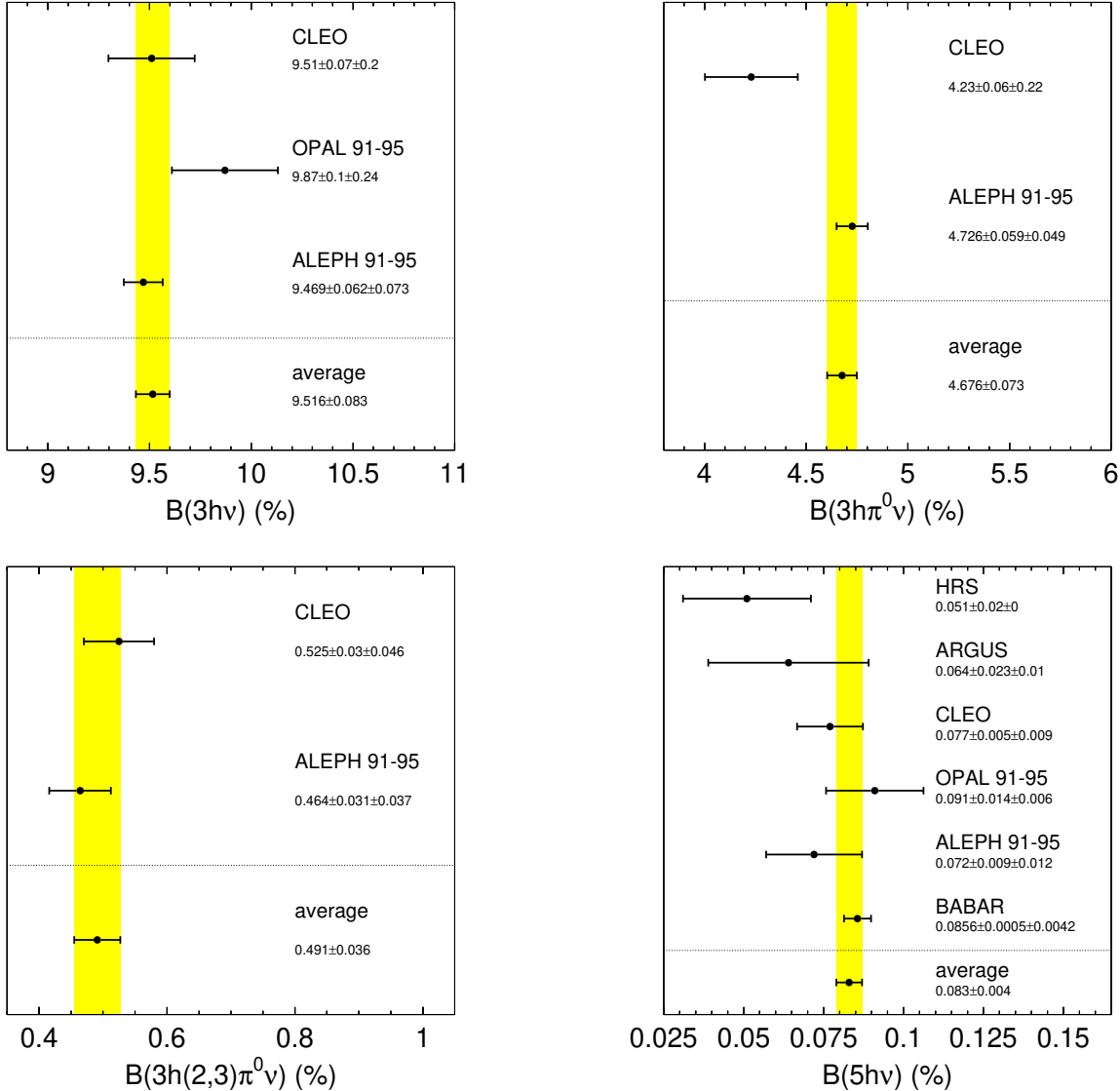


FIG. 6 Comparison of results on the branching fractions for $\tau^- \rightarrow 2h^-h^+\nu_\tau$, $2h^-h^+\pi^0\nu_\tau$, $2h^-h^+2(3)\pi^0\nu_\tau$ and $3h^-2h^+\nu_\tau$ (ALEPH Coll., 2005; ARGUS Coll., 1988; BABAR Coll., 2005b; CLEO Coll., 1993a,c, 1994a,b, 1995a, 1997b; HRS Colla., 1987; OPAL Coll., 1995b, 1998, 1999c). The world averages are indicated by the shaded vertical bands.

axial-vector states. This property places a strong requirement on the knowledge of the π^0 reconstruction efficiency in the detector.

Modes with a $K\bar{K}$ pair are not in general eigenstates of G -parity and contribute to both V and A channels. While the decay to K^-K^0 is pure vector, the situation is *a priori* not clear in the $K\bar{K}\pi$ channel, observed in three charged modes: $K^-K^+\pi^-$, $K^-K^0\pi^0$ and $K^0\bar{K}^0\pi^-$. Three sources of information exist on the possible V/A content in these decays:

1. In the ALEPH analysis of τ decay modes with kaons (ALEPH Coll., 1999b), an estimate of the vector contribution was obtained using the available e^+e^- annihilation data in the $K\bar{K}\pi$ channel, extracted in the $I = 1$ state. This contribution was found to be small, yielding the branching fraction $\mathcal{B}_{\text{CVC}}(\tau^- \rightarrow \nu_\tau(K\bar{K}\pi)^-) = (0.26 \pm 0.39) \times 10^{-3}$, which corresponds to an axial fraction of $f_{A,\text{CVC}} = 0.94^{+0.06}_{-0.08}$.
2. The CVC result is corroborated by a partial-wave and lineshape analysis of the a_1 resonance from τ decays in the $\nu_\tau\pi^-2\pi^0$ mode in (CLEO Coll., 2000a). The observation through unitarity of the opening

of the K^*K decay mode of the a_1 is postulated and the branching fraction $\mathcal{B}(a_1 \rightarrow K^*K) = (3.3 \pm 0.5)\%$ is derived. With the known decay rate of $\tau^- \rightarrow \nu_\tau a_1^-$, it is easy to see that such a result saturates, and even exceeds, the total rate for the $K\bar{K}\pi$ channel. The corresponding axial fraction is $f_{A,3\pi} = 1.30 \pm 0.24$.

3. A new piece of information, also contributed by CLEO, but conflicting with the two previous results, was recently published (CLEO Coll., 2004). It is based on a partial-wave analysis in the $K^-K^+\pi^-$ channel using two-body resonance production and including many possibly contributing channels. A much smaller axial contribution is found here: $f_{A,K\bar{K}\pi} = 0.56 \pm 0.10$.

Since the three determinations are inconsistent, a conservative value of $f_A = 0.75 \pm 0.25$ is assumed. It encompasses the range allowed by the previous results and still represents some progress over earlier analyses (ALEPH Coll., 1997b, 1998c), where a value of 0.5 ± 0.5 was used. For the decays into $K\bar{K}\pi\pi$ no information is available in this respect, and a fraction of 0.5 ± 0.5 is used.

The total nonstrange vector and axial-vector contributions obtained in (ALEPH Coll., 2005) are

$$\mathcal{B}_V = (31.82 \pm 0.18 \pm 0.12)\% , \quad (23)$$

$$R_{\tau,V} = 1.787 \pm 0.011 \pm 0.007 , \quad (24)$$

$$\mathcal{B}_A = (30.19 \pm 0.18 \pm 0.12)\% , \quad (25)$$

$$R_{\tau,A} = 1.695 \pm 0.011 \pm 0.007 , \quad (26)$$

where the second errors reflect the uncertainties in the V/A separation in the channels with $K\bar{K}$ pairs. Taking care of the (anti)correlations between the respective uncertainties, one obtains the difference between the vector and axial-vector components, which is physically related to the amount of nonperturbative contributions in the nonstrange hadronic τ decay width (see Section VII)

$$\mathcal{B}_{V-A} = (1.63 \pm 0.34 \pm 0.24)\% , \quad (27)$$

$$R_{\tau,V-A} = 0.092 \pm 0.018 \pm 0.014 , \quad (28)$$

where the second error has the same meaning as in Eqs. (23) and (25). The ratio

$$\frac{R_{\tau,V-A}}{R_{\tau,V+A}} = 0.026 \pm 0.007 \quad (29)$$

is a measure of the relative importance of nonperturbative contributions. Its smallness, in spite of our subtraction of observables with very different spectral contributions from hadronic resonances, represents a proof of the remarkable property that is referred to as quark-hadron duality (Shifman *et al.*, 1979). It is the basis of the QCD analyses of hadronic τ decays presented in this review.

The inclusive vector and axial-vector branching fractions provide the normalization of the corresponding spectral functions, which will be discussed below and which are the ingredients for the vacuum polarization calculations and the QCD analysis of hadronic τ decays.

IV. TAU HADRONIC SPECTRAL FUNCTIONS

The τ is the only lepton of the three-generation SM that is heavy enough to decay into hadrons. It is therefore an ideal laboratory for studying the charged weak hadronic currents and QCD. In analogy to the purely leptonic τ decays, the invariant amplitude for the hadronic decays can be written in form of a factorized current-current interaction

$$\mathcal{M}(\tau^- \rightarrow \text{hadrons}^- \nu_\tau) = \frac{G_F}{\sqrt{2}} |V_{\text{CKM}}| \ell_\mu h^\mu , \quad (30)$$

with the corresponding nonstrange or strange CKM matrix element $|V_{\text{CKM}}|$, and where ℓ_μ describes the leptonic $V - A$ current

$$\ell_\mu = \bar{\nu}_\tau \gamma_\mu (1 - \gamma_5) \tau \quad (31)$$

of the weak interaction. The hadronic transition current h_μ is the piece of interest here. It probes the matrix element of the left-handed charged current between the vacuum and the hadronic final state. Restricting to a $V - A$ structure, one can write

$$h_\mu = \langle \text{hadrons} | V_\mu(0) - A_\mu(0) | 0 \rangle. \quad (32)$$

The differential τ hadronic width can be expressed as follows

$$d\Gamma(\tau^- \rightarrow \text{hadrons}^- \nu_\tau) = \frac{G_F^2}{4M_\tau} |V_{\text{CKM}}|^2 L_{\mu\nu} H^{\mu\nu} d\text{PS}, \quad (33)$$

with the leptonic (hadronic) tensor $L_{\mu\nu}$ ($H_{\mu\nu}$) and the Lorentz invariant phase space element $d\text{PS}$. Seen from the hadronic rest system, the tensor product simplifies to a sum over so-called structure functions and kinematic factors (Kühn and Mirkes, 1992).

For the simplest hadronic decay modes $\tau^- \rightarrow h^- \nu_\tau$ ($h = \pi, K$), the structure functions reduce to δ -distributions, whereas resonances appear in τ decays into multiple hadrons. The hadronic structure is described by spectral functions. The quantum number corresponding to the (conserved) vector and axial-vector currents is the isotopic G -parity. It is a generalized multiplicative symmetry of multi-pion systems under the successive operations C and R , where C conjugates the charge and R rotates the system around the second axis in the $I = 1$ isospace. The measurement of the τ vector and axial-vector current spectral functions requires the selection and identification of τ decay modes with a defined G -parity $G = +1$ and $G = -1$, and hence hadronic channels with an even and odd number of neutral *or* charged pions, respectively. Since hadronic final states of different G -parity differ also in their J^P quantum numbers, there is no interference between these two states. Hence the total hadronic width separates into $\Gamma_{\text{tot}} = \Gamma_V + \Gamma_A$.

A. Definitions

The spectral function v_1 (a_1, a_0), where the subscript refers to the spin J of the hadronic system, is defined for a nonstrange ($|\Delta S| = 0$) or strange ($|\Delta S| = 1$) vector (axial-vector) hadronic τ decay channel $V^- \nu_\tau$ ($A^- \nu_\tau$). The spectral function is obtained by dividing the normalized invariant mass-squared distribution $(1/N_{V/A})(dN_{V/A}/ds)$ for a given hadronic mass \sqrt{s} by the appropriate kinematic factor

$$v_1(s)/a_1(s) = \frac{m_\tau^2}{6|V_{\text{CKM}}|^2 S_{\text{EW}}} \frac{\mathcal{B}(\tau^- \rightarrow V^-/A^- \nu_\tau)}{\mathcal{B}(\tau^- \rightarrow e^- \bar{\nu}_e \nu_\tau)} \times \frac{dN_{V/A}}{N_{V/A} ds} \left[\left(1 - \frac{s}{m_\tau^2}\right)^2 \left(1 + \frac{2s}{m_\tau^2}\right) \right]^{-1}, \quad (34)$$

$$a_0(s) = \frac{m_\tau^2}{6|V_{\text{CKM}}|^2 S_{\text{EW}}} \frac{\mathcal{B}(\tau^- \rightarrow \pi^-(K^-) \nu_\tau)}{\mathcal{B}(\tau^- \rightarrow e^- \bar{\nu}_e \nu_\tau)} \frac{dN_A}{N_A ds} \left(1 - \frac{s}{m_\tau^2}\right)^{-2}, \quad (35)$$

where S_{EW} accounts for short distance electroweak radiative corrections (Marciano and Sirlin, 1988) (see Section V.A for the relevant values of S_{EW}). Because of CVC there is no $J = 0$ contribution to the nonstrange vector spectral function, while the main contributions to a_0 are from the pion or kaon poles, with $dN_A/N_A ds = \delta(s - m_{\pi,K}^2)$. They are connected through partial conservation of the axial-vector current (PCAC) to the corresponding decay constants, $f_{\pi,K}$. The spectral functions are normalized by the ratio of the vector/axial-vector branching fraction $\mathcal{B}(\tau^- \rightarrow V^-/A^- \nu_\tau)$ to the branching fraction of the massless leptonic, *i.e.*, electron, channel (discussed in Section III.B).

The values for the CKM matrix elements V_{ud} and V_{us} have been recently much debated, because the determinations from nuclear β decays and semileptonic kaon decays did not satisfy the unitarity relation in the first row of the CKM matrix, that is $|V_{ud}|^2 + |V_{us}|^2 + |V_{ub}|^2 = 1$ (for this comparison, the V_{ub} element has a negligible contribution). The situation has improved with the availability of new results from $K_{\ell 3}$ and $K_{\mu 2}$ decays with revisited corrections from chiral perturbation theory on one hand, and more precise radiative corrections for the nuclear β decays (Marciano, 2005) on the other hand. The current results (Isidori, 2005),

which are still preliminary²,

$$|V_{ud}| = 0.9739 \pm 0.0003 \quad \text{nuclear } \beta \text{ decays ,} \quad (36)$$

$$|V_{us}| = 0.2248 \pm 0.0016 \quad K_{\ell 3} + K_{\mu 2} , \quad (37)$$

are consistent with CKM unitarity and provide a new level of precision in this sector. The $|V_{ud}|$ value gives $|V_{us}| = 0.2269 \pm 0.0013$ if CKM unitarity is used.

Using unitarity and analyticity, the spectral functions are connected to the imaginary part of the two-point correlation (or hadronic vacuum polarization) functions

$$\begin{aligned} \Pi_{ij,U}^{\mu\nu}(q) &\equiv i \int d^4x e^{iqx} \langle 0 | T(U_{ij}^\mu(x) U_{ij}^\nu(0)^\dagger) | 0 \rangle \\ &= (-g^{\mu\nu} q^2 + q^\mu q^\nu) \Pi_{ij,U}^{(1)}(q^2) + q^\mu q^\nu \Pi_{ij,U}^{(0)}(q^2) \end{aligned} \quad (38)$$

of vector ($U_{ij}^\mu = V_{ij}^\mu = \bar{q}_j \gamma^\mu q_i$) or axial-vector ($U_{ij}^\mu = A_{ij}^\mu = \bar{q}_j \gamma^\mu \gamma_5 q_i$) color-singlet quark currents in corresponding quantum states and for time-like momenta-squared $q^2 > 0$. Lorentz decomposition is used to separate the correlation function into its $J = 1$ and $J = 0$ parts. The polarization function $\Pi_{ij,U}^{\mu\nu}(s)$ have a branch cut along the real axis in the complex $s = q^2$ plane. Their imaginary parts give the spectral functions defined in (34), for nonstrange (strange) quark currents

$$\text{Im} \Pi_{\bar{u}d(s),V/A}^{(1)}(s) = \frac{1}{2\pi} v_1/a_1(s) , \quad \text{Im} \Pi_{\bar{u}d(s),A}^{(0)}(s) = \frac{1}{2\pi} a_0(s) , \quad (39)$$

which provide the basis for comparing short-distance theory with hadronic data.

The analytic vacuum polarization function $\Pi_{ij,U}^{(J)}(q^2)$ obeys the dispersion relation

$$\Pi_{ij,U}^{(J)}(q^2) = \frac{1}{\pi} \int_0^\infty ds \frac{\text{Im} \Pi_{ij,U}^{(J)}(s)}{s - q^2} + \text{subtractions} , \quad (40)$$

where the unknown but in general irrelevant subtraction constants can be removed by taking the derivative of $\Pi_{ij,U}(q^2)$. The dispersion relation allows one to connect the experimentally accessible spectral functions to the correlation functions $\Pi_{ij,U}^{(J)}(q^2)$, which can be derived from theory (QCD).

B. The physical mass spectra

The measurement of the τ spectral functions defined in Eq. (34) requires the determination of the invariant mass-squared distributions, obtained from the experimental distributions after unfolding from the effects of measurement distortion. The unfolding procedure used by the ALEPH collaboration (ALEPH Coll., 1997b, 1998c) follows a method based on the regularized inversion of the simulated detector response matrix using the Singular Value Decomposition (SVD) technique (Höcker and Kartvelishvili, 1996). The regularization function applied³ minimizes the average curvature of the distribution. The optimal choice of the regularization strength is found by means of the Monte Carlo simulation where the true distribution is known and chosen to be close to the expected physical distribution. The OPAL collaboration (OPAL Coll., 1999b) employs a similar regularized unfolding technique (Blobel, 1984), which is however based on cubic splines instead of the binned histograms used by ALEPH. Due to the superior mass resolution, the CLEO collaboration considers it to be sufficient to only apply a bin-to-bin migration correction (CLEO Coll., 2000d).

To measure exclusive spectral functions, individual unfolding procedures with specific detector response matrices and regularization parameters are applied for each τ decay channel considered. An iterative procedure is followed to correct the Monte Carlo spectral functions used to subtract the cross feed among the modes.

² We thank V. Cirigliano and G. Isidori for their advice on the current best values for $|V_{ud}|$ and $|V_{us}|$.

³ Regularization is necessary since in certain cases the unfolding produces results with unphysical behavior: statistically insignificant components in the detector response matrix can lead to large oscillations in the unfolded distribution. The regularization is achieved by applying a smooth damping function to the unfolded distribution.

Before unfolding the mass distributions, the τ and non- τ backgrounds are subtracted. In the case of τ feed-through the Monte Carlo distributions normalized to the measured branching fractions are used. When the spectral functions are measured for the nonstrange exclusive final states, the contributions from strange modes classified in the same topology are subtracted using their Monte Carlo spectral functions normalized by the measured branching fractions.

C. Systematic uncertainties

The systematic uncertainties affecting the decay classification of the exclusive modes are contained in the systematic errors on the branching fractions. Therefore, only the systematic effects that distort the shape of the unfolded mass-squared distributions, and not its normalization, need to be examined.

Comparisons of data and simulated Monte Carlo distributions are made. Biases that occur in these comparisons are corrected and the uncertainties on these corrections are taken as input for the evaluation of the systematic errors. For each possible effect, the whole analysis chain, including the unfolding procedure, is repeated. This generates new mass distributions under the systematic change, which are compared bin-by-bin to the nominal ones, hence providing covariance matrices of the spectral function for the studied effect. The overall systematic covariance matrices are obtained as the sum of the matrices for each effect.

The systematic studies include the effects from the photon and π^0 energy calibration and resolution, the photon detection efficiency (especially in the energy threshold region), the shapes of the distributions of mainly the electromagnetic shower variables used by the experiments to correctly identify reconstructed photons from fake ones, the estimate of the number of fake photons, the proximity in the calorimeter of other photon showers (required mainly for the LEP experiments, where the emitted particles are confined in a narrow cone around the decay axis) and of energy deposition by charged particles, and the separation between radiative and π^0 decay photons for residual single photons. The photon and π^0 reconstruction represents the main part of the uncertainty for the determination of spectral functions. Similarly, the effects of momentum calibration and resolution uncertainties in the reconstruction of charged tracks are checked, accompanied by tests of the reconstruction efficiency of highly collimated multi-prong events (LEP), and the simulation of secondary nuclear interactions. Moreover, systematic errors introduced by the unfolding procedure are tested by comparing known, true distributions to their corresponding unfolded ones.

D. Inclusive nonstrange spectral functions

1. Vector and axial-vector spectral functions

The inclusive τ vector and axial-vector spectral functions are shown in the upper and lower plots of Fig. 7, respectively. The left hand plots give the ALEPH result (ALEPH Coll., 1997b, 1998c, 2005) together with its most important exclusive contributions, and the right hand plots compare ALEPH with OPAL (OPAL Coll., 1999b). The agreement between the experiments is satisfying with the exception of the $\pi^-\pi^0$ (vector) mode, where some discrepancies occur. We note that the branching fraction used for this mode to obtain the inclusive spectral function is not the same in both experiments. The branching fraction used by ALEPH (ALEPH Coll., 2005) exceeds the one used by OPAL (OPAL Coll., 1999b) by 0.9% (relative).

The curves in the left hand plots of Fig. 7 represent the naive parton model prediction (dotted) and the improved (massless) perturbative QCD prediction (solid), assuming the relevant physics to be governed by short distances (Section VII). The difference between the two curves is due to higher order terms in the strong coupling $(\alpha_s(s)/\pi)^n$ with $n = 1, 2, 3$. At high energies the spectral functions are assumed to be dominated by continuum production, which locally agrees with perturbative QCD. This asymptotic region is not yet reached at $s = m_\tau^2$ for the vector and axial-vector spectral functions.

To build the vector spectral function ALEPH has measured the two- and four-pion final states exclusively, while only parts of the six-pion state. The total six-pion branching fraction has been determined using isospin symmetry (ALEPH Coll., 1997b). However, one has to account for the fact that the six-pion channel is contaminated by isospin-violating $\tau^- \rightarrow \eta(3\pi)^-\nu_\tau$ decays, as reported by CLEO (CLEO Coll., 1997a; Weinstein, 2001). A small fraction of the $\omega\pi^-\nu_\tau$ decay channel that is not reconstructed in the four-pion final state is added using the simulation. Similarly, one corrects for the $\eta\pi^-\pi^0\nu_\tau$ decay mode where the η decays into pions. For the $\eta \rightarrow 2\gamma$ mode, the τ decay is classified in the $h^-3\pi^0\nu_\tau$ final state, since the two-photon mass is inconsistent with the π^0 mass and consequently each photon is reconstructed as a π^0 . The $K^-K^0\nu_\tau$

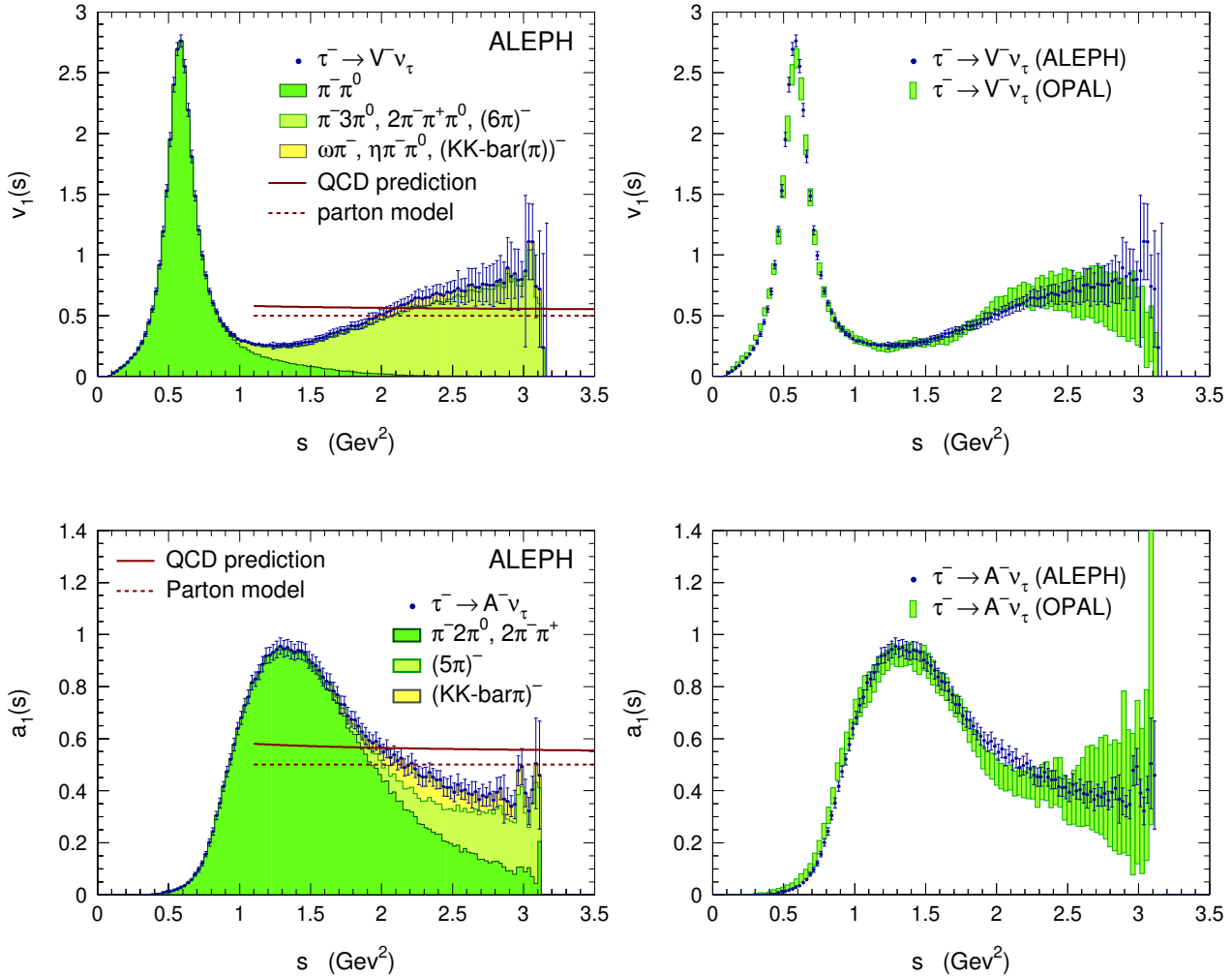


FIG. 7 Left hand plots: the inclusive vector (upper) and axial-vector (lower) spectral functions as measured in (ALEPH Coll., 2005). The shaded areas indicate the contributing exclusive τ decay channels. The curves show the predictions from the naive parton model (dotted) and from massless perturbative QCD using $\alpha_s(M_Z^2) = 0.120$ (solid). Right hand plots: comparison of the inclusive vector (upper) and axial-vector (lower) spectral functions obtained by ALEPH and OPAL (OPAL Coll., 1999b).

mass distribution is taken entirely from the simulation (recall that this mode is pure vector). The spectral functions for the final states $K\bar{K}\pi$ and $K\bar{K}\pi\pi$ (see Section III.E for the discussion on the G -parity of these modes) are obtained from the Monte Carlo simulation, where large systematic errors are applied to cover this approximation (ALEPH Coll., 1997b).

In analogy to the vector spectral function, the inclusive axial-vector spectral function is obtained by summing up the exclusive axial-vector spectral functions with the addition of small unmeasured modes taken from the Monte Carlo simulation. The small fraction of the $\omega\pi^-\pi^0\nu_\tau$ decay channel that is not accounted for in the $2\pi^-\pi^+2\pi^0\nu_\tau$ final state is added from the simulation. Also considered are the axial-vector $\eta(3\pi)^-\nu_\tau$ final states (CLEO Coll., 1997a; Weinstein, 2001). CLEO observed that the dominant part of this mode issues from the $\tau^-\rightarrow f_1(1285)\pi^-\nu_\tau$ intermediate state, with $\mathcal{B}(\tau^-\rightarrow f_1\pi^-\nu_\tau) = (0.068 \pm 0.030)\%$, measured in the $f_1\rightarrow\eta\pi^+\pi^-$ and $f_1\rightarrow\eta 2\pi^0$ decay modes (CLEO Coll., 1997a; Weinstein, 2001). Since the f_1 meson is isoscalar, the branching fractions relate as $\mathcal{B}(\tau^-\rightarrow\eta\pi^-\pi^+\pi^-\nu_\tau) = 2 \times \mathcal{B}(\tau^-\rightarrow\eta\pi^-\pi^0\nu_\tau)$. The distributions are taken from the ordinary six-pion phase space simulation accompanied by large systematic errors. The $K\bar{K}\pi$ final states contribute mostly to the inclusive axial-vector spectral function, with errors that are fully anticorrelated with the inclusive vector spectral function. The invariant mass distributions for these channels

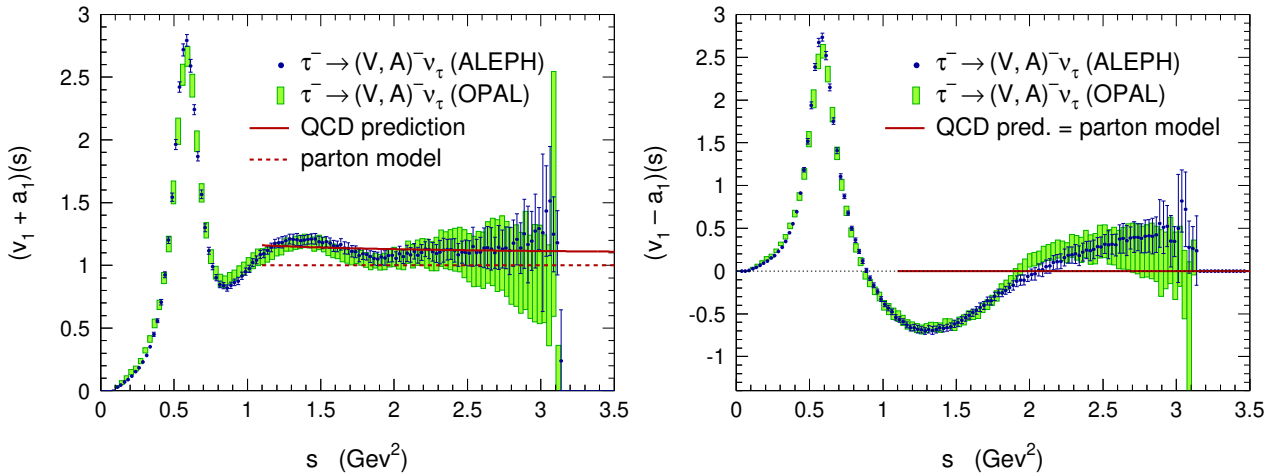


FIG. 8 Inclusive vector plus axial-vector (left) and vector minus axial-vector spectral function (right) as measured in (ALEPH Coll., 2005) (dots with errors bars) and (OPAL Coll., 1999b) (shaded one standard deviation errors). The lines show the predictions from the naive parton model (dotted) and from massless perturbative QCD using $\alpha_s(M_Z^2) = 0.120$ (solid). They cancel to all orders in the difference.

are taken from the simulation.

2. Inclusive $V \pm A$ spectral functions

For the total $v_1 + a_1$ hadronic spectral function it is not necessary to distinguish the current properties of the nonstrange decays. The one, two and three-pion final states dominate and their exclusive measurements are added with proper accounting for the (anti-)correlations. The remaining contributing topologies are treated inclusively, *i.e.*, without separation of the vector and axial-vector decay modes. This reduces the statistical uncertainty. The effect of the feed-through between τ final states on the invariant mass spectrum is described by the Monte Carlo simulation and resolution effects are corrected by the data unfolding. In this procedure the simulated mass distributions are iteratively corrected using the exclusive vector/axial-vector unfolded mass spectra. Also, one does not have to separate the vector/axial-vector currents of the $K\bar{K}\pi$ and $K\bar{K}\pi\pi$ modes. The $v_1 + a_1$ spectral functions for ALEPH and OPAL are plotted in the left hand plot of Fig. 8. The improvement in precision when comparing to a sum of the two parts in Fig. 7 is significant at higher mass-squared values.

One nicely identifies the oscillating behavior of the spectral function and, unlike the vector/axial-vector spectral functions, it does approximately reach the asymptotic limit predicted by perturbative QCD at $s \rightarrow m_\tau^2$. Also, the $V + A$ spectral function, including the pion pole, exhibits the features expected from global quark-hadron duality: despite the huge oscillations due to the prominent π , $\rho(770)$, a_1 and $\rho(1450)$ resonances, the spectral function qualitatively averages out to the quark contribution from perturbative QCD.

In the case of the $v_1 - a_1$ spectral function, uncertainties on the V/A separation are reinforced due to their anticorrelation. In addition, anticorrelations in the branching fractions between τ final states with adjacent numbers of pions increase the errors. The $v_1 - a_1$ spectral functions for ALEPH and OPAL are shown in the right hand plot of Fig. 8. The oscillating behavior of the respective v_1 and a_1 spectral functions is emphasized and the asymptotic regime is not reached at $s = m_\tau^2$. However again, the strong oscillation generated by the hadron resonances mostly averages out to zero, as predicted by perturbative QCD.

E. Strange spectral functions

The total $|\Delta S| = 1$ spectral function from the ALEPH analysis is shown in Fig. 9. The spectra for the $\bar{K}\pi$ and $\bar{K}\pi\pi$ modes are obtained from the corrected mass spectra, taking into account acceptance and bin migration corrections. The spectrum for the $\bar{K}\pi$ mode is taken from the $K^-\pi^0$ and $K_s^0\pi^-$ final states because

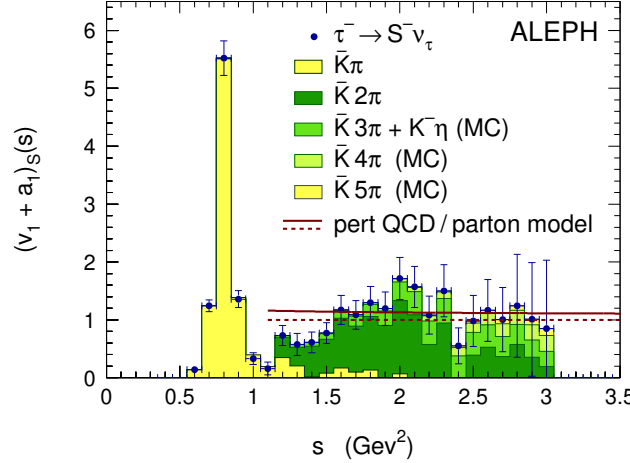


FIG. 9 Inclusive hadronic vector plus axial-vector spectral function from τ decays into $S = \pm 1$ final states with its different contributions as indicated (ALEPH Coll., 1999b). The kaon pole is not included in this plot. The shapes for the $K^-\eta$ and $\bar{K}n\pi$ ($n \geq 3$) modes are taken from the Monte Carlo simulation. The parton model prediction is given by the solid straight line.

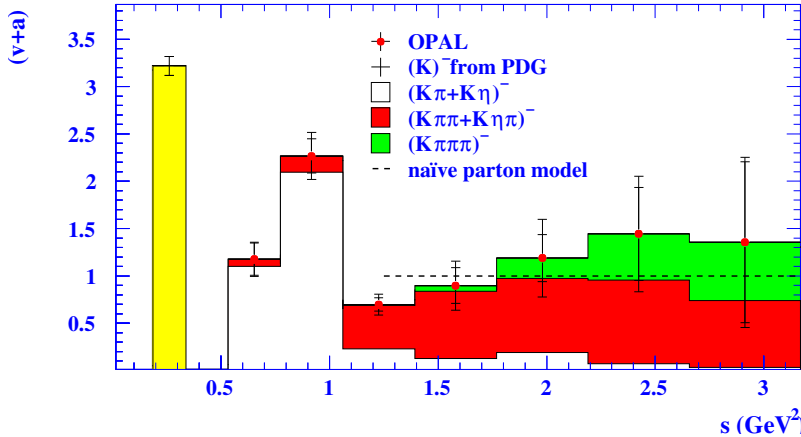


FIG. 10 Inclusive hadronic vector plus axial-vector spectral function from τ decays into strange final states with its different contributions indicated (OPAL Coll., 2004). The parton model prediction is given by the dashed straight line.

of their superior mass resolution as compared to the higher statistics $K_L^0\pi$ state where the K_L^0 detection suffers from poor energy resolution. For the other modes a phase-space generator is used to simulate the mass distributions. The contributions from the respective channels are normalized to the corresponding branching fractions.

The $K^*(892)^-$ resonance stands out clearly on the low mass side, while within a large uncertainty (dominated by background subtraction in the $(\bar{K}\pi\pi)^-$ modes) the higher energy part is consistent with the parton model (or perturbative QCD) expectation.

The spectral function from (OPAL Coll., 2004) is given in Fig. 10. Since OPAL normalizes each channel using the corresponding world average branching fraction, which is dominated by the ALEPH measurement, the added information is on the shape, limited by the relatively low statistics. As a consequence the OPAL and ALEPH spectral functions are correlated.

V. COMPARING TAU SPECTRAL FUNCTIONS WITH ELECTRON-POSITRON ANNIHILATION DATA VIA THE CONSERVED VECTOR CURRENT

The vacuum polarization functions (38) for the various types of quark currents ij carry the dynamical information for the theoretical evaluation of total cross sections and decay widths. In the limit of isospin invariance the vector current is conserved (CVC), so that the spectral function of a vector τ decay mode $X^-\nu_\tau$ in a given isospin state for the hadronic system is related to the e^+e^- annihilation cross section of the corresponding isovector final state X^0

$$\sigma_{e^+e^- \rightarrow X^0}^{I=1}(s) = \frac{4\pi\alpha^2}{s} v_{1, X^-}(s) , \quad (41)$$

where α is the electromagnetic fine structure constant.

A. Isospin breaking and radiative corrections

Since the breaking of isospin symmetry is expected at some level, in particular from electromagnetic effects, it is useful to carefully write down all the factors involved in the comparison of τ and e^+e^- spectral functions in order to make explicit the possible sources causing the breakdown of CVC. For the dominant $\pi\pi$ spectral functions, we have on the e^+e^- side

$$\sigma(e^+e^- \rightarrow \pi^+\pi^-) = \frac{4\pi\alpha^2}{s} v_0(s) , \quad (42)$$

where the spectral function $v_0(s)$ is related to the pion form factor $F_\pi^0(s)$ by

$$v_0(s) = \frac{\beta_0^3(s)}{12\pi} |F_\pi^0(s)|^2 , \quad (43)$$

and where $\beta_0^3(s)$ is the threshold kinematic factor. Similarly, on the τ side the relation between spectral function (34) and the charged pion form factor reads

$$v_-(s) = \frac{\beta^3(s)}{12\pi} |F_\pi^-(s)|^2 . \quad (44)$$

Isospin symmetry implies $v_-(s) = v_0(s)$. The threshold functions $\beta_{0,-}$ are defined by

$$\beta_{0,-} = \beta(s, m_{\pi^-}, m_{\pi^+, 0}) , \quad (45)$$

where

$$\beta(s, m_1, m_2) = \left[\left(1 - \frac{(m_1 + m_2)^2}{s} \right) \left(1 - \frac{(m_1 - m_2)^2}{s} \right) \right]^{1/2} . \quad (46)$$

The experiments measure τ decays inclusively with respect to radiative photons, *i.e.*, for $\tau^- \rightarrow \nu_\tau \pi^- \pi^0(\gamma)$. The measured spectral function is hence $v^*(s) = v_-(s) G(s)$, where $G(s)$ is a radiative correction.

Several levels of SU(2) breaking can be identified:

- *Electroweak radiative corrections to τ decays* are contained in the S_{EW} factor (Braaten and Li, 1990; Marciano and Sirlin, 1988), which is dominated by short-distance effects. It is expected to be weakly dependent on the specific hadronic final state, as verified for the $\tau^- \rightarrow (\pi^-, K^-)\nu_\tau$ decays (Decker and Finkemeier, 1993). Detailed calculations have been performed for the $\pi^-\pi^0$ channel (Cirigliano *et al.*, 2001, 2002), which also confirm the relative smallness of the long-distance contributions. The total correction is $S_{\text{EW}} = S_{\text{EW}}^{\text{had}} S_{\text{EM}}^{\text{had}} / S_{\text{EM}}^{\text{lep}}$, where $S_{\text{EW}}^{\text{had}}$ is the leading-log short-distance electroweak factor (which vanishes for leptons) and $S_{\text{EM}}^{\text{had,lep}}$ are the nonleading electromagnetic corrections. The latter corrections have been calculated at the quark level (Braaten and Li, 1990), at the hadron level for the $\pi^-\pi^0$ decay mode (Cirigliano *et al.*, 2001), and for leptons (Braaten and Li, 1990; Marciano and Sirlin, 1988). The total correction amounts to (Davier *et al.*, 2003a) $S_{\text{EW}}^{\text{incl}} = 1.0198 \pm 0.0006$ for the inclusive hadron decay rate and $S_{\text{EW}}^{\pi\pi^0} = (1.0232 \pm 0.0006) \cdot G_{\text{EM}}^{\pi\pi^0}(s)$ for the $\pi\pi^0$ decay mode, where $G_{\text{EM}}^{\pi\pi^0}(s)$ is an s -dependent long-distance radiative correction (Cirigliano *et al.*, 2001).

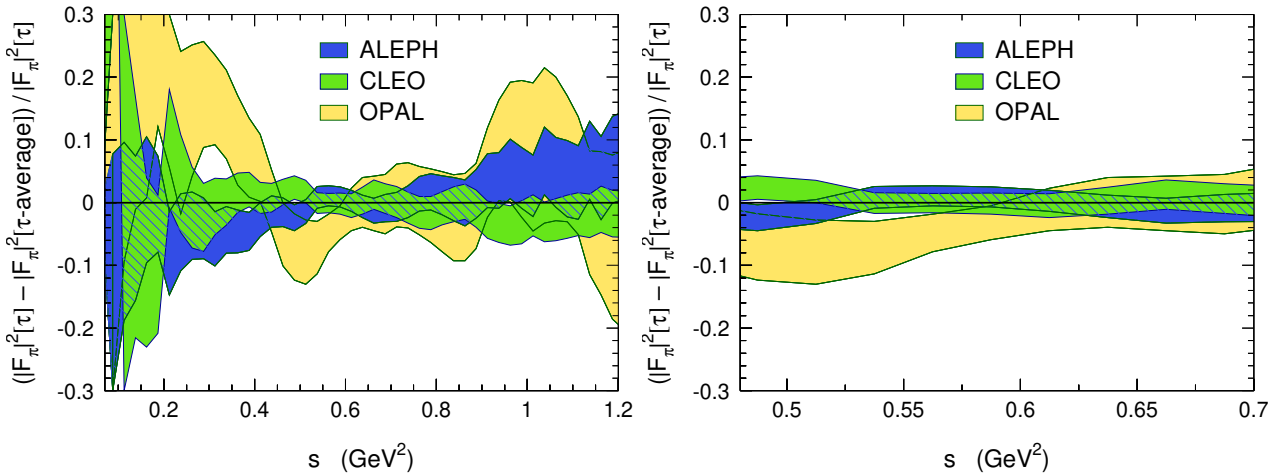


FIG. 11 The left figure shows a relative comparison of the $\pi^+\pi^-$ spectral functions extracted from τ data from the different experiments, expressed as a ratio to the average τ spectral function. The right figure emphasizes the ρ region. For CLEO only the statistical errors are shown.

- *The pion mass splitting* breaks isospin symmetry in the spectral functions (Alemany *et al.*, 1998; Czyż and Kühn, 2001) since $\beta_-(s) \neq \beta_0(s)$.
- Isospin symmetry is also broken in *the pion form factor* due to the π mass splitting (Alemany *et al.*, 1998; Cirigliano *et al.*, 2001).
- A similar effect is expected from *the rho mass splitting*. The theoretical expectation (Bijnens and Gospodzinsky, 1996) gives a limit (< 0.7 MeV), but this is only a rough estimate. Hence the question must be investigated experimentally, the best approach being the explicit comparison of τ and $e^+e^- 2\pi$ spectral functions, after correction for the other isospin-breaking effects. No correction for ρ mass splitting is applied initially.
- Explicit *electromagnetic decays* such as $\pi\gamma$, $\eta\gamma$, $\ell^+\ell^-$ and $\pi\pi\gamma$ introduce small differences between the widths of the charged and neutral ρ 's.
- Isospin violation in the strong amplitude through the *mass difference between u and d quarks* is expected to be negligible.
- When comparing τ with e^+e^- data, an obvious and locally large correction must be applied to the τ spectral function to introduce the effect of $\rho\omega$ *mixing*, only present in the neutral channel. This correction is computed using the parameters determined by the e^+e^- experiments in their form factor fits to the $\pi^+\pi^-$ lineshape modeling $\rho\omega$ interference (CMD-2 Coll., 2004).

B. Tau spectral functions and e^+e^- data

Data from τ decays into two- and four-pion final states $\tau^- \rightarrow \nu_\tau \pi^- \pi^0$, $\tau^- \rightarrow \nu_\tau \pi^- 3\pi^0$ and $\tau^- \rightarrow \nu_\tau 2\pi^- \pi^+ \pi^0$, are available from ALEPH (ALEPH Coll., 2005), CLEO (CLEO Coll., 2000c,d) and OPAL (OPAL Coll., 1999b). For the two-pion final states, they are compared in Fig. 11 in the region around the ρ resonance. For this comparison, each data set is normalized to the world average branching fraction and plotted with respect to their weighted average. The two most precise results from ALEPH and CLEO are in agreement. The statistics are comparable in the two cases, however due to a flat acceptance in ALEPH and a strongly increasing one (with the mass-squared) in CLEO, ALEPH data are more precise below the ρ peak, while CLEO has the better precision above. In the following we will use the $\tau^- \rightarrow \pi^- \pi^0 \nu_\tau$ spectral function averaged over the three experiments.

The exclusive low-energy e^+e^- cross sections have been mainly measured by experiments running at e^+e^- colliders in Novosibirsk and Orsay. The most precise $e^+e^- \rightarrow \pi^+\pi^-$ measurements come from CMD-2, which

are now available in their final form (CMD-2 Coll., 2004), after a significant revision where problems related to radiative corrections have been removed. The overall systematic error of the final data is quoted to be 0.6% and is dominated by the uncertainties in the radiative corrections (0.4%).

Recently, new data on the $\pi^+\pi^-$ spectral function in the mass region between 0.60 and 0.97 GeV were presented by the KLOE collaboration (KLOE Coll., 2005), using the—for the purpose of precision measurements—innovative technique of the radiative return (Binner *et al.*, 1999; Czyż *et al.*, 2002). The statistical precision of these data by far outperforms the Novosibirsk sample, but the systematic errors are about twice as large as those assigned by CMD-2.

C. Comparing τ with e^+e^- data

1. The 2π spectral function

The 2π spectral functions extracted from τ decays and e^+e^- annihilation data are compared in Fig. 12. The e^+e^- data are taken from (CMD-2 Coll., 2004; DM1 Coll., 1978; DM2 Coll., 1989; OLYA Coll., 1979; OLYA, CMD Colls., 1985; TOF Coll., 1981). All error bars shown contain statistical and systematic errors. Visually, the agreement appears to be satisfactory, however the large dynamical range involved does not permit an accurate test. To do so, the e^+e^- data are plotted as a point-by-point ratio to the τ spectral function in Fig. 13. In these latter plots we also show more recent e^+e^- -annihilation results from the SND collaboration (SND-2 Coll., 2005), and from the radiative return analysis performed by the KLOE collaboration (KLOE Coll., 2005). Several observations can be made:

- A significant discrepancy, mainly above the ρ peak is found between τ and the e^+e^- data from CMD-2 as well as older data from OLYA.
- Overall, the KLOE data seem to confirm the trend exhibited by the other (older) e^+e^- data.
- Some disagreement between KLOE and CMD-2 occurs on the low mass side (KLOE data are large), on the ρ peak (KLOE below CMD-2) as well as on the high mass side (KLOE data are low).
- A significant discrepancy between the (most recent) SND data and KLOE is observed in the energy domain above the $\rho(770)$ peak. The SND data largely dissolve the discrepancy observed with the τ data.

At this stage, the τ spectral function has not been corrected for a possible $\rho^-\rho^0$ mass and width splitting (ALEPH Coll., 2005; Davier, 2003; Ghozzi and Jegerlehner, 2004). In contrast to earlier experimental (ALEPH Coll., 1997b) and theoretical results (Bijnens and Gosdzinsky, 1996), a combined pion form factor fit to the new precise data on τ spectral functions and e^+e^- leads to $m_{\rho^-} - m_{\rho^0} = (2.4 \pm 0.8)$ MeV (Section V.D.2), while no significant width splitting is observed within the fit error of 1.0 MeV.

Considering the mass splitting in the isospin-breaking correction of the τ spectral function tends to locally improve though not restore the agreement between τ and CMD-2 data, leaving an overall normalization discrepancy. Increasing the $\Gamma_{\rho^-} - \Gamma_{\rho^0}$ width splitting by +3 MeV improves the agreement between τ and KLOE data in the peak region, while it cannot correct the discrepancies in the tails. Note that a correction of the mass splitting alone would *increase* the discrepancy between the τ and e^+e^- -based results for $a_\mu^{\text{had,LO}}$ (Section VI.F).

No convincing theoretical solution for a τ -vs- e^+e^- discrepancy has been suggested to date. A possible S -wave contribution to the τ decay amplitude via exchange of a charged Higgs boson (Morse, 2004) has been found too small to explain the observation (Gao, 2004). The possibility of contributions from tensor couplings introduced by a new force has been outlined in (Chizhov, 2003).

In light of the new SND data (SND-2 Coll., 2005), it seems appropriate to consider the possibility of a bias in the KLOE results, and one may also question the very small systematic uncertainties claimed by CMD-2. We also point out that the application of the τ long-distance correction $G_{\text{EM}}^{\pi\pi^0}(s)$ (Cirigliano *et al.*, 2001) worsens the agreement with the SND data in the energy domain above the $\rho(770)$ peak.

2. The 4π spectral functions

The spectral function measurements of the τ vector-current final states $\pi^-3\pi^0$ and $2\pi^-\pi^+\pi^0$ are compared to the cross sections of the corresponding e^+e^- annihilation into the isovector states $2\pi^-2\pi^+$ and $\pi^-\pi^+2\pi^0$.

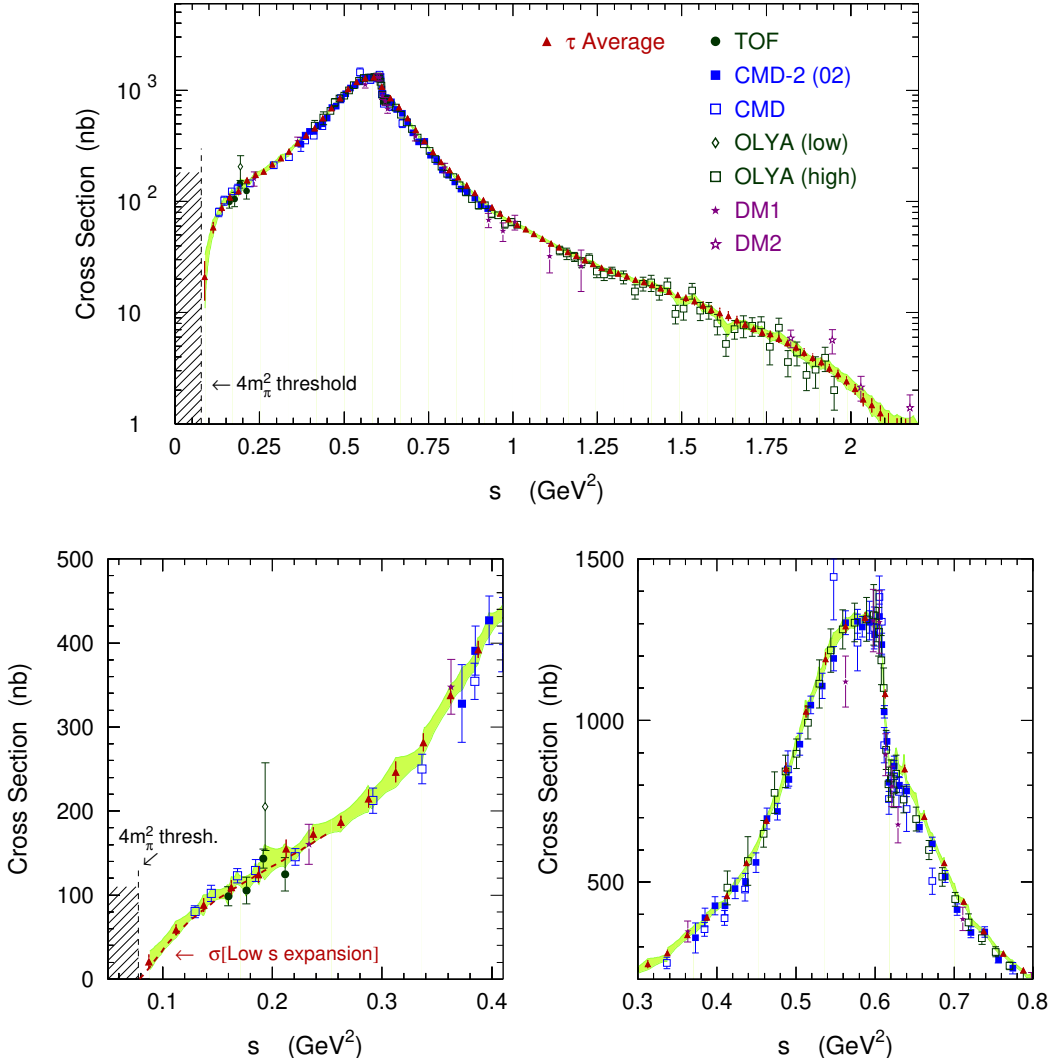


FIG. 12 Comparison of the $\pi^+\pi^-$ spectral functions from isospin-breaking corrected τ data (world average) expressed as e^+e^- cross sections, and e^+e^- annihilation. The band indicates the combined τ and e^+e^- result within 1σ errors. It is given for illustration purpose only. A compendium of references for the e^+e^- data is given in (Davier *et al.*, 2003a,b).

Using Eq. (35) and isospin invariance, the following relations hold

$$\sigma_{e^+e^- \rightarrow \pi^+\pi^-\pi^+\pi^-}^{I=1} = 2 \cdot \frac{4\pi\alpha^2}{s} v_{1,\pi^-3\pi^0\nu_\tau}, \quad (47)$$

$$\sigma_{e^+e^- \rightarrow \pi^+\pi^-\pi^0\pi^0}^{I=1} = \frac{4\pi\alpha^2}{s} [v_{1,2\pi^-\pi^+\pi^0\nu_\tau} - v_{1,\pi^-3\pi^0\nu_\tau}]. \quad (48)$$

The comparison of these cross sections is given in Fig. 14 for $2\pi^+2\pi^-$ (left hand plot) and $\pi^+\pi^-2\pi^0$ (right hand plot). The latter mode suffers from discrepancies between the results from the various e^+e^- experiments. The τ data, combining two measured spectral functions according to Eq. (48), and (coarsely) corrected for isospin breaking originating from the pion mass splitting (Czyz and Kühn, 2001), lie somewhat in between, with large uncertainties above 1.4 GeV because of the lack of statistics and a large feed-through background in the mode with three neutral pions. In spite of these difficulties the $\pi^-3\pi^0$ spectral function is in agreement with e^+e^- data as can be seen in Fig. 14. Due to the inconsistencies among the e^+e^- experiments a quantitative test of CVC in the $\pi^+\pi^-2\pi^0$ channel is premature.

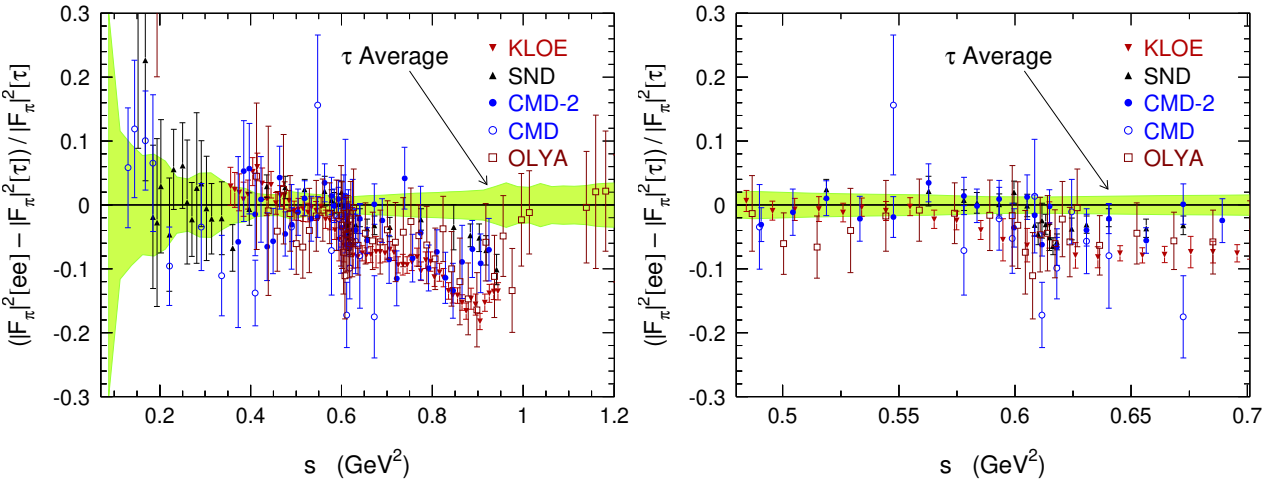


FIG. 13 Relative comparison of the isospin-breaking corrected τ data (world average) and $\pi^+\pi^-$ spectral functions from e^+e^- annihilation, expressed as a ratio to the τ spectral function. The shaded band gives the uncertainty on the τ spectral function. The right hand plot zooms into the $\rho(770)$ peak region where the data density is high. The ρ - ω mixing has been phenomenologically corrected using a fit to the CMD-2 data. The larger mixing observed in the SND data, expressed as a 40% increase in the value for the $\omega \rightarrow \pi^+\pi^-$ branching fraction (SND-2 Coll., 2005), is responsible for the residual effect after correction seen in the right hand plot.

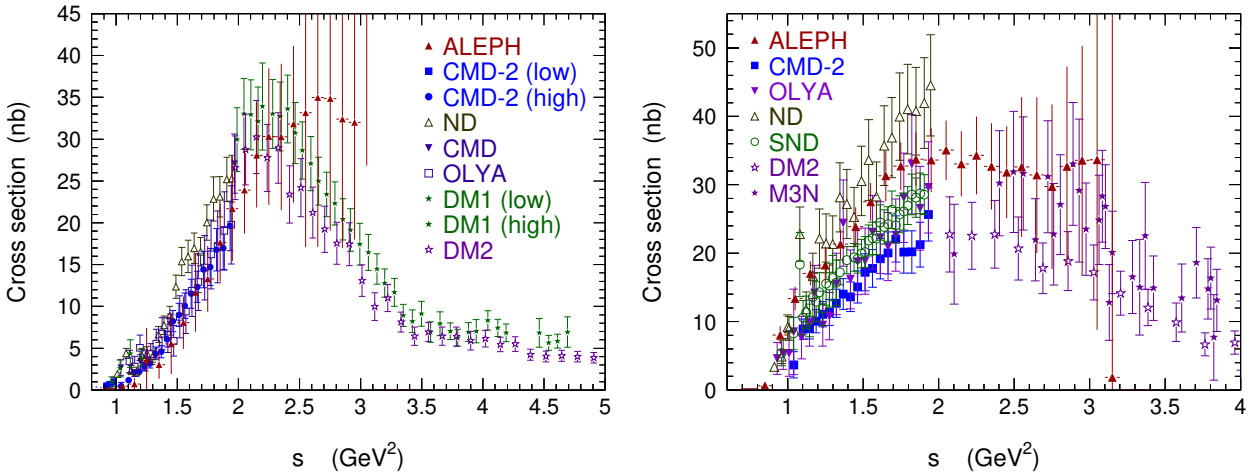


FIG. 14 Comparison of the $2\pi^+2\pi^-$ (left) and $\pi^+\pi^-2\pi^0$ (right) spectral functions from e^+e^- and isospin-breaking corrected τ data (ALEPH), expressed as e^+e^- cross sections. References for the e^+e^- data are given in (Davier *et al.*, 2003a,b).

3. Branching fractions in τ decays and CVC

It is instructive to compare the τ and e^+e^- spectral functions in a more quantitative way by calculating weighted integrals over the mass range of interest up to the τ mass. One convenient choice is provided by the τ branching fractions, which for the spin one part involve as a weight the kinematic factor $(1-s/m_\tau^2)^2(1+2s/m_\tau^2)$ coming from the $V-A$ charged current in τ decay. It is then possible to directly compare the measured τ branching fractions to their prediction through isospin invariance (CVC), with the e^+e^- isovector spectral functions as input.

Using the universality-improved branching fraction (13), one finds the results given for the dominant chan-

TABLE IV Branching fractions of τ vector decays into 2 and 4 pions in the final state (ALEPH Coll., 2005). Second column: τ decay measurements. Third column: results inferred from e^+e^- spectral functions using the isospin relations (41,44,47) and correcting for isospin breaking (Davier *et al.*, 2003a,b). The 2 pion prediction does not include the recent KLOE and SND data. Experimental errors, including uncertainties on the integration procedure, and theoretical errors (missing radiative corrections for e^+e^- , and isospin-breaking corrections and $|V_{ud}|$ for τ) are shown separately. Last column: differences between the direct measurements in τ decays and the CVC evaluations, where the various errors have been added in quadrature.

Mode	τ	Branching fractions (in %)		$\Delta(\tau - e^+e^-)$
		e^+e^- via CVC		
$\tau^- \rightarrow \nu_\tau \pi^- \pi^0$	25.47 ± 0.13	$24.52 \pm 0.26_{\text{exp}} \pm 0.11_{\text{rad}} \pm 0.12_{\text{SU(2)}}$ 0.31		$+0.95 \pm 0.33$
$\tau^- \rightarrow \nu_\tau \pi^- 3\pi^0$	0.98 ± 0.09	$1.09 \pm 0.06_{\text{exp}} \pm 0.02_{\text{rad}} \pm 0.05_{\text{SU(2)}}$ 0.08		-0.11 ± 0.12
$\tau^- \rightarrow \nu_\tau 2\pi^- \pi^+ \pi^0$	4.59 ± 0.09	$3.63 \pm 0.19_{\text{exp}} \pm 0.04_{\text{rad}} \pm 0.09_{\text{SU(2)}}$ 0.21		$+0.96 \pm 0.23$

nels in Table IV. The errors quoted for the CVC values are split into uncertainties from (*i*) the experimental input (the e^+e^- annihilation cross sections) and the numerical integration procedure, (*ii*) additional radiative corrections applied to some of the e^+e^- data (Davier *et al.*, 2003a), and (*iii*) the isospin-breaking corrections when relating τ and e^+e^- spectral functions.

As expected from the preceding discussion, a discrepancy is observed for the $\tau^- \rightarrow \pi^- \pi^0 \nu_\tau$ branching fraction, with a difference of $(0.95 \pm 0.13_\tau \pm 0.26_{\text{ee}} \pm 0.11_{\text{rad}} \pm 0.12_{\text{SU(2)}})\%$, where the uncertainties are from the τ branching fraction, e^+e^- cross section, e^+e^- missing radiative corrections and isospin-breaking corrections (also including the uncertainty on $|V_{ud}|$), respectively. Adding all errors in quadrature gives a 2.9σ effect. Including the new SND measurements (SND-2 Coll., 2005) into the $\pi^+ \pi^-$ data sample would decrease this discrepancy to approximately 2.5σ . The improvement would have been stronger, if we had discarded older data sets. In effect, using only SND data in the region where these are available [0.39–0.97 GeV], and all other data elsewhere, one finds for the predicted branching fraction: $\mathcal{B}_{\text{CVC}}(\tau^- \rightarrow \nu_\tau \pi^- \pi^0) = (25.12 \pm 0.36)\%$, which is in agreement with the τ result⁴. More information on this comparison is displayed in Fig. 15, where we also give the results for using only CMD-2 and only KLOE data, respectively, in the available energy regions (and the average of all other data elsewhere). The discrepancy between the e^+e^- -based prediction using the KLOE data and the τ result is at the 3.8σ level.

The situation in the 4π channels is different. While there is agreement for the $\pi^- 3\pi^0$ mode within a relative accuracy of 12%, the comparison is not satisfactory for $2\pi^- \pi^+ \pi^0$. In the latter case, the relative difference is very large, $(23 \pm 6)\%$, compared to a reasonable level of isospin symmetry breaking. As such, it rather points to experimental problems that require further investigation. These are emphasized by the scatter observed among the different e^+e^- results.

D. Fits to the $\pi\pi$ spectral function

Phenomenological fits to the pion form factor have been performed by the ALEPH and CLEO collaborations (ALEPH Coll., 1997b, 2005; CLEO Coll., 2000d). Appropriate parameterizations, *e.g.*, the one proposed in (Kühn and Santamaria, 1990), employ relativistic P -wave Breit-Wigner propagators, and coherent summation of the resonance amplitudes using the isobar model. The $\pi\pi$ spectral function is dominated by the broad ρ resonance, parameterized by both collaborations following Gounaris-Sakurai (Gounaris and Sakurai, 1968) (GS). The GS parameterization takes into account analyticity and unitarity properties. We will in the

⁴ However, we point out that the scarce SND data points in the tails of the $\rho(770)$ resonance, where the line shape is concave, may lead to an overestimate of the integral computed by the trapezoidal rule as it is done here.

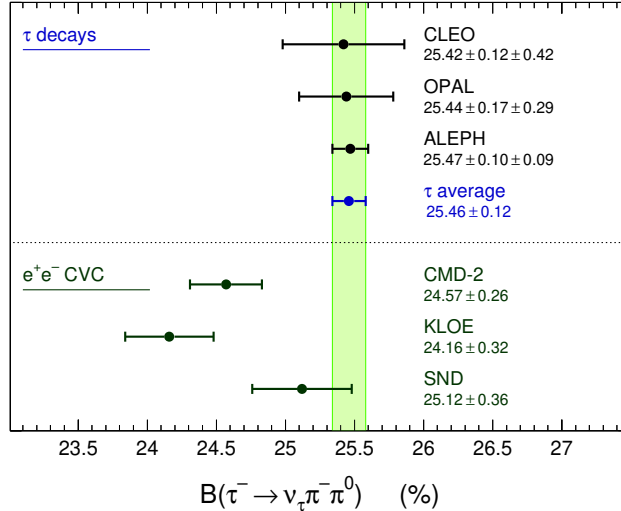


FIG. 15 The measured branching fractions for $\tau^- \rightarrow \pi^- \pi^0 \nu_\tau$ (ALEPH Coll., 2005; CLEO Coll., 1994a; OPAL Coll., 1998) compared to the predictions from the $e^+e^- \rightarrow \pi^+\pi^-$ spectral functions, applying the isospin-breaking correction factors discussed in Section V.A. For the e^+e^- results we have used only the data from the indicated experiments where they are available (0.61–0.96 GeV for CMD-2, 0.60–0.97 GeV for KLOE, and 0.39–0.97 GeV for SND), and all data combined in the remaining energy domains below m_τ . Since the compatibility between the e^+e^- data is marginal (*cf.* Fig. 13), we have refrained from taking their average.

following discuss the fits performed in (ALEPH Coll., 2005).

Assuming vector dominance, the pion form factor is given by interfering amplitudes from the known isovector meson resonances $\rho(770)$, $\rho(1450)$ and $\rho(1700)$ with relative strengths 1 , β , and γ . Although one could expect from the quark model that β and γ are real and respectively negative and positive, the phase of β , ϕ_β , is left free in the fits, and only the much smaller γ is assumed to be real for lack of precise experimental information at large masses. Taking into account ρ - ω mixing, one writes for the $\pi^+\pi^-$ form factor in e^+e^- annihilation

$$F_\pi^{I=1,0}(s) = \frac{\text{BW}_{\rho(770)}(s) \frac{1+\delta \text{BW}_{\omega(783)}(s)}{1+\delta} + \beta \text{BW}_{\rho(1450)}(s) + \gamma \text{BW}_{\rho(1700)}(s)}{1 + \beta + \gamma}, \quad (49)$$

with the Breit-Wigner propagators

$$\text{BW}_{\rho(m_\rho)}^{\text{GS}}(s) = \frac{m_\rho^2(1 + d \cdot \Gamma_\rho/m_\rho)}{m_\rho^2 - s + f(s) - i\sqrt{s}\Gamma_\rho(s)}, \quad (50)$$

where

$$f(s) = \Gamma_\rho \frac{m_\rho^2}{k^3(m_\rho^2)} \left[k^2(s) (h(s) - h(m_\rho^2)) + (m_\rho^2 - s) k^2(m_\rho^2) \frac{dh}{ds} \Big|_{s=m_\rho^2} \right]. \quad (51)$$

The P -wave energy-dependent width is given by

$$\Gamma_\rho(s) = \Gamma_\rho(m_\rho^2) \frac{m_\rho}{\sqrt{s}} \left(\frac{k(s)}{k(m_\rho^2)} \right)^3, \quad (52)$$

where $k(s) = \frac{1}{2}\sqrt{s}\beta_\pi^-(s)$ and $k(m_\rho^2)$ are pion momenta in the ρ rest frame. The function $h(s)$ is defined as

$$h(s) = \frac{2}{\pi} \frac{k(s)}{\sqrt{s}} \ln \frac{\sqrt{s} + 2k(s)}{2m_\pi}, \quad (53)$$

with $dh/ds|_{m_\rho^2} = h(m_\rho^2) [(8k^2(m_\rho^2))^{-1} - (2m_\rho^2)^{-1}] + (2\pi m_\rho^2)^{-1}$. Since interference with the isospin-violating electromagnetic $\omega \rightarrow \pi^+\pi^-$ decay occurs only in e^+e^- annihilation δ is fixed to zero when fitting τ data. The

TABLE V Combined fit to the pion form factor-squared to ALEPH, CLEO τ and all e^+e^- data, where vacuum polarization and known sources of isospin violation have been excluded from the latter data. The parameterization of the $\rho(770)$, $\rho(1450)$ and $\rho(1700)$ line shapes follows the Gounaris-Sakurai formula. Separate masses and widths are fit for the $\rho(770)$, while common values are kept for the higher vector mesons. All mass and width values are in units of MeV and the phases are in degrees. The value of the χ^2 estimator per degree of freedom (DF) is also quoted.

Simultaneous fit to τ and e^+e^- spectral functions ($\chi^2/DF = 383/326$)					
$m_{\rho^-}(770)$	775.5 ± 0.6	$\Gamma_{\rho^-}(770)$	148.2 ± 0.8	δ	$(2.03 \pm 0.10) \times 10^{-3}$
$m_{\rho^0}(770)$	773.1 ± 0.5	$\Gamma_{\rho^0}(770)$	148.0 ± 0.9	ϕ_δ	(13.0 ± 2.3)
$m_{\rho}(1450)$	1409 ± 12	$\Gamma_{\rho}(1450)$	501 ± 37	β	0.166 ± 0.005
$m_{\rho}(1700)$	1740 ± 20	$\Gamma_{\rho}(1700)$	$\equiv 235$	ϕ_β	177.8 ± 5.2
				γ	0.071 ± 0.006
				ϕ_γ	$\equiv 0$

normalization $BW_{\rho(m_\rho)}^{\text{GS}}(0) = 1$ fixes the parameter $d = f(0)/(\Gamma_\rho m_\rho)$, which is found to be (Gounaris and Sakurai, 1968)

$$d = \frac{3}{\pi} \frac{m_\pi^2}{k^2(m_\rho^2)} \ln \frac{m_\rho + 2k(m_\rho^2)}{2m_\pi} + \frac{m_\rho}{2\pi k(m_\rho^2)} - \frac{m_\pi^2 m_\rho}{\pi k^3(m_\rho^2)} . \quad (54)$$

1. Fit to τ data

The fit of the GS model to the isovector τ data establishes the need for the $\rho(1450)$ contribution to the weak pion form factor (ALEPH Coll., 1997b, 2005). Only weak evidence is found for a $\rho(1700)$ contribution lying close to the τ end-point. Most of the fit parameters exhibit large correlations, which have to be taken into account when interpreting the results. The ρ mass uncertainty is found to be dominated by systematic effects, the largest being the knowledge of the π^0 energy scale (calibration).

2. Combined fit to τ and e^+e^- data

The ALEPH collaboration has performed a combined fit using τ (ALEPH and CLEO) and e^+e^- data (not yet including KLOE and SND) in order to better constrain the lesser known parameters in the phenomenological form factor (ALEPH Coll., 1997b, 2005). For this study, the τ spectral function is duly corrected for the isospin-breaking effects identified in Section V.A. Also photon vacuum polarization contributions are removed in the e^+e^- spectral function since they are absent in the τ data. In this way, the mass and width of the dominant $\rho(770)$ resonance in the two isospin states can be determined. For the subleading amplitudes from the higher vector mesons, isospin symmetry is assumed so that common masses and widths can be used in the fit.

The result of the combined fit is given in Table V. The differences between the masses and widths of the charged and neutral $\rho(770)$'s are found to be (ALEPH Coll., 2005)

$$m_{\rho^-} - m_{\rho^0} = (2.4 \pm 0.8) \text{ MeV} , \quad (55)$$

$$\Gamma_{\rho^-} - \Gamma_{\rho^0} = (0.2 \pm 1.0) \text{ MeV} . \quad (56)$$

The mass splitting is somewhat larger than the theoretical prediction (< 0.7 MeV) (Bijnens and Gospodzinsky, 1996), but only at the 2σ level. The expected width splitting, from known isospin breaking, but not taking into account any ρ mass splitting, is (0.7 ± 0.3) MeV (Cirigliano *et al.*, 2001; Davier *et al.*, 2003a). However, if the mass difference is taken as an experimental fact, a larger width difference would be expected. From the chiral model of the ρ resonance (Cirigliano *et al.*, 2001; Gómez Dumm *et al.*, 2000; Guerrero and Pich, 1997), one expects

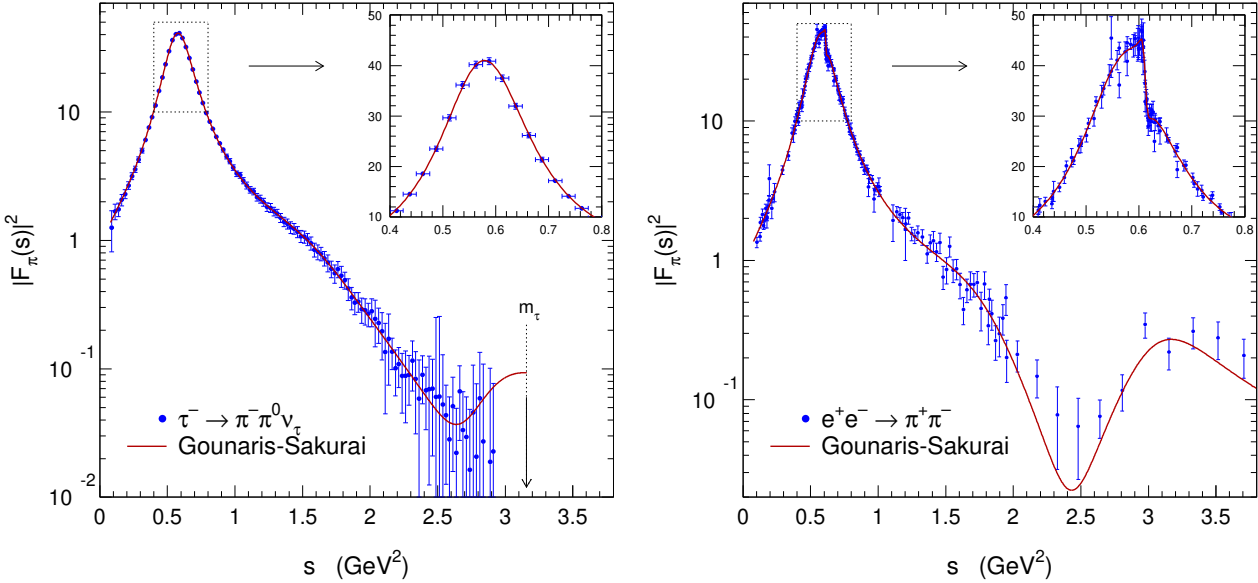


FIG. 16 Phenomenological fit to the ALEPH $\pi^-\pi^0$ spectral function (left) and to e^+e^- annihilation data (right) using the Gounaris-Sakurai parameterization. The fits are taken from (ALEPH Coll., 2005).

$$\Gamma_{\rho^0} = \Gamma_{\rho^-} \left(\frac{m_{\rho^0}}{m_{\rho^-}} \right)^3 \left(\frac{\beta_0}{\beta_-} \right)^3 + \Delta\Gamma_{\text{EM}} \quad (57)$$

where $\Delta\Gamma_{\text{EM}}$ is the width difference from electromagnetic decays (as discussed above). Using (55) leads to a total width difference of (2.1 ± 0.5) MeV, which is only marginally consistent with the observed value.

Since the τ results from ALEPH, CLEO and OPAL have been shown to be consistent, the question of the correction of the observed ρ mass splitting when relating τ to e^+e^- data is more relevant. However, a combined fit using τ and e^+e^- data, and requiring for consistency the constraint from Eq. (57), has a χ^2 probability of only 0.6% (ALEPH Coll., 2005). In fact, correcting for different masses extracted from the fit, and using the corresponding constrained widths, improves the agreement between the τ and e^+e^- line shapes, but at the expense of a significant discrepancy in normalization⁵. As seen in the previous applications, the situation should improve with the inclusion of the new SND data (SND-2 Coll., 2005). Also the observed ρ mass difference (55) is expected to decrease in this case.

VI. TAU DECAYS AND HADRONIC VACUUM POLARIZATION

Hadronic vacuum polarization in the photon propagator plays an important role in precision tests of the SM. This is the case for the evaluation of the electromagnetic coupling at the Z mass scale, $\alpha(M_Z^2)$, which receives a contribution $\Delta\alpha_{\text{had}}(M_Z^2)$ of the order of 2.8×10^{-2} . This correction must be known to a relative accuracy of better than 1% so that it does not limit the accuracy on the indirect determination of the Higgs boson mass from the measurement of $\sin^2\theta_W$. Another example is provided by the anomalous magnetic moment $a_\mu = (g_\mu - 2)/2$ of the muon, where the lowest-order hadronic vacuum polarization component $a_\mu^{\text{had,LO}}$ is the leading contributor to the uncertainty of the theoretical prediction.

Starting from (Bouchiat and Michel, 1961; Cabibbo and Gatto, 1960, 1961) there is a long history of calculating the contributions from hadronic vacuum polarization in these processes. As they cannot be

⁵ It should be noted that a correction for this apparent ρ mass splitting increases the present discrepancy for the muon anomalous magnetic moment between the estimates based on τ and e^+e^- spectral functions (Davier, 2003). See the discussion in Section VI.

obtained from first principles because of the low energy scale involved, the computation relies on analyticity and unitarity so that the relevant integrals can be expressed in terms of an experimentally determined spectral function, which is proportional to the cross section for e^+e^- annihilation into hadrons. The accuracy of the calculations has therefore followed the progress in the quality of the corresponding data (Eidelman and Jegerlehner, 1995). Because the data were not always suitable, it was deemed necessary to resort to other sources of information. One such possibility was the use of the vector spectral functions derived from the study of hadronic τ decays for the energy range less than m_τ (Alemany *et al.*, 1998). Also, it was demonstrated that essentially perturbative QCD could be applied to energy scales as low as 1–2 GeV (ALEPH Coll., 1998c; OPAL Coll., 1999b), thus offering a way to replace poor e^+e^- data in some energy regions by a reliable and precise theoretical prescription (Davier and Höcker, 1998a,b; Erler, 1999; Groote *et al.*, 1998; Kühn and Steinhauser, 1998; Martin and Zeppenfeld, 1995). Finally, without any further theoretical assumption, it was proposed to use QCD sum rules (Davier and Höcker, 1998b; Groote *et al.*, 1998) in order to improve the evaluation in energy regions dominated by resonances where one has to rely on experimental data. The complete theoretical prediction includes in addition quantum electrodynamics (QED), weak and higher order hadronic contributions.

Since in this review of hadronic τ decays we are mostly dealing with the low energy region⁶, common to both τ and e^+e^- data, and because of the current interest in the muon magnetic moment prompted by the excellence of the recent experimental results (see below), the emphasis will be on $a_\mu^{\text{had,LO}}$ rather than $\Delta\alpha_{\text{had}}(M_Z^2)$. We note that the presently achieved accuracy on $\Delta\alpha_{\text{had}}(M_Z^2)$ is meeting the goals for the LEP/SLC/FNAL global electroweak fit. However the situation will change in the long run when very precise determinations of $\sin^2\theta_W$, as could be available from the beam polarization asymmetry at the International Linear Collider, require a significant increase in the accuracy of $\Delta\alpha_{\text{had}}(M_Z^2)$ (Abe *et al.*, 2001).

A. Muon magnetic anomaly

One of the great successes of the Dirac equation (Dirac, 1928) was its prediction that the magnetic dipole moment, $\vec{\mu}$, of a spin $|\vec{s}| = 1/2$ particle such as the electron (or muon) is given by

$$\vec{\mu}_\ell = g_\ell \frac{e}{2m_\ell} \vec{s}, \quad \ell = e, \mu \dots \quad (58)$$

with gyromagnetic ratio $g_\ell = 2$, a value already implied by early atomic spectroscopy. Later it was realized that a relativistic quantum field theory such as QED can give rise via quantum fluctuations to a shift in g_ℓ

$$a_\ell \equiv \frac{g_\ell - 2}{2}, \quad (59)$$

called the magnetic anomaly. In a now classic QED calculation, Schwinger (Schwinger, 1948) found the leading (one loop) effect (Fig. 17, lower-left) $a_\ell = \alpha/(2\pi) \simeq 0.00116$, with $\alpha \equiv e^2/(4\pi) \simeq 1/137.036$, which agreed beautifully with experiment (Nagle *et al.*, 1947a,b), thereby providing strong confidence in the validity of perturbative QED. Today, the tradition of testing QED and its $SU(3)_C \times SU(2)_L \times U(1)_Y$ SM extension is continued (which includes strong and electroweak interactions) by measuring a_ℓ^{exp} for the electron and muon even more precisely and comparing with a_ℓ^{SM} expectations, calculated to much higher order in perturbation theory. Such comparisons test the validity of the SM and probe for new physics effects, which if present in quantum loop fluctuations should cause disagreement at some level. An experiment underway at Harvard (Gabrielse and Tan, 1994) aims to improve the best present measurement (Van Dyck *et al.*, 1987) of a_e by about a factor of 15. Combined with a much improved independent determination of α , it would significantly test the validity of perturbative QED. It should be noted, however, that a_e is in general not very sensitive to new physics at a high mass scale Λ because its effect on a_e is expected to be quadratic in $1/\Lambda$ (Czarnecki and Marciano, 2001)

$$\Delta a_e(\Lambda) \sim \mathcal{O}\left(\frac{m_e^2}{\Lambda^2}\right) \quad (60)$$

⁶ It is the property of the dispersion relation describing the hadronic contribution to $(g-2)_\mu$ that the $\pi\pi$ spectral function provides the major part of the total hadronic vacuum polarization contribution, so that the experimental effort focuses on this channel.

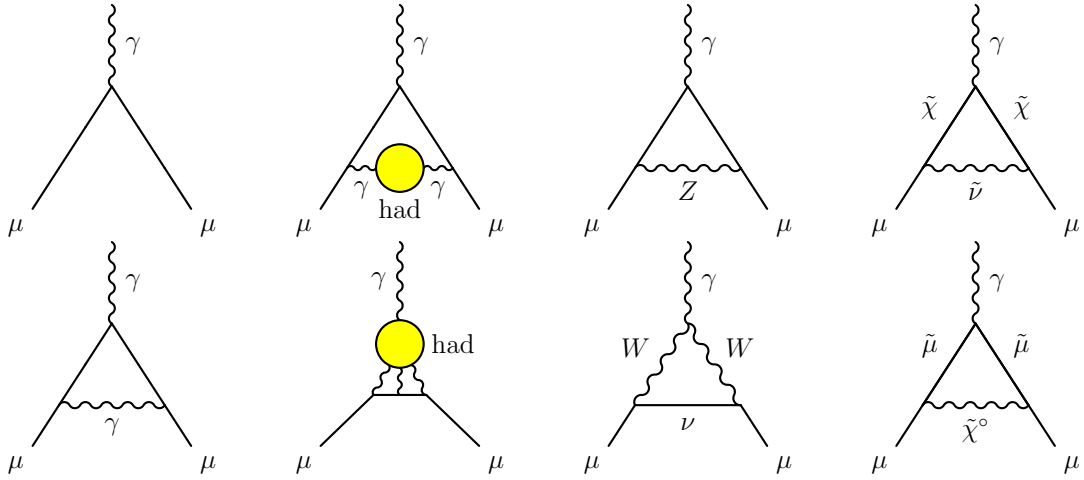


FIG. 17 Representative diagrams contributing to a_μ . First column: lowest-order diagram (upper) and first order QED correction (lower); second column: lowest-order hadronic contribution (upper) and hadronic light-by-light scattering (lower); third column: weak interaction diagrams; last column: possible contributions from lowest-order Supersymmetry.

and, hence, highly suppressed by the smallness of the electron mass. It would be much more sensitive if Δa_e were linear in $1/\Lambda$; but that is unlikely if chiral symmetry is present in the $m_e \rightarrow 0$ limit.

The muon magnetic anomaly has recently been measured with a relative precision of 5×10^{-7} by the E821 collaboration at Brookhaven National Laboratory (Muon ($g-2$) Coll., 2004). Combined with the older, less precise results from CERN (Bailey *et al.*, 1977), and averaging over charges, gives

$$a_\mu^{\text{exp}} = (11\,659\,208.0 \pm 5.8) \times 10^{-10}. \quad (61)$$

Although the accuracy is 200 times worse than a_e^{exp} , a_μ is about $m_\mu^2/m_e^2 \simeq 40,000$ times more sensitive to new physics and hence a better place (by about a factor of 200) to search for a deviation from the SM expectation. Of course, strong and electroweak contributions to a_μ are also enhanced by m_μ^2/m_e^2 relative to a_e ; so, they must be evaluated much more precisely in any meaningful comparison of a_μ^{SM} with Eq. (61). Fortunately, the recent experimental progress in a_μ^{exp} has stimulated much theoretical improvement of a_μ^{SM} , uncovering errors and inspiring new computational approaches along the way, among these the use of hadronic τ decays.

It is convenient to separate the SM prediction for the anomalous magnetic moment of the muon into its different contributions,

$$a_\mu^{\text{SM}} = a_\mu^{\text{QED}} + a_\mu^{\text{weak}} + a_\mu^{\text{had}}, \quad (62)$$

where $a_\mu^{\text{QED}} = (11\,658\,472.0 \pm 0.2) \times 10^{-10}$ is the pure electromagnetic contribution (see (Czarnecki and Marciano, 1999; Hughes and Kinoshita, 1999) and references therein),⁷ $a_\mu^{\text{weak}} = (15.4 \pm 0.1 \pm 0.2) \times 10^{-10}$, with the first error being the hadronic uncertainty and the second due to the Higgs mass range, accounts for corrections due to exchange of the weakly interacting bosons up to two loops (Czarnecki *et al.*, 2003) (see third column in Fig. 17). The term a_μ^{had} can be further decomposed into

$$a_\mu^{\text{had}} = a_\mu^{\text{had,LO}} + a_\mu^{\text{had,HO}} + a_\mu^{\text{had,LBL}}, \quad (63)$$

where $a_\mu^{\text{had,LO}}$ is the lowest-order contribution from hadronic vacuum polarization and $a_\mu^{\text{had,HO}}$ the corresponding higher-order part (Section VI.E). At the 3-loop level in α , the so-called hadronic light-by-light (LBL)

⁷ An improved calculation including all mass-dependent α^4 QED contributions has been published recently with a slightly different result (Kinoshita and Nio, 2004): $a_\mu^{\text{QED}} = 116\,584\,719.58(0.02)(1.15)(0.85) \times 10^{-11}$, where 0.02 and 1.15 are uncertainties in the α^4 and α^5 terms and 0.85 is from the uncertainty in α measured by atom interferometry.

scattering contributions, $a_\mu^{\text{had,LBL}}$, must be estimated in a model-dependent approach. Those estimates have been plagued by errors, which now seem to be sorted out (Section VI.E). Nevertheless, the remaining overall uncertainties from hadronic vacuum polarization and LBL scattering in a_μ^{had} represent the main theoretical error in a_μ^{SM} .

Owing to unitarity and to the analyticity of the vacuum-polarization function⁸, the lowest-order hadronic vacuum polarization contribution to a_μ can be computed via the dispersion integral (Gourdin and de Rafael, 1969)

$$a_\mu^{\text{had,LO}} = \frac{1}{3} \left(\frac{\alpha}{\pi} \right)^2 \int \frac{ds}{4m_\pi^2} \frac{K(s)}{s} R^{(0)}(s) , \quad (64)$$

where $K(s)$ is the QED kernel (Brodsky and Rafael, 1968),

$$K(s) = x^2 \left(1 - \frac{x^2}{2} \right) + (1+x)^2 \left(1 + \frac{1}{x^2} \right) \left[\ln(1+x) - x + \frac{x^2}{2} \right] + x^2 \ln x \frac{1+x}{1-x} , \quad (65)$$

with $x = (1 - \beta_\mu)/(1 + \beta_\mu)$ and $\beta_\mu = (1 - 4m_\mu^2/s)^{1/2}$. In Eq. (64), $R^{(0)}(s)$ denotes the ratio of the “bare” cross section for e^+e^- annihilation into hadrons to the pointlike muon-pair cross section at center-of-mass energy \sqrt{s} . The bare cross section is defined as the measured cross section corrected for initial-state radiation, electron-vertex loop contributions and vacuum-polarization effects in the photon propagator. As the only QED effect, photon radiation in the final state is to be included. The reason for using the bare (*i.e.*, lowest-order) cross section is that a full treatment of higher orders is anyhow needed at the level of a_μ , so that the use of the “dressed” cross section would entail the risk of double-counting some of the higher-order contributions.

The function $K(s) \sim 1/s$ in Eq. (64) gives a strong weight to the low-energy part of the integral. About 91% of the total contribution to $a_\mu^{\text{had,LO}}$ is accumulated at center-of-mass energies \sqrt{s} below 1.8 GeV and 73% of $a_\mu^{\text{had,LO}}$ is covered by the $\pi\pi$ final state, which is dominated by the $\rho(770)$ resonance.

⁸ Defining the photon vacuum polarization function as the spin-one component of the time-ordered product of two electromagnetic currents, $\Pi_\gamma(q^2)$, according to Eq. (38), and benefiting from the cancellation of all contributions from self energy and vertex correction graphs in perturbation theory (Ward identities), so that only vacuum polarization modifies the charge of an elementary particle, one can write for the running electron charge (charge screening) at energy scale s

$$\alpha(s) = \frac{\alpha(0)}{1 - \Delta\alpha(s)} ,$$

where $\alpha(0)$ is the fine structure constant in the long-wavelength Thomson limit and $\Delta\alpha(s) = \Delta\alpha_{\text{lep}}(s) + \Delta\alpha_{\text{had}}(s) = -4\pi\alpha\text{Re}[\Pi_\gamma(s) - \Pi_\gamma(0)]$. The leptonic part $\Delta\alpha_{\text{lep}}(s)$ is calculable within QED and known up to three loops (Steinhauser, 1998). However, quark loops are modified by long-distance hadronic physics that cannot be calculated within QCD. Instead, the optical theorem

$$12\pi\text{Im}\Pi_\gamma(s) = \frac{\sigma(e^+e^- \rightarrow \text{hadrons})}{\sigma(e^+e^- \rightarrow \mu^+\mu^-)} \equiv R(s) ,$$

and, owing to the analyticity of Π_γ , the dispersion relation

$$\Pi_\gamma(s) - \Pi_\gamma(0) = \frac{s}{\pi} \int_0^\infty ds' \frac{\text{Im}\Pi_\gamma(s')}{s'(s' - s) - i\varepsilon} ,$$

lead to

$$\Delta\alpha_{\text{had}}(s) = -\frac{\alpha(0)s}{3\pi} \text{Re} \int_0^\infty ds' \frac{R(s')}{s'(s' - s) - i\varepsilon} ,$$

Its r.h.s. can be obtained with the use of experimental data for $R(s)$. Similarly, one obtains Eq. (64) for the hadronic vacuum polarization contribution to a_μ .

B. Input data and their treatment

The information used for the evaluation of the integral (64) comes mainly from direct measurements of the cross sections in e^+e^- annihilation and via CVC from τ spectral functions. In addition to the data with the two- and four-pion final states shown in Section V.B, other final states and at different energies are also used (References for experimental data can be found in (Davier *et al.*, 2003a)). However, due to the higher hadron multiplicity at energies above ~ 2.5 GeV, the exclusive measurement of the many hadronic final states is not practicable. Consequently, the experiments at the high-energy colliders ADONE, SPEAR, DORIS, PETRA, PEP, VEPP-4, CESR and BEPC have measured the total inclusive cross section ratio R . In some cases measurements are incomplete, as for example $e^+e^- \rightarrow K\bar{K}\pi\pi$ or $e^+e^- \rightarrow 6\pi$, and one has to rely on isospin symmetry to estimate or bound the unmeasured cross sections (Davier *et al.*, 2003a). To obtain the corresponding e^+e^- annihilation cross sections using the τ data, the isospin rotations (41, 47) are applied, and all identified sources of isospin breaking are corrected.

In general, the integrals themselves are evaluated using the trapezoidal rule⁹, *i.e.*, combining adjacent measurement points by linear interpolation. Even if this method is straightforward and free from theoretical assumptions (other than CVC in the τ case), its numerical calculation requires special care. The finite and variable distance between adjacent measurements creates systematic uncertainties that have to be estimated. The combination of measurements from different experiments taking into account correlations—both within each data set and between different experiments—requires a well-defined statistical procedure to ensure the correct propagation of the measurement errors.

To exploit the maximum information from available data, weighted measurements of different experiments at a given energy should be combined instead of calculating the integrals for every experiment and finally averaging them. Different averaging methods are used in the literature varying from classical χ^2 minimization methods (Alemany *et al.*, 1998; Davier *et al.*, 2003a; Menke, 2001), to the so-called clustering method (Hagiwara *et al.*, 2004) in which a cluster of arbitrary size is predefined and precise data are used to rescale imprecise measurements within the (correlated) systematic errors of the imprecise data set.

C. Special cases

1. The threshold region

To overcome the lack of precise data at threshold energies and to benefit from the analyticity property of the pion form factor, a third order expansion in s is used:

$$F_\pi^0 = 1 + \frac{1}{6}\langle r_\pi^2 \rangle s + c_1 s^2 + c_2 s^3 + O(s^4) . \quad (66)$$

Exploiting precise results from space-like data (NA7 Coll., 1986), the pion charge radius-squared is constrained to

$$\langle r_\pi^2 \rangle = (0.439 \pm 0.008) \text{ fm}^2 , \quad (67)$$

and the two parameters $c_{1,2}$ are fit to the data in the range $[2m_\pi, 0.6 \text{ GeV}]$. Good agreement is observed in the low energy region where the expansion should be reliable (*cf.* Fig. 18). Since the fits incorporate unquestionable constraints from first principles, this parameterization is used for evaluating the integrals in the range up to 0.5 GeV (Davier *et al.*, 2003a).

⁹ The trapezoidal rule is the simplest prescription to interpolate adjacent measurements. It is superior to the other simple approach, the use of rectangular bins with variable bin size, determined by the energy distance of adjacent measurements, once strongly varying energy-dependent kernel functions occur. However, the trapezoidal rule can also give rise to biased integral evaluations. In effect, strongly concave functions, like the tails of narrow resonances with few available measurement points, systematically overestimate the integral when using the trapezoidal rule. In these cases, a phenomenological fit to the data points should be performed (Davier *et al.*, 2003a).

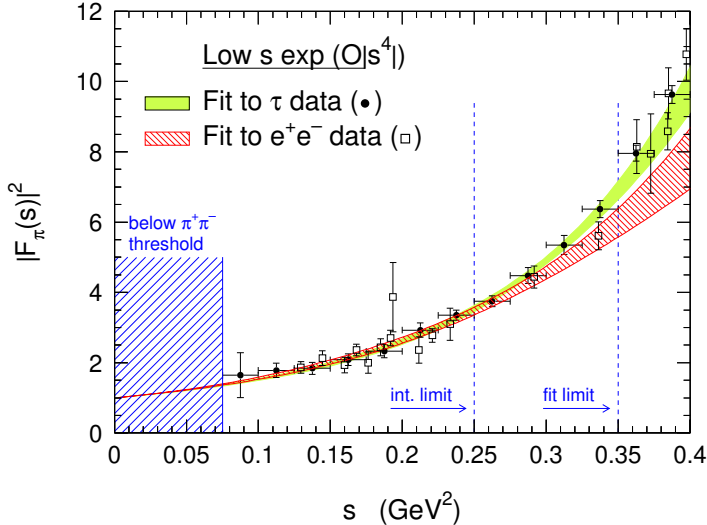


FIG. 18 Fit of the pion form factor from $4m_\pi^2$ to 0.35 GeV^2 using a third-order Taylor expansion with the constraints at $s = 0$ and the measured pion r.m.s. charge radius from space-like data (NA7 Coll., 1986). The result of the fit is integrated only up to 0.25 GeV^2 . The e^+e^- data do not yet include the recent SND measurement (SND-2 Coll., 2005).

2. QCD for the high energy contributions

Since problems still remain regarding the spectral functions from low-energy data, the prediction from essentially perturbative QCD is used above an energy of 1.8 and 5 GeV, respectively. The details of the calculation can be found in (Davier and Höcker, 1998a,b) and in the references therein.

The perturbative QCD prediction uses a next-to-next-to-leading order $O(\alpha_s^3)$ expansion of the Adler D -function (Gorishnii *et al.*, 1991; Surguladze and Samuel, 1991), with second-order quark mass corrections included (Chetyrkin *et al.*, 1996). $R(s)$ is obtained by evaluating numerically a contour integral in the complex s plane. Nonperturbative effects are considered through the Operator Product Expansion, giving small power corrections controlled by gluon and quark condensates. The value $\alpha_s(M_Z^2) = 0.1193 \pm 0.0026$, used for the evaluation of the perturbative part, is taken as the average of the results from the analyses of τ decays (ALEPH Coll., 1998c) (see Section VII) and of the Z width in the global electroweak fit (LEP EWG, 2002). Uncertainties on the QCD prediction are taken to be equal to the common error on $\alpha_s(M_Z^2)$, to half of the quark mass corrections and to the full nonperturbative contributions. A local test of the QCD prediction can be performed in the energy range between 1.8 and 3.7 GeV. The contribution to $a_\mu^{\text{had,LO}}$ in this region is computed to be $(33.87 \pm 0.46) \times 10^{-10}$ using QCD, to be compared with the result, $(34.9 \pm 1.8) \times 10^{-10}$ from the data. The two values agree within the 5% accuracy of the measurements.

The evaluation of $a_\mu^{\text{had,LO}}$ was shown to be improved by applying QCD sum rules (Davier and Höcker, 1998b; Groote *et al.*, 1998). The latest full reanalyses (Davier *et al.*, 2003a,b) however did not consider this possibility since the main problem at energies below 2 GeV was the inconsistency between the e^+e^- and τ input data, which had to be resolved with priority. Also the improvement provided by the use of QCD sum rules results from a balance between the experimental accuracy of the data and the theoretical uncertainties. With an increase in the experimental precision, the gain from the theoretical constraint would be smaller than before.

D. Results for the lowest order hadronic vacuum polarization

Many calculations of the hadronic vacuum polarization contribution have been carried out in the past, taking advantage of the e^+e^- data available at that time and benefiting from a more complete treatment of isospin-breaking corrections (Cirigliano *et al.*, 2001, 2002). In this review, we will follow the latest published analysis by (Davier *et al.*, 2003b) (and the update (Höcker, 2004) including data from KLOE, see also the result in (Troconiz and Yndurain, 2004)), which considers input from both τ and e^+e^- data.

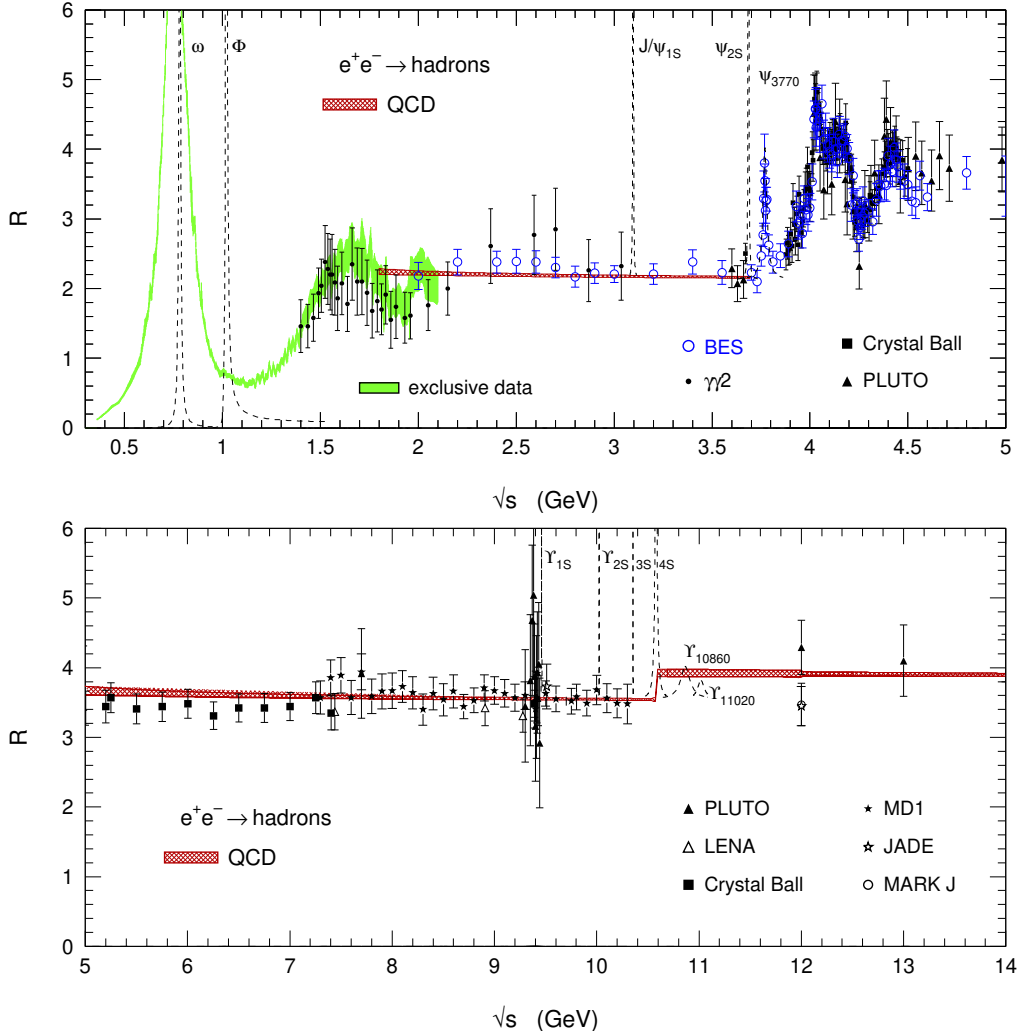


FIG. 19 Compilation of the data contributing to $a_\mu^{\text{had,LO}}$. Shown is the total hadronic over muonic cross section ratio R . The shaded band below 2 GeV represents the sum of the exclusively measured channels, with the exception of the contributions from the narrow resonances that are given as dashed lines. All data points shown correspond to inclusive measurements. The cross-hatched band gives the prediction from (essentially) perturbative QCD (see text).

Figure 19 gives a panoramic view of the e^+e^- data in the relevant energy range. The shaded band represents the sum of the exclusive channels. The QCD prediction is indicated by the cross-hatched band. Note that the QCD band is plotted taking into account the thresholds for open flavor B states, in order to facilitate the comparison with the data in the continuum. However, for the evaluation of the integral, the $b\bar{b}$ threshold is taken at twice the pole mass of the b quark, so that the contribution includes the narrow Υ resonances, according to global quark-hadron duality.

Compiling all contributions, the e^+e^- -based result (including the KLOE data, but not yet SND) for the lowest-order hadronic contribution is (Höcker, 2004)

$$a_\mu^{\text{had,LO}} = (693.4 \pm 5.3 \pm 3.5_{\text{rad}}) \times 10^{-10}, \quad (68)$$

where the second error is due to the treatment of (potentially) missing radiative corrections in the older data (Davier *et al.*, 2003a). The new KLOE data decreased the contribution by about 3×10^{-10} . For a comparison we also give the results without KLOE for the e^+e^- and τ -based analyses (Davier *et al.*, 2003b): $a_\mu^{\text{had,LO}}[e^+e^- \text{-based}] = (696.3 \pm 6.2_{\text{exp}} \pm 3.6_{\text{rad}}) \times 10^{-10}$ and $a_\mu^{\text{had,LO}}[\tau \text{-based}] = (711.0 \pm 5.0_{\text{exp}} \pm 0.8_{\text{rad}} \pm 2.8_{\text{SU}(2)}) \times 10^{-10}$.

E. Hadronic three-loop effects

The three-loop hadronic contributions to a_μ^{SM} involve one hadronic vacuum polarization insertion with an additional loop (either photonic or another leptonic or hadronic vacuum polarization). They can be evaluated (Krause, 1997) with the use of the same $e^+e^- \rightarrow \text{hadrons}$ data sets used for $a_\mu^{\text{had,LO}}$. Denoting that subset of $\mathcal{O}(\alpha/\pi)^3$ hadronic contributions $a_\mu^{\text{had,NLO}}$, we quote here the result of a recent analysis (Hagiwara *et al.*, 2004),

$$a_\mu^{\text{had,NLO}} = (-9.8 \pm 0.1) \times 10^{-10}, \quad (69)$$

which is consistent with earlier studies (Alemany *et al.*, 1998; Krause, 1997). It would change by about -0.3×10^{-10} if the τ data were also used.

More controversial are the hadronic light-by-light scattering contributions illustrated in the lower diagram of the second column in Fig. 17. Since it invokes a four-point correlation function, a dispersion relation approach using data is not possible and a first-principles calculation (*e.g.*, lattice gauge theory (Blum, 2003)) has so far not been carried out. Instead, calculations involving pole insertions, short distance quark loops (Bijnens *et al.*, 1996; Hayakawa *et al.*, 1996) and charged-pion loops have been individually performed in a large N_C QCD approach. The pseudoscalar poles (π^0, η and η') dominate such a calculation. Unfortunately, in early studies the sign of the contribution was incorrect. Its correction (Bijnens *et al.*, 2002; Blokland *et al.*, 2002; Hayakawa and Kinoshita, 1998; Knecht and Nyffeler, 2002; Knecht *et al.*, 2002) led to a large shift in the a_μ^{SM} prediction. A representative estimate (Davier *et al.*, 2003a) of the LBL contribution, which includes π, η and η' poles as well as other resonances, charged pion loops and quark loops, currently gives $a_\mu^{\text{had,LBL}} \simeq (8.6 \pm 3.5) \times 10^{-10}$ (representative).

A new analysis of LBL scattering (Melnikov and Vainshtein, 2004) takes into account the proper matching of the asymptotic short distance behavior of pseudoscalar and axial-vector contributions with the free quark loop behavior. It yields the somewhat larger result $a_\mu^{\text{had,LBL}} = (13.6 \pm 2.5) \times 10^{-10}$.

As pointed out in (Davier and Marciano, 2004), several small but (likely) negative contributions such as charged pion loops and scalar resonances were not included in (Melnikov and Vainshtein, 2004) and could reduce somewhat the magnitude of the result. The authors (Melnikov and Vainshtein, 2004) provide a consistency check on their result much in the spirit of the EW hadronic triangle diagram study (Czarnecki *et al.*, 2003; Vainshtein, 2003) discussed in (Davier and Marciano, 2004). Using constituent quark masses in the LBL diagram combined with a pion pole contribution that properly accounts for the chiral properties of massless QED and avoiding short distance double counting, they find $a_\mu^{\text{had,LBL}} \simeq 12.0 \times 10^{-10}$ with about half of the contribution coming from quark diagrams and the other half from the pion pole. Using that result along with an inflated error assigned so that the representative result and the one obtained in (Melnikov and Vainshtein, 2004) overlap within their errors, (Davier and Marciano, 2004) suggest the value

$$a_\mu^{\text{had,LBL}} \simeq (12.0 \pm 3.5) \times 10^{-10}. \quad (70)$$

Further resolution of the LBL scattering contribution is very important.

Combining Eqs. (69) and (70), one finds

$$a_\mu^{\text{had,3-loop}} = (2.2 \pm 3.5) \times 10^{-10}, \quad (71)$$

which we identify with $a_\mu^{\text{had,HO}}$ in Eq. (63).

F. Comparing a_μ between theory and experiment

Summing the results from the previous sections on a_μ^{QED} , a_μ^{EW} , $a_\mu^{\text{had,LO}}$, $a_\mu^{\text{had,NLO}}$, and $a_\mu^{\text{had,LBL}}$, one obtains the SM prediction for a_μ . The newest e^+e^- -based result reads (Höcker, 2004)

$$a_\mu^{\text{SM}} = (11\,659\,182.8 \pm 6.3_{\text{had,LO+NLO}} \pm 3.5_{\text{had,LBL}} \pm 0.3_{\text{QED+EW}}) \times 10^{-10}. \quad (72)$$

This value can be compared to the present measurement (61); adding all errors in quadrature, the difference between experiment and theory is

$$a_\mu^{\text{exp}} - a_\mu^{\text{SM}} = (25.2 \pm 9.2) \times 10^{-10}, \quad (73)$$

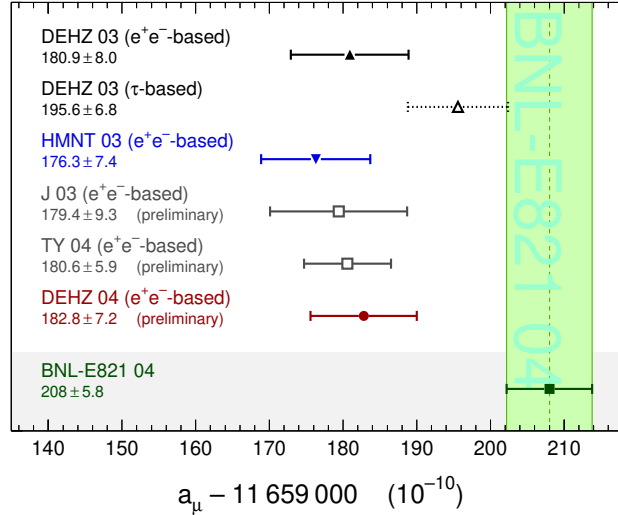


FIG. 20 Comparison of the result (72) (Höcker, 2004) labelled DEHZ 04 with the BNL measurement (Muon ($g - 2$) Coll., 2004). Also given are the previous estimate (Davier *et al.*, 2003b), where the triangle with the dotted error bar indicates the τ -based result, as well as the estimates from (Hagiwara *et al.*, 2004; Jegerlehner, 2003; Troconiz and Yndurain, 2004), not yet including the KLOE data.

which corresponds to 2.7 “standard deviations” (to be interpreted with care due to the dominance of experimental and theoretical systematic errors in the SM prediction). A graphical comparison of the result (72) with previous evaluations (also those containing τ data) and the experimental value is given in Fig. 20.

Whereas the evaluation based on the e^+e^- data only disagrees with the measurement, the evaluation including the tau data is consistent with it. The dominant contribution to the discrepancy between the two evaluations stems from the $\pi\pi$ channel with a difference of $(-11.9 \pm 6.4_{\text{exp}} \pm 2.4_{\text{rad}} \pm 2.6_{\text{SU}(2)} (\pm 7.3_{\text{total}})) \times 10^{-10}$, and a more significant energy-dependent deviation¹⁰. As a consequence, during the previous evaluations of $a_\mu^{\text{had},\text{LO}}$, the results using respectively the τ and e^+e^- data were quoted individually, but on the same footing since the e^+e^- -based evaluation was dominated by the data from a single experiment (CMD-2).

The seeming confirmation of the e^+e^- data by KLOE could lead to the conclusion that the τ -based result be discredited for the use in the dispersion integral (Höcker, 2004). However, the newest SND data (SND-2 Coll., 2005) alter this picture in favor of the τ data, along with prompting doubts on the validity of the KLOE results (see discussion in Section V.C). Comparing the SND and CMD-2 data in the overlapping energy region between 0.61 GeV and 0.96 GeV, the SND-based evaluation of $a_\mu^{\text{had},\text{NLO}}$ is found to be larger by $(9.1 \pm 6.3) \times 10^{-10}$. However, once these two experiments are averaged using the trapezoidal rule, the increase over the CMD-2 only evaluation is reduced to 2×10^{-10} due to the much smaller systematic errors and the higher density of the CMD-2 measurements.

The proper response to the problems in the LO hadronic contribution is to further improve the experimental precision by a renewed experimental effort, and to continue to improve theory. In this respect, new $e^+e^- \rightarrow$ hadrons data and further study of LBL scattering could potentially reduce the overall theoretical uncertainty. The excitement that was caused by the deviation (73) stems from the expectation that new physics could cause an effect of similar magnitude. In the next section, we briefly review several examples (following (Davier and Marciano, 2004)).

¹⁰ The systematic problem between τ and e^+e^- data is more noticeable when comparing the $\tau^- \rightarrow \pi^-\pi^0\nu_\tau$ branching fraction with the prediction obtained from integrating the corresponding isospin-breaking-corrected e^+e^- spectral function (*cf.* Section V).

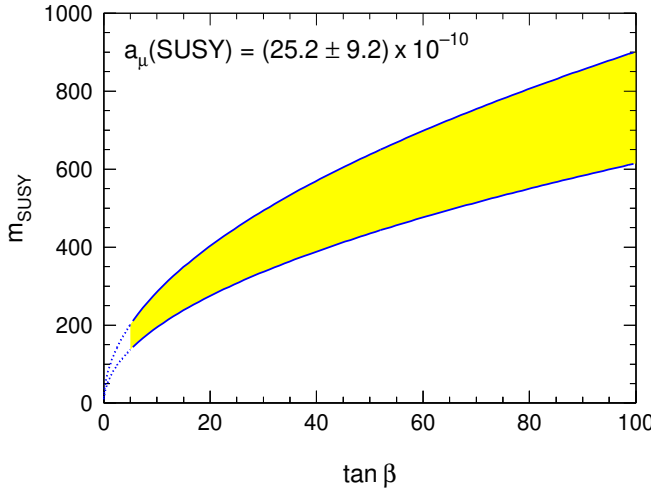


FIG. 21 Supersymmetric scale m_{SUSY} as a function of $\tan\beta$ assuming the discrepancy (73) is entirely due to SUSY contributions, and that the SUSY particles have degenerate masses.

G. New physics contributions

A deviation of about $\sim 25 \times 10^{-10}$ in $\Delta a_\mu = a_\mu^{\text{exp}} - a_\mu^{\text{SM}}$ would have interesting interpretations if truly due to new physics. The leading contender for causing such an effect is Supersymmetry. Indeed, supersymmetric contributions to a_μ can stem from sneutrino-chargino and smuon-neutralino loops as illustrated in the right hand diagrams of Fig. 17. Those diagrams actually describe 2-chargino and 4-neutralino states and could include 3-generation slepton mixing. In general, a broad range of predictions are possible depending on particle masses, couplings etc. For illustration purposes, we assume degenerate masses m_{SUSY} in all loops (Ibrahim and Nath, 1998; Moroi, 1996) (not a realistic assumption but one that should roughly approximate expectations). Then in terms of $\tan\beta = \langle\phi_2\rangle/\langle\phi_1\rangle$, the ratio of Higgs vacuum expectations and the sign of μ ($\text{sgn}\mu$), the higgsino mass parameter, one finds (for $\tan\beta \geq 3$) $a_\mu^{\text{SUSY}} \simeq (\text{sgn}\mu) \times 13.0 \times 10^{-10} (100 \text{ GeV}/m_{\text{SUSY}})^2 \tan\beta$, where 2-loop leading-log QED suppression effects have been included (Czarnecki and Marciano, 2001). Equating that prediction with the deviation (73) suggests $\mu > 0$ and $m_{\text{SUSY}} \simeq 72\sqrt{\tan\beta} \text{ GeV}$ (see Fig. 21).

The $\mu > 0$ scenario is also favored by $b \rightarrow s\gamma$ data, and for $3 \leq \tan\beta \leq 40$ the corresponding SUSY mass scale is the range $106 \text{ GeV} \leq m_{\text{SUSY}} \leq 570 \text{ GeV}$. Hence a deviation in Δa_μ of about the apparent magnitude is a relatively generic prediction of low mass SUSY models. If SUSY is eventually discovered at high-energy colliders and the masses measured, one can use Δa_μ to determine $\tan\beta$.

Another generic possibility (Marciano, 1996) is new physics related to the origin of the muon mass via loop effects (radiative muon mass scenarios). In such schemes (Czarnecki and Marciano, 2001) the muon mass originates from a chiral symmetry breaking loop effect with its origin coming from a high scale M , which can arise from dynamics, extra dimensions, multi-Higgs, softly broken SUSY, etc. One finds generically $a_\mu(M) \simeq C(m_\mu^2/M^2)$ where C is $\mathcal{O}(1)$ rather than (α/π) . A deviation of $\Delta a_\mu \simeq 25 \times 10^{-10}$ corresponds to $M \simeq 2 \text{ TeV}$, an interesting possibility. Indeed, if SUSY is not found at high energy colliders, it is highly likely that other $\mathcal{O}(1 \text{ TeV})$ scale physics emerges. If the Δa_μ deviation is related, it would suggest that mass generating new physics is at hand.

Other forms of new physics (Czarnecki and Marciano, 2001) such as Z' or W_R bosons, anomalous W dipole moments etc. generally lead to unobservable small Δa_μ . So, SUSY with its relatively low mass scale and $\tan\beta$ enhancement along with models with no α/π suppression are the more natural candidates to explain a deviation in Δa_μ from zero.

H. Conclusions and perspectives

After considerable effort, the experiment E821 at Brookhaven has improved the determination of a_μ by about a factor of 14 relative to the classic CERN results of the 1970's (Bailey *et al.*, 1977; Farley and Picasso, 1990). The result is still statistics limited and could be improved by another factor of 2 or so (to a precision

of 3.0×10^{-10}) before systematic effects become a limitation. Pushing the experiment to that level seems to be an obvious goal for the near term. In the longer term, a new experiment with improved muon acceptance and magnetic fields could potentially reach 0.6×10^{-10} (Hertzog, 2005; Roberts, 1999).

In spite of the new and precise data on the two-pion spectral function from the KLOE and SND collaborations, the lowest-order hadronic vacuum-polarization contribution remains the most critical component in the SM prediction of a_μ . The publication of the KLOE results led to an outward confirmation of the discrepancy between the τ data and e^+e^- annihilation observed in the $\pi^+\pi^-$ channel (Davier *et al.*, 2003b). Including the KLOE data in the hadronic evaluation, the e^+e^- -based SM prediction of a_μ was found to differ from the experimental value by 2.7 “standard deviations”.

An opposite point view is advocated in (Maltman, 2005). A QCD sum-rule analysis of low-energy e^+e^- data results in the value $\alpha_s(M_Z^2) = 0.1150 \pm 0.0024$, which is somewhat lower than the world average (Particle Data Group, 2004), 0.1187 ± 0.0020 , and even less consistent with the average 0.1200 ± 0.0020 , which excludes τ data (for the sake of comparison) and heavy quarkonium results (the accuracy of which has been questioned in (Brambilla *et al.*, 2004)). The same analysis using the τ vector spectral function provides agreement, with a value of $\alpha_s(M_Z^2) = 0.1201 \pm 0.0021$. Although the disagreement between the e^+e^- data and other measurements is not yet significant, the observed trend is worth more investigations¹¹. It is supported by the newest measurement from SND that tend to amend the compatibility with the τ data in the 2 pion channel.

The further improvement of the e^+e^- data is the better route and one is looking forward to the forthcoming results on the low- and high-energy two-pion spectral function from the CMD-2 collaboration. These data will help to significantly reduce the systematic uncertainty due to the corrective treatment of radiative effects, often omitted by part by the previous experiments. The initial-state-radiation program of the BABAR collaboration has already proved its performance by publishing the spectral functions for $\pi^+\pi^-\pi^0$ (BABAR Coll., 2004) and $2\pi^+2\pi^-$ (BABAR Coll., 2005a), while results for the two-pion final state are expected. All sources considered, and assuming all discrepancies to be resolved, it appears however difficult to reach an uncertainty much better than 3×10^{-10} in this sector¹².

The 30% uncertainty in the hadronic LBL contribution (3.5×10^{-10}) is largely model-dependent. Here one could conceive that further work following the approach of (Melnikov and Vainshtein, 2004) or lattice calculations could help to reduce the error. Doing much better will be difficult, but an improvement in the precision by about a factor of 2 would well match short-term experimental capabilities.

If the above experimental and theoretical improvements do occur, they will lead to a total uncertainty in $\Delta a_\mu = a_\mu^{\text{exp}} - a_\mu^{\text{SM}}$ of about 5.0×10^{-10} , *i.e.*, a factor of 2 reduction with respect to today. This would provide an important step towards a better test of the SM. The result could be used in conjunction with future collider discoveries to sort out the properties of new physics (*e.g.*, the size of $\tan\beta$ in SUSY) or to further constrain possible appendages to the SM.

VII. HADRONIC TAU DECAYS AND QCD

Tests of Quantum Chromodynamics and the precise measurement of the strong coupling constant α_s at the τ mass scale (Braaten, 1989; Braaten *et al.*, 1992; Le Diberder and Pich, 1992b; Narison and Pich, 1988), carried out for the first time by the ALEPH (ALEPH Coll., 1993) and CLEO (CLEO Coll., 1995b) collaborations have triggered many theoretical developments. They concern primarily the perturbative expansion for which different optimized rules have been suggested. Among these are contour-improved (resummed) fixed-order perturbation theory (Le Diberder and Pich, 1992a; Pivovarov, 1991, 1992), effective charge and minimal sensitivity schemes (Dhar, 1983; Dhar and Gupta, 1984; Grunberg, 1980, 1984; Stevenson, 1981), the large- β_0 expansion (Altarelli *et al.*, 1995; Ball *et al.*, 1995; Neubert, 1996), as well as combinations of these approaches. Moreover, with the publication of the full vector and axial-vector spectral functions by ALEPH (ALEPH Coll., 1997b, 1998c) and OPAL (OPAL Coll., 1999b) it became possible to directly study the nonperturbative properties of QCD through vector minus axial-vector sum rules. These analyses are described in Section IX.

¹¹ We note that the rather high spectral moments used in (Maltman, 2005) should be inspected for the possibility of systematic deviations from the Operator Product Expansion, which—if present—could affect the reliability of the result.

¹² We also point out that lattice gauge theories with dynamical fermions can in principle provide a determination of $a_\mu^{\text{had,LO}}$ (Blum, 2003).

One could wonder how τ decays may allow us to learn something about perturbative QCD. The hadronic decay of the τ is dominated by resonant single particle final states. The corresponding QCD interactions that bind the quarks and gluons into these hadrons necessarily involve small momentum transfers, which are outside the domain of perturbation theory. On the other hand, perturbative QCD describes interactions of quarks and gluons with large momentum transfer. Indeed, it is the inclusive character of the sum of all hadronic τ decays that allows us to probe fundamental short distance physics. Inclusive observables like the total hadronic τ decay rate R_τ (20) can be accurately predicted as function of $\alpha_s(m_\tau^2)$ using perturbative QCD, and including small nonperturbative contributions within the framework of the Operator Product Expansion (OPE) (Shifman *et al.*, 1979). In effect, R_τ is a doubly inclusive observable since it is the result of an integration over all hadronic final states at a given invariant mass and further over all masses between m_π and m_τ . Hadronic τ decays are more inclusive than e^+e^- annihilation data, since vector and axial-vector contributions are of approximately equal size, while the isospin-zero component in e^+e^- data is three times smaller than the isovector part, which is (about) equal to the vector contribution in τ decays. The scale m_τ lies in a compromise region where $\alpha_s(m_\tau^2)$ is large enough so that R_τ is sensitive to its value, yet still small enough so that the perturbative expansion converges safely and nonperturbative power terms are small.

If strong and electroweak radiative corrections are neglected, the theoretical parton level prediction for $SU_C(N_C)$, $N_C = 3$ reads

$$R_\tau = N_C (|V_{ud}|^2 + |V_{us}|^2) = 3 , \quad (74)$$

so that we can estimate a perturbative correction to this value of approximately 21% to obtain (20), assuming other sources to be small. One realizes the increase in sensitivity to α_s compared to the Z hadronic width, where due to the three times smaller $\alpha_s(M_Z^2)$ the perturbative QCD correction reaches only about 4%.

The nonstrange inclusive observable R_τ can be theoretically separated into contributions from specific quark currents, namely vector (V) and axial-vector (A) $\bar{u}d$ and $\bar{u}s$ quark currents. It is therefore appropriate to decompose

$$R_\tau = R_{\tau,V} + R_{\tau,A} + R_{\tau,S} , \quad (75)$$

where for the strange hadronic width $R_{\tau,S}$ vector and axial-vector contributions are not separated so far due to the lack of the corresponding experimental information for the Cabibbo-suppressed modes. Parton level and perturbative prediction do not distinguish vector and axial-vector currents. Thus the corresponding naive predictions become $R_{\tau,V/A} = (N_C/2)|V_{ud}|^2$ and $R_{\tau,S} = N_C|V_{us}|^2$, which add up to Eq. (74).

A crucial issue of the QCD analysis at the τ mass scale concerns the reliability of the theoretical description, *i.e.*, the use of the OPE to organize the perturbative and nonperturbative expansions, and the control of unknown higher-order terms in these series. A reasonable stability test is to continuously vary m_τ to lower values $\sqrt{s_0} \leq m_\tau$ for both theoretical prediction and measurement, which is possible since the shape of the full τ spectral function is available. The kinematic factor that takes into account the τ phase space suppression at masses near to m_τ is correspondingly modified so that $\sqrt{s_0}$ represents the new mass of the τ .

A. Renormalization group equations

Like in QED, the subtraction of divergences in QCD is equivalent to the renormalization of the coupling ($\alpha_s \equiv g_s^2/4\pi$), the quark masses (m_q), etc, and the fields in the bare (superscript B) Lagrangian such as $\alpha_s^B = s^\varepsilon Z_{\alpha_s} \alpha_s$, $m_q^B = s^\varepsilon Z_m m_q$, etc. Here s is the renormalization scale, ε the dimensional regularization parameter, and Z denotes a series of renormalization constants obtained from the generating functional of the bare Green's function. The renormalization procedure introduces an energy scale, s , which represents the point at which the subtraction to remove the divergences is actually performed. This leads to the differential *Renormalization Group Equations* (RGE)

$$\frac{da_s}{d\ln s} = \beta(a_s) = -a_s^2 \sum_n \beta_n a_s^n , \quad (76)$$

$$\frac{1}{m_q} \frac{dm_q}{d\ln s} = \gamma(\alpha_s) = -a_s \sum_n \gamma_n a_s^n , \quad (77)$$

with $a_s = \alpha_s/\pi$. Expressed in the *modified minimal subtraction renormalization scheme* ($\overline{\text{MS}}$) (Bardeen *et al.*, 1978; t'Hooft *et al.*, 1972) and for three active quark flavors at the τ mass scale, the perturbative coefficients,

known to four loops (van Ritbergen *et al.*, 1997a,b), are¹³

$$\beta_0 = 2.25, \quad \beta_1 = 4, \quad \beta_2 \approx 10.05989, \quad \beta_3 \approx 47.22804, \quad (78)$$

$$\gamma_0 = 1, \quad \gamma_1 = 3.79166, \quad \gamma_2 \approx 12.42018, \quad \gamma_3 \approx 44.26278. \quad (79)$$

The solutions for the evolutions (76) and (77) are obtained from integration¹⁴ (Chetyrkin *et al.*, 1997b; Stevenson, 1981)

$$\ln \frac{s}{\Lambda^2} = \int_0^{a_s(s)} da'_s \left(\frac{1}{\beta(a'_s)} + \frac{1}{\beta_0(a'_s)^2 + \beta_1(a'_s)^3} \right) + \int_{a_s(s)}^{\infty} da'_s \frac{1}{\beta_0(a'_s)^2 + \beta_1(a'_s)^3} \quad (80)$$

$$\approx \frac{1}{\beta_0} \left[\frac{1}{a_s} + \frac{\beta_1}{\beta_0} \ln a_s + \left(\frac{\beta_2}{\beta_0} - \frac{\beta_1^2}{\beta_0^2} \right) a_s + \left(\frac{\beta_3}{2\beta_0} - \beta_1\beta_2 + \frac{\beta_1^3}{2\beta_0^3} \right) a_s^2 \right] + C, \quad (81)$$

$$\ln \frac{m_q(s)}{m_q(s_0)} = \int_{a_s(s_0)}^{a_s(s)} da'_s \frac{\gamma(a'_s)}{\beta(a'_s)}, \quad (82)$$

where the $\overline{\text{MS}}$ asymptotic scale parameter Λ and the RG-invariant quark mass \hat{m}_q (which appears after evaluating the integral (82)) are fixed by referring to known values $a_s(s_0)$ and $m_q(s_0)$, respectively, at scale s_0 . The explicit solution of the integral (80) implies the integration constant $C = (\beta_1/\beta_0^2) \ln \beta_0$, which is chosen to suppress terms $\propto \ln(s/\Lambda^2)$ (Bardeen *et al.*, 1978; Furmanski and Petronzio, 1982) (the reader is referred to (Chetyrkin *et al.*, 1997b) for a discussion of other suitable choices).

For most practical purposes, it is however unnecessary to explicitly perform the integrations (80, 82), since the evolution of the differential RGEs can be solved numerically by means of *single-step integration* using a modified Euler method. It consists of Taylor-developing, say, Eq. (76) around the reference scale s_0 in powers of $\eta \equiv \ln(s/s_0)$, and reordering the perturbative series in powers of $a_s \equiv a_s(s_0)$,

$$\begin{aligned} a_s(s) = & a_s - \beta_0 \eta a_s^2 + (-\beta_1 \eta + \beta_0^2 \eta^2) a_s^3 + \left(-\beta_2 \eta + \frac{5}{2} \beta_0 \beta_1 \eta^2 - \beta_0^3 \eta^3 \right) a_s^4 \\ & + \left(-\beta_3 \eta + \frac{3}{2} \beta_1^2 \eta^2 + 3\beta_0 \beta_2 \eta^2 - \frac{13}{3} \beta_0^2 \beta_1 \eta^3 + \beta_0^4 \eta^4 \right) a_s^5 \end{aligned} \quad (83)$$

¹³ The full expressions for an arbitrary number of quark flavors (n_f) are (van Ritbergen *et al.*, 1997a,b)

$$\begin{aligned} \beta_0 &= \frac{1}{4} \left(11 - \frac{2}{3} n_f \right), \quad \beta_1 = \frac{1}{16} \left(102 - \frac{38}{3} n_f \right), \quad \beta_2 = \frac{1}{64} \left(\frac{2857}{2} - \frac{5033}{18} n_f + \frac{325}{54} n_f^2 \right), \\ \beta_3 &= \frac{1}{256} \left[\frac{149753}{6} + 3564 \zeta_3 - \left(\frac{1078361}{162} + \frac{6508}{27} \zeta_3 \right) n_f + \left(\frac{50065}{162} + \frac{6472}{81} \zeta_3 \right) n_f^2 + \frac{1093}{729} n_f^3 \right], \end{aligned}$$

and

$$\begin{aligned} \gamma_0 &= 1, \quad \gamma_1 = \frac{1}{16} \left(\frac{202}{3} - \frac{20}{9} n_f \right), \quad \gamma_2 = \frac{1}{64} \left[1249 - \left(\frac{2216}{27} + \frac{160}{3} \zeta_3 \right) n_f - \frac{140}{81} n_f^2 \right], \\ \gamma_3 &= \frac{1}{256} \left[\frac{4603055}{162} + \frac{135680}{27} \zeta_3 - 8800 \zeta_5 + \left(-\frac{91723}{27} - \frac{34192}{9} \zeta_3 + 880 \zeta_4 + \frac{18400}{9} \zeta_5 \right) n_f \right. \\ &\quad \left. + \left(\frac{5242}{243} + \frac{800}{9} \zeta_3 - \frac{160}{3} \zeta_4 \right) n_f^2 + \left(-\frac{332}{243} + \frac{64}{27} \zeta_3 \right) n_f^3 \right], \end{aligned}$$

¹⁴ where the $\zeta_{i=\{3,4,5\}} = \{1.2020569, \pi^4/90, 1.0369278\}$ are the Riemann ζ -functions.

Note that the integration is only defined for a non-vanishing derivative $\beta(a_s) \neq 0$. Vanishing $\beta(a_s)$ may indeed occur for example in effective charge schemes with large K_4 or K_5 coefficients (see later in this section). An iterative solution of the four-loop β function has been computed in (Chetyrkin *et al.*, 1997b), which we give here for completeness

$$\begin{aligned} a_s(s) = & \frac{1}{\beta_0 L} - \frac{b_1 \ln L}{(\beta_0 L)^2} + \frac{1}{(\beta_0 L)^3} \left[b_1^2 \left(\ln^2 L - \ln L - 1 \right) + b_2 \right] \\ & + \frac{1}{(\beta_0 L)^4} \left[b_1^3 \left(-\ln^3 L + \frac{5}{2} \ln^2 L + 2 \ln L - \frac{1}{2} \right) - 3b_1 b_2 \ln L + \frac{b_3}{2} \right], \end{aligned}$$

where $L = \ln(s/\Lambda^2)$, $b_i = \beta_i/\beta_0$ and terms of order $\mathcal{O}(L^{-5})$ have been neglected.

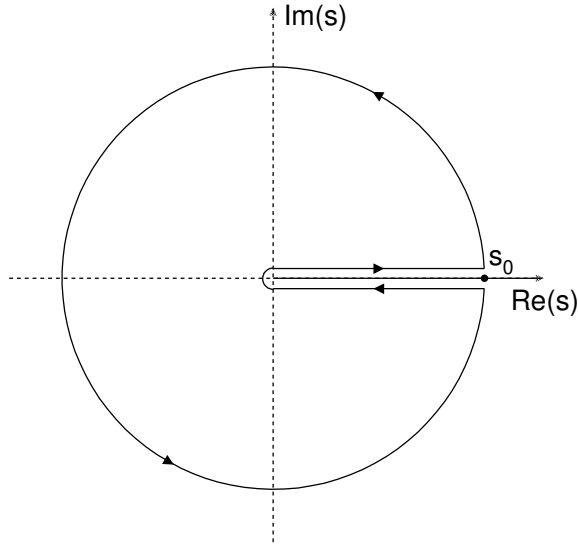


FIG. 22 Integration contour for the r.h.s. in Eq. (85).

$$\begin{aligned}
& + \left(-\beta_4\eta + \frac{7}{2}\beta_1\beta_2\eta^2 + \frac{7}{2}\beta_0\beta_3\eta^2 - \frac{35}{6}\beta_0\beta_1^2\eta^3 - 6\beta_0^2\beta_2\eta^3 + \frac{77}{12}\beta_0^3\beta_1\eta^4 - \beta_0^5\eta^5 \right) a_s^6 \\
& + \mathcal{O}(a_s^7) .
\end{aligned}$$

For later use, we have expressed the expansion up to order a_s^6 , which involves the unknown five-loop coefficient β_4 . An efficient integration of the RGEs can also be obtained using the CERNLIB routine ‘RKSTP’, which performs a 4th order Runge-Kutta single step approximation with excellent accuracy.

B. Theoretical prediction of R_τ

According to Eq. (39) the absorptive parts of the vector and axial-vector two-point correlation functions $\Pi_{ud,V/A}^{(J)}(s)$, with the spin J of the hadronic system, are proportional to the τ hadronic spectral functions with corresponding quantum numbers. The nonstrange ratio $R_{\tau,V+A}$ can be written as an integral of these spectral functions over the invariant mass-squared s of the final state hadrons (Braaten *et al.*, 1992)

$$R_{\tau,V+A}(s_0) = 12\pi S_{\text{EW}} \int_0^{s_0} \frac{ds}{s_0} \left(1 - \frac{s}{s_0}\right)^2 \left[\left(1 + 2\frac{s}{s_0}\right) \text{Im}\Pi^{(1)}(s + i\epsilon) + \text{Im}\Pi^{(0)}(s + i\epsilon) \right], \quad (84)$$

where $\Pi^{(J)}$ can be decomposed as $\Pi^{(J)} = |V_{ud}|^2 \left(\Pi_{ud,V}^{(J)} + \Pi_{ud,A}^{(J)} \right)$. The lower integration limit is zero because the pion pole is at zero mass in the chiral limit.

The correlation function $\Pi^{(J)}$ is analytic in the complex s plane everywhere except on the positive real axis where singularities exist. Hence by Cauchy’s theorem, the imaginary part of $\Pi^{(J)}$ is proportional to the discontinuity across the positive real axis

$$\frac{1}{\pi} \int_0^{s_0} ds w(s) \text{Im}\Pi(s) = -\frac{1}{2\pi i} \oint_{|s|=s_0} ds w(s) \Pi(s), \quad (85)$$

where $w(s)$ is an arbitrary analytic function, and the contour integral runs counter-clockwise around the circle from $s = s_0 + i\epsilon$ to $s = s_0 - i\epsilon$ as indicated in Fig. 22.

The energy scale $s_0 = m_\tau^2$ is large enough that contributions from nonperturbative effects are expected to be subdominant and the use of the OPE is appropriate. The kinematic factor $(1 - s/s_0)^2$ suppresses the

contribution from the region near the positive real axis where $\Pi^{(J)}(s)$ has a branch cut and the OPE validity is restricted due to large possible quark-hadron duality violations (Braaten, 1988; Poggio *et al.*, 1976).

The theoretical prediction of the vector and axial-vector ratio $R_{\tau,V/A}$ can hence be written as

$$R_{\tau,V/A} = \frac{3}{2} |V_{ud}|^2 S_{\text{EW}} \left(1 + \delta^{(0)} + \delta'_{\text{EW}} + \delta_{ud,V/A}^{(2,m_q)} + \sum_{D=4,6,\dots} \delta_{ud,V/A}^{(D)} \right), \quad (86)$$

with the massless perturbative contribution $\delta^{(0)}$, the residual non-logarithmic electroweak correction $\delta'_{\text{EW}} = 0.0010$ (Braaten and Li, 1990) (*cf.* the discussion on radiative corrections in Section V.A), and the dimension $D = 2$ contribution $\delta_{ud,V/A}^{(2,m_q)}$ from quark masses, which is lower than 0.1% for u, d quarks. The term $\delta^{(D)}$ denotes the OPE contributions of mass dimension D

$$\delta_{ud,V/A}^{(D)} = \sum_{\text{dim}\mathcal{O}=D} C_{ud,V/A}(s, \mu) \frac{\langle \mathcal{O}_{ud}(\mu) \rangle_{V/A}}{(-\sqrt{s_0})^D}, \quad (87)$$

where the scale parameter μ separates the long-distance nonperturbative effects, absorbed into the vacuum expectation elements $\langle \mathcal{O}_{ud}(\mu) \rangle$, from the short-distance effects that are included in the Wilson coefficients $C_{ud,V/A}(s, \mu)$ (Wilson, 1969). Note that $\delta_{ud,V+A}^{(D)} = (\delta_{ud,V}^{(D)} + \delta_{ud,A}^{(D)})/2$.

1. The Adler function

The perturbative prediction used by the experiments follows the work of (Le Diberder and Pich, 1992a). The perturbative contribution is given in the chiral limit. Effects from quark masses have been calculated in (Chetyrkin and Kwiatkowski, 1993) and are found to be well below 1% for the light quarks. As a consequence, the contributions from vector and axial-vector currents coincide to any given order of perturbation theory and the results are flavor independent.

For the evaluation of the perturbative series, it is convenient to introduce the analytic Adler function (Adler, 1974)

$$D(s) \equiv -s \frac{d\Pi(s)}{ds} = \frac{s}{\pi} \int_0^\infty ds' \frac{\text{Im}\Pi(s')}{(s' - s)^2}, \quad (88)$$

where the second identity is the dispersion relation (*cf.* Section VI.A). The derivative of the correlator avoids extra subtractions (renormalization) on the r.h.s. of Eq. (88), which are unrelated to QCD dynamics. The function $D(s)$ calculated in perturbative QCD within the $\overline{\text{MS}}$ renormalization scheme depends on a non-physical parameter μ occurring as $\ln(\mu^2/s)$. Furthermore it is a function of α_s . On the other hand, since $D(s)$ is connected to a physical quantity, the spectral function $\text{Im}\Pi(s)$, it cannot depend on the subjective choice of μ . This can be achieved if α_s becomes a function of μ providing independence of $D(s)$ of the choice of μ . Nevertheless, in the realistic case of a truncated series, some μ dependence remains and represents an irreducible systematic uncertainty. $D(s)$ is then a function of μ^2/s , α_s and can be understood as an effective charge (see below) that obeys the RGE. Choosing $\mu^2 = s$, the perturbative series reads

$$D(\alpha_s(s)) = \sum_{n=0}^{\infty} r_n a_s^n(s), \quad (89)$$

with renormalization scheme dependent coefficients r_n .

To introduce the Adler function in Eqs. (84) and (85) one uses partial integration

$$\oint_{|s|=s_0} ds g(s) \Pi(s) = - \oint_{|s|=s_0} \frac{ds}{s} (G(s) - G(s_0)) s \frac{d\Pi(s)}{ds}, \quad (90)$$

with the kernel $g(s) = (1 - s/s_0)^2 (1 + 2s/s_0)/s_0$ and $G(s) = \int_0^s ds' g(s')$. This gives (Le Diberder and Pich, 1992a)

$$1 + \delta^{(0)} = -2\pi i \oint_{|s|=s_0} \frac{ds}{s} \left[1 - 2\frac{s}{s_0} + 2\left(\frac{s}{s_0}\right)^3 - \left(\frac{s}{s_0}\right)^4 \right] D(s). \quad (91)$$

The perturbative expansion of the Adler function can be inferred from the third-order calculation of the e^+e^- inclusive cross section ratio $R_{e^+e^-}(s) = \sigma(e^+e^- \rightarrow \text{hadrons}(\gamma))/\sigma(e^+e^- \rightarrow \mu^+\mu^-(\gamma))$ (Cemmaster and Gonsalves, 1980; Chetyrkin *et al.*, 1979; Dine and Sapirostein, 1979; Gorishnii *et al.*, 1991; Le Diberder and Pich, 1992a; Surguladze and Samuel, 1991)

$$D(s) = \frac{1}{4\pi^2} \sum_{n=0}^{\infty} \tilde{K}_n(\xi) a_s^n(-\xi s) , \quad (92)$$

with the $\tilde{K}_n(\xi)$ functions up to order $n = 5$ (Le Diberder and Pich, 1992a)

$$\begin{aligned} \tilde{K}_0(\xi) &= K_0 , & \tilde{K}_1(\xi) &= K_1 , & \tilde{K}_2(\xi) &= K_2 + L , \\ \tilde{K}_3(\xi) &= K_3 + (b_1 + 2K_2)L + L^2 \\ \tilde{K}_4(\xi) &= K_4 + (b_2 + 2b_1K_2 + 3K_3)L + \left(\frac{5}{2}b_1 + 3K_2\right)L^2 + L^3 , \\ \tilde{K}_5(\xi) &= K_5 + (b_3 + 2b_2K_2 + 3b_1K_3 + 4K_4)L + \left(\frac{3}{2}b_1^2 + 3b_2 + 7b_1K_2 + 6K_3\right)L \\ &\quad + \left(\frac{13}{3}b_1 + 4K_2\right)L^3 + L^4 , \end{aligned} \quad (93)$$

where $b_i = \beta_i/\beta_0$ and $L = \beta_0 \ln \xi$. The factor $\xi = s/s_0$ in Eq. (92) represents the arbitrary renormalization scale ambiguity of which the Adler function (88) is independent. The ξ dependence of the $K_i(\xi)$ coefficients is determined by inserting the expansion (83) into (92), and equating the two series obtained for $\xi = 1$ and arbitrary ξ at each order in a_s .¹⁵ The coefficients K_n are known up to third order in α_s^3 . For $n \geq 2$ they depend on the renormalization scheme used, while the first two coefficients are universal

$$K_0 = 1 , \quad K_1 = 1 , \quad K_2(\overline{\text{MS}}) = F_3(\overline{\text{MS}}) , \quad K_3(\overline{\text{MS}}) = F_4(\overline{\text{MS}}) + \frac{1}{3}\pi^2\beta_0^2 , \quad (94)$$

where $F_3(\overline{\text{MS}}) = 1.9857 - 0.1153 n_f$ and $F_4(\overline{\text{MS}}) = -6.6368 - 1.2001 n_f - 0.0052 n_f^2$ are the coefficients of the perturbative series of $R_{e^+e^-}$. For $n_f = 3$ one has $K_2 = 1.640$ and $K_3 = 6.371$. With the series (92), inserted in the r.h.s of Eq. (91), one obtains the perturbative expansion

$$\delta^{(0)} = \sum_{n=1}^5 \tilde{K}_n(\xi) A^{(n)}(a_s) , \quad (95)$$

with the functions

$$\begin{aligned} A^{(n)}(a_s) &= \frac{1}{2\pi i} \oint_{|s|=s_0} \frac{ds}{s} \left[1 - 2\frac{s}{s_0} + 2\left(\frac{s}{s_0}\right)^3 - \left(\frac{s}{s_0}\right)^4 \right] a_s^n(-\xi s) \\ &= \frac{1}{2\pi} \int_{-\pi}^{\pi} d\varphi [1 + 2e^{i\varphi} - 2e^{i3\varphi} - e^{i4\varphi}] a_s^n(\xi s_0 e^{i\varphi}) , \end{aligned} \quad (96)$$

¹⁵ Note that this procedure corresponds to a fixed-order perturbation theory rule since known higher order pieces of the expansion (83) are neglected when solving

$$\frac{\partial}{\partial \xi} \sum_{n=0}^N \tilde{K}_n(\xi) a_s^n(-\xi s) = \frac{\beta(a_s^n(-\xi s))}{\xi} \sum_{n=0}^N (n+1) \tilde{K}_n(\xi) a_s^n(-\xi s) + \sum_{n=0}^N a_s^{n+1}(-\xi s) \frac{\partial \tilde{K}_n(\xi)}{\partial \xi} \sim \mathcal{O}(a_s^{N+1}) ,$$

for a truncated series with maximum known order N . A resummation of the subleading logarithms has been proposed in (Dams and Kleiss, 2004).

where $s = -s_0 e^{i\varphi}$ has been substituted in the second line and the integral path proceeds according to Fig. 22. Formally, the integrals (96) also obey an RGE (Le Diberder and Pich, 1992a)

$$\xi \frac{\partial A^{(n)}(a_s(-\xi s))}{\partial \xi} = n \sum_{k=1} \beta_k A^{(n+k)}(a_s(-\xi s)) . \quad (97)$$

2. Fixed-order perturbation theory (FOPT)

Inserting the series (83) in Eq. (95), evaluating the contour integral, and collecting the terms with equal powers in a_s leads to the familiar expression (Le Diberder and Pich, 1992a)

$$\delta^{(0)} = \sum_n \left[\tilde{K}_n(\xi) + g_n(\xi) \right] \left(\frac{\alpha_s(\xi s_0)}{\pi} \right)^n , \quad (98)$$

where the g_n are functions of $\tilde{K}_{m < n}$ and $\beta_{m < n-1}$, and of elementary integrals with logarithms of power $m < n$ in the integrand. Setting $\xi = 1$ and replacing all known β_i and K_i coefficients by their numerical values, Eq. (98) simplifies to

$$\begin{aligned} \delta^{(0)} = & a_s(s_0) + (1.6398 + 3.5625) a_s^2(s_0) + (6.371 + 19.995) a_s^3(s_0) \\ & + (K_4 + 78.003) a_s^4(s_0) \\ & + (K_5 + 14.250 K_4 - 391.54) a_s^5(s_0) \\ & + (K_6 + 17.813 K_5 + 45.112 K_4 + 1.58333 \beta_4 - 8062.1) a_s^6(s_0) , \end{aligned} \quad (99)$$

where for the purpose of later studies we have kept terms up to sixth order. When two numbers are given in the parentheses, the first number is K_n , while the second is g_n .

The FOPT series is truncated at given order despite the fact that parts of the higher coefficients $g_{n>4}(\xi)$ are known to all orders and could be resummed. These known parts are the higher (up to infinite) order terms of the expansion (83) that are functions of $\beta_{n \leq 3}$ and $K_{n \leq 3}$ only. In effect, beyond the use of the perturbative expansion of the Adler function (92), two approximations have been used to obtain the FOPT series (99): (i) the RGE (76) has been Taylor-expanded and terms higher than the given FOPT order have been truncated, and (ii) this Taylor expansion is used to predict $a_s(-s)$ on the entire $|s| = s_0$ contour.

3. Contour-improved fixed-order perturbation theory (CIPT)

A more promising approach to the solution of the contour integral (96) is to perform a direct numerical evaluation by means of single-step integration and using the solution of the RGE to four loops as input for the running $a_s(-\xi s)$ at each integration step (Le Diberder and Pich, 1992a; Pivovarov, 1991, 1992). It implicitly provides a partial resummation of the (known) higher order logarithmic integrals and improves the convergence of the perturbative series. While for instance the third order term in the expansion (99) contributes with 17% to the total (truncated) perturbative prediction, the corresponding term of the numerical solution amounts only to 6% (assuming $\alpha_s(m_\tau^2) = 0.35$). This numerical solution of Eq. (95) will be referred to as *contour-improved* fixed-order perturbation theory (CIPT) in the following.

Single-step integration also avoids the Taylor approximation of the RGE on the entire contour, since a_s is iteratively computed from the previous step using the full known RGE.¹⁶ Figure 23 shows the comparison between the iteratively evolved $\alpha_s(m_\tau^2 e^{i\varphi})$ (referred to as the exact solution), and the fourth-order Taylor expansion (83) on the circle $\varphi = -\pi \dots \pi$ (Menke, 1998). The differences appear to be significant far away from the reference value at ($\varphi = 0$). However, as shown below, the numerical effect of this discrepancy on the contour integral is small compared to the main difference between FOPT and CIPT, which is the truncation of the perturbative series after integration.

¹⁶ It has been tested that the single-step integration, *i.e.*, $a_s(\xi s_0 e^{i(\varphi + \Delta\varphi)})$ is computed from $a_s(\xi s_0 e^{i\varphi})$, using a modified Euler method (that is, a Taylor expansion of a_s in each integration step), or using explicit 4th order Runge-Kutta integration, leads to the same result, as far as the step size is chosen to be small enough (1000 integration steps on the contour are found to be largely sufficient).

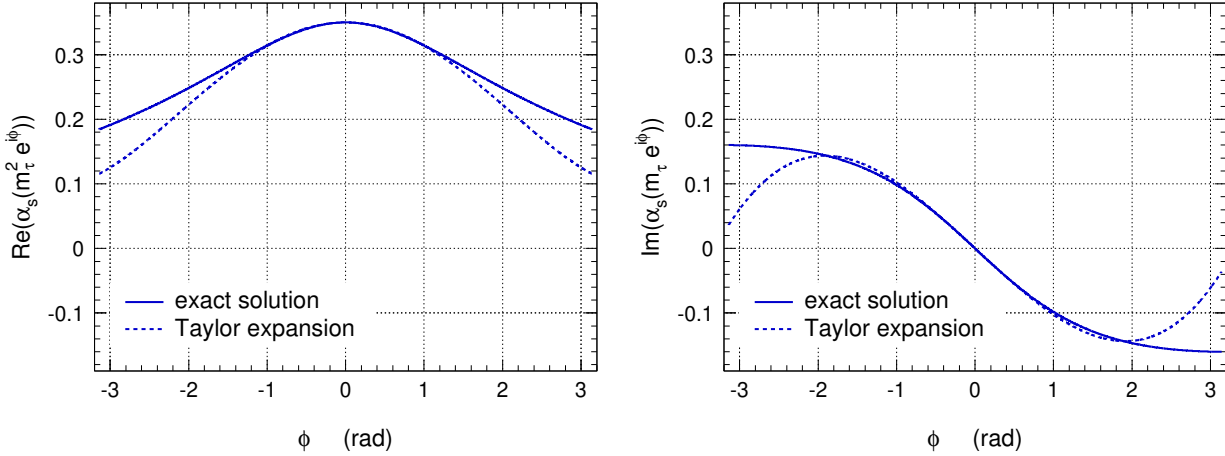


FIG. 23 Comparison between the iteratively evolved $\alpha_s(m_t^2 e^{i\varphi})$ (exact solution) and the fourth-order Taylor expansion (83) on the circle $\varphi = -\pi \dots \pi$ (Menke, 1998). This example uses $\alpha_s(m_t^2) = 0.35$.

4. Effective charge perturbation theory (ECPT)

Inspired by the pioneering work in (Dhar, 1983; Dhar and Gupta, 1984; Grunberg, 1980, 1984; Stevenson, 1981) the use of effective charges to approach the perturbative prediction of R_τ has become quite popular in the recent past (Körner *et al.*, 2001a; Maxwell and Tonge, 1996, 1998; Racza, 1998). The advocated advantage of this technique is that the perturbative prediction of the effective charge is renormalization scheme (RS) and scale invariant since it is a physical observable. The effective τ charge is defined by

$$a_\tau = \delta^{(0)}, \quad (100)$$

and obeys the RGE

$$\frac{da_\tau}{d\ln s} = \beta_\tau(a_\tau) = -a_\tau^2 \sum_{n=0}^{\infty} \beta_{\tau,n} a_\tau^n. \quad (101)$$

The first two terms in the expansion of β_τ are universal (*i.e.*, RS-independent), while the higher order terms must be computed using perturbation theory. The prescription for this computation is obtained from the relation between the renormalization scheme and scale used to obtain the FOPT coefficients in the series (98), and the requirement of RS and scale invariance. Since a_τ is scheme and scale invariant, its evolution coefficients $\beta_{\tau,i}$ have the same property. “*Another way of looking at this is to say that the method of effective charges involves a specific choice of renormalization scheme and scale (...), so that the energy evolution of the observable is identical to the beta-function evolution of the coupling*” (Dinsdale and Maxwell, 2004).

The function β_τ is obtained from the equation

$$\frac{da_\tau}{da_s} = \frac{d\beta_\tau(a_\tau)}{d\beta(a_s)}, \quad (102)$$

which, setting $\xi = 1$, can be rewritten in the form

$$\beta_\tau(a_\tau) = \frac{da_\tau}{d\ln s} = \frac{da_\tau}{da_s} \frac{da_s}{d\ln s} \Big|_{a_s=a_s(a_\tau)} = \frac{da_\tau}{da_s} \beta(a_s) \Big|_{a_s=a_s(a_\tau)}. \quad (103)$$

Inserting Eq. (98) for a_τ on the l.h.s. and the r.h.s. of Eq. (103), and equating the coefficients for each order

in a_s leads to the coefficients¹⁷

$$\beta_{\tau,2} = \beta_2 - \beta_1 c_2 + \beta_0 (-c_2^2 + c_3) , \quad (104)$$

$$\beta_{\tau,3} = \beta_3 - 2\beta_2 c_2 + \beta_1 c_2^2 + 2\beta_0 (2c_2^3 - 3c_2 c_3 + c_4) , \quad (105)$$

$$\begin{aligned} \beta_{\tau,4} = & \beta_4 - 3\beta_3 c_2 + \beta_2 (4c_2^2 - c_3) + \beta_1 (-2c_2 c_3 + c_4) \\ & + \beta_0 (-14c_2^4 + 28c_2^2 c_3 - 5c_3^2 - 12c_2 c_4 + 3c_5) , \end{aligned} \quad (106)$$

where $c_i = K_i + g_i(1)$ (*cf.* Eq. 98) and $\beta_{\tau,0} = \beta_0$, $\beta_{\tau,1} = \beta_1$ because $K_0 = K_1 = 1$. Inserting the known β_i and c_i coefficients, one finds (Körner *et al.*, 2001a)

$$\begin{aligned} \beta_{\tau,2} &= -12.320 , \\ \beta_{\tau,3} &= -182.72 + 4.5 K_4 , \\ \beta_{\tau,4} &= -236.2 + \beta_4 - 40.27 K_4 + 6.75 K_5 , \\ \beta_{\tau,5} &= 16427 - 20.80 \beta_4 + \beta_5 - 521.6 K_4 - 65.79 K_5 + 9 K_6 , \end{aligned} \quad (107)$$

with a noticeable sign alteration for $\beta_{\tau,2}$ (and also for $\beta_{\tau,3}$ if $K_4 < 40$).

Neglecting nonperturbative contributions, one has

$$a_\tau(s_0) = R_{\tau,V+A}(s_0)/(3|V_{ud}|^2) - 1 , \quad (108)$$

which using Eq. (22) and the $|V_{ud}|$ value given in Section IV yields $a_\tau(m_\tau^2) = 0.2219 \pm 0.0055$.

5. Estimating unknown higher order perturbative coefficients

Compared with the $\overline{\text{MS}}$ RGE (76) the $\beta_\tau(a_\tau)$ series is significantly less convergent, taking into account that $a_\tau(m_\tau^2) \simeq 1.8 \times a_s(m_\tau^2)$. This property has been used in the past to estimate an effective K_4^{eff} coefficient, which was found to be $K_4^{\text{eff}} \sim 27$ (Kataev and Starshenko, 1995). It approximates the true value of K_4 in the limit of vanishing higher order contributions. In effect, the derivative of $a_\tau(m_\tau^2)$ with respect to K_4 is large¹⁸

$$\left. \frac{da_\tau(m_\tau^2)}{dK_4} \right|_{a_\tau(m_\tau^2)=0.22, K_4=25} \simeq 0.0020 , \quad (109)$$

so that the precise experimental error on $a_\tau(m_\tau^2)$ allows us to predict K_4 with an accuracy of a few units, if we assume that the subleading contributions can be neglected. However, this assumption is unfounded since, taking naively the unknown higher order coefficients to grow like a geometric series, *i.e.*, $z_n \sim z_{n-1}^2/z_{n-2}$, with $z = \beta, K$, and using the estimate $K_4 = 25$ so that $K_5 \sim 98$, $\beta_{\tau,4} \sim -360$ (with $\beta_4 \sim 222$), one finds

$$\left. \frac{da_\tau(m_\tau^2)}{dK_5} \right|_{a_\tau(m_\tau^2), K_4, K_5, \beta_4, \dots} \simeq 0.0004 , \quad (110)$$

which is not small with respect to (109), in particular considering the coarseness of the assumptions that went into the estimate (110). It is found that even the sixth-order coefficient is not negligible. Assuming the same geometric growth, one would expect $K_6 \sim 395$ with a derivative of $da_\tau(m_\tau^2)/dK_6 \sim 5 \times 10^{-5}$, which appears small. However, considering that the uncertainty on K_6 is at least of the same size as its estimated value (which is probably still optimistic) generates an uncertainty in $a_\tau(m_\tau^2)$ that is equivalent to $\sigma(K_4) \sim 10$.

¹⁷ For completeness we also give the sixth-order coefficient, which is later needed for extrapolation tests

$$\begin{aligned} \beta_{\tau,5} = & \beta_5 - 4\beta_4 c_2 + 2\beta_3 (4c_2^2 - c_3) + 4\beta_2 (-2c_2^3 + c_2 c_3) + \beta_1 (-6c_2^4 + 16c_2^2 c_3 - 3c_3^2 - 8c_2 c_4 + 2c_5) \\ & + 4\beta_0 (12c_2^5 - 30c_2^3 c_3 + 12c_2 c_3^2 + 14c_2^2 c_4 - 4c_3 c_4 - 5c_2 c_5 + c_6) . \end{aligned}$$

¹⁸ One can obtain the solution for $a_\tau(m_\tau^2)$ as a function of the β_τ coefficients without explicitly integrating the RGE (101), by using as fixed point of the differential equation the one-loop solution at $s \rightarrow \infty$, $\Lambda^2 = se^{-1/(\beta_0 a_\tau(s))}$, so that the four-loop $a_\tau(\infty \rightarrow m_\tau^2)$ evolution reproduces the experimental value. This gives $\Lambda = 0.41$ GeV.

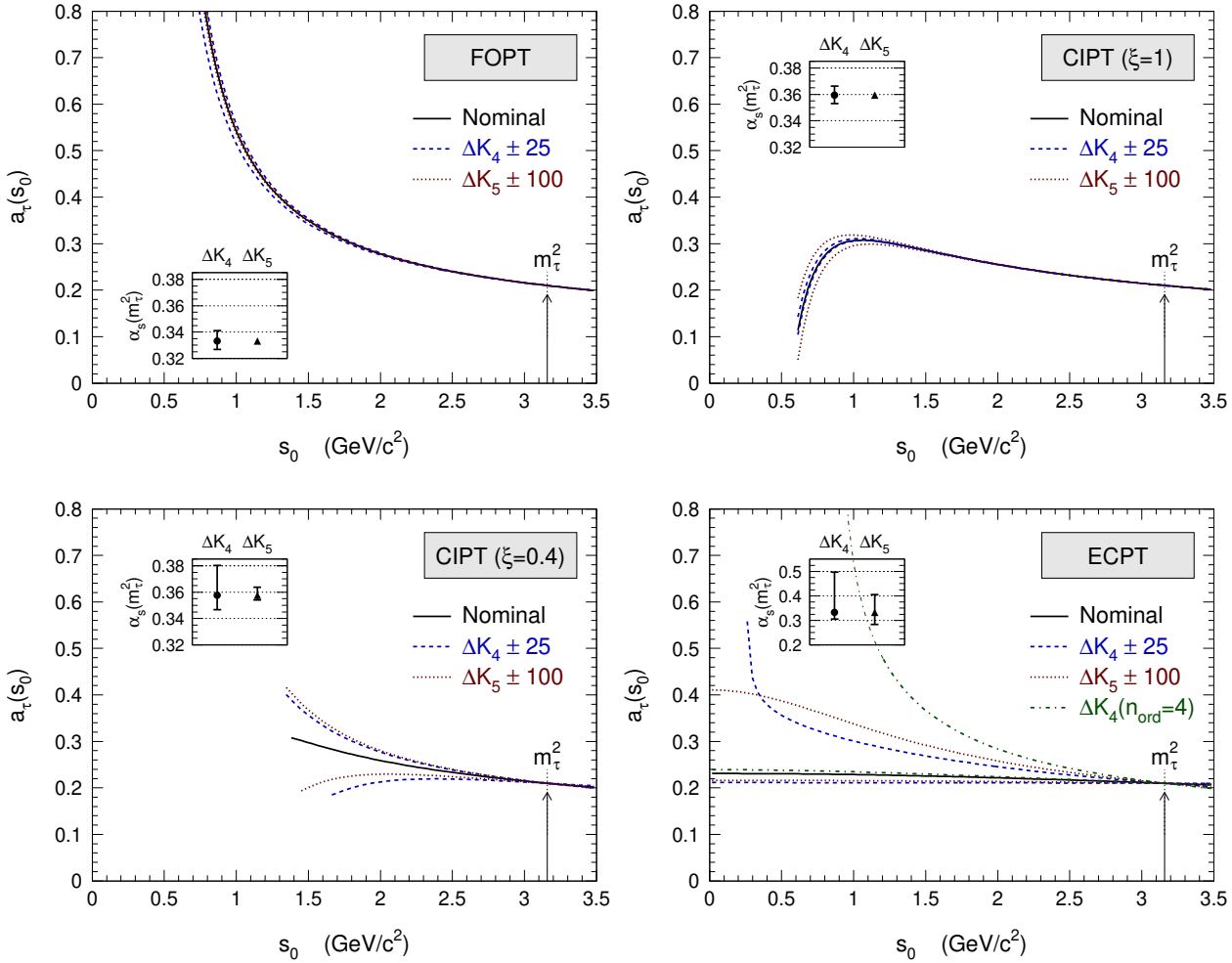


FIG. 24 Evolution of $a_\tau(s_0)$ for the different perturbative methods, and for variations of the unknown higher order perturbative coefficients K_4 (dashed) and K_5 (dotted). All methods are normalized to $a_\tau(m_\tau^2) = 0.22$. The inserted frames give the $\alpha_s(m_\tau^2)$ values derived from this a_τ value in the respective methods. The error bars show the uncertainties, added in quadrature, from the K_4 and K_5 variations quoted on the plots.

Taking correspondingly the fifth-order uncertainty of the order of the estimated value of K_5 , we conclude that the systematic uncertainty on K_4 obtained with the effective charge scheme is at least of the order of $\sigma(K_4) \sim 23$.

Another method to estimate K_4^{eff} has been suggested in (Le Diberder, 1995). It consists of increasing the sensitivity of the CIPT prediction of $\delta^{(0)}$ on K_4 by reducing the renormalization scale ξ in Eq. (95). The result 27 ± 5 is consistent with the one obtained from ECPT. However, these methods are not independent as can be seen in the following. Using the integral (80), and taking $s \rightarrow \infty$ so that $a_\tau, a_s \rightarrow 0$, we can write (Stevenson, 1981)

$$\ln \frac{s}{\Lambda^2} - \ln \frac{s}{\Lambda_\tau^2} = 2 \ln \frac{\Lambda_\tau}{\Lambda} = \frac{1}{\beta_0 a_s(s)} - \frac{1}{\beta_0 a_\tau(s)} + \mathcal{O}(a_s) = c_2 + \mathcal{O}(a_s) , \quad (111)$$

$$\iff \Lambda_\tau \simeq \Lambda e^{c_2/\beta_0} \approx 3.2 \Lambda . \quad (112)$$

Since the asymptotic scale parameters are reciprocal to the scale, transforming FOPT into ECPT is equivalent to reducing the renormalization scale, at lowest order.

In terms of the measurement of $\alpha_s(m_\tau^2)$ the three perturbative methods FOPT, CIPT and ECPT use similar information. However their dependence on the unknown higher order coefficients $K_{n \geq 4}$ can be dramatically

different. Figure 24 shows the evolution of $a_\tau(s_0)$ for FOPT, CIPT with renormalization scales $\xi = 1$ and $\xi = 0.4$, and ECPT, all normalized to $a_\tau(m_\tau^2) = 0.22$. The solid lines correspond to fifth order perturbation theory with assumed $K_4 = 25$, $K_5 = 98$, and for variations of these (dashed and dotted lines). One observes relatively small dependence for FOPT and CIPT with $\xi = 1$, while large and very large effects are found with CIPT ($\xi = 0.4$) and ECPT. The latter effect provides the sensitivity to estimate the unknown coefficients. To better analyze this sensitivity, we have compared the ΔK_4 variation in fifth-order ECPT to the fourth-order effect (dashed-dotted line in the lower right hand plot of Fig. 24). Including the bold estimate for the next order significantly reduces the dependence on the K_4 term. This cancellation becomes obvious when looking at the numerical expansion (107): the K_4 coefficient enters $\beta_{\tau,3}$ and $\beta_{\tau,4}$ with different signs, and with a larger coefficient at fifth order to compensate for the a_τ suppression. A similar behavior is observed for K_5 when turning on the sixth-order term. We conclude that as for the K_4 term, the strong K_5 dependence observed in ECPT is (by part) an artifact of the truncation of the perturbative series, and it is therefore dangerous to use it for an estimate of the unknown coefficients.

The embedded frames in Fig. 24 give the $\alpha_s(m_\tau^2)$ values derived from the given a_τ value in the respective methods. The error bars indicate the uncertainty, added in quadrature, from the K_4 and K_5 variations quoted on the figures. One observes that the difference in α_s between FOPT and CIPT is not covered by the uncertainties on K_4 and K_5 . This is because the main contribution to the difference in these methods is due to the truncation of the *known* higher order terms of the Taylor expansion after the contour integration, rather than due to the unknown coefficients. Due to the good convergence of these series, the dependence on the K_5 coefficient is marginal.

It should be mentioned that a large computational effort is underway with the goal to calculate the K_4 coefficient. The large number of five-loop diagrams needed to calculate the two-point current correlator at this order is somewhat discouraging, however the results on two gauge invariant subsets are already available. The subset of order $\mathcal{O}(\alpha_s^4 n_f^3)$ was evaluated long ago through the summation of renormalon chains (Beneke, 1993), while the much harder subset $\mathcal{O}(\alpha_s^4 n_f^2)$ was recently calculated (Baikov *et al.*, 2002). The known parts amount to about half of the expected K_4 coefficient assuming a geometric growth. Using the results of (Kataev and Starshenko, 1995) for different n_f obtained with the effective charge method, it is possible to compare the n_f^2 estimated term at the α_s^4 order of the Adler function expansion ($3.64 n_f^2$), with the newly computed one ($1.875 n_f^2$). The difference provides a conservative estimate for the uncertainty of the ECPT procedure to predict the full K_4 term, as one could expect the sum of all $\alpha_s^4 n_f^i$ terms to be closer to the true value than the term-by-term comparison. A successful test of the procedure has been performed for K_3 , where all the $\alpha_s^3 n_f^i$ terms are exactly known. The two unknown remaining terms $\mathcal{O}(\alpha_s^4 n_f^1)$ and $\mathcal{O}(\alpha_s^4 n_f^0)$, the direct calculation of which is prevented by the present computing power available to this project, have been estimated (Baikov *et al.*, 2003) to be

$$K_4 = -0.01009 n_f^3 + 1.875 n_f^2 - 31.8 n_f + 105.7, \quad (113)$$

where the first two terms are known exactly. The calculation for $n_f = 3$ yields $K_4 \simeq 27$ with an uncertainty estimated to ± 16 in (Baikov *et al.*, 2003).

6. Infrared behavior of the effective charge

It has been pointed out in (Brodsky *et al.*, 2002) that a physical coupling should have a finite infrared behavior and should therefore not suffer from the Landau-pole that makes the $\overline{\text{MS}}$ (but also momentum subtraction schemes) break down below some scale $\sqrt{s} \sim 1$ GeV. The universal two-loop function $\beta_\tau(a_\tau)$ does however suffer from a singularity at $\sqrt{s} \sim 1.1$ GeV (for $a_\tau(m_\tau^2) = 0.22$). Only adding the negative three-loop coefficient regularizes $\beta_\tau(a_\tau)$ and leads to a freezing $a_\tau(s \rightarrow 0) \simeq 0.62$. Adding higher orders does not qualitatively alter this behavior, however the freezing value is very unstable against variations of the unknown coefficients (which again exhibits the mediocre convergence of the ECPT series). The lower right hand plot of Fig. 24 shows the evolution of $a_\tau(s)$ for different orders and assumptions upon the unknown higher order coefficients.

7. The large- β_0 expansion

Perturbative series in quantum field theory¹⁹

$$R_N = \sum_{n=0}^N r_n \alpha^{n+1} , \quad (114)$$

be they abelian or not, are divergent at $N \rightarrow \infty$ for any value of α . Because the number of Feynman graphs increases at each order n , one expects a factorial growth of the perturbative coefficients of the corresponding S -matrix series

$$r_n \sim K a^n n! n^\gamma , \quad (115)$$

with constant K , a , γ . The divergent behavior of perturbative expansions often has physical significance: it indicates the nonperturbative structure of the vacuum and its excitations. To be a useful approximation of the true value R , the series (114) must be *asymptotic* to R for given α , *i.e.*, it exists a number K_N so that²⁰

$$|R - R_N| < K_{N+1} \alpha^{N+2} . \quad (116)$$

If $r_n \sim K_n$, the best approximation of R is achieved when the series is truncated at its minimal (absolute) term and the truncation error can be roughly estimated by the size of the minimal term. The accuracy in the point of minimal sensitivity depends on the strength of the perturbative expansion parameter (the coupling). The larger it is, the lower the order when minimal sensitivity is reached, and the worse is the approximation. Note that as long as the computed order is below the order of minimal sensitivity, there is no actual difference between a divergent or a convergent series.

A convenient way to deal with this divergence is to consider the Borel transform

$$B[R](t) \equiv \sum_{n=0}^{\infty} \frac{r_n}{n!} t^n , \quad (117)$$

which is believed to have a finite radius of convergence in the t -plane (Mueller, 1993). The n^{th} fixed order perturbation coefficient is then generated by the n^{th} derivative

$$r_n = \left. \frac{d^n B[R](t)}{dt^n} \right|_{t=0} . \quad (118)$$

The explicit factor $n!$ in the denominator of $B[R](t)$ makes the Borel-transformed series much better behaved. Summing up all orders leads to the integral representation²¹

$$R(\alpha) = \int_0^\infty dt e^{-t/\alpha} B[R](t) . \quad (119)$$

If the integral exists, it gives the Borel sum of the original divergent series. Existence requires that $B[R](t)$ has no singularities in the integration range. However, for a factorial behavior akin to Eq. (115) (non-alternating series), the Borel transform is given by $B[R](t) \propto (1 - at)^{-1-\gamma}$. Hence, if γ is positive there exists a singularity $t = 1/a$ so that the integral (119) does not exist. Indeed, “*the divergent behavior of the original series is encoded in the singularities of its Borel transform*” (Beneke, 1999). One notices that the larger a , *i.e.*, the faster diverging the series is, the closer to zero moves the singularity.

¹⁹ The suppression of the constant term in the definition of Eq. (114) is convenient to avoid $1/\alpha$ terms in the definition of the Borel integral (119). It is without consequence for the following discussion.

²⁰ Our discussion of renormalons has greatly benefited from the comprehensive review given in (Beneke, 1999).

²¹ The Borel integral is easily derived by using the integral representation $n! = \int_0^\infty dv \exp(-v) v^n$, and exchanging summation and integration in Eq. (114) (see, *e.g.*, (Lovett-Turner and Maxwell, 1994)). Note however that this interchange is formally not justified in presence of the Landau pole for the coupling constant.

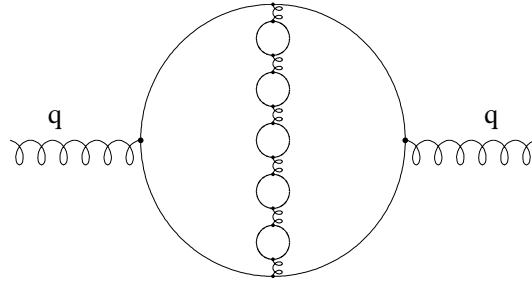


FIG. 25 Multi-fermion loop insertion (renormalons) into a fermion anti-fermion vacuum polarization diagram.

Let us consider a renormalized fermion-loop insertion into a quark-antiquark vacuum polarization diagram (*cf.* one bubble in Fig. 25). Assuming dominance of the $(\beta_0 a_s(-s))^n$ term (the *large- β_0 expansion*), it is possible to resum this chain with a large number of n bubbles. Higher order terms of the β -function are neglected. This assumption is supported empirically by the observation that the β_0 term dominates second order radiative corrections for many observables in the $\overline{\text{MS}}$ scheme (Ball *et al.*, 1995). This procedure provides a *naive non-abelianization* of the theory since lowest order radiative corrections do not include gluon self-coupling. At sufficiently large orders of n vacuum polarization bubbles, the coefficients diverge as

$$r_n \sim C_k n! n^{\gamma_k} (\beta_0/k)^n , \quad (120)$$

with constant C_k, γ_k, k .

Following this line, the Adler function can be expanded as (Beneke and Braun, 1995)

$$D(s) = 1 + a_s \sum_{n=0}^N a_s^n (d_n \beta_0^n + \delta_n) , \quad (121)$$

where the coefficients d_n are computed in terms of fermion bubble diagrams²² (see Fig. 25). The $\overline{\text{MS}}$ Borel transform of Eq. (121) is given by (Beneke, 1993; Broadhurst, 1993)

$$B[D](u) = \frac{32\pi}{3} e^{\frac{5}{3}u} \frac{u}{1 - (1-u)^2} \sum_{k=2}^{\infty} \frac{(-1)^k k}{(k^2 - (1-u)^2)^2} , \quad (122)$$

where $u = -\beta_0 t$, and where we have chosen the renormalization scale to be equal to the momentum scale. Neglecting the corrections δ_n , the series (121) leads to the large- β_0 expansion of $D(s)$. The first elements of the series are

$$\begin{aligned} d_0 &= 1 , & d_1 \beta_0 &= 0.496 , & d_2 \beta_0^2 &= 15.71 , \\ d_3 \beta_0^3 &= 24.83 , & d_4 \beta_0^4 &= 787.8 , & d_5 \beta_0^5 &= -1991 , \end{aligned} \quad (123)$$

²² One identifies the coefficients d_n in Eq. (121) with their leading- n_f pieces $d_n^{[n]}$ in the expression $d_n = d_n^{[n]} n_f^k + \dots + d_n^{[0]}$. It has been shown in (Broadhurst, 1993) that the $d_n^{[n]}$ in $\overline{\text{MS}}$ are given by ($s = \mu^2$)

$$d_n^{[n]} = 2^{1-n} n! \sum_{k=0}^n \left(-\frac{5}{9} \right)^k \frac{\Psi_{n+2-k}^{[n+2-k]}}{k!(n-k)!} ,$$

with the generating function

$$\Psi_m^{[m]} = \frac{3^{2-m}}{2} \left(\frac{d}{dx} \right)^{m-2} P(x) \Big|_{x=1} , \quad \text{and} \quad P(x) = \frac{32}{3(1+x)} \sum_{k=2}^{\infty} \frac{(-1)^k k}{(k^2 - x^2)^2} .$$

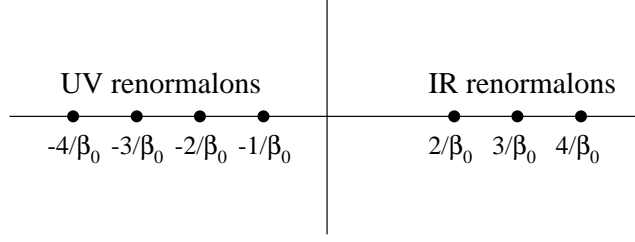


FIG. 26 Ultraviolet (UV) and infrared (IR) renormalons in the Borel plane of the Adler function.

which compare only coarsely with the exact terms (94) where these are known. The Borel transform $B[D](u)$ has singularities on the real axis, which can be distinguished in infrared (IR renormalons) for small virtuality, and ultraviolet singularities (UV renormalons) for high virtuality of the exchanged gluon. One finds an infinite sequence of IR (UV) renormalons at positive (negative) integer u , with the exception of $u = 1$ (see Fig. 26).

The integral (119) may still be solvable in presence of renormalons by acquiring an imaginary part from moving the integration contour above or below the real axis. The associated ambiguity is exponentially small in the expansion parameter α , and is therefore of nonperturbative origin. Correspondingly, the IR poles give rise to ambiguities when one uses the generators (118) to recompute $D(s)$ from its Borel transform. Using in first order

$$a_s(s) = \frac{1}{\beta_0 \ln(s/A^2)}, \quad (124)$$

one obtains for the associated ambiguity for $u = 2, 3, \dots$

$$\Delta D(s) \sim e^{-u/(\beta_0 a_s)} = \left(\frac{A^2}{s} \right)^u. \quad (125)$$

These IR renormalons proportional to $(A^2/s)^u$ are reabsorbed into the nonperturbative terms of the OPE. The absence of a $u = 1$ IR renormalon is thereby related to the impossibility to build a gauge invariant operator of dimension $D = 2$, which is an important property that is exploited for the determination of α_s from R_τ . The lowest IR renormalon is hence of the order $(A^2/s)^2$. On the contrary to the UV renormalons, this term is scale independent and cannot be decreased (Beneke and Zakharov, 1992). It should therefore have physical meaning and can be identified with the gluon condensate $\langle 0 | G_{\mu\nu} G^{\mu\nu} | 0 \rangle$ as the leading infrared contribution to the Adler function. However, while IR renormalons lead to nonperturbative operators for power corrections, it does not necessarily contain all of them. For example, at $D = 4$ one misses the quark condensate $\langle 0 | \bar{q}q | 0 \rangle$, which is generated by chiral symmetry breaking that does not occur in perturbation theory.

Due to asymptotic freedom, governed by the negative sign in front of the RGE β -function, the UV renormalons arise on the negative real axis²³ (on the contrary to QED where they occur on the positive side) so that they are outside the integration range of (119) and insofar harmless, that is, Borel-summable (Mueller, 1993). Let us return for a moment to the series (114) in the large- β_0 expansion. For large n , the factorial growth of the perturbation series is dominated by the contribution of the leading UV renormalon $k = -1$ with alternating coefficients $r_n \sim n! n^\gamma (-\beta_0)^n$. A guess at which order N_{\min} minimal sensitivity is achieved can be obtained from the argument that the series is convergent, *i.e.*, reliable at order $n + 1$ if $\alpha(r_{n+1}/r_n < 1)$. Considering leading IR and UV renormalons only, one finds from the asymptotic behavior (120) $r_{n+1}/r_n \sim n\beta_0/2$ (IR) and $r_{n+1}/r_n \sim -n\beta_0$ (UV). Hence the breakdown of convergence is first caused by the UV renormalon and $N_{\min} \sim 1/(\beta_0 a_s)$ is of order one. A series truncated at finite order brings an intrinsic limitation of accuracy along with it. The associated error is reasonably estimated with the magnitude of the order $N = N_{\min}$ term

²³ In QCD, the presence of IR renormalons implies that nonperturbative corrections should be added to define the theory unambiguously. The same is true for UV renormalons in QED. This corresponds to the observation of large coupling constants in the respective energy regimes.

of the perturbative series. That gives using Eqs. (120) and (124) for the leading UV renormalon

$$\begin{aligned}
|r_N| a_s^N &\sim N! N^\gamma (-\beta_0 a_s)^N \\
&\simeq N^N e^{-N} \sqrt{2\pi N} N^\gamma (-\beta_0 a_s)^N \quad (\text{Stirling formula}) \\
&\sim e^{-1/(\beta_0 a_s)} (\beta_0 a_s)^{-\gamma} \sqrt{2\pi/(\beta_0 \alpha_s)} \\
&\sim \frac{\Lambda^2}{s} \times \text{logarithms} ,
\end{aligned} \tag{126}$$

where we have fixed the renormalization scale at $\mu^2 = s$. The truncation of the perturbative series is accompanied by an uncertainty which scales like $1/s$, *i.e.*, with apparent dimension $D = 2$. This contribution is however not to be confounded with nonperturbative IR renormalon ambiguities. Furthermore it has been shown in (Beneke and Zakharov, 1992) that the truncation uncertainty at N_{\min} scales actually as $\Lambda^2 s / \mu^4$ once the renormalization scheme dependence of Λ is taken into account.

Similarly to Eq. (121) the R_τ FOPT series (98) can be written as

$$\delta^{(0)}(s) = 1 + a_s \sum_{n=0}^N a_s^n (d_n^\tau \beta_0^n + \delta_n^\tau) , \tag{127}$$

where $d_n^\tau \beta_0^n + \delta_n^\tau = K_{n+1} + g_{n+1}(1)$. Inserting Eq. (122) into (91), and taking advantage of the factorized s dependence in the large- β_0 expansion, the Borel transform of (127) is (Beneke, 1993)

$$B[R_\tau](u) = B[D](u) \frac{\sin(\pi u)}{\pi} \left(\frac{1}{u} + \frac{2}{1-u} + \frac{3}{3-u} \frac{1}{4-u} \right) . \tag{128}$$

The first elements of the series are

$$\begin{aligned}
d_0^\tau &= 1 , & d_1^\tau \beta_0 &= 5.119 , & d_2^\tau \beta_0^2 &= 28.78 , \\
d_3^\tau \beta_0^3 &= 156.6 , & d_4^\tau \beta_0^4 &= 900.9 , & d_5^\tau \beta_0^5 &= 4867 .
\end{aligned} \tag{129}$$

They compare reasonably well with the exact terms (99) where these are known. In this approach, the unknown fixed-order fourth-order coefficient is estimated to be $K_4 \sim 79$, which is significantly larger than the estimate based on ECPT, and also larger than the one obtained from the large- β_0 expansion of the Adler function (123).

Apart from the conceptual interest in the study of renormalons, the main question regarding the concrete use of the large- β_0 expansion certainly is: how large are the uncertainties? From Eq. (129) we see that the series is positive and that minimal sensitivity is reached at $n \sim 5$. On the other hand, the resummation of the known $g_n(\xi)$ coefficients (99) shows that large negative coefficients occur at higher order FOPT so that one would need a far larger than a geometric growth of the K_n coefficients to keep the series positive. A direct comparison between the large- β_0 expansion coefficients for the Adler function (123) with the exact calculation (94) reveals an oscillating behavior of the large- β_0 series, *i.e.*, small d_n coefficients for n -even and large d_n for n -odd. For example, the large- β_0 d_3 coefficient is substantially overestimated. One also has to worry about important contributions from the d_5 term, which is found to be 788. As a consequence, our conclusion is that the uncertainties associated with the large- β_0 expansion are not under sufficient control to improve the perturbative prediction of R_τ . It is also an unreliable estimator of the uncertainty of the perturbative series.

8. Comparison of the perturbative methods

Some comparisons between the fixed-order PT methods have already been given for the discussion of the estimate of the unknown higher order coefficients in Section VII.B.5. The slow convergence of ECPT (and CIPT at small renormalization scales, $\xi \ll 1$) has been pointed out in this respect. To further study the convergence of the perturbative series, we give in Table VI the contributions of the different orders in PT to $\delta^{(0)}$ for the various approaches and using $\alpha_s(m_\tau^2) = 0.35$. We assumed here $K_4 = 25$ and a geometric growth of all other unknown PT and RGE coefficients. In the case of CIPT the results are given for the various techniques used to evolve $\alpha_s(s_0 e^{i\varphi})$: the truncated Taylor expansion (83), Runge-Kutta integration of the RGE with $\xi = 1$, and Runge-Kutta integration with $\xi = 0.4$.

TABLE VI Massless perturbative contribution to $R_\tau(m_\tau^2)$ for the various methods considered, and at orders $n \geq 1$ with $\alpha_s(m_\tau^2) = 0.35$. The value of K_4 is set to 25, while all unknown higher order $K_{n>4}$ and $\beta_{n>3}$ coefficients are assumed to follow a geometric growth.

Pert. Method	δ^0							
	$n = 1$	$n = 2$	$n = 3$	$(n = 4)$	$(n = 5)$	$(n = 6)$	$\sum_{n=1}^4$	$\sum_{n=1}^6$
FOPT ($\xi = 1$)	0.1114	0.0646	0.0365	0.0159	0.0010	-0.0086	0.2283	0.2208
CIPT (Taylor RGE, $\xi = 1$)	0.1573	0.0317	0.0126	0.0042	0.0011	0.0001	0.2058	0.2070
CIPT (full RGE, $\xi = 1$)	0.1524	0.0311	0.0129	0.0046	0.0013	0.0002	0.2009	0.2025
CIPT (full RGE, $\xi = 0.4$)	0.2166	-0.0133	0.0006	-0.0007	0.0010	-0.0007	0.2032	0.2048
ECPT	0.1442	0.2187	-0.1195	-0.0344	-0.0160	-0.0120	0.2090	0.1810
Large- β_0 expansion	0.1114	0.0635	0.0398	0.0241	0.0155	0.0093	0.2388	0.2636

As advocated in (Le Diberder and Pich, 1992a), faster convergence is observed for CIPT compared to FOPT yielding a significantly smaller error associated with the renormalization scale ambiguity (while, somewhat counter intuitive, the uncertainty due to the unknown K_4 and higher order coefficients is similar in both approaches). Our coarse extrapolation of the higher order coefficients could indicate that minimal sensitivity is reached at $n \sim 5$ for FOPT, while the series further converges for CIPT. Although the Taylor expansion in the CIPT integral exhibits significant deviations from the exact solution on the integration circle (*cf.* Fig. 23), the actual numerical effect from this on $\delta^{(0)}$ is small (*cf.* second and third column in Table VI). As discussed in Section VII.B.4, the convergence of the ECPT series is much worse than for FOPT and CIPT. Consequently, the difference between truncation at $n = 4$ and $n = 6$ is expected to be significant. A similar behavior is observed for the large- β_0 expansion.

The CIPT series is found to be better behaved than FOPT (as well as ECPT) and is therefore to be preferred for the numerical analysis of the τ hadronic width. As a matter of fact, the difference in the result observed when using a Taylor expansion and truncating the perturbative series after integrating along the contour (FOPT) with the exact result at given order (CIPT) is exhibiting the incompleteness of the perturbative series. However, it is even worse than that since large known coefficients are neglected in FOPT so that the difference between CIPT and FOPT is actually overstating the perturbative truncation uncertainty. This can be verified by studying the behavior of this difference for the various orders in perturbation theory given in Table VI. The CIPT-vs.-FOPT discrepancy increases with the addition of each order, up to order four where a maximum is reached. Adding the fifth order does not reduce the effect, and only beyond fifth order the two evaluations become asymptotic to each other. As a consequence varying the unknown higher order coefficients and using the difference between FOPT and CIPT as indicator of the theoretical uncertainties overemphasizes the truncation effect.

9. Quark-mass and nonperturbative contributions

Following SVZ (Shifman *et al.*, 1979), the first contribution to R_τ beyond the $D = 0$ perturbative expansion is the non-dynamical quark mass correction of dimension²⁴ $D = 2$, *i.e.*, corrections in powers of $1/s_0$. The leading $D = 2$ corrections induced by the light-quark masses are computed using the running quark masses evaluated at the two-loop level. Evaluation of the contour integral in FOPT leads to (Braaten *et al.*, 1992)

$$\begin{aligned} \delta_{ij,V/A}^{(2\text{-mass})} &= -8 \left(1 + \frac{16}{3}a_s(s_0)\right) \frac{m_i^2(s_0) + m_j^2(s_0)}{s_0} \\ &\pm 4 \left(1 + \frac{25}{3}a_s(s_0)\right) \frac{m_i(s_0)m_j(s_0)}{s_0}, \end{aligned} \quad (130)$$

²⁴ Corrections of dimension $D = 2$ refer to the mass dependence of the perturbative OPE coefficients of the unit operator.

where $m_i(s_0)$ are the running quark masses evaluated at the scale s_0 using the RGE γ -function (77). The following values are used by ALEPH for the renormalization group invariant quark mass parameters \hat{m}_i defined in (82)

$$\hat{m}_u = (8.7 \pm 1.5) \text{ MeV} , \quad \hat{m}_d = (15.4 \pm 1.5) \text{ MeV} , \quad \hat{m}_s = (270 \pm 30) \text{ MeV} . \quad (131)$$

The dimension $D = 4$ operators have dynamical contributions from the gluon condensate $\langle a_s GG \rangle$ and light u, d quark condensates $\langle m_i q_i q_j \rangle$, which are the matrix elements of the gluon field strength-squared and the scalar quark densities, respectively. Remaining $D = 4$ operators are running quark masses to the fourth power. Inserting the Wilson coefficients of these operators (Becchi *et al.*, 1981; Broadhurst, 1981; Chetyrkin *et al.*, 1985; Generalis, 1989) in the contour integral one obtains (Braaten *et al.*, 1992)

$$\begin{aligned} \delta_{ij,V/A}^{(4)} = & \frac{11}{4} \pi^2 a_s^2(s_0) \frac{\langle a_s GG \rangle}{s_0^2} \\ & + 16\pi^2 \left[1 + \frac{9}{2} a_s^2(s_0) \right] \frac{\langle (m_i \mp m_j) (\bar{q}_i q_i \mp \bar{q}_j q_j) \rangle}{s_0^2} \\ & - 18\pi^2 a_s^2(s_0) \left[\frac{\langle m_i \bar{q}_i q_i + m_j \bar{q}_j q_j \rangle}{s_0^2} + \frac{4}{9} \sum_k \frac{\langle m_k \bar{q}_k q_k \rangle}{s_0^2} \right] \\ & - \left[\frac{48}{7} \frac{1}{a_s(s_0)} - \frac{22}{7} \right] \frac{\langle m_i(s_0) \mp m_j(s_0) \rangle \langle m_i^3(s_0) \mp m_j^3(s_0) \rangle}{s_0^2} \\ & \pm 6 \frac{\langle m_i(s_0) m_j(s_0) \rangle \langle m_i(s_0) \mp m_j(s_0) \rangle^2}{s_0^2} + 36 \frac{\langle m_i^2(s_0) m_j^2(s_0) \rangle}{s_0^2} . \end{aligned} \quad (132)$$

Where two signs are given the upper (lower) one is for V (A). The gluon condensate vanishes in first order $\alpha_s(s_0)$. However, there appear second order terms in the Wilson coefficients due to the s dependence of a_s , which after integration becomes a_s^2 .

The contributions from dimension $D = 6$ operators are complex. The most important operators arise from four-quark dynamical effects of the form $\bar{q}_i \Gamma_1 q_j \bar{q}_k \Gamma_2 q_l$. Other operators, such as the triple gluon condensate whose Wilson coefficient vanishes at order α_s , or those which are suppressed by powers of quark masses, are neglected in the evaluation of the contour integrals performed in (Braaten *et al.*, 1992). The large number of independent operators of the four-quark type occurring in the $D = 6$ term can be reduced by means of the *factorization* (or *vacuum saturation*) assumption (Shifman *et al.*, 1979) to leading order α_s . The operators are then expressed as products of scale dependent two-quark condensates $\alpha_s(\mu) \langle \bar{q}_i q_i(\mu) \rangle \langle \bar{q}_j q_j(\mu) \rangle$. To take into account possible deviations from the vacuum saturation assumption, one can introduce an effective scale independent operator $\rho \alpha_s \langle \bar{q} q \rangle^2$ that replaces the above product. The effective $D = 6$ term obtained in this way is (Braaten *et al.*, 1992)

$$\delta_{ij,V/A}^{(6)} \simeq \left(\begin{array}{c} -7 \\ -11 \end{array} \right) \frac{256\pi^4}{27} \frac{\rho \alpha_s \langle \bar{q} q \rangle^2}{s_0^3} , \quad (133)$$

predicting a different sign and hence a partial cancellation between vector and axial-vector contributions²⁵

The dimension $D = 8$ contribution has a structure of nontrivial quark-quark, quark-gluon and four-gluon condensates whose explicit form is given in (Broadhurst, 1985). For the theoretical prediction of R_τ it is custom to absorb the complete long and short distance part into the scale invariant phenomenological $D = 8$ operator $\langle \mathcal{O}_8 \rangle$, which is fit simultaneously with α_s and the other unknown nonperturbative operators to date.

Higher order contributions from $D \geq 10$ operators are expected to be small as, equivalent to the gluon condensate, constant terms and terms in leading order α_s vanish in Eq. (85) after integrating over the contour.

²⁵ It has been pointed out in (Chetyrkin and Kwiatkowski, 1993) that Eq. (133) assumes that the same ρ parameter can be used for both vector and axial-vector contributions.

C. Results

It was shown in (Le Diberder and Pich, 1992b) that one can exploit the shape of the spectral functions to obtain additional constraints on $\alpha_s(s_0)$ and—more importantly—on the nonperturbative effective operators. The τ *spectral moments* at $s_0 = m_\tau^2$ are defined by

$$R_{\tau,V/A}^{k\ell} = \int_0^{m_\tau^2} ds \left(1 - \frac{s}{m_\tau^2}\right)^k \left(\frac{s}{m_\tau^2}\right)^\ell \frac{dR_{\tau,V/A}}{ds} , \quad (134)$$

where $R_{\tau,V/A}^{00} = R_{\tau,V/A}$. The factor $(1 - s/m_\tau^2)^k$ suppresses the integrand at the crossing of the positive real axis where the validity of the OPE less certain (Braaten, 1988) and the experimental accuracy is statistically limited. Its counterpart $(s/m_\tau^2)^\ell$ projects upon higher energies. The spectral information is used to fit simultaneously $\alpha_s(m_\tau^2)$ and the effective operators $\langle a_s GG \rangle$, $\rho \alpha_s \langle \bar{q}q \rangle^2$ and $\langle \mathcal{O}_D \rangle$ for dimension $D = 4, 6$ and 8 , respectively. Due to the intrinsic experimental correlations only five moments are used as input to the fit.

In analogy to R_τ , the contributions to the moments originating from perturbative and nonperturbative QCD are decomposed through the OPE

$$R_{\tau,V/A}^{k\ell} = \frac{3}{2} |V_{ud}|^2 S_{EW} \left(1 + \delta^{(0,k\ell)} + \delta'_{EW} + \delta_{ud,V/A}^{(2-\text{mass},k\ell)} + \sum_{D=4,6,\dots} \delta_{ud,V/A}^{(D,k\ell)} \right) . \quad (135)$$

The prediction of the perturbative contribution takes the form

$$\delta^{(0,k\ell)} = \sum_{n=1}^3 \tilde{K}_n(\xi) A^{(n,k\ell)}(a_s) , \quad (136)$$

with the functions

$$A^{(n,k\ell)}(a_s) = \frac{1}{2\pi i} \oint_{|s|=m_\tau^2} \frac{ds}{s} \left[2\Gamma(3+k) \left(\frac{\Gamma(1+\ell)}{\Gamma(4+k+\ell)} + 2 \frac{\Gamma(2+\ell)}{\Gamma(5+k+\ell)} \right) - I\left(\frac{s}{s_0}, 1+\ell, 3+k\right) - 2I\left(\frac{s}{s_0}, 2+\ell, 3+k\right) \right] a_s^n(-\xi s) , \quad (137)$$

which make use of the elementary integrals $I(\gamma, a, b) = \int_0^\gamma t^{a-1} (1-t)^{b-1} dt$. The contour integrals are numerically solved for the running $a_s(-\xi s)$ (CIPT).

In the chiral limit²⁶ and neglecting the small logarithmic s dependence of the Wilson coefficients, the dimension D nonperturbative contributions in Expression (135) read

$$\delta_{ud,V/A}^{(D,k\ell)} = 8\pi^2 \left(\begin{array}{cccccc} (D=2) & (D=4) & (D=6) & (D=8) & (D=10) & (k,\ell) \\ 1 & 0 & -3 & -2 & 0 & (0,0) \\ 1 & 1 & -3 & -5 & -2 & (1,0) \\ 0 & -1 & -1 & 3 & 5 & (1,1) \\ 0 & 0 & 1 & 1 & -3 & (1,2) \\ 0 & 0 & 0 & -1 & -1 & (1,3) \end{array} \right) \sum_{\text{dim}\mathcal{O}=D} C^{(1+0)}(\mu) \frac{\langle \mathcal{O}_D(\mu) \rangle_{V/A}}{m_\tau^D} , \quad (138)$$

where the matrix is defined by the choice of the coefficients for the moments $k = 1$, $\ell = 0, 1, 2, 3$ and the corresponding dimension D . For completeness, we also give the coefficients for dimension $D = 10$, which is not considered by the experiments since they do not contribute to $R_{\tau,V/A}^{00}$ at leading order. With increasing weight ℓ the contributions from low dimensional operators vanish. For example, the only nonperturbative contribution to the moment $R_{\tau,V/A}^{13}$ stems from dimension $D = 8$ and beyond. Hence, in a fit using spectral

²⁶ In the chiral limit, vector and axial-vector currents are conserved so that $s\Pi_V^{(0)} = s\Pi_A^{(0)} = 0$.

moments, $D = 8$ will be determined by $R_{\tau,V/A}^{13}$. This observation is in some sense a “paradox”, as higher moments project upon higher masses on the contrary to R_τ and the spirit of the OPE, where the higher dimension terms are enhanced at small s_0 .

For practical purpose it is more convenient to define moments that are normalized to the corresponding $R_{\tau,V/A}$ in order to decouple the normalization from the shape of the τ spectral functions

$$D_{\tau,V/A}^{kl} = \frac{R_{\tau,V/A}^{kl}}{R_{\tau,V/A}}. \quad (139)$$

The two sets of experimentally almost uncorrelated observables— $R_{\tau,V/A}$ on one hand and the spectral moments on the other hand—yield independent constraints on $\alpha_s(m_\tau^2)$ and thus provide an important test of consistency. The correlation between these observables is completely negligible in the $V + A$ case where $R_{\tau,V+A}$ is calculated from the difference $R_\tau - R_{\tau,S}$, which has no correlation with the hadronic invariant mass spectrum. One experimentally obtains the $D_{\tau,V/A}^{kl}$ by integrating the weighed normalized invariant mass-squared spectrum. The corresponding theoretical predictions are easily modified.

1. The ALEPH determination of $\alpha_s(m_\tau^2)$ and nonperturbative contributions

Combined fits to experimental spectral moments and the extraction of $\alpha_s(m_\tau^2)$ together with the leading nonperturbative operators have been performed by ALEPH, CLEO and OPAL (ALEPH Coll., 1993, 1998c, 2005; CLEO Coll., 1995b; OPAL Coll., 1999b) using similar strategies and inputs. Let us follow in this report the most recent analysis performed by the ALEPH collaboration (ALEPH Coll., 2005).

Since the determination of α_s should be model-independent, the experiments proceed by fitting simultaneously the nonperturbative operators, which is possible since the correlations between these and α_s turn out to be small enough. The theoretical framework and its intrinsic uncertainties were the subject of the previous section. Minor additional contributions originate from the CKM matrix element $|V_{ud}|$, the electroweak radiative correction factor S_{EW} , the light quark masses $m_{u,d}$ and the quark condensates (Section VII.B.9). The largest contributions have their origin in the truncation of the perturbative expansion. Although it introduces some double-counting for the systematic error, the procedure used in (ALEPH Coll., 2005) considers separate variations of the unknown higher order coefficient K_4 and the renormalization scale. The renormalization scale is varied around m_τ from 1.1 to 2.5 GeV with the variation over half of the range taken as systematic uncertainty. Taking advantage of the new theoretical developments discussed above, the value $K_4 = 25 \pm 25$ is used in (ALEPH Coll., 2005).

The fit minimizes the χ^2 of the differences between measured and adjusted quantities contracted with the inverse of the sum of the experimental and theoretical covariance matrices. The results of (ALEPH Coll., 2005) are listed in Table VII, separately for the CIPT and FOPT prescriptions for the perturbative term. Table VIII gives the corresponding correlation matrices of the fit parameters. The limited number of observables and the strong correlations between the spectral moments explain the large correlations observed, especially between the nonperturbative operators, which are solely determined by the shapes of the spectral functions. The precision of $\alpha_s(m_\tau^2)$ obtained with the two perturbative methods employed is comparable, however their central values differ by 0.01–0.02, which is larger than the theoretical errors assigned. The $\delta^{(2)}$ term is theoretical only with quark masses varying within their allowed ranges (131). The quark condensates in the $\delta^{(4)}$ term are obtained from PCAC, while the gluon condensate is determined by the fit. The main contributions to the theoretical uncertainty on $\alpha_s(m_\tau^2)$ are listed in Table IX. The fact that the χ^2 value of the axial-vector fit is better with FOPT than with CIPT should not—in our view— affect the conclusion in favor of the latter method, reached in Sections VII.B.8 and VII.B.3 on the basis of a better perturbative behavior, but it may require further studies.

The final result on $\alpha_s(m_\tau^2)$ given by (ALEPH Coll., 2005) is taken as the arithmetic average of the CIPT and FOPT values given in Table VII, with half of their difference added as additional theoretical error $\alpha_s(m_\tau^2) = 0.340 \pm 0.005_{\text{exp}} \pm 0.014_{\text{th}}$. The first error accounts for the experimental uncertainty and the second error gives the uncertainty related to the theoretical prediction of the spectral moments including the ambiguity between CIPT and FOPT.

There is a remarkable agreement within statistical errors between the $\alpha_s(m_\tau^2)$ determinations using the vector and axial-vector data. This provides an important consistency check of the results, since the two corresponding spectral functions are experimentally independent and manifest a quite different resonant behavior. The results are displayed in Fig. 27.

TABLE VII Fit results (ALEPH Coll., 2005) for $\alpha_s(m_\tau^2)$ and the nonperturbative contributions for vector, axial-vector and $V + A$ combined fits using the corresponding experimental spectral moments as input parameters. Where two errors are given the first is experimental and the second theoretical. The $\delta^{(2)}$ term is theoretical only with quark masses varying within their allowed ranges (see text). The quark condensates in the $\delta^{(4)}$ term are obtained from PCAC, while the gluon condensate is determined by the fit. The total nonperturbative contribution is the sum $\delta_{\text{NP}} = \delta^{(4)} + \delta^{(6)} + \delta^{(8)}$. Results are given separately for the CIPT and FOPT perturbative prescriptions.

Parameter	Vector (V)	Axial-Vector (A)	$V + A$
$\alpha_s(m_\tau^2)$ (CIPT)	$0.355 \pm 0.008 \pm 0.009$	$0.333 \pm 0.009 \pm 0.009$	$0.350 \pm 0.005 \pm 0.009$
$\alpha_s(m_\tau^2)$ (FOPT)	$0.331 \pm 0.006 \pm 0.012$	$0.327 \pm 0.007 \pm 0.012$	$0.331 \pm 0.004 \pm 0.012$
$\delta^{(2)}$ (CIPT)	$(-3.3 \pm 3.0) \times 10^{-4}$	$(-5.1 \pm 3.0) \times 10^{-4}$	$(-4.4 \pm 2.0) \times 10^{-4}$
$\delta^{(2)}$ (FOPT)	$(-3.0 \pm 3.0) \times 10^{-4}$	$(-5.0 \pm 3.0) \times 10^{-4}$	$(-4.0 \pm 2.0) \times 10^{-4}$
$\langle a_s GG \rangle$ (GeV 4) (CIPT)	$(0.4 \pm 0.3) \times 10^{-2}$	$(-1.3 \pm 0.4) \times 10^{-2}$	$(-0.5 \pm 0.3) \times 10^{-2}$
$\langle a_s GG \rangle$ (GeV 4) (FOPT)	$(1.5 \pm 0.3) \times 10^{-2}$	$(-0.2 \pm 0.4) \times 10^{-2}$	$(0.6 \pm 0.2) \times 10^{-2}$
$\delta^{(4)}$ (CIPT)	$(4.1 \pm 1.2) \times 10^{-4}$	$(-5.7 \pm 0.1) \times 10^{-3}$	$(-2.7 \pm 0.1) \times 10^{-3}$
$\delta^{(4)}$ (FOPT)	$(6.8 \pm 1.0) \times 10^{-4}$	$(-5.3 \pm 0.1) \times 10^{-3}$	$(-2.4 \pm 0.1) \times 10^{-3}$
$\delta^{(6)}$ (CIPT)	$(2.85 \pm 0.22) \times 10^{-2}$	$(-3.23 \pm 0.26) \times 10^{-2}$	$(-2.1 \pm 2.2) \times 10^{-3}$
$\delta^{(6)}$ (FOPT)	$(2.70 \pm 0.25) \times 10^{-2}$	$(-2.96 \pm 0.31) \times 10^{-2}$	$(-1.6 \pm 2.5) \times 10^{-3}$
$\delta^{(8)}$ (CIPT)	$(-9.0 \pm 0.5) \times 10^{-3}$	$(8.9 \pm 0.6) \times 10^{-3}$	$(-0.3 \pm 4.8) \times 10^{-4}$
$\delta^{(8)}$ (FOPT)	$(-8.6 \pm 0.6) \times 10^{-3}$	$(8.6 \pm 0.6) \times 10^{-3}$	$(1.2 \pm 5.2) \times 10^{-4}$
Total δ_{NP} (CIPT)	$(1.99 \pm 0.27) \times 10^{-2}$	$(-2.91 \pm 0.20) \times 10^{-2}$	$(-4.8 \pm 1.7) \times 10^{-3}$
Total δ_{NP} (FOPT)	$(1.91 \pm 0.31) \times 10^{-2}$	$(-2.63 \pm 0.25) \times 10^{-2}$	$(-3.9 \pm 2.0) \times 10^{-3}$
χ^2/DF (CIPT)	0.52	5.71	3.84
χ^2/DF (FOPT)	0.01	0.63	0.11

TABLE VIII Correlation matrices for the fits given in Table VII for vector (left table), axial-vector (middle) and $V + A$ (right table) using CIPT (ALEPH Coll., 2005).

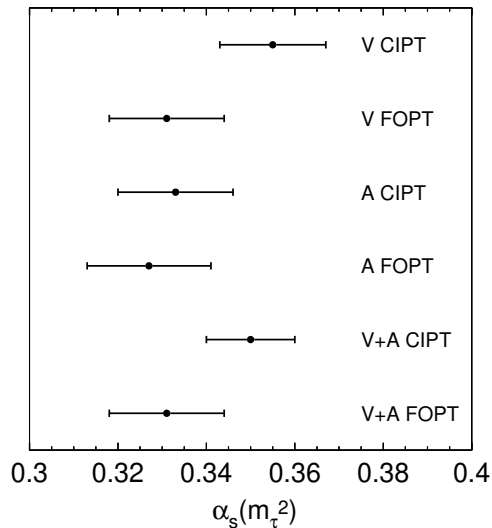
Parameter	$\langle a_s GG \rangle_V$	$\delta_V^{(6)}$	$\delta_V^{(8)}$	$\langle a_s GG \rangle_A$	$\delta_A^{(6)}$	$\delta_A^{(8)}$	$\langle a_s GG \rangle_{V+A}$	$\delta_{V+A}^{(6)}$	$\delta_{V+A}^{(8)}$
$\alpha_s(m_\tau^2)$	-0.39	-0.28	-0.34	-0.57	0.52	-0.55	-0.37	0.38	-0.45
$\langle a_s GG \rangle$	1	0.44	0.46	1	-0.81	0.80	1	-0.65	0.65
$\delta^{(6)}$	-	1	-0.98	-	1	-0.99	-	1	-0.98
$\delta^{(8)}$	-	-	1	-	-	1	-	-	1

The advantage of separating the vector and axial-vector channels and comparing to the inclusive $V + A$ fit becomes obvious in the adjustment of the leading nonperturbative contributions of dimension $D = 6$ and $D = 8$, which approximately cancel in the inclusive sum. This cancellation of the nonperturbative terms increases the confidence in the $\alpha_s(m_\tau^2)$ determination from the inclusive $V + A$ observables. The gluon condensate is determined by the first $k = 1$, $\ell = 0, 1$ moments, which receive lowest order contributions. It is observed that the values obtained in the V and A fits are not very consistent, which could indicate problems in the validity of the OPE approach used once the nonperturbative terms become significant. Taking the value obtained in the $V + A$ fit, where nonperturbative effects are small, and adding as systematic uncertainties half of the difference between the vector and axial-vector fits as well as between the CIPT and FOPT results, ALEPH measures the gluon condensate to be

$$\langle a_s GG \rangle = (0.001 \pm 0.012) \text{ GeV}^4. \quad (140)$$

TABLE IX Sources of theoretical uncertainties and their impact on $R_{\tau,V+A}$ and $\alpha_s(m_\tau^2)$ (ALEPH Coll., 2005).

Error source	Value $\pm \Delta^{\text{th}}$	$\Delta^{\text{th}} R_{\tau,V+A}$		$\Delta^{\text{th}} \alpha_s(m_\tau^2)$	
		CIPT	FOPT	CIPT	FOPT
S_{EW}	1.0198 ± 0.0006		0.002		0.001
$ V_{ud} $	0.9745 ± 0.0004		0.002		0.001
K_4	25 ± 25	0.015	0.009	0.007	0.003
R-scale μ	$m_\tau^2 \pm 2 \text{ GeV}^2$	0.012	0.035	0.006	0.011
Total errors		0.019	0.036	0.009	0.012

FIG. 27 Results for $\alpha_s(m_\tau^2)$ from the fits of $R_{\tau,V,A,V+A}$ and the moments $D_{V,A,V+A}^{k\ell}$ using the CIPT and FOPT perturbative expansions. The measurements are correlated due to the theoretical errors (see Table VII).

This result does not provide evidence for a nonzero gluon condensate, but it is consistent with and has comparable accuracy to the independent value obtained using charmonium sum rules and e^+e^- data in the charm region, $(0.011 \pm 0.009) \text{ GeV}^4$ in a combined determination with the c quark mass (Ioffe and Zyablyuk, 2003).

The $D = 6, 8$ nonperturbative contributions are obtained after averaging the FOPT and CIPT values:

$$\begin{aligned} \delta_V^{(6)} &= (2.8 \pm 0.3) \times 10^{-2}, & \delta_V^{(8)} &= (-8.8 \pm 0.6) \times 10^{-3}, \\ \delta_A^{(6)} &= (-3.1 \pm 0.3) \times 10^{-2}, & \delta_A^{(8)} &= (8.7 \pm 0.6) \times 10^{-3}, \\ \delta_{V+A}^{(6)} &= (-1.8 \pm 2.4) \times 10^{-3}, & \delta_{V+A}^{(8)} &= (0.5 \pm 5.1) \times 10^{-4}. \end{aligned} \quad (141)$$

The remarkable feature is the approximate cancellation of these contributions in the $V+A$ case, both for $D = 6$ and $D = 8$. This property was predicted (Braaten *et al.*, 1992) for $D = 6$ using the simplifying assumption of vacuum saturation for the matrix elements of four-quark operators, yielding $\delta_V^{(6)}/\delta_A^{(6)} = -7/11 = -0.64$, in fair agreement with the above results which reads -0.90 ± 0.18 . The estimate (Braaten *et al.*, 1992) for $\delta_V^{(6)} = (2.5 \pm 1.3) \times 10^{-2}$ agrees well with the experimental result.

The total nonperturbative $V+A$ correction, $\delta_{\text{NP},V+A} = (-4.3 \pm 1.9) \times 10^{-3}$, is an order-of-magnitude smaller than the corresponding values in the V and A components, $\delta_{\text{NP},V} = (2.0 \pm 0.3) \times 10^{-2}$ and $\delta_{\text{NP},A} = (-2.8 \pm 0.3) \times 10^{-2}$.

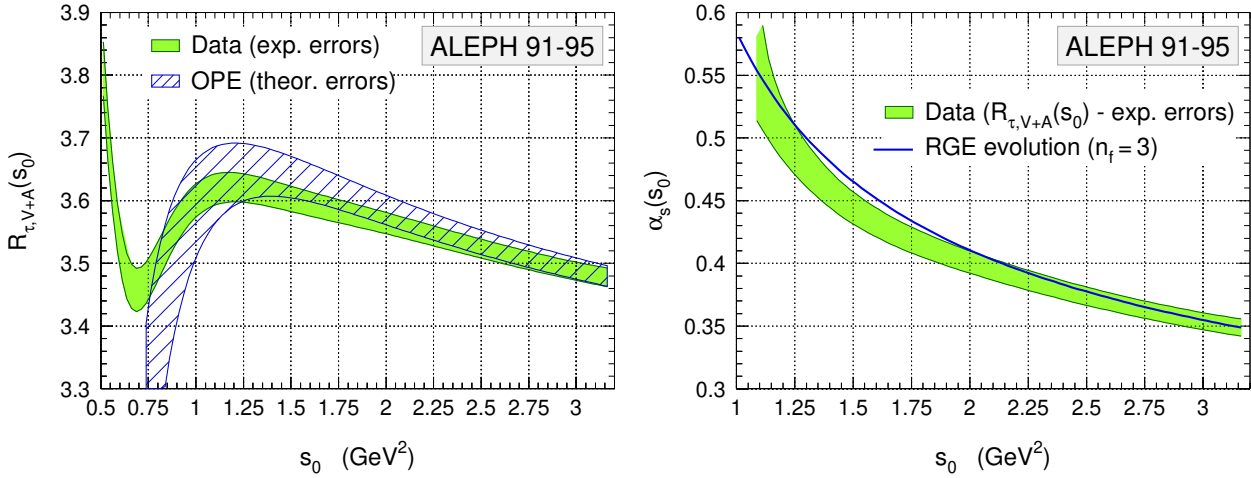


FIG. 28 Left: The ratio $R_{\tau,V+A}$ versus the square “ τ mass” s_0 . The curves are plotted as error bands to emphasize their strong point-to-point correlations in s_0 . Also shown is the theoretical prediction using CIPT and the results for $R_{\tau,V+A}$ and the nonperturbative terms from Table VII. Right: The running of $\alpha_s(s_0)$ obtained from the fit of the theoretical prediction to $R_{\tau,V+A}(s_0)$ using CIPT. The shaded band shows the data including only experimental errors. The curve gives the four-loop RGE evolution for three flavors.

2. The OPAL results

The OPAL analysis (OPAL Coll., 1999b) makes use of the spectral functions shown in Fig. 7 and provides also a complete description in terms of QCD of their vector and axial-vector data. It proceeds along very similar lines as the ALEPH analysis, with the difference that OPAL has chosen to quote their results separately for three prescriptions for the perturbative expansion, respectively CIPT, FOPT and with renormalon chains, *i.e.*

$$\alpha_s(m_\tau^2) = \begin{cases} 0.348 \pm 0.009_{\text{exp}} \pm 0.019_{\text{th}} & \text{CIPT ,} \\ 0.324 \pm 0.006_{\text{exp}} \pm 0.013_{\text{th}} & \text{FOPT ,} \\ 0.306 \pm 0.005_{\text{exp}} \pm 0.011_{\text{th}} & \text{renormalon .} \end{cases} \quad (142)$$

The OPAL results using CIPT and FOPT agree with those from ALEPH. The quoted theoretical uncertainties are consistently treated between the two analyses, with the important difference that the more recent ALEPH analysis (ALEPH Coll., 2005) uses a reduced uncertainty range for the K_4 parameter ($K_4 = 25 \pm 25$) as compared to $K_4 = 50 \pm 50$ in the 1998 analysis (ALEPH Coll., 1998c) and $K_4 = 25 \pm 50$ in OPAL. The justification of the smaller K_4 uncertainty was provided in Section VII.B.1. As for the value obtained with the renormalon chains, we refer to our discussion in Sections VII.B.7 and VII.B.8 where we concluded that however interesting this approach is, its performance for a reliable and precise determination of $\alpha_s(m_\tau^2)$ is not adequate. OPAL also derives values for the gluon condensate: averaging the results of the CIPT and FOPT analyses, one obtains $\langle a_s GG \rangle = (0.005 \pm 0.017) \text{ GeV}^4$, in agreement with ALEPH.

3. Running of $\alpha_s(s)$ below m_τ^2

Using the spectral functions, one can simulate the physics of a hypothetical τ lepton with a mass $\sqrt{s_0}$ smaller than m_τ through Eq. (84). Assuming quark-hadron duality, the evolution of $R_\tau(s_0)$ provides a direct test of the running of $\alpha_s(s_0)$, governed by the RGE β -function. On the other hand, it is also a test of the stability of the OPE approach in τ decays. The studies performed in this section employ only CIPT. Results

obtained with FOPT are similar²⁷ and differ mostly in the central $\alpha_s(m_\tau^2)$ value.

The functional dependence of $R_{\tau,V+A}(s_0)$ is plotted in the left hand plot of Fig. 28 together with the theoretical prediction using the results of Table VII. The spreads due to uncertainties are shown as error bands. The correlations between two adjacent points in s_0 are large as the only new information is provided by the small mass difference between the two points and the slightly modified weight functions. Moreover they are reinforced by the original experimental and theoretical correlations. Below 1 GeV² the error of the theoretical prediction of $R_{\tau,V+A}(s_0)$ starts to blow up due to the increasing uncertainty from the unknown K_4 perturbative term; errors of the nonperturbative contributions are *not* contained in the theoretical error band. Figure 28 (right) shows the plot corresponding to Fig. 28 (left), translated into the running of $\alpha_s(s_0)$, *i.e.*, the experimental value for $\alpha_s(s_0)$ has been individually determined at every s_0 from the comparison of data and theory. Also plotted is the four-loop RGE evolution using three quark flavors.

It is remarkable that the theoretical prediction using the parameters determined at the τ mass and $R_{\tau,V+A}(s_0)$ extracted from the measured $V + A$ spectral function agree down to $s_0 \sim 0.8$ GeV². The agreement is good to about 2% at 1 GeV². This result, even more directly illustrated by the right hand plot of Fig. 28, demonstrates the validity of the perturbative approach down to masses around 1 GeV, well below the τ mass scale. The agreement with the expected scale evolution between 1 and 1.8 GeV is an interesting result, considering the relatively low mass range, where α_s is seen to decrease by a factor of 1.6 and reaches rather large values ~ 0.55 at the lowest masses. This behavior provides confidence that the $\alpha_s(m_\tau^2)$ measurement is on solid phenomenological ground.

4. Final assessment on the $\alpha_s(m_\tau^2)$ determination

Although the recent ALEPH evaluation of $\alpha_s(m_\tau^2)$ represents the state-of-the art, several remarks can be made:

- The analysis is based on the ALEPH spectral functions and branching fractions, ensuring a good consistency between all the observables, but not exploiting the full experimental information currently available from other experiments. Since the result on $\alpha_s(m_\tau^2)$ is limited by theoretical uncertainties, one should expect only a small improvement of the final error in this way, however it can influence the central value.
- One example for this is the evaluation of the strange component. Some discrepancy is observed between the ALEPH measurement of the $(K\pi\pi)^-\nu$ mode and the CLEO and OPAL results, as discussed in Section III.C. Although this could still be the result of a statistical fluctuation, their average provides a significant shift in the central value compared to using the ALEPH number alone. Another improvement is the substitution of the measured branching fraction for the $K^-\nu$ mode by the more precise value predicted from $\tau-\mu$ universality (see Eq. (16)). Both operations have the effect to increase the strange $R_{\tau,S}$ ratio from 0.1603 ± 0.0064 , as obtained by ALEPH, to 0.1686 ± 0.0047 for the world average.
- One can likewise substitute the world average value for the universality-consolidated value of the electronic branching fraction given in Eq. (13), $\mathcal{B}_e^{\text{uni}} = (17.818 \pm 0.032)\%$, to the corresponding ALEPH result, $\mathcal{B}_e = (17.810 \pm 0.039)\%$, with little effect on the central value, but some improvement in the precision.
- Most of the theoretical uncertainty originates from the limited knowledge of the perturbative expansion, only predicted to third order. This problem was discussed in detail in Section VII.B.1 and, among the standard FOPT and CIPT approaches, strong arguments have been presented in favor of the latter one. We therefore take the result from the CIPT expansion, not introducing any additional uncertainty spanning the difference between FOPT and CIPT results. The dominant theoretical errors are from the uncertainty in K_4 and from the renormalization scale dependence, both covering the effect of truncating the series after the estimated fourth order.

²⁷ As already indicated by the smaller χ^2 value of the spectral moments fit (see Table VII), the agreement between the FOPT evolution computation and the data is better than it is when using CIPT.

From this analysis, one finds the new value for the nonstrange ratio,

$$\begin{aligned} R_{\tau,V+A} &= R_\tau - R_{\tau,S} \\ &= (3.640 \pm 0.010) - (0.1686 \pm 0.0047) \\ &= 3.471 \pm 0.011, \end{aligned} \quad (143)$$

to be compared to the ALEPH value of 3.482 ± 0.014 . The result (143) translates into an updated determination of $\alpha_s(m_\tau^2)$ from the inclusive $V + A$ component using the CIPT approach

$$\alpha_s(m_\tau^2) = 0.345 \pm 0.004_{\text{exp}} \pm 0.009_{\text{th}}, \quad (144)$$

with improved experimental and theoretical precision over the ALEPH result.

5. Evolution to M_Z^2

It is customary to compare α_s values, obtained at different renormalization scales, at the scale of the Z -boson mass. To do this, one evolves the α_s result using the RGE (76). A difficulty arises from the quark thresholds: in the $\overline{\text{MS}}$ scheme, or any of its modifications such as $\overline{\text{MS}}$, the beta function governing the running of the strong coupling constant is independent of quark masses. This simplifies the calculation of QCD corrections beyond the one-loop level. On the other hand, decoupling of heavy quarks (Appelquist and Carazzzone, 1975) is not manifest in each order of perturbation theory (Bernreuther, 1983). A heavy quark decoupling is realized in momentum-space dependent renormalization schemes (MO). The RGE in an MO scheme involves the scaling-function $\beta_{\text{MO}} = \beta(\alpha'_s, m'_i, a')$ that depends on the coupling $\alpha'_s(\mu^2)$, the quark masses $m'_i(\mu^2)$ and a gauge parameter $a'(\mu^2)$, where the primes stand for the scheme dependence of the parameters. Quark-loop calculations in this scheme appear rather complicated, however the mass dependence of the β -function provides a suppression of heavy-quark effects at scales much smaller than the masses of these quarks, *i.e.*, it decouples heavy quarks from the light-particle Green's function to each order in perturbation theory.

To obtain decoupling in $\overline{\text{MS}}$ schemes, one builds in the decoupling region, $\mu \ll \overline{m}_q^{(n_f)}(\mu^2)$, where $\overline{m}^{(n_f)}(\mu^2)$ is the running $\overline{\text{MS}}$ mass of the heavy quark with flavor f , an effective field theory that behaves as if only light quarks up to flavor $n_f - 1$ were present. Matching conditions connect the parameters of the low energy effective Lagrangian to the full theory. The coupling constant of the effective theory can then be developed in a power series of the coupling constant of the full theory with coefficients that depend on $x = \ln(\mu^2/\overline{m}_q^2)$. Doing so one obtains for the matching of a_s and the light quark masses between the “light” flavor $n_f - 1$ and the heavy-quark flavor n_f (Bernreuther and Wetzel, 1982; Chetyrkin *et al.*, 1997b, 1998a; van Ritbergen *et al.*, 1997a; Rodrigo *et al.*, 1998; Wetzel, 1982)

$$\begin{aligned} a_s^{(n_f)}(\mu^2) &= a_s^{(n_f-1)}(\mu^2) \left[1 + \sum_{k=1}^{\infty} C_k(x) \left(a_s^{(n_f-1)}(\mu^2) \right)^k \right], \\ \overline{m}_q^{(n_f)}(\mu^2) &= \overline{m}_q^{(n_f-1)}(\mu^2) \left[1 + \sum_{k=1}^{\infty} H_k(x) \left(a_s^{(n_f-1)}(\mu^2) \right)^k \right]. \end{aligned} \quad (145)$$

There is no straightforward choice of the matching scale μ . However, to acquire good convergence of the perturbative expansion, one should satisfy $\mu/\overline{m}_q \sim \mathcal{O}(1)$. Since vacuum polarization of quark pairs modifies the coupling constant, we believe that the scale $\mu = 2\overline{m}_q$ is quite meaningful. The effect from this scale ambiguity is part of the systematic error assigned to the RGE evolution (see below).

The functions $C_k(x)$ and $H_k(x)$ are derived by inserting the RGE-based Taylor expansions (Eq. (83) and equivalent for the quark masses) into Eq. (145), and solving for each order in $a_s^{(n_f-1)}$ the corresponding coupled differential equations (Rodrigo *et al.*, 1998)

$$C_1 = \frac{1}{6}x, \quad C_2 = c_{2,0} + \frac{19}{24}x + \frac{1}{36}x^2, \quad (146)$$

$$C_3 = c_{3,0} + \left[\frac{241}{54} + \frac{13}{4}c_{2,0} - \left(\frac{325}{1728} + \frac{1}{6}c_{2,0} \right) n_f \right] x + \frac{511}{576}x^2 + \frac{1}{216}x^3, \quad (147)$$

$$H_1 = 0, \quad H_2 = d_{2,0} + \frac{5}{36} x - \frac{1}{12} x^2, \quad (148)$$

$$H_3 = d_{3,0} + \left[\frac{1627}{1296} - c_{2,0} + \frac{35}{6} d_{2,0} + \left(\frac{35}{648} - \frac{1}{3} d_{2,0} \right) n_f + \frac{5}{6} \zeta_3 \right] x - \frac{299}{432} x^2 - \left(\frac{37}{216} - \frac{1}{108} n_f \right) x^3, \quad (149)$$

where the integration coefficients $c_{i,0}$, $d_{i,0}$ are computed in the $\overline{\text{MS}}$ scheme at the scale of the quark masses (*i.e.*, $m_q = \overline{m}_q(m_q)$) (Bernreuther and Wetzel, 1982; Chetyrkin *et al.*, 1997b; Rodrigo *et al.*, 1998; Wetzel, 1982)

$$c_{1,0} = d_{1,0} = 0, \quad c_{2,0} = -\frac{11}{72}, \quad c_{3,0} = \frac{82043}{27648} \zeta_3 - \frac{575263}{124416} + \frac{2633}{31104} n_f, \quad d_{2,0} = -\frac{89}{432}. \quad (150)$$

The evolution of the $\alpha_s(m_\tau^2)$ measurement from the inclusive $V + A$ observables given in Eq. (144), based on Runge-Kutta integration of the RGE (76) to N³LO (see Section VII.A), and three-loop quark-flavor matching (145), gives

$$\begin{aligned} \alpha_s(M_Z^2) &= 0.1215 \pm 0.0004_{\text{exp}} \pm 0.0010_{\text{th}} \pm 0.0005_{\text{evol}}, \\ &= 0.1215 \pm 0.0012. \end{aligned} \quad (151)$$

The first two errors originate from the $\alpha_s(m_\tau^2)$ determination given in Eq. (144), and the last error stands for ambiguities in the evolution due to uncertainties in the matching scales of the quark thresholds (Rodrigo *et al.*, 1998). This evolution error receives contributions from the uncertainties in the c -quark mass (0.00020, m_c varied by ± 0.1 GeV) and the b -quark mass (0.00005, m_b varied by ± 0.1 GeV), the matching scale (0.00023, μ varied between $0.7 m_q$ and $3.0 m_q$), the three-loop truncation in the matching expansion (0.00026) and the four-loop truncation in the RGE equation (0.00031), where we used for the last two errors the size of the highest known perturbative term as systematic uncertainty. These errors have been added in quadrature. The result (151) is a determination of the strong coupling at the Z mass scale with a precision of 1%.

The evolution path of $\alpha_s(m_\tau^2)$ is shown in the upper plot of Fig. 29. The two discontinuities are due to the quark-flavor matching at $\mu = 2\overline{m}_q$. One could prefer to avoid the discontinuities by choosing $\mu = \overline{m}_q$ so that the logarithms in Eq. (145) vanish, and the matching becomes (almost) smooth. However, in this case, one must first evolve from m_τ down to \overline{m}_c to match the c -quark flavor, before evolving to \overline{m}_b . The effect on $\alpha_s(M_Z^2)$ from this ambiguity is within the assigned systematic uncertainty for the evolution.

6. Comparison with other determinations of $\alpha_s(M_Z^2)$

The evolution of $\alpha_s(m_\tau^2)$ in Fig. 29 is compared with other independent measurements compiled in (Bethke, 2004). These include from the low to the high energy scale:

DIS (Bj-SR): $\alpha_s(1.58 \text{ GeV}) = 0.375^{+0.062}_{-0.081}$ (Ellis and Karliner, 1995) was obtained using the polarized structure function data for protons $g_1^p(x)$ and neutrons $g_1^n(x)$ from the CERN SMC (Adams *et al.*, 1994) and SLAC E142 (E143 Coll., 1995) experiments, based on the Bjorken sum rule (Bjorken, 1970) at N²LO (Larin *et al.*, 1991; Larin and Vermaseren, 1991)

$$\int_0^1 [g_1^p(x) - g_1^n(x)] dx = \frac{1}{3} \left| \frac{g_A}{g_V} \right| \left[1 - \frac{\alpha_s}{\pi} - 3.58 \left(\frac{\alpha_s}{\pi} \right)^2 - 20.2 \left(\frac{\alpha_s}{\pi} \right)^3 \right]. \quad (152)$$

Here g_V and g_A are the vector and axial-vector coupling constants of the neutron decay, $|g_A/g_V| = -1.2573 \pm 0.0028$ (determined assuming CVC), and the last two coefficients are calculated for three active flavors. No explicit corrections for nonperturbative higher twist effects²⁸ were applied to derive this result. However an estimate of the size of the perturbative $\mathcal{O}(\alpha_s^4)$ term was taken into account.

²⁸ Interactions involving more than one parton, like secondary interactions of quarks with the target remnant, give rise to additional contributions to the structure functions. These “higher twist” terms are classified according to their Q^2 dependence $1/Q^{2n}$, where $n = 0$ is leading twist (twist two), $n = 1$ is twist four, etc.

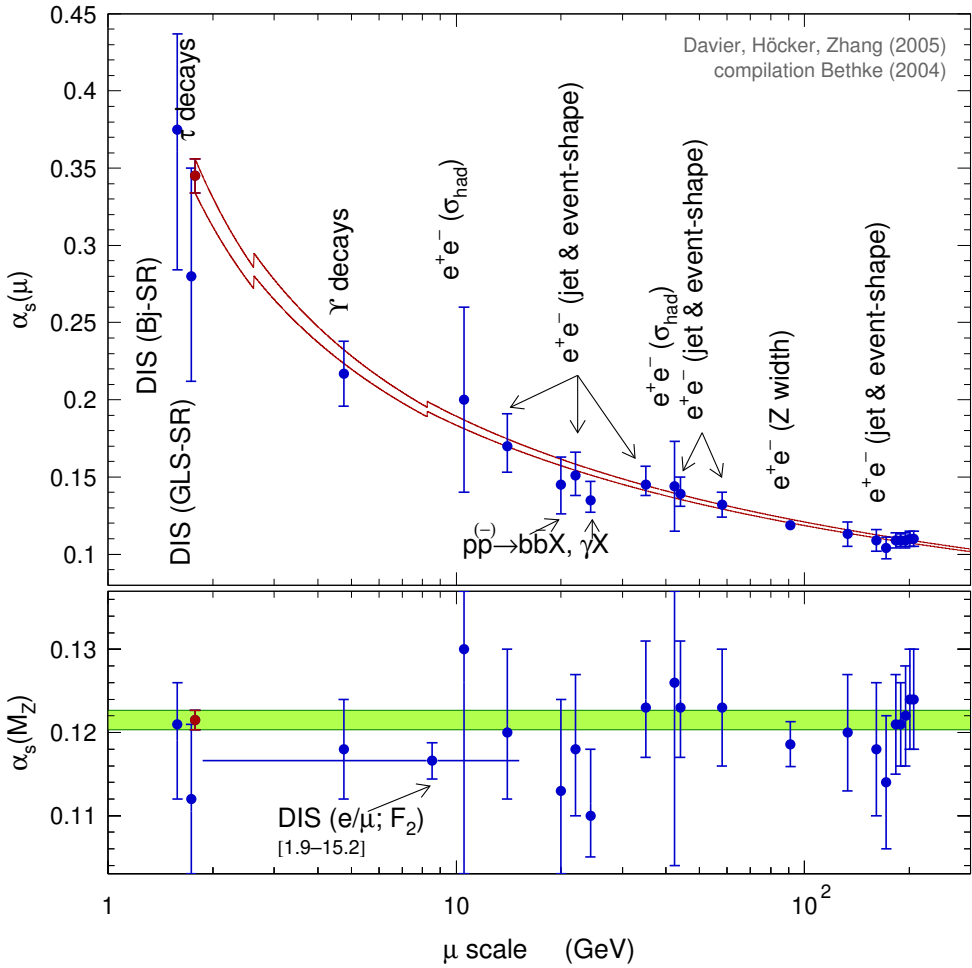


FIG. 29 Top: The evolution of $\alpha_s(m_\tau^2)$ (144) to higher scales μ using the four-loop RGE and the 3-loop matching conditions applied at the heavy quark-pair thresholds (hence the discontinuities at $2m_c$ and $2m_b$). The evolution is compared with other independent measurements (see text) covering scales varying over more than two orders magnitude. The experimental values are briefly discussed in the text; they are mostly taken from the compilation (Bethke, 2004). Bottom: The corresponding extrapolated α_s values at M_Z . The shaded band displays the τ decay result within errors.

DIS (GLS-SR): $\alpha_s(1.73 \text{ GeV}) = 0.280 \pm 0.061_{\text{exp}}^{+0.035}_{-0.030}|_{\text{th}}$ is an update of the analysis using structure function F_3 data in the Q^2 range from 1 to 15.5 GeV^2 performed by the CCFR collaboration (CCFR Coll., 1998). It uses the Gross-Llewellyn-Smith (GLS) sum rule (Gross and Llewellyn-Smith, 1969) at N^2LO (Chýla and Kataev, 1992; Larin *et al.*, 1991; Larin and Vermaseren, 1991)

$$\int_0^1 F_3(x, Q^2) dx \equiv 3 \left[1 - \frac{\alpha_s}{\pi} - 3.58 \left(\frac{\alpha_s}{\pi} \right)^2 - 19.0 \left(\frac{\alpha_s}{\pi} \right)^3 \right], \quad (153)$$

given for three active flavors. The systematic uncertainty is dominated by the extrapolation of the GLS integral to the region $x < 0.01$ where no measurements exist, and to $x > 0.5$, which is substituted by the structure function F_2 from SLAC data (Withlow *et al.*, 1992). The theoretical error is dominated by uncertainties in the higher twist corrections.

γ decays: $\alpha_s(m_b)|_{m_b=4.75 \text{ GeV}} = 0.217 \pm 0.021$ was found together with the bottom quark pole mass m_b from sum rules for the γ system in N^2LO , resumming all $\mathcal{O}(\alpha_s^2, \alpha_s v, v^2)$ terms with v being the velocity of the heavy quark (Penin and Pivovarov, 1998).

e^+e^- (σ_{had}): $\alpha_s(10.52 \text{ GeV}) = 0.20 \pm 0.06$ was determined in N²LO by CLEO (CLEO Coll., 1998) using the total e^+e^- hadronic cross section according to

$$R = \frac{\sigma(e^+e^- \rightarrow \text{hadrons})}{\sigma(e^+e^- \rightarrow \mu^+\mu^-)} = 3 \sum_i Q_i^2 \left[1 + \frac{\alpha_s}{\pi} + 1.52 \left(\frac{\alpha_s}{\pi} \right)^2 - 11.5 \left(\frac{\alpha_s}{\pi} \right)^3 \right], \quad (154)$$

where Q_i are the electric charges of quark flavors i that are produced at center-of-mass energy just below the $\Upsilon(4S)$ resonance in the e^+e^- continuum. Another measurement $\alpha_s(42.4 \text{ GeV}) = 0.175 \pm 0.028$ was obtained with the use of data from PETRA and TRISTAN in the center-of-mass energy range from 20 to 65 GeV (Bethke, 2000; Haidt, 1995).

e^+e^- (**jet & event-shape**): Using data from PETRA, TRISTAN, SLC and LEP1,2 over a large energy range, several determinations of α_s were obtained based on the jet rate and event-shape variables that are sensitive to gluon radiation governed by the strong coupling constant. The observables are calculated in resummed NLO (*i.e.*, NLO matched with next-to-leading order logarithms). In all these determinations, the theoretical uncertainty from the renormalization scale uncertainty is the dominant error source. At low PETRA energy the hadronization uncertainty is also important. See references in (Bethke, 2000).

$p\bar{p} \rightarrow b\bar{b}X$: $\alpha_s(20 \text{ GeV}) = 0.145^{+0.012}_{-0.010}|_{\text{exp}}^{+0.013}_{-0.016}|_{\text{th}}$ was obtained by UA1 (UA1 Coll., 1996) from a measurement of the cross section of the process $p\bar{p} \rightarrow b\bar{b}X$ for which NLO QCD predictions exist. The theoretical error includes uncertainties due to different sets of structure functions, renormalization/factorization scale uncertainties and the b -quark mass.

$p\bar{p}, pp \rightarrow \gamma X$: $\alpha_s(24.3 \text{ GeV}) = 0.135 \pm 0.006_{\text{exp}}^{+0.011}_{-0.005}|_{\text{th}}$ was determined by UA6 (UA6 Coll., 1999) in NLO from a measurement of the cross section difference $\sigma(p\bar{p} \rightarrow \gamma X) - \sigma(pp \rightarrow \gamma X)$ such that the poorly known contributions of the sea quarks and gluon distributions in the proton cancel. The theoretical error includes uncertainties from the scale choice and from the variation of the parton distribution functions.

e^+e^- (**Z width**): $\alpha_s(M_Z)_{Z \text{ width}} = 0.1186 \pm 0.0027$ was determined from the hadronic width at the Z^0 resonance by a global fit to all electroweak data in N²LO (LEP EWWG, 2004).

A comparison is best achieved by extrapolating these measurements to M_Z as shown in the lower plot in Fig. 29. The most precise result at the M_Z scale stems from τ decays (151), which is a 1.1% determination limited in accuracy by theoretical uncertainties in the perturbative expansion. The significant improvement in precision compared to the previous ALEPH result (ALEPH Coll., 1998c), $0.1202 \pm 0.0008_{\text{exp}} \pm 0.0024_{\text{th}} \pm 0.0010_{\text{evol}}$, is due to the higher statistics and the more detailed experimental analysis, but mostly because of the smaller theory uncertainty assigned to the perturbative expansion and our conclusion to lift the ambiguity between CIPT and FOPT.

Another precise determination (DIS ($e/\mu; F_2$) [1.9 – 15.2] GeV), $\alpha_s(M_Z^2) = 0.1166 \pm 0.009_{\text{stat}} \pm 0.0020_{\text{syst}}$ (Bethke, 2004; Santiago and Yndurain, 2001), obtained using the structure function F_2 from deep inelastic electron (e) and muon (μ) scattering (DIS) data in the Q^2 range between 3.5 GeV² and 230 GeV² is also shown. The analyses use N²LO calculations wherever available. The systematic error is mostly theoretical including higher twist effects and an estimate of the N³LO corrections, and is doubled to account for missing contributions associated with the renormalization scale and scheme uncertainties.

7. A measure of asymptotic freedom between m_τ^2 and M_Z^2

The τ -decay and Z -width determinations have comparable accuracies, which are however very different in nature. The τ value is dominated by theoretical uncertainties, whereas the determination at the Z resonance, benefiting from the much larger energy scale and the correspondingly small uncertainties from the truncated perturbative expansion, is limited by the experimental precision on the electroweak observables, essentially the ratio of leptonic to hadronic peak cross sections. The consistency between the two results provides the most powerful present test of the evolution of the strong interaction coupling, over a range of s spanning more than three orders of magnitude, as it is predicted by the nonabelian nature of the QCD gauge theory. The difference between the extrapolated τ -decay value and the measurement at the Z is:

$$\alpha_s^\tau(M_Z^2) - \alpha_s^Z(M_Z^2) = 0.0029 \pm 0.0010_\tau \pm 0.0027_Z, \quad (155)$$

which agrees with zero with a relative precision of 2.4%.

In fact, the comparison of these two values is valuable since they are among the most precise single measurements and they are widely spaced in energy scale. Thus it allows one to perform an accurate test of asymptotic freedom. Let us consider the following evolution estimator (DELPHI Coll., 2004) for the inverse of $\alpha_s(s)$,

$$r(s_1, s_2) = 2 \cdot \frac{\alpha_s^{-1}(s_1) - \alpha_s^{-1}(s_2)}{\ln s_1 - \ln s_2}, \quad (156)$$

which reduces to the logarithmic derivative of $\alpha_s^{-1}(s)$ when $s_1 \rightarrow s_2$,

$$\begin{aligned} \frac{d\alpha_s^{-1}}{d\ln\sqrt{s}} &= -\frac{2\pi\beta(s)}{\alpha_s^2}, \\ &= \frac{2\beta_0}{\pi} \left(1 + \frac{\beta_1}{\beta_0} \frac{\alpha_s}{\pi} + \dots\right), \end{aligned} \quad (157)$$

with the notations of Eq. (76). At first order, the logarithmic derivative is driven by β_0 .

The τ and Z experimental determinations of $\alpha_s(s)$ yield the value

$$r_{\text{exp}}(m_\tau^2, M_Z^2) = 1.405 \pm 0.053, \quad (158)$$

which agrees with the QCD prediction using the RGE to N³LO, and three-loop quark-flavor matching (145), as discussed in Section VII.C.5,

$$r_{\text{QCD}}(m_\tau^2, M_Z^2) = 1.353 \pm 0.006. \quad (159)$$

This is to our knowledge the most precise experimental test of the asymptotic freedom property of QCD at present. It can be compared to an independent determination (DELPHI Coll., 2004), using an analysis of event shape observables at LEP between the Z energy and 207 GeV, $r(M_Z^2, (207 \text{ GeV})^2) = 1.11 \pm 0.21$, for a QCD expectation of 1.27.

VIII. SPECTRAL FUNCTIONS OF TAU FINAL STATES WITH STRANGENESS

Complete experimental studies of the Cabibbo-suppressed decays of the τ became available at LEP (ALEPH Coll., 1999b), allowing to initiate systematic QCD studies (Chen, 1998; Chen *et al.*, 1999; Davier, 1997; Davier *et al.*, 2001; Höcker, 1997) of the effect induced by the strange quark mass in the τ decay width (Braaten *et al.*, 1992; Chetyrkin and Kwiatkowski, 1993; Chetyrkin and Kühn, 1997; Chetyrkin *et al.*, 1997a, 1998b; Kambor and Maltman, 2000, 2001; Körner *et al.*, 2001b; Maltman, 1998a; Pich and Prades, 1998, 1999, 2000; Prades and Pich, 1999; Prades, 1999). Indeed, from the separate measurement of the strangeness $S = 0$ and $S = -1$ τ decay widths, it is possible to pin down the SU(3) breaking effects and to obtain information on the strange quark mass. Recent experimental information (CLEO Coll., 1999b; OPAL Coll., 2004) can now be included in addition to the ALEPH data. In this section the current situation on the physics of τ decays with net strangeness is reviewed, with emphasis on the determination of the strange quark mass and the CKM element $|V_{us}|$.

A. Strange spectral functions

The experimental determination of nonstrange and strange (subscript S) spectral functions has been presented and discussed in Section IV. As shown in Section VII.C, one uses the spectral functions, or equivalently the fully corrected mass-squared distributions, to construct the spectral moments

$$R_{\tau,(S)}^{k\ell} = \int_0^{m_\tau^2} ds \left(1 - \frac{s}{m_\tau^2}\right)^k \left(\frac{s}{m_\tau^2}\right)^\ell \frac{dR_{\tau,(S)}}{ds}, \quad (160)$$

where $R_{\tau,(S)}^{00} = R_{\tau,(S)}$.

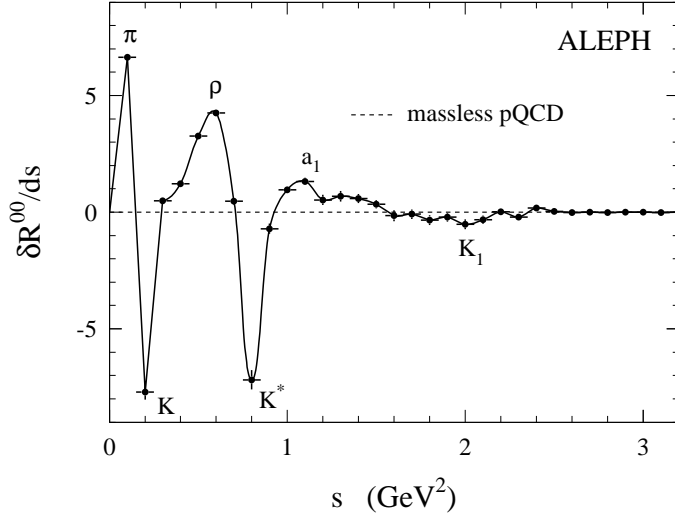


FIG. 30 Integrand of Eq. (160) with $(k = 0, \ell = 0)$ for the difference (161) of the Cabibbo-corrected nonstrange and strange invariant mass spectra from (ALEPH Coll., 1999b). The contribution from massless perturbative QCD (pQCD) vanishes. To guide the eye, the solid line interpolates between the bins of constant 0.1 GeV^2 width.

TABLE X Spectral moments $\delta R_\tau^{k\ell}$ from (ALEPH Coll., 1999b) and (OPAL Coll., 2004). ALEPH uses its spectral function (SF), the components of which are normalized by its own branching ratios (\mathcal{B}), while OPAL normalizes its spectral functions with the world average (WA) branching fractions. The error combines the uncertainties from the measurements (dominant) and from $|V_{us}|$.

(k, ℓ)	ALEPH SF + \mathcal{B}	OPAL SF + WA \mathcal{B}
(0,0)	0.39 ± 0.14	0.26 ± 0.12
(1,0)	0.38 ± 0.08	0.28 ± 0.09
(2,0)	0.37 ± 0.05	0.30 ± 0.07
(3,0)	0.40 ± 0.04	0.33 ± 0.05
(4,0)	0.40 ± 0.04	0.34 ± 0.04

To reduce the theoretical uncertainties and emphasize the SU(3) breaking component originating from the larger s quark mass, it is convenient to consider the difference between nonstrange and strange spectral moments, properly normalized with their respective CKM matrix elements (ALEPH Coll., 1999b)

$$\delta R_\tau^{k\ell} = \frac{1}{|V_{ud}|^2} R_{\tau,S=0}^{k\ell} - \frac{1}{|V_{us}|^2} R_{\tau,S=-1}^{k\ell}, \quad (161)$$

for which the massless perturbative contribution vanishes.

The ALEPH results for the spectral moments $\delta R_\tau^{k\ell}$ are given in Table X (ALEPH Coll., 1999b). We recall that their values are strongly correlated since they originate from the same invariant mass spectrum, which has large statistical errors.

It can be observed that the central values stay rather constant between $k = 0$ and $k = 4$, while the errors decrease. They decrease because moments with higher k values emphasize the accurately measured K and $K^*(892)$ channels. The contributions from $K(n\pi)$, $n \geq 2$ modes to the moments are negligible for $k > 2$. The error from $|V_{us}|$ is also reduced as $R_{\tau,S}^{k0}$ decreases with k . The contribution from the various decay modes to δR_τ^{00} is visualized in Fig. 30. The experimental moments (161) within their 1σ error bands are shown in Fig. 31.

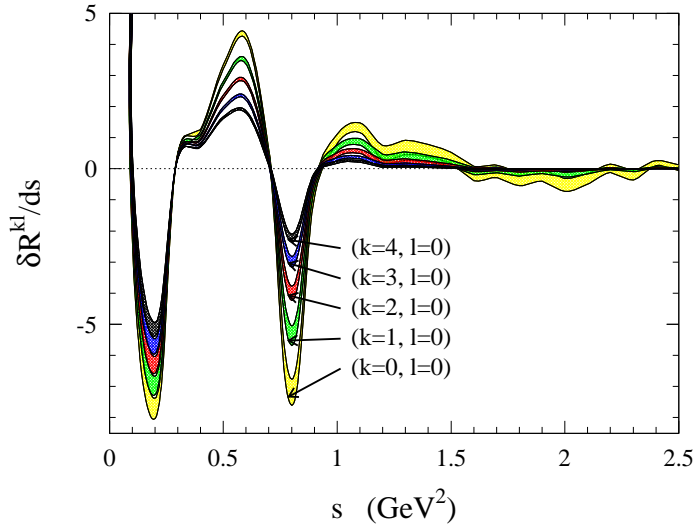


FIG. 31 Integrand of Eq. (160) for the moments $k = 0, \dots, 4$ and $\ell = 0$ of the difference (161). The data are from (ALEPH Coll., 1999b). The widths of the interpolating bands correspond to one standard deviation.

B. Theoretical analysis of $R_{\tau,S}$

The inclusive τ decay ratio into strange hadronic final states

$$R_{\tau,S} = \frac{\Gamma(\tau^- \rightarrow \text{hadrons}_{S=-1}^- \nu_\tau)}{\Gamma(\tau^- \rightarrow e^- \bar{\nu}_e \nu_\tau)} , \quad (162)$$

can be used through the framework of the OPE to determine $m_s(s)$ at the scale $s = m_\tau^2$ (Chen, 1998; Chen *et al.*, 1999; Davier, 1997; Höcker, 1997). However, the perturbative expansion computed for the mass term in (Chetyrkin and Kwiatkowski, 1993) was shown to be incorrect (Maltman, 1998a). After correction the series shows a problematic convergence behavior (Chetyrkin *et al.*, 1998b; Maltman, 1998a; Pich and Prades, 1998; Prades and Pich, 1999; Prades, 1999), which is discussed in detail below.

Following (Braaten *et al.*, 1992) we recall the theoretical prediction for the inclusive vector plus axial-vector hadronic decay rate, given by

$$R_\tau(m_\tau^2) = 12\pi S_{\text{EW}} \int_0^{m_\tau^2} \frac{ds}{m_\tau^2} \left(1 - \frac{s}{m_\tau^2}\right)^2 \left[\left(1 + 2\frac{s}{m_\tau^2}\right) \text{Im}\Pi^{(1+0)}(s + i\epsilon) - 2\frac{s}{m_\tau^2} \text{Im}\Pi^{(0)}(s + i\epsilon) \right] , \quad (163)$$

with the two-point correlation functions $\Pi^{(J)} = |V_{ud}|^2 \Pi_{ud,V+A}^{(J)} + |V_{us}|^2 \Pi_{us,V+A}^{(J)}$ for the hadronic final state of spin J . The choice of the particular spin combination for the correlators taken in Eq. (163) is justified in (Braaten *et al.*, 1992). Using the OPE (Shifman *et al.*, 1979), Eq. (163) for the strange part can be decomposed as

$$R_{\tau,S} = 3|V_{us}|^2 S_{\text{EW}} \left(1 + \delta^{(0)} + \delta'_{\text{EW}} + \delta_S^{(2,m_q)} + \sum_{D=4,6,\dots} \delta_S^{(D)} \right) . \quad (164)$$

The $\delta^{(0)}$ term is the perturbative part of mass dimension $D = 0$, known to third order in the expansion with $a_s = \alpha_s(m_\tau^2)/\pi$, and discussed in detail in Section VII.B.1. The residual non-logarithmic electroweak correction $\delta'_{\text{EW}} \simeq 0.0010$ (Braaten and Li, 1990) is neglected in the following. Throughout this section, all QCD observables are expressed in the $\overline{\text{MS}}$ renormalization scheme.

1. Evidence for the effect of a massive strange quark

From the result obtained for the world average branching fraction for inclusive τ decays to strange hadronic final states in Table (II), one obtains

$$R_{\tau,S} = 0.1666 \pm 0.0048 , \quad (165)$$

using the value for $\mathcal{B}_e^{\text{uni}}$ given in Section III.B. This result can be compared with the QCD prediction for a massless strange quark neglecting the nonperturbative contributions,

$$R_{\tau,S}^{(0)} = 3|V_{us}|^2 S_{\text{EW}} \left(1 + \delta^{(0)} \right) = 0.1847 \pm 0.0029 , \quad (166)$$

where the quoted error reflects the uncertainties on mostly $|V_{us}|$ and to a lesser extent $\alpha_s(m_\tau^2)$. The two values differ by 3.2σ , in the direction predicted for a non-zero m_s value ($\delta_S^{(2,m_q)}$ has a negative sign). This is an indication for the effect of a massive strange quark in a single observable (although not the most sensitive one), which is essentially predicted by perturbative QCD.

2. Convergence of the perturbative series

The $\delta_S^{(2,m_q)}$ term in Eq. (164) is the mass contribution of dimension $D = 2$, which is in practice only relevant for the strange quark mass. Fixed-order perturbation theory (FOPT) gives (Chetyrkin and Kwiatkowski, 1993; Maltman, 1998a)

$$\delta_S^{(2,m_s)} = -8 \frac{m_s^2(m_\tau^2)}{m_\tau^2} \left[1 + \frac{16}{3} a_s + 46.00 a_s^2 + \left(283.6 + \frac{3}{4} x_3^{(1+0)} \right) a_s^3 + \dots \right] . \quad (167)$$

The third order coefficient $x_3^{(1+0)}$ occurring in the expansion of the massive $J = 1 + 0$ correlator has been recently calculated (Baikov *et al.*, 2004), while the $J = 0$ correlator was already known up to third order. Previous analyses used an estimate for $x_3^{(1+0)}$, however it turns out to be of minor numerical importance. The true value (Baikov *et al.*, 2004) is $x_3^{(1+0)} = 202.3$, while the naive estimate, assuming a geometric growth of the perturbative coefficients, gives $x_3^{(1+0)} \simeq x_2^{(1+0)} (x_2^{(1+0)} / x_1^{(1+0)}) \simeq 165$, which was taken with a 200% uncertainty.

Setting $\alpha_s(m_\tau^2) = 0.334$, one finds for Eq. (167)

$$\delta_S^{(2,m_s)} = -8 \frac{m_s^2(m_\tau^2)}{m_\tau^2} (1 + 0.57 + 0.52 + 0.52 + \dots) , \quad (168)$$

which converges badly.

A contour-improved analysis (CIPT) for the dimension $D = 2$ contribution has been used in (Chetyrkin *et al.*, 1998b; Pich and Prades, 1998; Prades and Pich, 1999; Prades, 1999). It consists of a direct numerical evaluation of the contour integral derived from Eq. (163), using the solution of the renormalization group equation (RGE) to four loops as input to the running $\alpha_s(s)$ and $m_s(s)$. This provides a resummation of all known higher order logarithmic integrals and has been found to improve the convergence of the massless perturbative series. With the above value for α_s , the contour-improved evaluation of the perturbative series reads

$$\delta_{S,\text{CIPT}}^{(2,m_s)} = -8 \frac{m_s^2(m_\tau^2)}{m_\tau^2} (0.97 + 0.49 + 0.38 + 0.33 + \dots) , \quad (169)$$

with somewhat improved but still unsatisfactory convergence.

Independently of whether FOPT or CIPT is used, the origin of the convergence problem is found in the $J = 0$ component as defined in Eq. (163). Using FOPT the series reads

$$\delta_S^{(2,m_s)}(J = 0) = -8 \frac{m_s^2(m_\tau^2)}{m_\tau^2} (0.41 + 0.32 + 0.32 + 0.37 + \dots) , \quad (170)$$

while the $J = 1 + 0$ part converges well,

$$\delta_S^{(2,m_s)}(J = 1 + 0) = -8 \frac{m_s^2(m_\tau^2)}{m_\tau^2} (0.56 + 0.16 + 0.05 - 0.05 + \dots) . \quad (171)$$

Similar but worse convergence problems occur in the mass corrections to the (k, ℓ) $J = 0$ moments.

3. Phenomenological analysis

The phenomenological analysis is performed using the OPE framework including the light quark masses and the $D = 4$ quark-mass corrections. Higher dimension terms are assumed to be numerically insignificant compared to the present experimental uncertainty so that for all practical purposes the strange quark mass can be obtained from the relation

$$m_s^2(m_\tau^2) \simeq \frac{m_\tau^2}{\Delta_{k\ell}(a_s)} \left[\frac{\delta R_\tau^{k\ell}}{24S_{\text{EW}}} + 2\pi^2 \frac{\langle \delta O_4(m_\tau^2) \rangle}{m_\tau^4} Q_{k\ell}(a_s) \right] , \quad (172)$$

where $\Delta_{k\ell}(a_s)$ and $Q_{k\ell}(a_s)$ are the pQCD series, defined in (Pich and Prades, 1999, 2000), associated with the $D = 2$ and $D = 4$ contributions to $\delta R_\tau^{k\ell}$, and

$$\begin{aligned} \langle \delta O_4(m_\tau^2) \rangle &= \langle 0 | m_s \bar{s}s - m_d \bar{d}d | 0 \rangle (m_\tau^2) \\ &\simeq -(1.5 \pm 0.4) \times 10^{-3} \text{ GeV}^4 . \end{aligned} \quad (173)$$

As discussed above, the QCD series for $\Delta_{k\ell} = \Delta_{k\ell}^{(1+0)} + \Delta_{k\ell}^{(0)}$ are problematic, since they exhibit bad convergence originating from the longitudinal component ($\Delta_{k\ell}^{(0)}$) (Maltman, 1998a; Pich and Prades, 1998, 1999, 2000; Prades and Pich, 1999; Prades, 1999). The value of the strong coupling constant is taken to be $\alpha_s(m_\tau^2) = 0.334 \pm 0.022$, from the analyses of the nonstrange $V + A$ moments $R_\tau^{k\ell}$. Correlations between $\alpha_s(m_\tau^2)$ and the moments $\delta R_{k\ell}$ are negligible since the uncertainty on the former value is dominated by theory and on the latter one by the measurement of the strange component. Using these inputs, the pQCD series $\Delta_{k\ell}$ can be displayed up to third order using CIPT, separating the $(1 + 0)$ and (0) series ($a_s = 0.106$):

$$\begin{aligned} \Delta_{00}^{(1+0)}(a_s) &= 0.565 + 0.161 + 0.049 - 0.038 + \dots \\ \Delta_{10}^{(1+0)}(a_s) &= 0.684 + 0.251 + 0.144 + 0.042 + \dots \\ \Delta_{20}^{(1+0)}(a_s) &= 0.791 + 0.338 + 0.248 + 0.142 + \dots \\ \Delta_{30}^{(1+0)}(a_s) &= 0.893 + 0.428 + 0.363 + 0.264 + \dots \\ \Delta_{40}^{(1+0)}(a_s) &= 0.993 + 0.523 + 0.493 + 0.413 + \dots \\ \\ \Delta_{00}^{(0)}(a_s) &= 0.408 + 0.320 + 0.323 + 0.375 + \dots \\ \Delta_{10}^{(0)}(a_s) &= 0.355 + 0.307 + 0.338 + 0.435 + \dots \\ \Delta_{20}^{(0)}(a_s) &= 0.324 + 0.305 + 0.360 + 0.505 + \dots \\ \Delta_{30}^{(0)}(a_s) &= 0.306 + 0.309 + 0.389 + 0.587 + \dots \\ \Delta_{40}^{(0)}(a_s) &= 0.295 + 0.317 + 0.421 + 0.680 + \dots . \end{aligned} \quad (174)$$

The exhibited behavior is that of asymptotic series close to their point of minimum sensitivity and a prescription is needed to evaluate the expansions and to make a reasonable estimate of their uncertainties.

C. Several approaches

The bad convergence properties of the perturbative QCD expansion can be alleviated in several ways.

1. Summing up the full known terms

One could try to work with the full series up to the highest known order (third), observing that the terms in the overall expansion show a reasonable rate of decrease, at least in the CIPT approach. Fourth order coefficients can be estimated, using for instance the principle of minimal sensitivity (Stevenson, 1981) or the simplistic geometric growth rule. The latter method was used in early analyses (Chen, 1998; Chen *et al.*, 1999; Davier, 1997; Höcker, 1997).

2. Optimal truncation of the series

Examination of examples of asymptotic series suggests that a reasonable procedure is to truncate the expansion where the terms reach their minimum value. The precise prescription—cutting at the minimum, or one order before or after, including the full last term or only a fraction of it—is arbitrary and this ambiguity must be reflected by a specific uncertainty attached to the procedure. In (Chen *et al.*, 2001; Davier *et al.*, 2001) the adopted rule was to keep all terms up to (and including) the minimal one and to assign as a systematic uncertainty the value of the last term retained. It follows that the Δ_{k0} series are summed up to third order for $k = 0, 1$, second order for $k = 2$ and first order for $k = 3, 4$.

3. Removing the longitudinal parts

The kaon pole and other spin-0 components

Since the culprit is the longitudinal expansion, it could be wise to remove the longitudinal piece beforehand from the inclusive data and to apply the QCD analysis only to the well-behaved $(1+0)$ part²⁹. This method was already used in (ALEPH Coll., 1999b), where it was noted that the dominant contribution to the strange $J = 0$ component is given by the kaon pole.

Other longitudinal contributions can be identified: *(i)* off-shell vector K^* resonances can generate a 0^+ component (Finkemeier and Mirkes, 1996), however too small to have a significant effect in the analysis, and *(ii)* production of the scalar $K_0^*(1430)$ resonance. The $K_0^*(1430)$ state decays almost exclusively into $K\pi$ with a branching fraction of $(93 \pm 10)\%$ (Particle Data Group, 2004). A fit to the $K^-\pi^0$ mass distribution measured by ALEPH (ALEPH Coll., 1999b) results in the branching fraction $\mathcal{B}(\tau \rightarrow \bar{K}_0^*(1430)\nu_\tau) = (0.0 \pm 2.5) \times 10^{-4}$. Hence 0^+ contributions are suppressed ($< 1.6 \times 10^{-2}$) compared to the dominant $J^P = 1^-$ production. This is expected from chiral symmetry breaking, with $J = 0$ contributions reduced by $\sim (m_K/m_\tau)^4$ as discussed in (Finkemeier and Mirkes, 1996), not including the τ kinematic factor, which suppresses higher mass states.

No direct estimate of extra 0^- components beyond the single K can be made from the present data in the $\bar{K}\pi\pi$ modes. This is due to the lack of statistics and to the background subtraction, especially in the high mass region where some evidence for a broad pseudoscalar state at 1460 MeV exists (Particle Data Group, 2004). A contribution (upper limit) equal to the 0^+ one is assumed in this case.

The ALEPH evaluation of the $J = 0$ contributions to $R_{\tau,S}$ gives

$$R_{\tau,S}^{(0)}(K) = -0.00615 \pm 0.00026, \quad (175)$$

$$R_{\tau,S}^{(0)}(\text{other } 0^-, 0^+) = -0.0015 \pm 0.0015, \quad (176)$$

leading to the result

$$\delta R_\tau^{00}(J = 0) = 0.147 \pm 0.031, \quad (177)$$

where the $J = 0$ contributions in the nonstrange part are assumed to be saturated by the pion pole and have been computed to be -0.0078 . Similarly, one estimates the $J = 0$ contributions for all (k, ℓ) moments and subtracts them from the measured moments.

²⁹ A drawback of this procedure is that it reduces the inclusiveness of the data and hence makes the phenomenological analysis more vulnerable to quark-hadron duality violations.

TABLE XI The strange quark mass at m_τ determined from each of the $\delta R_\tau^{k\ell}$ experimental moments (Chen *et al.*, 2001). The breakdown of the different sources of uncertainties corresponds to: experimental, $|V_{us}|$, $\alpha_s(m_\tau^2)$, quark condensates, truncation of the perturbative series $\Delta_{k0}(a_s)$, and the renormalization scale ambiguity. The last column gives the total theoretical uncertainty excluding the contribution from $|V_{us}|$, which is separately quoted. Errors have been symmetrized for reading convenience.

(k, ℓ)	m_s (MeV)	exp.	σ_{m_s} (MeV)					R-scale	th.
			$ V_{us} $	α_s	$\langle m_s \bar{s}s \rangle$	trunc.			
(0,0)	132	26	13	2	4	9	9	14	
(1,0)	120	13	9	3	4	10	11	16	
(2,0)	117	10	7	3	6	14	14	21	
(3,0)	117	9	8	2	8	19	16	27	
(4,0)	103	7	5	3	9	20	19	29	

Other spin-0 components: phenomenological parameterizations

Here the additional scalar and pseudoscalar components are obtained from hadronic phenomenological parameterizations using resonances and coupled-channel dispersion analyses (Jamin *et al.*, 2002; Maltman and Kambor, 2002). The 0^\pm spectral functions constructed in this way rely on not well-established resonances with poorly known couplings, however they probably provide a realistic level for these contributions. Even with their intrinsically large uncertainties they are an order of magnitude more precise than the experimental estimate from ALEPH (Eq.(176)). In the analysis of (Gámiz *et al.*, 2003) the corresponding contribution to $R_{\tau,s}$ yields

$$\delta R_\tau^{00}(J=0, \text{ph}) = 0.155 \pm 0.005 , \quad (178)$$

where “ph” stands for phenomenological parameterizations. The quoted uncertainty in this method is clearly much smaller than in Eq. (177). It reflects the fact that pieces of the spin-0 spectral functions can be reconstructed using known resonances.

D. Results and discussion

Results are given first with the method presented in Section VIII.C.2 using optimal truncation of the perturbative series (Chen *et al.*, 2001), the stability of the results is then checked and different analyses are compared.

1. Results with the truncation method

With the truncation prescription given for the perturbative expansion $\Delta_{k\ell}(a_s)$ and the data from ALEPH, the strange quark mass can be derived from each experimental δR_τ^{k0} moment. The results are quoted in Table XI. The values obtained for $m_s(m_\tau^2)$ are moderately stable between $k = 0$ and $k = 4$. Indeed there is a small decrease, which could be of statistical nature but could also indicate a deterioration of the validity of the OPE, since larger k values emphasize the low-mass contributions rendering the approach effectively less inclusive. Also given in Table XI is the breakdown of the error on $m_s(m_\tau^2)$ into its contributions: whereas the experimental uncertainty dominates at small k , the theoretical uncertainty, which receives its main contribution from the truncation of the perturbative series and the renormalization scale, increases with k and dominates for $k \geq 1$. To estimate the latter uncertainty, the renormalization scale is varied from $0.75 m_\tau$ to $2 m_\tau$. All the theoretical errors are added in quadrature. Since the square of the strange quark mass is determined the errors on $m_s(m_\tau^2)$ are asymmetric.

Accounting errors for each, the truncation and the renormalization scale, both related to the limited number of terms in the perturbative expansion, can be considered to be a conservative approach. One can moreover check the quoted systematic uncertainty by modifying the truncation procedure: cutting off the expansion one

order less than the minimum term yields $m_s(m_\tau^2)$ values ranging from 143 MeV (for $k = 0$) to 127 MeV (for $k = 4$), showing a slightly better relative stability, but deviating from the nominal results given in Table XI by values consistent with the quoted truncation errors. Another test of the handling of the perturbative series and its poor convergence is obtained by comparing the chosen contour-improved method (CIPT) to the more standard procedure of fixed order expansion without partial resummation (FOPT). The latter method provides $m_s(m_\tau^2)$ values in the range 121 MeV ($k = 0$) to 119 MeV ($k = 4$), *i.e.*, remarkably stable and consistent with the nominal values within the uncertainties relevant to the treatment of the perturbative series.

The $|V_{us}|$ uncertainty is never dominant for any value of k . Other sources of systematic effects are negligible: in particular, the uncertainties from S_{EW} and higher order nonperturbative operators $\langle \delta O_6 \rangle$ (using the estimate of (Pich and Prades, 1999, 2000)) lie in the range 0.3 to 0.6 MeV.

To optimize experimental and theoretical sensitivities, a combined fit to several moments is performed. The overall sensitivity increases up to $k = 2$ while no significant improvement occurs for larger k values and the adjusted $m_s(m_\tau^2)$ value remains relatively stable. Keeping only lower k moments is also justified in view of a possible breakdown of the OPE for higher moments and their worse perturbative convergence (*cf.* Eq. (174)). The constrained fit of the $k = 0, 1, 2$ moments takes into account the very large correlations between the experimental values and yields the result

$$\begin{aligned} m_s(m_\tau^2) &= (120 \pm 11_{\text{exp}} \pm 8_{|V_{us}|} \pm 19_{\text{th}}) \text{ MeV} \\ &= (120^{+21}_{-26}) \text{ MeV}, \end{aligned} \quad (179)$$

where the theoretical error includes an uncertainty of 12 MeV, which accounts for the stability of the result when using different moments. All theoretical errors have been added in quadrature. For reading convenience, the errors in the first line of Eq. (179) have been symmetrized.

2. Verifying the stability of the results

As shown in the analysis of the nonstrange τ decays in (ALEPH Coll., 1998c), one can test the validity of the QCD analysis by simulating the physics of a hypothetical τ lepton of lower mass, $\sqrt{s_0} \leq m_\tau$. This is obtained by replacing m_τ^2 by s_0 everywhere in Eqs. (160, 163), and correcting the latter equation for the modified kinematic factor. Under the assumption of quark-hadron duality, the evaluation of the observables as function of s_0 represents a test of the OPE approach, since the energy dependence of the theoretical predictions is determined once the parameters of the theory are fixed. The results of this exercise are given in Fig. 32, showing the variation with s_0 of the first four δR_τ^{k0} moments, and the value for $m_s(s_0)$ derived from each moment. The bands indicate the experimental and theoretical uncertainties. The agreement between data and theory, perfect at $s_0 = m_\tau^2$ by construction, remains acceptable for lower s_0 values, down to 1.6 (2.4) GeV² for $k = 0$ (4). For the first three moments used in the final determination, the running observed in data follows the RGE evolution down to about 2 GeV². The validity of using higher moments thus appears more questionable. It should be pointed out that the s_0 dependence of the theoretical prediction is obtained following the truncation method defined in Section VIII.B.3 and applied at $s_0 = m_\tau^2$. If the same rule had been consistently used at each s_0 point a better scaling agreement would have been found, at the price of introducing steps in the prediction, corresponding to dropped terms in the expansion (according to the truncation prescription). This observation provides another consistency test of the procedure, with however some warning concerning the use of the high moments.

3. Comparison between the different analyses

Several analyses of the ALEPH strange spectral function have been performed in order to extract $m_s(m_\tau^2)$.

- In (ALEPH Coll., 1999b), a rather conservative road was followed, using only the $1 + 0$ part and a prudent estimate of the removed longitudinal part as discussed in Section VIII.C.3. A price was paid in the experimental sensitivity, leading to large errors. Also, the experimental moments were fit, not only to the strange quark mass, but also to the values of the nonperturbative operators $\langle \delta O_6 \rangle$ and $\langle \delta O_8 \rangle$. The value found by ALEPH is $m_s(m_\tau^2) = (176^{+37}_{-48})_{\text{exp}}^{+24}_{-28} \pm 14_{\text{meth}}$ MeV.
- The analysis of (Körner *et al.*, 2001b) uses the ALEPH δR_τ^{00} moment and obtains $m_s(m_\tau^2) = (130 \pm 27_{\text{exp}} \pm 9_{\text{th}})$ MeV. It advocates contour-improved resummation and employs an effective charge as well

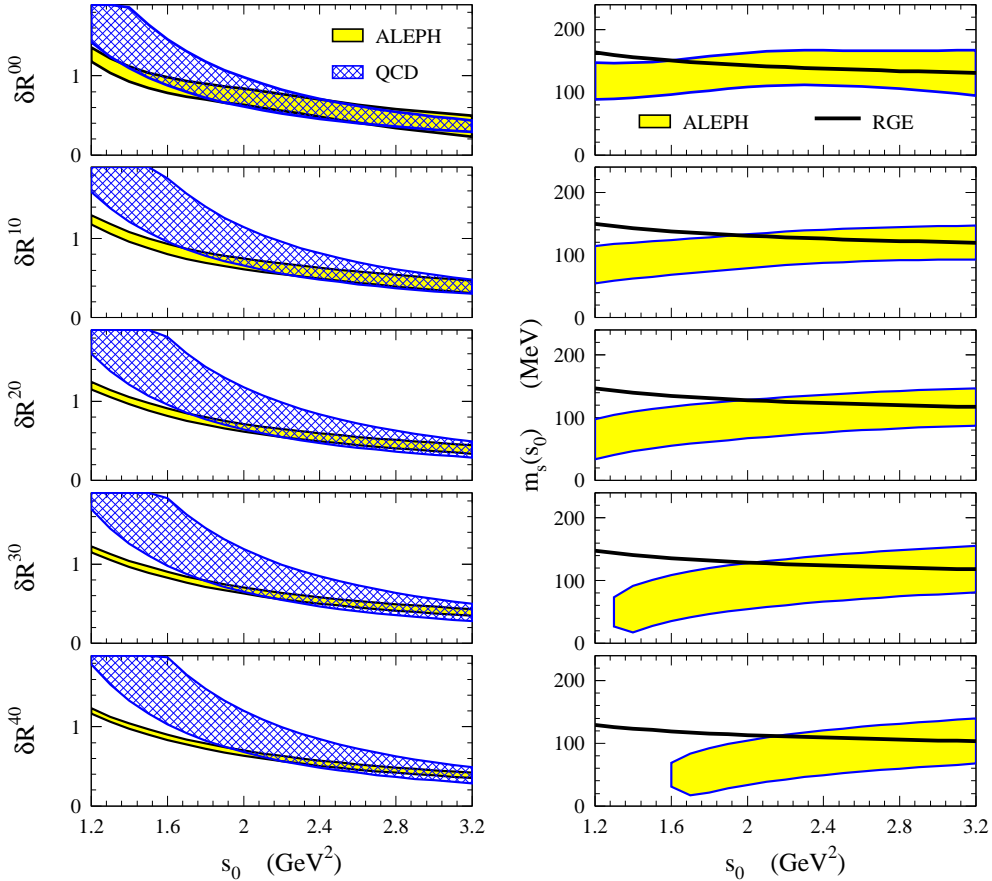


FIG. 32 The observables $\delta R_\tau^{k0}(s_0)$ as a function of the “ τ -mass”-squared s_0 confronted with the QCD predictions (left plots), and the derived $m_s(s_0)$ compared with the QCD RGE running (right plots). The bands correspond to the experimental and theoretical uncertainties (left plots), and experimental errors only (right plots). By construction, data and theory agree at $s_0 = m_\tau^2$. The figure is taken from (Chen *et al.*, 2001).

as effective masses absorbing the higher perturbative terms. The small quoted theoretical uncertainty is not exhaustively motivated in their paper, and apparently no uncertainty is included from $|V_{us}|$, which should be of the order of ± 13 MeV.

- Another analysis (Kambor and Maltman, 2000, 2001) using the ALEPH data makes use of weight functions multiplying the correlators in Eq. (163). These weights are designed to improve the convergence of the perturbative series, while suppressing the less accurate high-mass part of the strange spectral function. This latter feature is similar to using higher moments in k and it is not entirely clear to what extent this procedure provides stable results and hence how reliable the answer is. Nevertheless that result is in good agreement with (179), with a smaller theoretical uncertainty, but apparently not including the effect from the renormalization scale ambiguity.

More recent analyses take advantage of new experimental input on the strange spectral function from (OPAL Coll., 2004) and improvements in branching fractions for some strange channels (see Table II).

- In (Gámiz *et al.*, 2003), the longitudinal part is subtracted using a phenomenological prescription according to Section VIII.C.3. The result $m_s(m_\tau^2) = (107 \pm 18)$ MeV is obtained by taking the weighted average of the m_s values from $k = 0, \dots, 4$ and $\ell = 0$ moments. This procedure is statistically hardly justified as the experimental moments are strongly correlated. The result is more precise than other determinations, however a large systematic trend is observed for different k values: the m_s central values decrease monotonically from 151 for $k = 0$ to 91 MeV for $k = 4$. No additional systematic uncertainty is

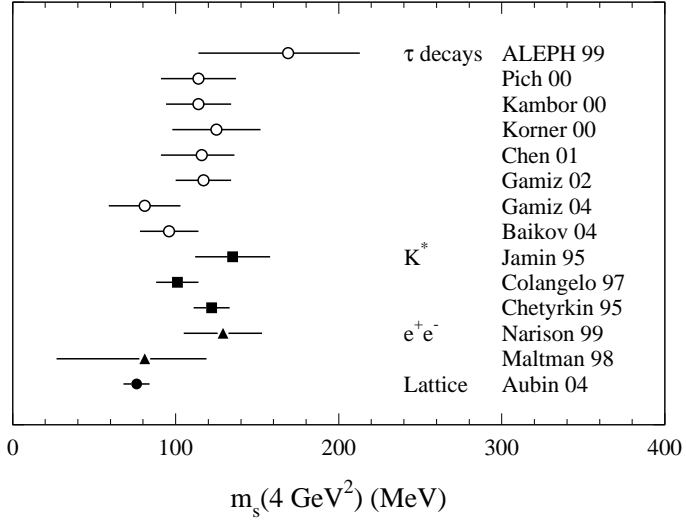


FIG. 33 Determinations of the $\overline{\text{MS}}$ mass $\overline{m}_s(4 \text{ GeV}^2)$ based on τ spectral functions and on other approaches: K^* and e^+e^- sum rules, lattice calculations.

included to account for this effect, which is larger than the final quoted error, dominated by the experimental error and the uncertainty on $|V_{us}|$. The updated value using the OPAL strange spectral function with world-average branching ratios yields (Gámiz *et al.*, 2005) a value $m_s(m_\tau^2) = (84 \pm 23)$ MeV.

- Another analysis (Baikov *et al.*, 2004) uses the full perturbative series for the $1 + 0$ correlator up to third order and an estimate of the fourth order contributions, while the longitudinal part is subtracted using the same phenomenological model as in (Gámiz *et al.*, 2003). The result, based on the $k = 3$ $\ell = 0$ moment, is $m_s(m_\tau^2) = (100^{+5}_{-3}|_{\text{th}}^{+17}_{-19}|_{\text{rest}})$ MeV. Here the first (quite small) error shall cover the uncertainties on the perturbative treatment, while the remaining error is dominated by the experimental and $|V_{us}|$ uncertainties. The same systematic trend is observed with $m_s(m_\tau^2)$ values ranging from 126 MeV for $k = 2$, to 82 MeV for $k = 4$.

The determinations of m_s from τ decays compare reasonably well to the results of analyses of the divergence of the vector and axial-vector current two-point function correlators (Becchi *et al.*, 1981; Chetyrkin *et al.*, 1995, 1997d; Colangelo *et al.*, 1997; Dominguez and de Rafael, 1987; Dominguez *et al.*, 1991; Gasser and Leutwyler, 1982; Jamin and Münz, 1995; Jamin, 1998; Kataev *et al.*, 1983; Narison, 1989). In these approaches the phenomenological information on the associated scalar and pseudoscalar spectral functions is reconstructed from phase-shift resonance analyses, which are yet incomplete over the considered mass range and need to be supplemented by other assumed ingredients, in particular the description of the continuum.

Another approach (Narison, 1995) considers the difference between isovector and hypercharge vector current correlators as related to the $I = 1$ and $I = 0$ spectral functions accessible in e^+e^- annihilation into hadrons at low energy. The author obtains $m_s(1 \text{ GeV}^2) = (198 \pm 29)$ MeV. This approach was criticized in (Maltman, 1998b), pointing out the possibility of large isospin breaking leading to a significant deviation for the extracted m_s value. Subsequently in (Narison, 1999), new SU(3)-breaking sum rules much less affected by SU(2) breaking were studied, with the result $m_s(1 \text{ GeV}^2) = (178 \pm 33)$ MeV.

Finally, lattice QCD calculations of m_s have been presented, but rarely published, with the exception of the recent result from (Aubin *et al.*, 2004) that uses an unquenched lattice QCD calculation with three dynamical quarks. The value given in the $\overline{\text{MS}}$ scheme, $m_s(4 \text{ GeV}^2) = (76 \pm 8)$ MeV, has a small error dominated by the uncertainty in the perturbative theory, needed to obtain the $\overline{\text{MS}}$ mass from the pole mass, itself calculated from the lattice bare mass. The included systematic uncertainty from the simulation on the lattice is quoted to be only 3 MeV, while the statistical error is negligible.

Available results on m_s are displayed in Fig. 33. They are scaled for convenience at a mass of 2 GeV, using the four-loop RGE γ -function (Larin *et al.*, 1997b). One observes a scatter among the values that exceeds the quoted uncertainties in some cases.

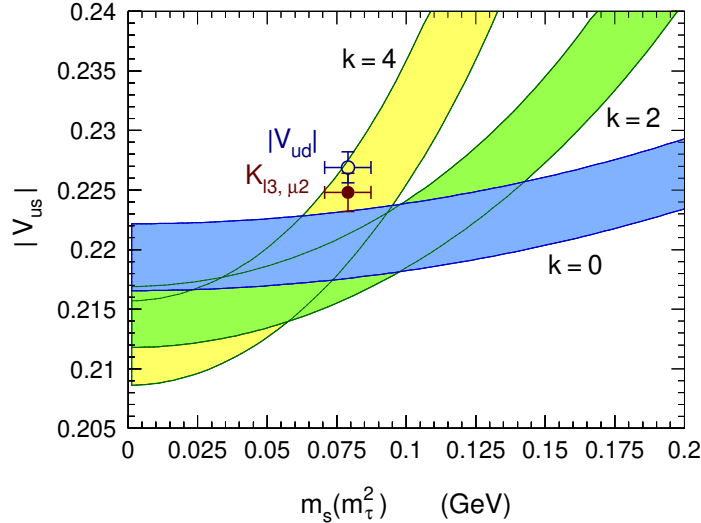


FIG. 34 The values of $|V_{us}|$ and $m_s(m_\tau^2)$ derived from the experimental strange and nonstrange moments obtained from the ALEPH spectral functions normalized to the world average branching ratios. The various curves correspond to the different $k, \ell = 0$ moments with k from 0 to 4. The width of the bands indicates the present experimental accuracy. The longitudinal components are subtracted using the K and π branching fractions together with $\tau-\mu$ universality, and the phenomenological contributions estimated in (Gámiz *et al.*, 2003). The data points indicate the $|V_{us}|$ and $m_s(m_\tau^2)$ results from outside τ physics. The two $|V_{us}|$ values shown correspond to the average of the K_{l3} and $K_{\mu 2}$ results (full circle), and to the $\sqrt{1 - |V_{ud}|^2}$ unitarity-based number (open circle) (Isidori, 2005).

E. Sensitivity to $|V_{us}|$ and concluding remarks on the m_s determinations

Before concluding the discussion of strange τ decays, it is useful to combine the available experimental information. Taking detector-corrected experimental mass spectra from (ALEPH Coll., 1999b), the world average branching fractions for the strange final states (Table II) and the value (16) for the $\tau^- \rightarrow K^- \nu_\tau$ branching ratio, an improved strange spectral function can be constructed. We shall use it in this last section.

Besides the strange quark mass, the detailed analysis of the strange τ width can bring independent information on the CKM matrix element $|V_{us}|$. In fact the present uncertainty on $|V_{us}|$ is a major contribution to the final error on m_s . One can turn the argument around and consider the possibility that data on strange τ decays could ultimately provide a powerful determination of $|V_{us}|$ (Gámiz *et al.*, 2003, 2005). Figure 34 illustrates the method: the bands show the regions in the $|V_{us}|$ -vs.- $m_s(m_\tau^2)$ plane which are allowed by the different moments δR_τ^{k0} for $J = 1 + 0$ (*i.e.*, longitudinal part excluded) within their total (experimental and theoretical) errors. It is found that the various moments are sensitive to $|V_{us}|$ and m_s in a different way. While higher- k moments exhibit a strong m_s dependence, δR_τ^{00} is particularly sensitive to $|V_{us}|$, almost independently of m_s . This property can be exploited to achieve a determination of $|V_{us}|$ from τ decays. Since the τ $SU(3)$ breaking relation (161) involves both $|V_{ud}|$ and $|V_{us}|$, unitarity of the CKM matrix is used ($|V_{ub}|$ being negligible) and only $|V_{us}|$ is kept as a variable.

Using as an independent determination the m_s value from recent lattice calculations (Aubin *et al.*, 2004) evolved to the τ scale, $m_s(m_\tau^2) = (79 \pm 8)$ MeV, one gets from δR_τ^{00} alone

$$|V_{us}| = 0.2204 \pm 0.0028_{\text{exp}} \pm 0.0003_{\text{th}} \pm 0.0001_{m_s}, \quad (180)$$

where the quoted errors are from the τ data (dominantly from the strange channels), the theory-at-large (S_{EW} , δO_4 , f_π , f_K , α_s , m_τ , the phenomenological longitudinal part), and m_s . The theoretical error is strongly reduced because the $(1 + 0)$ expansion of the $(0,0)$ moment is well behaved, in contrast to the higher moments. Thus the uncertainty on the result is dominated by the experimental error on the branching ratios for strange hadronic final states.

The present result is not yet competitive with the best determinations of $|V_{us}|$, but it is approaching these. Although it could be a statistical fluctuation, the fact that the result (180) is on the low side of the recent

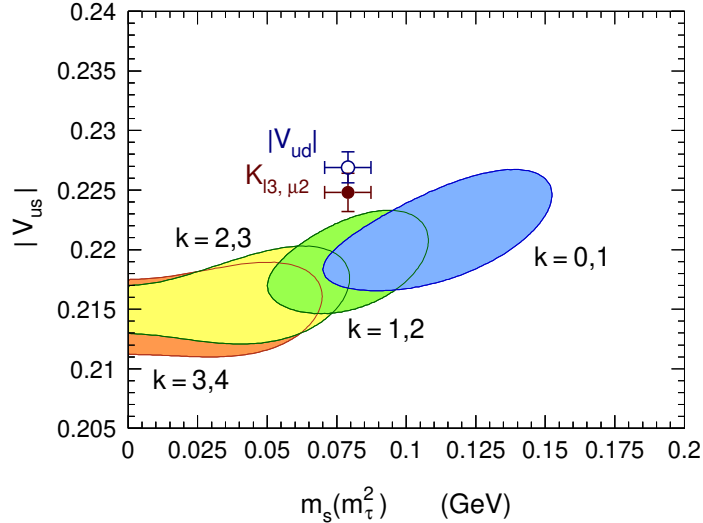


FIG. 35 The 68% CL contours in the $|V_{us}|$ -vs.- $m_s(m_\tau^2)$ plane from the fit of different pairs of moments derived from the experimental strange and nonstrange ALEPH spectral functions normalized to the world average branching ratios. The longitudinal components are subtracted using the τ - μ universality-improved K and π branching fractions, and the phenomenological contributions estimated in (Gámiz *et al.*, 2003). The results exhibit a systematic trend with the orders of the pair chosen. The data points show the best present knowledge of $|V_{us}|$ (the open circle determined using unitarity) and $m_s(m_\tau^2)$ from outside τ physics. The two $|V_{us}|$ values shown correspond to the average of the $K_{\ell 3}$ and $K_{\mu 2}$ results (full circle), and to the $\sqrt{1 - |V_{ud}|^2}$ unitarity-based number (open circle) (Isidori, 2005).

results from $K_{\ell 3}$ and $K_{\mu 2}$ decays may be worrisome. It could indicate that not all τ strange final states have been identified. In this context it is important to revisit in particular the branching ratio for the $\nu_\tau K^- \pi^+ \pi^-$ mode where the agreement is marginal between ALEPH on the low side, and CLEO and OPAL on the high side (Section III.C).

One could forecast a significant improvement with the analyses of high statistics τ samples available at the B Factories. The detectors at these facilities (*BABAR* and *Belle*) are equipped with powerful Cherenkov counters, well suited to separate kaons and pions in a large momentum domain, and one should expect significant improvement in the measurement of the small, statistics-limited strange branching fractions. Then it is conceivable that a competitive determination of $|V_{us}|$ can be obtained.

We now turn back to the m_s determination. In fact, owing to the availability of the different moments, it is possible to fit them simultaneously and to derive both $|V_{us}|$ and m_s . In doing so it is mandatory to take into account the strong correlations between the moments. With the present best data it seems not possible to achieve a consistent description of all five moments ($k = 0 - 4$) with a unique solution for $|V_{us}|$ and m_s . The situation is best illustrated in Fig. 35 showing the 68% CL contours when only pairs of moments are considered in the fit. Typical examples are given with the following “adjacent” k -pairs: going from $k = 0, 1$ through $k = 3, 4$ pairs clearly selects different regions in the plane. The situation is worse than it looks at first sight since the moments are highly correlated. Indeed, the correlation coefficient ranges from 0.68 ($k = 0 - 4$) to 0.99 ($k = 2 - 3, 3 - 4$). A fit of the three $k = 0, 2, 4$ moments (adding more does not extract any new information from the data) yields a χ^2 of 6.4 for 1 DF, corresponding to a goodness-of-fit probability of only 1%.

We are afraid that the pattern emerging from Fig. 35 undermines the reliability in the previous findings of m_s from τ decays, at least within their quoted errors. The more recent determinations (Baikov *et al.*, 2004; Gámiz *et al.*, 2005) have focused on the higher $k = 2, 3, 4$ moments (only the $k = 3$ moment is used in (Baikov *et al.*, 2004)) since they are more sensitive to m_s and they used a world average value for $|V_{us}|$. However, Fig. 35 shows that the data prefer a lower value, not consistent with the world average. This might be the result of the worse behavior of the perturbative expansion of the higher moments as detailed in Eq. (174), even for the $J = 1 + 0$ part. Another sign of potential problems is found in the m_s running study as function of s_0 in Section VIII.D.2, where the stability of the results for the higher moments could not be safely established.

It may be that some of these alarming features will disappear with better experimental data, especially if

systematic deviations are found. More precise data from the B Factories on the multi-hadronic strange final states will certainly add valuable information to this problem. As for the moment, whereas the $|V_{us}|$ measurement from the $k = 0$ SU(3) breaking moment appears solid, the m_s determination is unfortunately plagued with systematic effects and does not appear to be sufficiently robust for a precise and model-independent measurement.

IX. CHIRAL SYMMETRY AND QCD SUM RULES

In the limit of n_f massless quarks ($m_i = 0, i = u, d, \dots$), the QCD Lagrangian possesses a global $SU_L(n_f) \times SU_R(n_f)$ chiral symmetry between the left- and right-handed quarks in flavor space. The associated conserved Noether currents are the vector (V^μ) and axial-vector (A^μ) quark currents. The vector and axial-vector charges

$$Q_{V/A} = \int d^3x V^0/A^0(x) , \quad (181)$$

are the generators of the symmetry group. For a state $|\phi\rangle$, which is symmetric under $SU(3)_L \times SU(3)_R$, one then must have (Gasser and Leutwyler, 1982)³⁰

$$\langle \phi | A_\mu^a(x) A_\mu^b(y) | \phi \rangle = \langle \phi | V_\mu^a(x) V_\mu^b(y) | \phi \rangle \quad (a, b = 1, \dots, 8) , \quad (182)$$

which requires that for every contribution on the r.h.s. of Eq. (182) ($J^P = 0^+$ or 1^-) there exists a mass degenerate partner on the l.h.s. ($J^P = 0^-$ or 1^+). However, chiral symmetry, which should be a good symmetry for the light u, d, s quarks, is not observed in the low energy hadronic spectra of e^+e^- annihilation or τ spectral functions. In order to be consistent with this experimental fact, the chiral flavor group $SU(3)_L \times SU(3)_R$ is assumed to be spontaneously broken down to $SU(3)_{L+R}$ where the vacuum expectation values are symmetric

$$\langle \bar{u}u \rangle = \langle \bar{d}d \rangle = \langle \bar{s}s \rangle \neq 0 . \quad (183)$$

The spontaneously symmetry breaking of the axial charge generates an octet of massless pseudoscalar Goldstone mesons (Goldstone, 1961; Goldstone *et al.*, 1961; Nambu and Jona-Lasinio, 1961), which is identified with the 8 lightest hadronic states: $\pi^+, \pi^0, \pi^-, \eta, K^+, K^-, K^0$ and \bar{K}^0 . In this case, the axial-vector current is non-conserved and its divergence reads

$$\partial_\mu A_{ij}^\mu = (m_i + m_j) \bar{q}_i (i\gamma_5) q_j , \quad (184)$$

which is associated with the decay constant f_P of a pseudoscalar meson P with four momentum q_μ , defined as

$$\langle 0 | \partial_\mu A_P^\mu | P \rangle = \sqrt{2} f_P m_P^2 \quad \text{or:} \quad \langle 0 | A_P^\mu | P \rangle = \sqrt{2} f_P q^\mu . \quad (185)$$

The non-vanishing physical masses of the pseudoscalars reflect the fact that chiral symmetry is not exact in QCD. True zero u, d, s quark masses would generate massless pseudoscalar mesons. Explicit mass relations between the pseudoscalars can be deduced from Chiral Perturbation Theory (*cf.* Section IX.D).

There is no indication of spontaneously symmetry breaking of the vector charge (the vector charge operators annihilate the vacuum): no light scalars have been found experimentally, and vector mesons can be classified in degenerate multiplets, which are $SU(3)_V$ representations. Hence, the longitudinal part of the vector correlator in Eq. (38) vanishes $\Pi_{ij,V}^{(0)}(q^2) = 0$.

Reducing chiral symmetry to the nonstrange sector, *i.e.*, to $SU(2)_L \times SU(2)_R$, one has the Lorentz-decomposed two-point correlation function

$$\begin{aligned} \Pi_{ud,LR}^{\mu\nu}(q) &\equiv i \int d^4x e^{iqx} \langle 0 | T(L^\mu(x) R^\nu(0)^\dagger) | 0 \rangle \\ &= (-g^{\mu\nu} q^2 + q^\mu q^\nu) \Pi_{ud,LR}^{(1)}(q^2) + q^\mu q^\nu \Pi_{ud,LR}^{(0)}(q^2) , \end{aligned} \quad (186)$$

³⁰ The conserved right- ($R = V + A$) and left-handed ($L = V - A$) currents under $SU(3)_L \times SU(3)_R$ transform like $(\underline{8}, \underline{1})$ and $(\underline{1}, \underline{8})$, respectively. If $|\phi\rangle$ is invariant then $\langle \phi | RL | \phi \rangle = 0 \Rightarrow \langle \phi | V^2 - A^2 | \phi \rangle = 0$, which is Eq. (182).

where L^μ and R^μ are the left- and right-handed quark currents

$$L^\mu = \bar{u}\gamma^\mu(1 - \gamma_5)d, \quad R^\mu = \bar{u}\gamma^\mu(1 + \gamma_5)d. \quad (187)$$

With Eqs. (186) and (187) and the correlators for vector and axial-vector currents (38) one finds

$$\Pi_{\bar{u}d,LR}^{\mu\nu}(q) = \Pi_{\bar{u}d,V}^{\mu\nu}(q) - \Pi_{\bar{u}d,A}^{\mu\nu}(q). \quad (188)$$

In the chiral limit and for $q^2 \rightarrow \infty$, the correlator $\Pi_{\bar{u}d,LR}^{\mu\nu}(q)$ vanishes (which again implies the degeneracy of Eq. (182)). With the use of a dispersion relation and from the comparison of the $q^\mu q^\nu$ and the q^2 terms in Eq. (186), one obtains the two Weinberg sum rules (WSR) for u, d quark correlators (Weinberg, 1967)

$$1. \text{ WSR : } \int_0^{s_0 \rightarrow \infty} ds \text{Im} \left[\Pi_{\bar{u}d,V}^{(1)}(s) - \Pi_{\bar{u}d,A}^{(1)}(s) + \Pi_{\bar{u}d,V}^{(0)}(s) - \Pi_{\bar{u}d,A}^{(0)}(s) \right] = 0, \quad (189)$$

$$2. \text{ WSR : } \int_0^{s_0 \rightarrow \infty} ds s \text{Im} \left[\Pi_{\bar{u}d,V}^{(1)}(s) - \Pi_{\bar{u}d,A}^{(1)}(s) \right] = 0. \quad (190)$$

The upper integration bound s_0 is finite when integrating over experimental spectral functions, and the missing saturation of the integral at the cut-off is a source of systematic uncertainty. The first WSR can be simplified using the pion decay constant f_π defined in Eq. (185), which fixes the integral $\int ds \text{Im} \Pi_{\bar{u}d,A}^{(0)}(s) = f_\pi^2$, and the fact the longitudinal vector correlator vanishes. Defining

$$\rho_{V-A}(s) = v_1(s) - a_1(s), \quad (191)$$

the two Weinberg sum rules read

$$1. \text{ WSR : } \frac{1}{4\pi^2} \int_0^{s_0 \rightarrow \infty} ds \rho_{V-A}(s) = f_\pi^2, \quad (192)$$

$$2. \text{ WSR : } \frac{1}{4\pi^2} \int_0^{s_0 \rightarrow \infty} ds s \rho_{V-A}(s) = 0. \quad (193)$$

In the presence of non-zero quark masses, only the first WSR remains valid while the second WSR breaks down due to contributions from the difference of non-conserved currents of order m_q^2/s , leading to a quadratic divergence of the integral (Floratos *et al.*, 1979). However, convergence can be recovered by considering a *Borel-transformed* (also denoted *Laplace-transformed*) version of the second WSR (see Section IX.C), where the result is expressed as a function of the Borel parameter M^2 and the u, d running quark masses at scale M^2 and quark condensates in powers of $1/M^0, 1/M^2, \dots$ (Floratos *et al.*, 1979; Peccei and Solà, 1987; Shifman *et al.*, 1979).

Using a narrow-width approximation for the resonances and a saturation of the corresponding vector, axial-vector spectral functions by the π , $\rho(770)$ and $a_1(1260)$, Weinberg deduced from these sum rules the mass formula (Weinberg, 1967) $m_{a_1}/m_\rho \simeq 1.41$, which compares not too badly with the experimental value of 1.60 ± 0.05 (Particle Data Group, 2004), keeping in mind the coarseness of the approximation used.

Das, Mathur and Okubo (DMO) (Das *et al.*, 1967b) showed that the derivative of the vector minus axial-vector correlator $\Pi_{\bar{u}d,V-A}(q^2)$ taken at $q^2 = 0$ is connected with the radiative $\pi^- \rightarrow \ell^- \bar{\nu}_\ell \gamma$ decay axial-vector

form factor F_A via³¹

$$\left. \frac{d(q^2 \Pi_{\bar{u}d, V-A}(q^2))}{dq^2} \right|_{q^2=0} = \frac{1}{4\pi^2} \int_0^{s_0 \rightarrow \infty} ds \frac{1}{s} \rho_{V-A}(s) = f_\pi^2 \frac{\langle r_\pi^2 \rangle}{3} - F_A , \quad (195)$$

with the pion charge radius-squared $\langle r_\pi^2 \rangle$ given in Eq. (67). This relation has been used in the past to perform a finite energy sum-rule determination of the electric polarizability³² of the pion (Höcker, 1997; Kartvelishvili *et al.*, 1997; Margvelashvili, 1988; Menke, 1999). Equation (195) is an example for an *inverse moment spectral sum rule*. It is special because the integration kernel is singular at $s = 0$ so that its residue is sensitive to the chiral properties of the spectral functions (*cf.* Section IX.D).

The electromagnetic mass splitting between the charged and the neutral pion has been calculated using current algebra techniques in chiral symmetry by Das *et al.* (Das *et al.*, 1967a). They derived the Das-Guralnik-Low-Mathur-Young (DGLMY) sum rule

$$\begin{aligned} 16\pi^2 i \int \frac{d^4 q}{(2\pi)^4} \frac{1}{q^2} \int_0^{s_0 \rightarrow \infty} ds s \frac{\text{Im} \left[\Pi_{\bar{u}d, V}^{(1)}(s) - \Pi_{\bar{u}d, A}^{(1)}(s) \right]}{q^2 + s - i\epsilon} &= \frac{1}{4\pi^2} \int_0^{s_0 \rightarrow \infty} ds s \ln \frac{s}{\Lambda^2} \rho_{V-A}(s) \\ &= -\frac{4\pi f_\pi^2}{3\alpha} (m_{\pi^\pm}^2 - m_{\pi^0}^2) . \end{aligned} \quad (196)$$

Making use of the KSFR relation (Kawarabayashi and Suzuki, 1966; Riazuddin and Fayazuddin, 1966) and lowest resonance saturation, they obtained the relation

$$m_{\pi^\pm}^2 - m_{\pi^0}^2 = \frac{3\alpha m_\rho^2 \ln 2}{4\pi m_\pi} = 5.1 \text{ MeV} , \quad (197)$$

in approximate agreement with the experimental value of 4.59 MeV (Particle Data Group, 2004). Although apparently containing an arbitrary energy scale Λ , the sum rule (196) is actually independent of Λ by virtue of the second WSR. However, for finite s_0 a residual Λ dependence is maintained.

A. Chiral sum rules with τ spectral functions

The spectral integrals (189) through (196) are computed with variable upper integration bounds $s_0 \leq m_\tau^2$ using the experimental τ hadronic spectral functions and their respective covariance matrices. The availability of the covariance matrices allows one to perform a straightforward Gaussian error propagation taking into account the strong bin-to-bin correlations of the spectral functions³³. The vector minus axial-vector τ spectral

³¹ In cases where the radiated photon is real the differential decay rate can be written as

$$\frac{d^2 \Gamma_{\pi \rightarrow \ell \nu \gamma}}{dE_\gamma dE_\ell} = \frac{d^2 (\Gamma_{\text{IB}} + \Gamma_{\text{SD}} + \Gamma_{\text{INT}})}{dE_\gamma dE_\ell} , \quad (194)$$

where Γ_{IB} , Γ_{SD} and Γ_{INT} are the contributions from inner bremsstrahlung, structure-dependent radiation and their interference. The structure-dependent term is parameterized by using vector and axial-vector form factors $F_{V/A}$ (for the complete expression see Ref. (Particle Data Group, 2004)).

³² The electric polarizability α_E of a physical system can be classically understood as the proportionality constant that governs the induction of the dipole moment \mathbf{p} of a system in presence of an external electric field vector \mathbf{E} : $\mathbf{p} = \alpha_E \mathbf{E}$. The polarizability is an important quantity to characterize a particle, *i.e.*, in probing its inner structure. In chiral perturbation theory, it can be shown (Holstein, 1990; Terent'ev, 1973) that the polarizability of the pion is given by $\alpha_E = \alpha F_A / (m_\pi f_\pi^2)$, which gives (Höcker, 1997) $\alpha_E = (2.86 \pm 0.33) \times 10^{-4} \text{ fm}^3$. Using the value (67) for the pion charge radius-squared, the analysis of a Borel-improved DMO sum rule yields (Höcker, 1997) $\alpha_E = (2.96 \pm 0.32) \times 10^{-4} \text{ fm}^3$.

³³ The spectral integrals with weight function $w(s)$ are evaluated as

$$I(s_0) = \int_0^{s_0} ds w(s) [v_1(s) - a_1(s)] = \sum_{i=1}^{N_{\text{bin}}(s_0)} \Delta s_i w(s_i) [v_{1,i} - a_{1,i}] ,$$

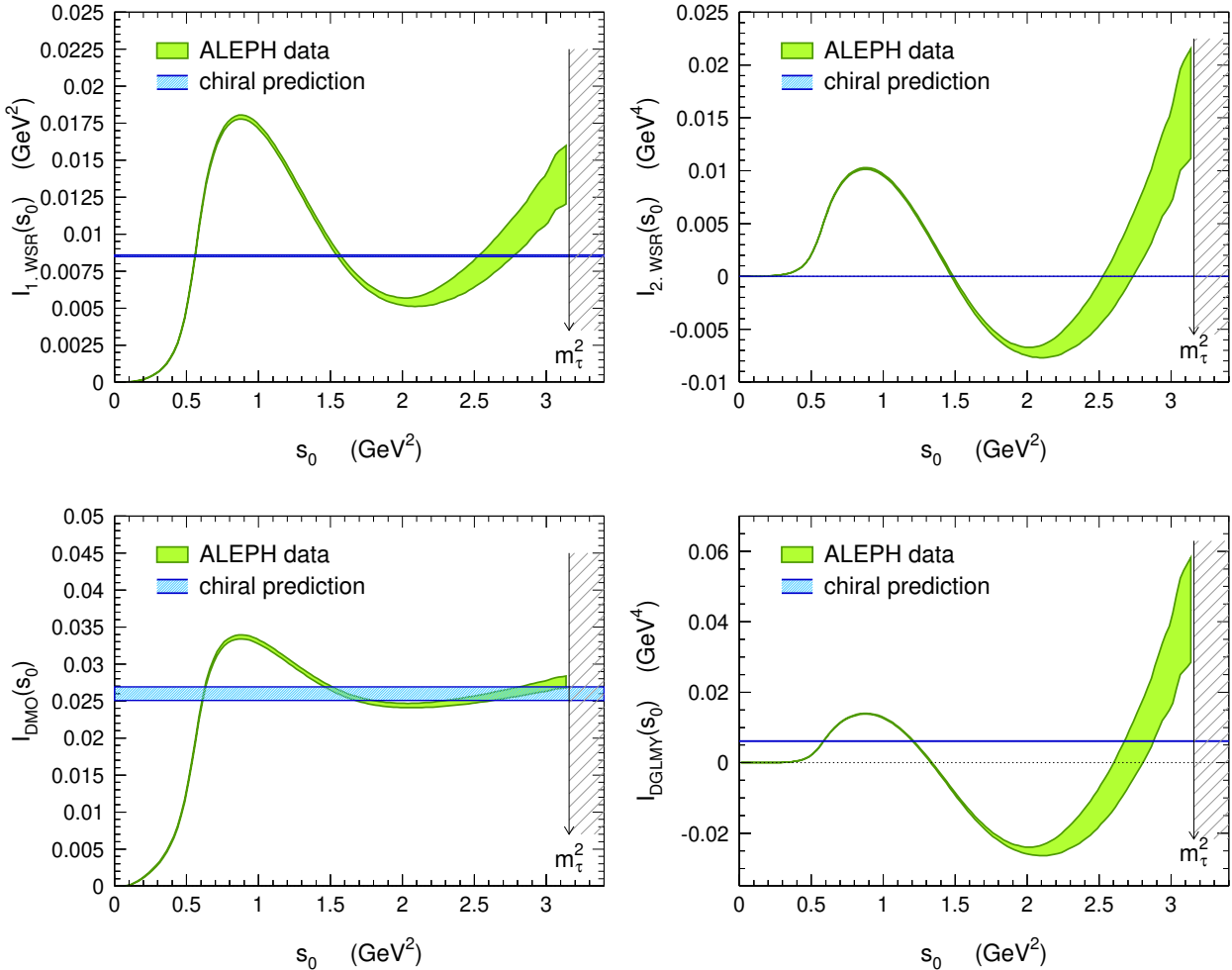


FIG. 36 The first and second Weinberg sum rules (upper left and right), and the DMO and DGLMY sum rules (lower left and right) versus the upper integration cut-off (s_0). The horizontal bands indicate the chiral predictions within errors, assuming full saturation of the integrals.

functions measured by ALEPH (ALEPH Coll., 2005) and OPAL (OPAL Coll., 1999b) have been shown in the right hand plot in Fig. 8. Local saturation of the spectral functions at the integral end point s_0 would require convergence of central values and all derivatives at zero. This is certainly not yet achieved at $s_0 = m_\tau^2$. We hence expect the sum rules not to be entirely satisfied for the τ spectral functions.

The sum rules (189) through (196) versus the upper integration cut-off $s_0 \leq m_\tau^2$ are plotted in Fig. 36 for the ALEPH spectral functions. The horizontal band depicts the chiral predictions of the integrals, neglecting OPE power corrections. One observes that only for the DMO sum rule (lower left plot), where contributions

and their errors-squared read

$$\sigma^2(I(s_0)) = \sum_{i,j=1}^{N_{\text{bin}}(s_0)} \Delta s_i \Delta s_j w(s_i) w(s_j) [C_{ij}^V + C_{ij}^A] ,$$

where the anti-correlations between v_1 and a_1 due to the estimates of the vector/axial-vector parts of the $K\bar{K}\pi(\pi)$ final states, and also due to experimental feed through between modes with adjacent numbers of pions, must be reabsorbed in the respective covariance matrices $C^{V/A}$, so that v_1 and a_1 can be assumed to be uncorrelated.

from higher masses are suppressed, saturation at the τ mass is approximately satisfied within errors. The other sum rules are not saturated at m_τ^2 , and no further conclusions can be drawn.

Many $V - A$ sum-rule analyses have been performed since the experimental spectral functions became available (Bijnens, 2001; Cirigliano *et al.*, 2003a,b; Ciulli *et al.*, 2003; Davier *et al.*, 1998; Dominguez and Schilcher, 2004; Ioffe and Zyablyuk, 2001; Peris *et al.*, 2001; Rojo and Latorre, 2004; Zyablyuk, 2004). Some of these will be discussed in the following.

B. Operator product expansion

Useful relations between the OPE terms and the spectral functions are obtained from projective sum rules (Kartvelishvili and Margvelashvili, 1992). The conservation of currents in the chiral limit implies $s \left[\Pi_{\bar{u}d,V}^{(1)}(s) - \Pi_{\bar{u}d,A}^{(1)}(s) \right] = 0$ in momentum space. For large space-like momenta $Q^2 = -s$ one can expand the dispersion relation of the $V - A$ correlator, and with the use of the first and the second WSR one obtains

$$\frac{1}{4\pi^2} \int_0^{s_0 \rightarrow \infty} ds \rho_{V-A}(s) \left[\frac{1}{s+Q^2} - \left(\frac{s^2}{Q^6} - \frac{s^3}{Q^8} + \dots \right) \right] \approx 0. \quad (198)$$

On the other hand, nonperturbative effects give rise to nonperturbative OPE contributions

$$\Pi_{\bar{u}d,V}^{(1)}(s) - \Pi_{\bar{u}d,A}^{(1)}(s) = \sum_{D=2,4,6,\dots} \frac{1}{(-s)^{D/2}} \sum_{\dim \mathcal{O}=D} C_{D,V-A}(s, \mu) \langle \mathcal{O}_D(\mu) \rangle_{V-A}, \quad (199)$$

where we shall omit the $V - A$ subscripts in the following. The dimension $D = 0$ contribution is of pure perturbative origin and is degenerate in all orders of perturbation theory for vector and axial-vector currents. To NLO in QCD one has

$$C_D(s, \mu) \langle \mathcal{O}_D(\mu) \rangle = a_D(\mu) + b_D \ln \left(\frac{s}{\mu^2} \right). \quad (200)$$

The explicit logarithmic dependence of the Wilson coefficients (the b_D terms) is known for $D = 2, 4, 6$, but not for higher dimensions. Comparing the coefficients of the corresponding powers between Eqs. (198) and (199), and using Eq. (85), leads for the non-logarithmic OPE terms to the sum rules (Cirigliano *et al.*, 2003a)

$$\begin{aligned} \frac{1}{4\pi^2} \int_0^{s_0} ds \left(\frac{s}{s_0} \right)^k \rho_{V-A}(s) &= -\frac{1}{2\pi i} \oint_{|s|=s_0} ds \frac{a_D}{(-s)^{D/2}} \left(\frac{s}{s_0} \right)^k \\ &= (-1)^k \frac{a_D}{s_0^k} \delta_{k,(D/2)-1}, \end{aligned} \quad (201)$$

where $\delta_{m,n}$ has the value 1 if $m = n$, and 0 elsewhere.

The validity of the OPE depends on the size of the cut-off scale s_0 . Apart from the saturation of the spectral integral, this represents a second source of systematic uncertainty related to the cut-off. The insertion of appropriate weight functions $w(s)$ under the spectral integral in (201) may help to reduce the impact of these systematics (see also the discussion in (Cirigliano *et al.*, 2003a,b)). While the impact of missing saturation can be reduced by suppressing the high-energy tail of the $V - A$ spectral function, the breakdown of the OPE due to quark-hadron duality violations is unavoidable to some extent³⁴. In practice, this duality violation is assumed to be absorbed by the OPE power operators that are fit phenomenologically to the spectral sum rules. The fit protects the physical observable (for instance the strong coupling constant as discussed in Section VII) that one is aiming to extract. If the nonperturbative corrections are found to be large, this

³⁴ Reference (Blok *et al.*, 1998) gives the following definition of quark-hadron duality. “In a nutshell, a *truncated* OPE is analytically continued, term by term, from the Euclidean to the Minkowski domain. A smooth quark curve obtained in this way is supposed to coincide at high energies (energy releases) with the actual hadronic cross section.”

protection mechanism may not work sufficiently well anymore, and duality violations can entail systematic errors. The optimization between saturation of the integral on one hand, and small duality violation on the other hand requires a compromise: if one aims at a minimum saturation loss, *i.e.*, small residual modulations of the spectral function in the vicinity of the cut-off s_0 , one has to apply a weight function that suppresses the high-energy tail³⁵. However, the stronger the suppression the larger the quark-hadron duality violation is expected to be.

Using the formulae of (Braaten *et al.*, 1992) and (Chetyrkin and Kwiatkowski, 1993) for the nonperturbative power expansion of the correlators, one obtains for the $V - A$ correlators the OPE (Davier *et al.*, 1998)

$$\begin{aligned} \Pi_{\overline{u}d, V-A}^{(0+1)}(-s) = & -\frac{a_s(s)}{\pi^2} \frac{\hat{m}^2(s)}{s} + \left(\frac{8}{3}a_s(s) + \frac{59}{3}a_s^2(s) \right) \frac{\hat{m}\langle \overline{u}u + \overline{d}d \rangle}{s^2} - \frac{16}{7\pi^2} \frac{\hat{m}^4(s)}{s^2} \\ & - 8\pi^2 a_s(\mu^2) \left[1 + \left(\frac{119}{24} - \frac{1}{2}L(s) \right) a_s(\mu^2) \right] \frac{\langle \mathcal{O}_6^1(\mu^2) \rangle}{s^3} \\ & + \frac{2\pi^2}{3} \left[3 + 4L(s) \right] a_s^2(\mu^2) \frac{\langle \mathcal{O}_6^2(\mu^2) \rangle}{s^3} + \frac{\langle \mathcal{O}_8 \rangle}{s^4}, \end{aligned} \quad (202)$$

$$\begin{aligned} \Pi_{\overline{u}d, V-A}^{(0)}(-s) = & -\frac{3}{\pi^2} \left[2a_s^{-1}(s) - 5 + \left(-\frac{21373}{2448} + \frac{75}{17}\zeta(3) \right) a_s(s) \right] \frac{\hat{m}^2(s)}{s} - 4\hat{C}(\mu^2) \frac{\hat{m}^2(\mu^2)}{s} \\ & - 2 \frac{\hat{m}\langle \overline{u}u + \overline{d}d \rangle}{s^2} - \frac{1}{7\pi^2} \left[\frac{53}{2} - 12a_s^{-1}(s) \right] \frac{\hat{m}^4(s)}{s^2}, \end{aligned} \quad (203)$$

with $a_s(s) = \alpha_s(s)/\pi$, $L(s) = \ln(s/\mu^2)$ and the dimension $D = 6$ operators

$$\begin{aligned} \mathcal{O}_6^1 & \equiv \overline{u}\gamma_\mu\gamma_5 T^a d\bar{d}\gamma^\mu\gamma_5 T^a u - \overline{u}\gamma_\mu T^a d\bar{d}\gamma^\mu T^a u, \\ \mathcal{O}_6^2 & \equiv \overline{u}\gamma_\mu\overline{d}d\gamma^\mu u - \overline{u}\gamma_\mu\gamma_5\overline{d}d\gamma^\mu\gamma_5 u, \end{aligned} \quad (204)$$

and where the SU(3) generators T^a are normalized so that $\text{tr}(T^a T^b) = \delta^{ab}/2$. The average mass \hat{m} stands for $(m_u + m_d)/2$, *i.e.*, SU(2) symmetry is assumed. The constant $\hat{C}(\mu^2)$ depends on the renormalization procedure and should not affect physical observables. Dimension $D = 2$ mass terms are calculated perturbatively to order α_s^2 , which suffices for the light u, d , quarks. The coefficient functions of the dimension $D = 4$ operators for vector and axial-vector currents have been calculated to subleading order in (Chetyrkin *et al.*, 1985; Generalis, 1989). Their vacuum expectation values are expressed in terms of the scale invariant gluon and quark condensates. Since the Wilson coefficients of the gluon condensate are symmetric for vector and axial-vector currents, they vanish in the difference. The expectation values of the dimension $D = 6$ operators (204) obey the inequalities $\langle \mathcal{O}_6^1(\mu^2) \rangle \geq 0$ and $\langle \mathcal{O}_6^2(\mu^2) \rangle \leq 0$, which can be derived from first principles. The corresponding coefficient functions were calculated in the chiral limit (Lanin *et al.*, 1986). Since $\langle \mathcal{O}_6^2(\mu^2) \rangle$ is subleading in $a_s(\mu^2)$, it is neglected in most phenomenological analyses. In leading order, one can use factorization of the matrix elements (that is, vacuum insertion) to rewrite $\langle \mathcal{O}_6^1 \rangle$ in the form³⁶

$$\langle \mathcal{O}_6^1 \rangle \propto -\frac{64}{9}\pi^2 a_s \langle 0|\overline{u}u|0 \rangle \langle 0|\overline{d}d|0 \rangle. \quad (205)$$

For the dimension $D = 8$ operators no higher order calculations are available in the literature, so that it is customary in the QCD sum-rule analyses to neglect their logarithmic s dependence. Again, the $J = 0$ contribution vanishes in the chiral limit. A factorization result similar to Eq. (205) can be derived, which now involves a five-dimensional quark-gluon mixed condensate (Grozin and Pinelis, 1986; Ioffe and Zyablyuk, 2001; Zyablyuk, 2004). Higher OPE dimensions are neglected (see (Zyablyuk, 2004) for an analysis that includes the relevant $D = 10$ operators).

³⁵ The suppression of the high-energy spectral function also reduces the experimental uncertainty on the integral since the statistical errors are large at the kinematic endpoint of the τ phase space.

³⁶ Following (Zyablyuk, 2004), factorization for the $D = 6$ operators can be written as $\langle (\overline{u}\lambda\Gamma_1 d)(\overline{d}\lambda\Gamma_2 u) \rangle = -(16/9)\text{Tr}[(u \otimes \overline{u})\Gamma_1 \langle d \otimes \overline{d} \rangle \Gamma_2]$, where Γ_i are Dirac matrices (acting on color, flavor and Lorentz indices), the factor 16/9 includes the SU(3) color number, and the 4×4 matrix $\langle q \otimes \overline{q} \rangle$ is proportional to the quark condensate $\langle q \otimes \overline{q} \rangle = -(1/4)\langle 0|\overline{q}q|0 \rangle$.

C. Borel and pinched weight sum rules

Many ways have been explored to improve the saturation of the integrals at finite cut-off scale s_0 , and to better control the validity of the OPE. In general, the approaches distinguish themselves by the definition of the weight $w(s)$ used under the integral

$$\frac{1}{4\pi^2} \int_0^{s_0} ds w(s) \rho_{V-A}(s) . \quad (206)$$

Since duality violations are expected to be largest in the vicinity of the timelike real axis (Poggio *et al.*, 1976), some authors suggest to use weights of the form $w_n(s) \propto (1 - s/s_0)^n$ (Le Diberder and Pich, 1992b) (*cf.* Section VII.C). The class of functions that satisfy $w(s_0) = 0$ is introduced as “pinched weights” in (Cirigliano *et al.*, 2003a,b). As mentioned before, pinched weights improve the experimental accuracy of the sum rule, but also reduce the effective inclusiveness of the spectrum, and hence make it more sensitive to duality violations.

Another way to improve the saturation of finite energy sum rules is to apply the Borel weight $w(s) = \exp(-s/M^2)$, emphasizing the lower resonances of the spectrum. Here, the OPE operators of dimension $D = n$ are suppressed as $\langle \mathcal{O}_{2n+2} \rangle / n!$, and all leading terms of the OPE vanish. The Borel-transformed sum rules give rise to nonperturbative corrections from quark condensates and non-vanishing quark masses that scale with the Borel parameter M^2 and with $\alpha_s(M^2)$. For example, the Borel-transformed first WSR reads (Floratos *et al.*, 1979; Narison, 1982; Pascual and de Rafael, 1982; Peccei and Solà, 1987)

$$\begin{aligned} \frac{1}{4\pi^2} \int_0^{s_0 \rightarrow \infty} ds e^{-s/M^2} \rho_{V-A}(s) &= f_\pi^2 \\ &+ \frac{\alpha_s(M^2)}{2\pi} \left[-\frac{m_u(M^2)m_d(M^2)}{\pi^2} - \frac{8}{3} \frac{f_\pi^2 m_\pi^2}{M^2} - \frac{32\pi}{9} \frac{(\langle 0|\bar{q}q|0 \rangle)^2}{M^4} + \dots \right] , \end{aligned} \quad (207)$$

where the current algebra Gell-Mann-Oakes-Renner relation

$$f_\pi^2 m_\pi^2 = -(m_u + m_d) \langle 0|\bar{u}u|0 \rangle , \quad (208)$$

obtained from Eqs. (184) and (185) has been used (Gell-Mann *et al.*, 1978), and where $m_u(M^2)$ and $m_d(M^2)$ denote the running light quark masses (see (Jamin, 2002) for a derivation of chiral corrections to Eq. (208), which are found to be of the order of -5%). The Borel sum rule is plotted in Fig. 37 (left hand) for $M = 1$ GeV. The comparison with Fig. 36 (upper left hand plot) exhibits the gain in experimental precision and in the approach to the asymptotic regime. Inserting the experimental values for the parameters on the r.h.s. of Eq. (207), and neglecting higher order nonperturbative contributions $\mathcal{O}(M^{-6})$ and contributions other than quark condensates, one obtains $(8.44 \pm 0.17) \times 10^{-3}$ GeV². From Fig. 37 we conclude that further nonperturbative power terms need to be added in order to satisfy the sum rule.

To reduce the correlation between the different operators, one can consider a Borel transformation in the complex plane of the Borel scale parameter, that is $M^2 \rightarrow M^2 \exp[i(\pi - \phi)]$. Keeping only the leading order coefficients a_D in Eq. (200), one finds for the real and imaginary parts of the Borel transformation (Zyablyuk, 2004)

$$\frac{1}{4\pi^2} \int_0^{s_0 \rightarrow \infty} e^{c_\phi} \cos(s_\phi) \rho_{V-A}(s) = f_\pi^2 + \sum_{k=1}^{\infty} (-1)^k \frac{\cos(k\phi) a_{2k+2}}{k! M^{2k}} , \quad (209)$$

$$\frac{1}{4\pi^2 M^2} \int_0^{s_0 \rightarrow \infty} e^{c_\phi} \sin(s_\phi) \rho_{V-A}(s) = \sum_{k=1}^{\infty} (-1)^k \frac{\sin(k\phi) a_{2k+2}}{k! M^{2k+2}} , \quad (210)$$

with $s_\phi = (s/M^2) \sin \phi$, $c_\phi = (s/M^2) \cos \phi$. If the sum rule is applied to the τ spectral functions, the argument of the cosine function must be negative to suppress the unknown $s_0 > m_\tau^2$ tail of the spectrum. In the case of $\phi = \pi(2k-1)/(2k)$ ($k = 2, 3, \dots$) for the real part (209), and $\phi = \pi(k-1)/k$ ($k = 3, 4, \dots$) for the imaginary part (210), the sum rules become projective with vanishing leading operators of dimension $D = 2k+2$. The

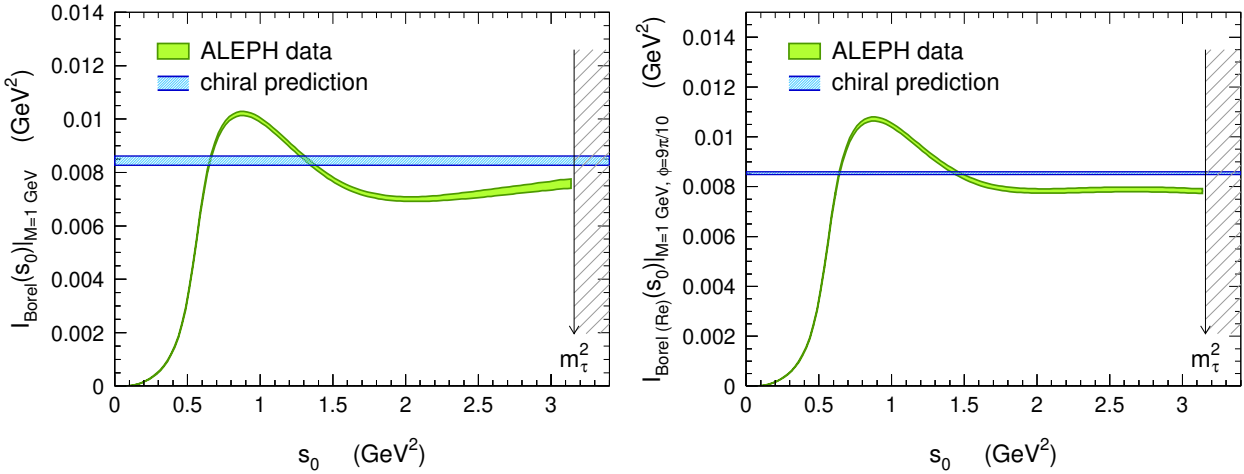


FIG. 37 The Borel sum rule (207) (left) and the real part of the complex Borel sum rule (209) for $\phi = 9\pi/10$ (right), at $M = 1 \text{ GeV}$, and as a function of the integral cut-off s_0 . The chiral prediction shown in the right hand plot does not include OPE power corrections.

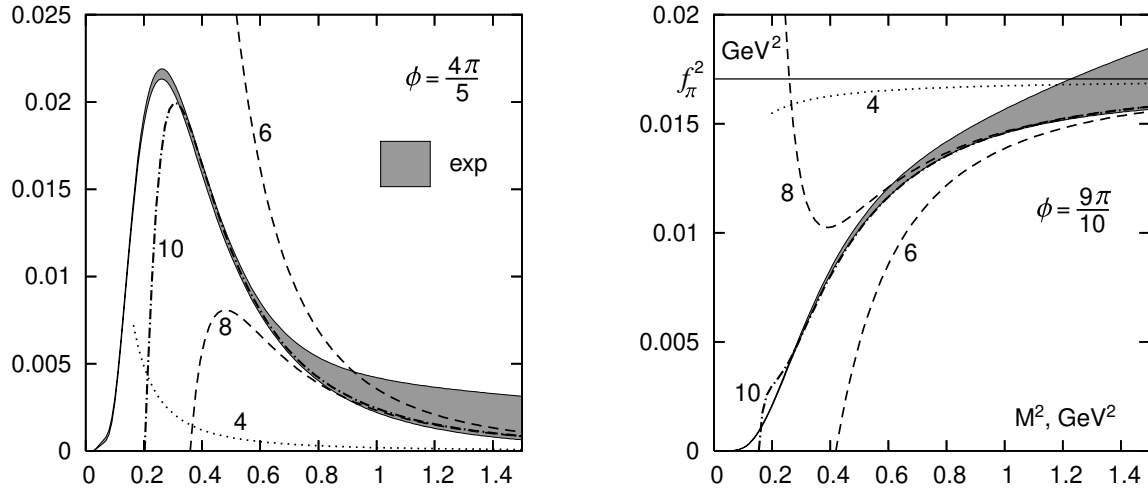


FIG. 38 Real part (209) of the Borel transformation for $\phi = 9\pi/10$, and its imaginary part (209) for $\phi = 4\pi/5$, as a function of the modulus M^2 of the Borel parameter. The leading order $D = 12$ operator a_{12} vanishes in these sum rules. The shaded band shows the ALEPH data (ALEPH Coll., 1997b, 1998c), and the lines display the leading order operator series, *i.e.*, neglecting all logarithmic terms. The numbers indicate the highest dimension considered in the operator sum. The figures are taken from (Zyablyuk, 2004).

real part for a particular working point chosen in (Zyablyuk, 2004) as a function of the cut-off s_0 is shown in the right hand plot of Fig. 37. The chiral prediction given contains the pion pole, but no OPE power corrections. The sum rule is well saturated at $s_0 = m_\tau^2$. The remaining discrepancy with the data is due to nonperturbative contributions. An update (Zyablyuk, 2004) of the numerical analysis performed in (Ioffe and Zyablyuk, 2001) finds for the leading $V - A$ operators using the ALEPH data (ALEPH Coll., 1998c)

$$a_6 = -(7.2 \pm 1.2) \times 10^{-3} \text{ GeV}^6, \quad (211)$$

$$a_8 = (7.8 \pm 2.5) \times 10^{-3} \text{ GeV}^8. \quad (212)$$

The author also estimates the leading $D = 10$ operator to be $a_{10} = -(4.4 \pm 2.8) \times 10^{-3} \text{ GeV}^{10}$, without however reporting the statistical correlations with a_6 and a_8 . The imaginary part (210) of the Borel sum rule

were used as input, as well as the angles $\phi = 2\pi/3, 3\pi/4, 4\pi/5$ for which the operators a_8, a_{10}, a_{12} vanish, respectively. For the Borel parameter M^2 a range between 0.4 and 1.0 GeV² is used, which is integrated over to determine an average χ^2 estimator (Zyablyuk, 2004) that is minimized in the fit. The fit results for the real and imaginary parts of the sum rules (209), (210), and for two working points in the parameter ϕ are shown in Fig. 38. The contribution from $D = 10$ is significant here.

D. Inverse moments sum rules and chiral perturbation theory

We have seen that at sufficiently high energies nonperturbative effects are parameterized by vacuum condensates, following the OPE rules. A particular role is played by the condensates that are order parameters of the spontaneous breakdown of chiral symmetry (SB χ S). They vanish at all orders of perturbation theory and control the high energy behavior of chiral correlation functions, such as the difference of vector and axial-vector current two-point functions. On the other hand, at low energies, SB χ S makes it possible to construct an effective theory of QCD, the Chiral Perturbation Theory (χ PT) (Gasser and Leutwyler, 1984; Weinberg, 1979), which uses the Goldstone bosons as fundamental fields and provides a systematic expansion of QCD correlation functions in powers of momenta and quark masses. Any missing information is then parameterized by low-energy coupling constants, which can be determined phenomenologically in low-energy experiments involving pions and kaons. The fundamental parameters describing chiral symmetry breaking, the running quark masses and the quark condensates appear both in low-energy χ PT and the high energy OPE expansion. For this reason it is useful to combine the two expansions in order to get a truly systematic approach to the chiral sum rules (Donoghue and Golowich, 1994). Such a combined approach is illustrated in (Davier *et al.*, 1998) through the determination of the L_{10} parameter of the chiral Lagrangian, including high-energy corrections coming from the OPE. The connection between the two domains is provided by the experimental τ spectral function ρ_{V-A} .

At leading order χ PT, L_{10} is obtained by the DMO sum rule (195)

$$\frac{1}{4\pi^2} \int_0^{s_0 \rightarrow \infty} ds \frac{1}{s} \rho_{V-A}(s) \simeq -4L_{10} . \quad (213)$$

As it stands the DMO sum rule (195) is subject to chiral corrections due to non-vanishing quark masses (Golowich and Kambor, 1997). On the other hand, the truncation of the integral at $s_0 \leq m_\tau^2$ introduces an error that competes with the low-energy chiral corrections. Both types of corrections can be systematically included through (i) the high-energy expansion in $\alpha_s(s_0)$ and in inverse powers of s_0 , and (ii) the low-energy expansion in powers of quark masses and of their logarithms.

In Section VII.C we have reviewed the simultaneous determination of the strong coupling constant and the OPE operators using the spectral weights

$$w^{(k,\ell)}(s) = \left(1 - \frac{s}{s_0}\right)^k \left(\frac{s}{s_0}\right)^\ell , \quad (214)$$

for $k, \ell \geq 0$. The extension of the spectral moment analysis to negative integer values of ℓ (“inverse moment sum rules”, (IMSR) (Golowich and Kambor, 1996)) requires, due to the pole at $s = 0$, a modified contour of integration in the complex plane, as illustrated in Fig. 39. This is where χ PT comes into play: along the small circle C_2 placed at the production threshold $s_{\text{th}} = 4m_\pi^2$ one can use χ PT predictions for the two-point correlators. Generalizing the spectral moments (134) to IMSR’s, one obtains for the Cauchy integral

$$R_{\tau,V/A}^{(k,\ell)} = 6\pi i |V_{ud}|^2 S_{\text{EW}} \oint_C \frac{ds}{s_0} w^{(k,\ell)}(s) \left[\left(1 + 2\frac{s}{s_0}\right) \Pi_{V/A}^{(0+1)}(s) - 2\frac{s}{s_0} \Pi_A^{(0)}(s) \right] , \quad (215)$$

where $C = C_1 + C_2$ for the inverse moments and $C = C_1$ for the positive moments (see Fig. 39).

The nonstrange correlators (38) are known up to two loops (Gasser and Leutwyler, 1984, 1985; Golowich and Kambor, 1995, 1998) in standard χ PT. The authors of (Davier *et al.*, 1998) use generalized χ PT (G χ PT (Knecht and Stern, 1995)) to $\mathcal{O}(p^4)$ one-loop order only. Standard χ PT assumes (Weinberg, 1977) the validity of Eq. (208) and $r \simeq 2m_K^2/m_\pi^2 - 1 \approx 25.9$, whereas G χ PT admits lower values of these two quantities (Fuchs *et al.*, 1990, 1991; Knecht and Stern, 1995). It is found that the present experimental precision

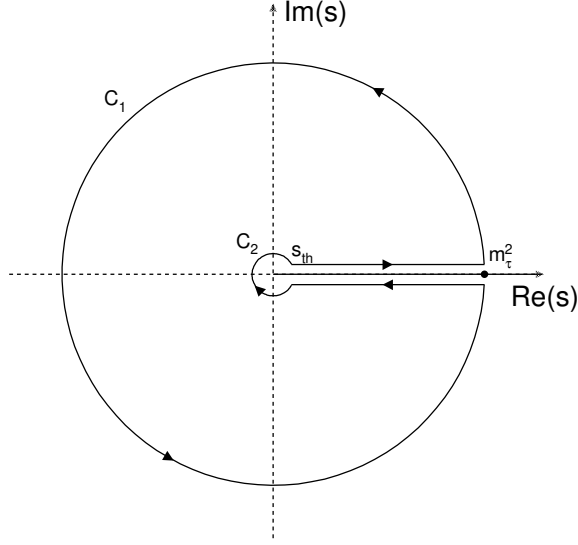


FIG. 39 Integration contour around the circles at $s = m_\tau^2$ and $s = s_{\text{th}}$.

of the nonstrange data does not allow to constrain the light quark masses, *i.e.*, the mass ratio $r = m_s/\hat{m}$, and hence to discriminate between the two approaches. The alterations of the standard $\mathcal{O}(p^4)$ results for nonstrange correlators introduced by $G\chi\text{PT}$ are marginal. They merely concern the symmetry breaking $J = 0$ component of the spectral functions and most of them are absorbed into the renormalization of f_π .

For the Cabibbo-allowed channel one finds for the χPT correlation functions (Davier *et al.*, 1998)

$$\Pi_{\overline{u}d,V}^{(0+1)}(s) = 4M_{KK}^r(s) + 8M_{\pi\pi}^r(s) - 4(L_{10}^r + 2H_1^r) , \quad (216)$$

$$\Pi_{\overline{u}d,V}^{(0)}(s) = 0 , \quad (217)$$

$$\Pi_{\overline{u}d,A}^{(0+1)}(s) = -\frac{2f_\pi^2}{s - M_\pi^2} - 4(2H_1^r - L_{10}^r) , \quad (218)$$

$$s\Pi_{\overline{u}d,A}^{(0)}(s) = -\frac{2f_\pi^2 M_\pi^2}{s - M_\pi^2} + 8\hat{m}^2(H_{2,2} - 2B_3) , \quad (219)$$

where $M_{PP'}^r(s)$ and $L_{PP'}(s)$ are loop integrals defined in (Gasser and Leutwyler, 1985). The superscript r refers to renormalized quantities, which depend on the scale $\mu_{\chi\text{PT}}$. The whole expressions are $\mu_{\chi\text{PT}}$ independent. The terms $H_{2,2}$ and B_3 are found to be finite, and do not need renormalization. The coefficients H_1^r and $H_{2,2}$ multiply contact terms of the sources. They are counterterms needed to renormalize the ultraviolet divergences of the Green functions and do not appear in physical observables. In the difference between vector and axial-vector correlators the constant H_1^r and all massless perturbative expressions cancel.

The analysis described in (Davier *et al.*, 1998) performs a fit of the OPE to the IMSR $R_{\tau,V-A}^{(1,-1)}$ (see the reference for the full expression of the evaluated Cauchy integral), and the spectral moments (134). The inner integration circle C_2 occurring in $R_{\tau,V-A}^{(1,-1)}$ introduces the sensitivity to the effective χPT parameter L_{10}^{eff} , which is determined by the fit. This quantity is a well defined observable. In the particular case of the one-loop $G\chi\text{PT}$ calculation, its expansion reads

$$L_{10}^{\text{eff}} = L_{10}^r(\mu_{\chi\text{PT}}) + \frac{1}{128\pi^2} \left(\ln \frac{m_\pi^2}{\mu_{\chi\text{PT}}^2} + 1 \right) + \frac{1}{384\pi^2} \ln \frac{m_K^2}{m_\pi^2} + \frac{2\hat{m}^2}{m_\tau^2} (2B_3 - \hat{H}_{2,2}) , \quad (220)$$

which is independent of $\mu_{\chi\text{PT}}$.

The spectral information is used to simultaneously determine L_{10}^{eff} and the nonperturbative phenomenological operators. For dimension $D = 6$ the contribution from \mathcal{O}_6^2 is neglected since it is large- N_C and α_s^2

suppressed. The results of the fit are reported as (Davier *et al.*, 1998)

$$L_{10}^{\text{eff}} = -(6.36 \pm 0.09_{\text{exp}} \pm 0.14_{\text{th}} \pm 0.07_{\text{fit}} \pm 0.06_{\text{OPE}}) \times 10^{-3} , \quad (221)$$

$$\langle \mathcal{O}_6 \rangle = (5.0 \pm 0.5_{\text{exp}} \pm 0.4_{\text{th}} \pm 0.2_{\text{fit}} \pm 1.1_{\text{OPE}}) \times 10^{-4} \text{ GeV}^6 , \quad (222)$$

$$\langle \mathcal{O}_8 \rangle = (8.7 \pm 1.0_{\text{exp}} \pm 0.1_{\text{th}} \pm 0.6_{\text{fit}} \pm 2.1_{\text{OPE}}) \times 10^{-3} \text{ GeV}^8 , \quad (223)$$

where $\mathcal{O}_6 = \mathcal{O}_6^1(m_\tau^2)$. The fit errors are separated in experimental (first errors) and theoretical (second errors) parts, and systematic fit uncertainties (third errors) are added. The last errors estimate the uncertainties due to the OPE breakdown (ALEPH Coll., 1998c). They are small for L_{10}^{eff} and dominant for the nonperturbative operators. Correlations between the fit parameters are found to be small, which improves the robustness of the result. Correcting for the factor of about -13 between the definition of $\langle \mathcal{O}_6 \rangle$ and a_6 of Eq. (211), the two estimates are in agreement. The results (222) and (223) have been confirmed in (OPAL Coll., 1999b) using OPAL data. In general it is observed that while all available sum-rule analyses³⁷ agree on the value for the $D = 6$ contribution to the $V - A$ correlator, the $D = 8$ contribution, due to its smallness, is less stable. It exhibits a model dependence that exceeds the experimental error in (223). For example, the analyses performed in (Bijnens, 2001; Cirigliano *et al.*, 2003b) find negative values for $\langle \mathcal{O}_8 \rangle$. We refer to the detailed comparisons of the various fit results for the nonperturbative power terms using the τ spectral functions in (Friot, 2004; Rojo and Latorre, 2004).

Expressing L_{10}^{eff} of Eq. (221) by means of Eq. (220) at the χ PT renormalization scale $\mu_{\chi\text{PT}} = m_\rho \simeq 770$ MeV, and neglecting the term $2\hat{m}^2(2B_3 - \hat{H}_{2,2})$, one obtains (Davier *et al.*, 1998)

$$L_{10}^r(m_\rho) = -(5.13 \pm 0.19) \times 10^{-3} , \quad (224)$$

where experimental and theoretical errors of different sources have been added in quadrature. This result can be compared with the value of L_{10}^r that is obtained from the one-loop expression of the axial form factor, F_A , of $\pi^- \rightarrow e^- \bar{\nu}_e \gamma$ decays (see (Bijnens and Talavera, 1997) for notations)

$$F_A = \frac{4\sqrt{2}m_\pi}{f_\pi} (L_9 + L_{10}) . \quad (225)$$

Using $L_9^r(m_\rho) = (6.78 \pm 0.15) \times 10^{-3}$ (Bijnens *et al.*, 1995a; Davier *et al.*, 1998; Gasser and Leutwyler, 1985) and $F_A = 0.0116 \pm 0.0016$ (Particle Data Group, 2004), one obtains $L_9 + L_{10} = (1.36 \pm 0.19) \times 10^{-3}$. This gives $L_{10}^r(m_\rho) = -(5.42 \pm 0.24) \times 10^{-3}$, in agreement with (224). Note that the quoted errors do not take into account uncertainties from higher order chiral corrections. Nonetheless, the determination of L_{10}^{eff} is independent of any chiral expansion: its value can be directly used in a two-loop analysis, where it suffices to include higher order corrections in Eq. (220).

The total purely nonperturbative contribution to $R_{\tau,V-A}$ found in the fit, taking into account the correlations between the operators, amounts to (Davier *et al.*, 1998)

$$R_{\tau,V-A} = 0.061 \pm 0.014 , \quad (226)$$

in agreement with the measurement 0.092 ± 0.023 (Eq. (28)).

A stability test of the results (221) through (223) at m_τ^2 is obtained by performing fits for variable “ τ masses” $s_0 \leq m_\tau^2$ (Davier *et al.*, 1998). The results of such fits are shown in Fig. 40. The horizontal bands give the results at m_τ^2 within one standard deviation (all errors added in quadrature). All curves exhibit a convergent behavior for $s_0 \rightarrow m_\tau^2$. Any deviation from the fit values for $s_0 > m_\tau^2$ should be covered by the “OPE” errors assigned to the results.

X. CONCLUSIONS AND PERSPECTIVES

The physics of hadronic τ decays has been the subject of much progress in the last decade, both at the experimental and the theoretical level. Somewhat unexpectedly, hadronic τ decays provide one of the most powerful testing grounds for QCD. This situation results from a number of favorable conditions:

³⁷ See also the detailed recent analysis (Catà *et al.*, 2005) on duality violations in $V - A$ sum rules, which came to late to be included in this review.

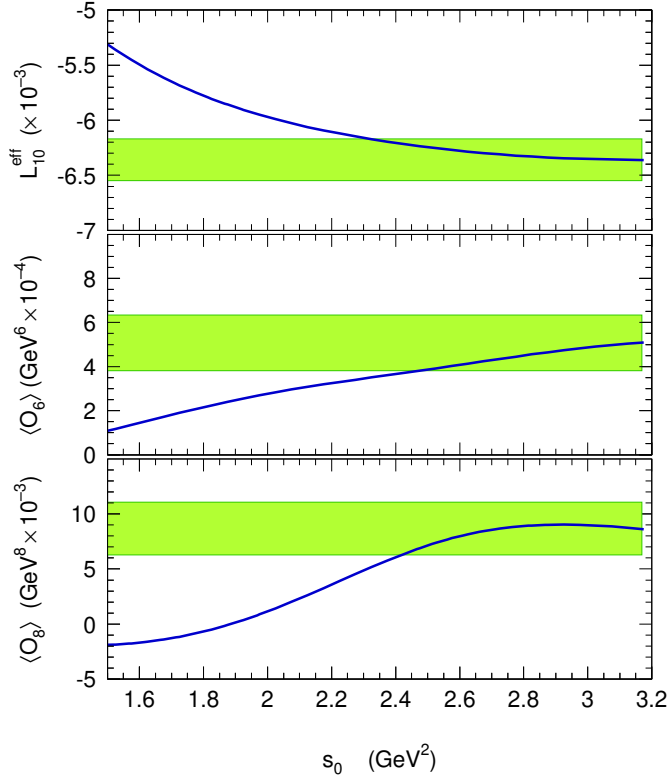


FIG. 40 Fit results for L_{10}^{eff} and the nonperturbative operators as a function of the “ τ mass” s_0 . The bands depict the values (221)–(223) within errors, obtained at m_τ^2 .

- The τ lepton is heavy enough to decay into a variety of hadrons, with net strangeness 0 and ± 1 .
- τ leptons are copiously produced in pairs at e^+e^- colliders, leading to simple event topologies without extra background particles.
- The experimental study of τ decays could be done with large data samples, either at LEP with high efficiency and small background, or at the $\Upsilon(4S)$ energy with much increased statistics, where the two experimental setups offer complementary advantages.
- As a consequence, τ decays are experimentally known to great details and their rates measured with high precision.
- The theoretical description of hadronic τ decays is based on solid ground and found to be dominated by perturbative QCD, as the result of several lucky circumstances, which shall be briefly recalled below.

The τ decay rates into hadrons are expressed through spectral functions of different final states with specific quantum numbers. The spectral functions are the basic ingredients to the theoretical description of these decays, since they represent the probability to produce a given hadronic system from the vacuum, as a function of its invariant mass-squared s . The spectral functions are dominated by known resonances, but tend to approach the quark-level asymptotic regime at m_τ^2 . They have been determined for individual hadronic modes, however they are conveniently summed and separated into their inclusive vector and axial-vector components for the nonstrange part, while the Cabibbo-suppressed strange part cannot be fully separated at present, due to the lack of necessary experimental information.

The nonstrange τ vector spectral functions can be compared to the corresponding quantities obtained in e^+e^- annihilation by the virtue of isospin symmetry. The $\mathcal{O}(\%)$ precision reached makes it necessary to correct for isospin-symmetry breaking. Beyond a first-order agreement, the detailed comparison unveils discrepancies with some e^+e^- data sets. Since the vector spectral functions are the necessary ingredients to compute vacuum polarization integrals, required for the evaluation of the running of $\alpha(s)$ or the anomalous magnetic moment

of the muon a_μ , this disagreement leads to different results when using τ or e^+e^- spectral functions. While the e^+e^- -based theoretical a_μ value disagrees with the measurement by 2.7 “standard deviations”, possibly indicating a contribution from physics beyond the Standard Model, the τ -based calculation is consistent with experiment. Although the use of e^+e^- data is *a priori* more direct, the physics at stake is such that the present situation must evolve, requiring more experimental and theoretical cross-checks. Newest e^+e^- results already indicate better agreement with the τ data.

The observation that hadronic τ spectral functions can provide precision information on perturbative QCD is surprising, considering the moderate energy scale involved in these decays. Hence it is useful to recall briefly the reasons behind this success:

- The total semileptonic decay rate normalized to the leptonic width, R_τ , is obtained by integrating over s the total spectral function weighed by a known kinematic function originating from the $V - A$ leptonic tensor. This integral can be transformed to a complex contour integral over a circle at $|s| = m_\tau^2$, hence involving only large complex s values where perturbative QCD can be applied.
- One factor in the weight function, $(1 - s/m_\tau^2)^2$, chops off the integrand in the vicinity of the real axis where poles of the current correlator are located.
- The invariant-mass spectra in the hadronic τ decays, dominated by resonances, are thus related to the quark-level contributions expected at large mass. This global quark-hadron duality is expected to work best in more inclusive situations. In the case of hadronic τ decays, this condition is particularly well met, with several resonance contributions in each of the equally important vector and axial-vector components.
- The perturbative expansion of the spectral function is known to third order in α_s , with some estimates of the fourth order coefficient.
- The perturbative and nonperturbative contributions can be treated systematically using the operator product expansion (OPE), giving corrections with inverse powers D of m_τ .
- The *a priori* dominant nonperturbative term from the gluon condensate ($D = 4$) is strongly suppressed by the second factor of the weight function, $(1 + 2s/m_\tau^2)$. This accidental fact renders hadronic τ decays particularly favorable since nonperturbative effects are expected to be small.
- The next $D = 6$ term is subject to a partial cancellation between the vector V and axial-vector A contributions, due to the $(1 - \gamma_5)$ factor in the W vertices.

These fortunate circumstances explain why hadronic τ decays can be globally described by perturbative QCD with very small nonperturbative corrections. This behavior has been verified model-independently using the measured spectral functions. From a simultaneous fit of the total hadronic rate, obtained with precision from the leptonic branching ratio, and spectral moments that are weighted integrals of the mass-squared distributions, the total nonperturbative contribution is found to be $\delta_{NP,V+A} = (-4.3 \pm 1.9) \times 10^{-3}$ relative to the $V + A$ hadronic width. This is almost a factor of 50 smaller than the α_s -dependent perturbative correction to R_τ . The predicted near-cancellation between the V and A contributions has been also observed, as $\delta_{NP,V} = (2.0 \pm 0.3) \times 10^{-2}$ and $\delta_{NP,A} = (-2.8 \pm 0.3) \times 10^{-2}$.

Several approaches are available to treat the perturbative expansion of the τ hadronic width. In fixed-order perturbation theory (FOPT), all contributions beyond the known orders of the Adler function are cut out, even if some parts resulting from the contour integral are calculable (and calculated). On the contrary, the contour-improved FOPT variant (CIPT) keeps all known terms. It has been shown that a faster convergence is achieved with CIPT and, since the FOPT expansion represents an unnecessary approximation, the CIPT approach should be preferred. Analyses using ALEPH and OPAL spectral functions give $\alpha_s(m_\tau^2)$ values that are in agreement. The robustness of the result can be established by comparing results from separate fits based on the V or A spectral functions, which are less inclusive and include larger, yet still small, nonperturbative contributions: their results are in reasonable agreement. A further test is achieved by partial integration of the spectral function up to a variable hypothetical τ mass s_0 less than m_τ^2 : the derived $\alpha_s(s_0)$ values are in agreement with the expected behavior from the QCD renormalization group down to s_0 values as low as 1 GeV^2 , where the OPE begins to break down. Therefore the moderately high mass of the τ lepton is shown to be fully adequate for a precision measurement of α_s .

Using the final spectral functions from ALEPH, supplemented by the world average leptonic and total strange hadronic fractions, the most precise determination of the strong coupling at the τ mass scale gives

$$\alpha_s(m_\tau^2) = 0.345 \pm 0.004_{\text{exp}} \pm 0.009_{\text{th}} . \quad (227)$$

Evolving this value to the Z mass, and adding experimental and theoretical errors in quadrature, gives $\alpha_s(M_Z^2)_\tau = 0.1215 \pm 0.0012$. Taken together with the measurement from the Z width at LEP, $\alpha_s(M_Z^2)_{Z \text{ width}} = 0.1186 \pm 0.0027$, the $\alpha_s(m_\tau^2)$ determination provides a powerful test of the running of α_s as predicted by QCD. The property of asymptotic freedom can be conveniently tested using the estimator

$$r(s_1, s_2) = \frac{\Delta \alpha_s^{-1}}{\Delta \ln \sqrt{s}} = 1.405 \pm 0.053 , \quad (228)$$

with $s_1 = m_\tau^2$ and $s_2 = M_Z^2$, while QCD predicts 1.353 ± 0.006 .

Further progress in the QCD analyses of τ decays will have to wait for a full calculation of the fourth-order coefficient K_4 in the Adler function expansion. Such a program is underway and will succeed with the availability of improved computing power. When K_4 is known, we expect the perturbative uncertainty to become really small: the errors on $\alpha_s(m_\tau^2)$ from K_5 , estimated assuming a geometric growth of the perturbative coefficients with 100% uncertainty, and from the renormalization scale will be 0.002 and 0.002, respectively. Using the existing data, the total error on $\alpha_s(m_\tau^2)$ will be reduced by a factor of 2 and reach a relative precision of 1.4%. Hence the calculation of K_4 will be highly rewarding.

Further progress can be considered with better quality data. Whereas ameliorating the precision on the branching ratios appears to be difficult, several areas could be improved with facilities such as the B Factories, affording very large statistics samples. Examples include the study of the high mass part of the spectrum near the τ -mass endpoint, limited at the moment by statistics. This will improve the knowledge of the spectral function in an interesting region and permit the study of the approach to the asymptotic regime. Such topics can also be covered at a τ -charm factory operating near the τ threshold. Detailed physics simulations are required to quantitatively assess the potential of these measurements.

The strange component of the τ hadronic width gives access to the study of flavor-symmetry breaking induced by the massive s quark as compared to the nearly massless u and d quarks. Although the expected shift in the strange hadronic width is indeed found experimentally, it turns out that a competitive determination of the strange quark mass m_s is difficult because of poor convergence of the mass-dependent perturbative series and lack of sufficient inclusiveness in the higher-order spectral moments that are most sensitive to m_s . Thus various analyses have given somewhat different results, depending on the moments used. The situation might improve with a better determined strange spectral function. Contrary to the situation for m_s , the determination of the CKM matrix element $|V_{us}|$ from the strange τ decays appears on safe grounds, since it relies directly on the non-weighted spectral function with maximum inclusiveness and a better control of the perturbative expansion. Present data yield

$$|V_{us}| = 0.2204 \pm 0.0028_{\text{exp}} \pm 0.0003_{\text{th}} \pm 0.0001_{m_s} , \quad (229)$$

where m_s has been taken from lattice calculations to be $m_s(m_\tau^2) = (79 \pm 8)$ MeV.

The study of strange τ decays can benefit significantly from the large statistical samples provided by the B Factories, complemented by the excellent $K - \pi$ separation available with the *BABAR* and *Belle* detectors. The prospects are excellent for improving over the present situation. As discussed above, the determination of $|V_{us}|$ is limited by the experimental error, while the theoretical uncertainty would permit the best measurement among all of this quantity. We express our wish that these experiments measure the various strange decay channels in a systematic way towards achieving this goal. It could also occur that the present unsatisfactory situation on the determination of m_s will improve during this process. In any case, better strange spectral functions are needed.

Another active field of research is the study of finite energy chiral sum rules, involving the nonstrange $V - A$ spectral function, which are of intrinsically nonperturbative nature. The analyses are divided into spectral moments that are weighted integrals over the $V - A$ spectral function with some high-mass damping function to reduce the systematic uncertainty due to the finite energy integral cut-off, and inverse moment sum rules, which, due to the singularity at $s = 0$, give direct access to the chiral structure of the QCD Lagrangian. The former sum rules are useful to analyze the nonperturbative structure of the OPE, since it allows one to measure the higher dimensional operators of the expansion independently of the perturbative contributions. Several analyses give agreeing results on the $D = 6$ contribution, while the much smaller $D = 8$ contribution

exhibits some model dependence. Even $D = 10$ has been considered and found to improve the fit, though not significantly. No sign of nonconvergence of the OPE has been detected at the τ -mass scale. Inverse moment sum rules have been traditionally used through the Das-Mathur-Okubo sum rule to determine the polarizability of the pion. In a more evolved later analysis the parameter L_{10} of the chiral Lagrangian has been determined, which at one-loop and expressed at the Chiral Perturbation Theory (χ PT) renormalization scale $\mu_{\chi\text{PT}} = m_\rho \simeq 770$ MeV, is found to be

$$L_{10}^r(m_\rho) = -(5.13 \pm 0.19) \times 10^{-3}, \quad (230)$$

where experimental and theoretical errors of different sources have been added in quadrature. This result is in agreement with, but more precise than corresponding determinations from the axial form factor of $\pi^- \rightarrow e^- \bar{\nu}_e \gamma$ decays.

While the study of hadronic τ decays has achieved a high status thanks to precise and complete sets of measurements and the development of the relevant theoretical framework, it is satisfying that advances are at hand both at the experimental and theoretical levels.

Acknowledgments

We are indebted to all our experimental and theoretical colleagues who have provided valuable contributions to the field of τ physics. During this work we benefited from helpful discussions with Georges Grunberg, François Le Diberder, William Marciano, Sven Menke, Antonio Pich, Joachim Prades, Jan Stern, and Konstantin Zyablyuk. We thank Konstantin Chetyrkin, Matthias Jamin, Sven Menke, Antonio Pich, Achim Stahl and Arkady Vainshtein for critically reading the document and providing helpful comments. Special thanks to Shaomin Chen and Changzheng Yuan for the fruitful collaboration on the spectral function measurements.

References

Abe, T., *et al.*, 2001, Linear Collider Physics Resource Book for Snowmass 2001, SLAC-R-570, [hep-ex/0106057].
 Adams, D., *et al.*, 1994, Phys. Lett. **B329**, 399.
 Adler, S., 1974, Phys. Rev. **D10**, 3714.
 ALEPH Collaboration (D. Decamp, *et al.*), 1992, Z. Phys. **C54**, 211.
 ALEPH Collaboration (D. Buskulic, *et al.*), 1993, Phys. Lett. **B307**, 209.
 ALEPH Collaboration (D. Buskulic, *et al.*), 1996a, Z. Phys. **C70**, 561.
 ALEPH Collaboration (D. Buskulic, *et al.*), 1996b, Z. Phys. **C70**, 579.
 ALEPH Collaboration (R. Barate, *et al.*), 1997a, Z. Phys. **C74**, 263.
 ALEPH Collaboration (R. Barate, *et al.*), 1997b, Z. Phys. **C76**, 15.
 ALEPH Collaboration (R. Barate, *et al.*), 1998a, Eur. Phys. J. **C1**, 65.
 ALEPH Collaboration (R. Barate, *et al.*), 1998b, Eur. Phys. J. **C4**, 29.
 ALEPH Collaboration (R. Barate, *et al.*), 1998c, Eur. Phys. J. **C4**, 409.
 ALEPH Collaboration (R. Barate, *et al.*), 1999a, Eur. Phys. J. **C10**, 1.
 ALEPH Collaboration (R. Barate, *et al.*), 1999b, Eur. Phys. J. **C11**, 599.
 ALEPH Collaboration (R. Barate, *et al.*), 2005, submitted to Phys. Rept., [hep-ex/0506072].
 Alemany, R., M. Davier, and A. Höcker, 1998, Eur. Phys. J. **C2**, 123.
 Altarelli, G., P. Nason, and G. Ridolfi, 1995, Z. Phys. **C68**, 257.
 Appelquist, T., and J. Carazzone, 1975, Phys. Rev. **D11**, 2856.
 ARGUS Collaboration (H. Albrecht, *et al.*), 1988, Phys. Lett. **B202**, 149.
 ARGUS Collaboration (H. Albrecht, *et al.*), 1993, Phys. Lett. **B316**, 608.
 Aubin, C., *et al.*, 2004, Phys. Rev. **D70**, 031504.
 BABAR Collaboration (B. Aubert, *et al.*), 2004, Phys. Rev. **D70**, 072004.
 BABAR Collaboration (B. Aubert, *et al.*), 2005a, Phys. Rev. **D71**, 052001.
 BABAR Collaboration (B. Aubert, *et al.*), 2005b, [hep-ex/0505004].
 Baikov, P.A., K.G. Chetyrkin, and J.H. Kühn, 2002, Phys. Rev. Lett. **88**, 012001.
 Baikov, P.A., K.G. Chetyrkin, and J.H. Kühn, 2003, Phys. Rev. **D67**, 074026.
 Baikov, P.A., K.G. Chetyrkin, and J.H. Kühn, 2004, “Strange quark mass from tau lepton decays with $\mathcal{O}(\alpha_s^3)$ accuracy”, [hep-ph/0412350].
 Bailey, J., *et al.*, 1977, Phys. Lett. **B68**, 191.
 Ball, P., M. Beneke, and V.M. Braun, 1995, Nucl. Phys. **B452**, 563.
 Bardeen, W.A., A.J. Buras, D.W. Duke, and T. Muta, 1978, Phys. Rev. **D18**, 3998.

Becchi, C., S. Narison, E. de Rafael, and F.J. Yndurain,, 1981, Z. Phys. **C8**, 335.

Beneke, M., 1992, Nucl. Phys. **B385**, 452.

Beneke, M., and V.I. Zakharov, 1992, Phys. Rev. Lett. **69**, 2472.

Beneke, M., 1993, Nucl. Phys. **B405**, 424.

Beneke, M., and V.M. Braun, 1999, Phys. Lett. **B348**, 513.

Beneke, M., 1999, Phys. Rept. **317**, 1.

Bernreuther, W., and W. Wetzel, 1982, Nucl. Phys. **B197**, 228; Erratum 1998, ibid **B513**, 758.

Bernreuther, W., 1983, Ann. Phys. **151**, 129.

BES Collaboration (J.Z. Bai, *et al.*), 2002, Phys. Rev. Lett. **88**, 101802.

Bethke, S., 2000, J. Phys. **G26**, R27.

Bethke, S., 2004, Nucl. Phys. (Proc. Suppl.) **135**, 345.

Bijnens, J., G. Ecker, and J. Gasser, 1995a, *The second DAΦNE Physics Handbook, Vol I* Eds. L. Maiani, G. Pancheri and N. Paver, INFN, Frascati, 125.

Bijnens, J., and P. Gosdzinsky, 1996, Phys. Lett. **B388**, 203.

Bijnens, J., E. Pallante, and J. Prades, 1996, Nucl. Phys. **B474**, 379.

Bijnens, J., and P. Talavera, 1997, Nucl. Phys. **B489**, 387.

Bijnens, J., E. Gàmiz, and J. Prades, 2001, JHEP **0110**, 009.

Bijnens, J., E. Pallante, and J. Prades, 2002, Nucl. Phys. **B626**, 410.

Binner, S., J.H. Kühn, and K. Melnikov, 1999, Phys. Lett. **B459**, 279.

Bjorken, J., 1970, Phys. Rev. **D1**, 1376.

Blobel, V., 1984, DESY-84/118.

Blok, B., M.A. Shifman, and D.-X. Zhang, 1998, Phys. Rev. **D57**, 2691; Erratum 1999, ibid **D59**, 019901.

Blokland, I., A. Czarnecki, and K. Melnikov, 2002, Phys. Rev. Lett. **88**, 071803.

Blum, T., 2003, Phys. Rev. Lett. **91**, 052001.

Bouchiat, C., and L. Michel, 1961, J. Phys. Radium **22**, 121.

Braaten, E., 1988, Phys. Rev. Lett. **60**, 1606.

Braaten, E., 1989, Phys. Rev. **D39**, 1458.

Braaten, E., and C.S. Li, 1990, Phys. Rev. **D42**, 3888.

Braaten, E., S. Narison, and A. Pich, 1992, Nucl. Phys. **B373**, 581.

Brambilla, N., *et al.*, 2004, The Quarkonium Working Group, [hep-ph/0412158], 399.

Broadhurst, D.J., 1981, Phys. Lett. **B101**, 423.

Broadhurst, D.J., and S.C. Generalis, 1985, Phys. Lett. **165**, 175.

Broadhurst, D.J., 1993, Z. Phys. **C58**, 339.

Brodsky, S.J., and E. de Rafael, 1968, Phys. Rev. **168**, 1620.

Brodsky, S.J., S. Menke, C. Merino, and J. Rathsmann, 2002, Phys. Rev. **D67**, 055008.

Brown, L.M., and F. Calogero, 1960, Phys. Rev. **120**, 653.

Cabibbo, N., and R. Gatto, 1960, Phys. Rev. Lett. **4**, 313; 1961, Phys. Rev. **124**, 1577.

Catà, O., M. Golterman, and S. Peris, 2005, [hep-ph/0506004].

CCFR Collaboration (J.H. Kim, *et al.*, 1998, Phys. Rev. Lett. **81**, 3595.

CELLO Collaboration (H.J. Behrend, *et al.*, 1990, Z. Phys. **C46**, 537.

Celmaster, W., and R.J. Gonsalves, 1980, Phys. Rev. Lett. **44**, 560.

Chen, S., 1998, Nucl. Phys. (Proc. Suppl.) **64**, 256.

Chen, S., M. Davier, and A. Höcker, 1999, Nucl. Phys. (Proc. Suppl.) **76**, 369.

Chen, S., *et al.*, 2001, Eur. Phys. J. **C22**, 31.

Chetyrkin, K.G., A.L. Kataev, and F.V. Tkachov, 1979, Phys. Lett. **85**, 277.

Chetyrkin, K.G., S.G. Gorishny, and V.P. Spiridonov, 1985, Phys. Lett. **B160**, 149.

Chetyrkin, K.G., and A. Kwiatkowski, 1993, Z. Phys. **C59**, 525.

Chetyrkin, K.G., C.A. Dominguez, D. Pirjol, and K. Schilcher, 1995, Phys. Rev. **D51**, 5090.

Chetyrkin, K.G., J.H. Kühn, and M. Steinhauser, 1996, Nucl. Phys. **B482**, 213.

Chetyrkin, K.G., and J.H. Kühn, 1997, Phys. Lett. **B406**, 102.

Chetyrkin, K.G., S.G. Gorishny, and V.P. Spiridonov, 1997a, Phys. Lett. **B390**, 309.

Chetyrkin, K.G., B.A. Kniehl, and M. Steinhauser, 1997b, Phys. Rev. Lett. **79**, 2184.

Chetyrkin, K.G., J.H. Kühn, and T. Teubner, 1997c, Phys. Rev. **D56**, 3011.

Chetyrkin, K.G., D. Pirjol, and K. Schilcher, 1997d, Phys. Lett. **B404**, 337.

Chetyrkin, K.G., B.A. Kniehl, and M. Steinhauser, 1998a, Nucl. Phys. **B510**, 61.

Chetyrkin, K.G., J.H. Kühn, and A.A. Pivovarov, 1998b, Nucl. Phys. **B533**, 473.

Chizhov, M.V., 2003, [hep-ph/0311360].

Chýla, J., and A.L. Kataev, 1992, Phys. Lett. **B297**, 385.

Cirigliano, V., G. Ecker, and H. Neufeld, 2001, Phys. Lett. **B513**, 361.

Cirigliano, V., G. Ecker, and H. Neufeld, 2002, JHEP **0208**, 002.

Cirigliano, V., J.F. Donoghue, E. Golowich, and K. Maltman, 2003a, Phys. Lett. **B555**, 71.

Cirigliano, V., E. Golowich, and K. Maltman, 2003b, Phys. Rev. **D68**, 054013.

Ciulli, C., S. Sebu, K. Schilcher, and H. Spiesberger, 2003, [hep-ph/0312212].
 CLEO Collaboration (M. Artuso, *et al.*), 1992, Phys. Rev. Lett. **69**, 3278.
 CLEO Collaboration (M. Procario, *et al.*), 1993a, Phys. Rev. Lett. **70**, 1207.
 CLEO Collaboration (D. Bortoletto, *et al.*), 1993b, Phys. Rev. Lett. **71**, 1791.
 CLEO Collaboration (D. Bortoletto, *et al.*), 1993c, Phys. Rev. Lett. **71**, 3762.
 CLEO Collaboration (M. Artuso, *et al.*), 1994a, Phys. Rev. Lett. **72**, 3762.
 CLEO Collaboration (O. Gibaut, *et al.*), 1994b, Phys. Rev. Lett. **73**, 934.
 CLEO Collaboration (M. Battle, *et al.*), 1994c, Phys. Rev. Lett. **73**, 1079.
 CLEO Collaboration (R. Balest, *et al.*), 1995a, Phys. Rev. Lett. **75**, 3809.
 CLEO Collaboration (T. Coan, *et al.*), 1995b, Phys. Lett. **B356**, 580.
 CLEO Collaboration (J. Bartelt, *et al.*), 1996, Phys. Rev. Lett. **76**, 4119.
 CLEO Collaboration (T. Bergfeld, *et al.*), 1997a, Phys. Rev. Lett. **79**, 2406.
 CLEO Collaboration (A. Anastassov, *et al.*), 1997b, Phys. Rev. **D55**, 2559.
 CLEO Collaboration (K. Edwards, *et al.*), 1997c, Phys. Rev. **D56**, 5297.
 CLEO Collaboration (R. Ammar, *et al.*), 1998, Phys. Rev. **D57**, 1350.
 CLEO Collaboration (M. Bishai, *et al.*), 1999a, Phys. Rev. Lett. **82**, 281.
 CLEO Collaboration (S. Richichi, *et al.*), 1999b, Phys. Rev. **D60**, 112002.
 CLEO Collaboration (D. Asner, *et al.*), 2000a, Phys. Rev. **D61**, 012002.
 CLEO Collaboration (T.E. Browder, *et al.*), 2000b, Phys. Rev. **D61**, 052004.
 CLEO Collaboration (K.W. Edwards, *et al.*), 2000c, Phys. Rev. **D61**, 072003.
 CLEO Collaboration (S. Anderson, *et al.*), 2000d, Phys. Rev. **D61**, 112002.
 CLEO Collaboration (A. Anastassov, *et al.*), 2001, Phys. Rev. Lett. **86**, 4467.
 CLEO Collaboration (R. A. Briere, *et al.*), 2003, Phys. Rev. Lett. **90**, 18182.
 CLEO Collaboration (T.E. Coan, *et al.*), 2004, Phys. Rev. Lett. **92**, 232001.
 CLEO Collaboration (K. Arms, *et al.*), 2005, [hep-ex/0501042].
 CMD-2 Collaboration (R.R. Akhmetshin, *et al.*), 2004, Phys. Lett. **B578**, 285.
 Colangelo, P., F. De Fazio, G. Nardulli, and N. Paver, 1997, Phys. Lett. **B408**, 340.
 Czarnecki, A., and W.J. Marciano, 1999, Nucl. Phys. (Proc. Suppl.) **B76**, 245.
 Czarnecki, A., and W. Marciano, 2001, Phys. Rev. **D64**, 013014.
 Czarnecki, A., W.J. Marciano, and A. Vainshtein, 2003, Phys. Rev. **D67**, 073006; see references to the earlier works therein.
 Czyż, H., and J.H. Kühn, 2001, Eur. Phys. J. **C18**, 497.
 Czyż, H., J.H. Kühn, G. Rodrigo, and M. Szopa, 2002, Eur. Phys. J. **C24**, 71; see also the later publications on the subject from these authors and collaborators.
 Dams, C., and R. Kleiss, 2004, [hep-ph/0412254].
 Das, T., *et al.*, 1967a, Phys. Rev. Lett. **18**, 759.
 Das, T., V.S. Mathur, and S. Okubo, 1967b, Phys. Rev. Lett. **19**, 859.
 Davier, M., 1997, Nucl. Phys. (Proc. Suppl.) **55C**, 395.
 Davier, M., L. Girlanda, A. Höcker, and J. Stern, 1998, Phys. Rev. **D58**, 096014.
 Davier, M., and A. Höcker, 1998a, Phys. Lett. **B419**, 419.
 Davier, M., and A. Höcker, 1998b, Phys. Lett. **B435**, 427.
 Davier, M., *et al.*, 2001, Nucl. Phys. (Proc. Suppl.) **B98**, 319.
 Davier, M., 2003, Proceedings of the Workshop on Hadronic Cross-Section at Low-Energy (SIGHAD03), Pisa, Italy, 8-10 Oct 2003, [hep-ex/0312065].
 Davier, M., S. Eidelman, A. Höcker, and Z. Zhang, 2003a, Eur. Phys. J. **C27**, 497.
 Davier, M., S. Eidelman, A. Höcker, and Z. Zhang, 2003b, Eur. Phys. J. **C31**, 503.
 Davier, M., and W.J. Marciano, 2004, Ann. Rev. Nucl. Part. Sci. **54**, 115.
 Davier, M., 2005, Nucl. Phys. (Proc. Suppl.) **B144**, 45.
 Decker, R., and E. Mirkes, 1993, Phys. Rev. **D47**, 4012.
 Decker, R., and M. Finkemeier, 1993, Phys. Rev. **D48**, 4203.
 DELPHI Collaboration (P. Abreu, *et al.*), 1998, Phys. Lett. **B426**, 411.
 DELPHI Collaboration (P. Abreu, *et al.*), 1999, Eur. Phys. J. **C10**, 201.
 DELPHI Collaboration (P. Abreu, *et al.*), 2001, Eur. Phys. J. **C20**, 617.
 DELPHI Collaboration (J. Abdallah, *et al.*), 2004, Eur. Phys. J. **C37**, 1.
 Dhar, A., 1983, Phys. Lett. **B128**, 407.
 Dhar, A., and V. Gupta, 1983, Phys. Rev. **D29**, 2822.
 Dine, M., and J.R. Sapirstein, 1979, Phys. Rev. Lett. **43**, 668.
 Dinsdale, M.J., and C.J. Maxwell, 2004, [hep-ph/0412118].
 Dirac, P.A.M., 1928, Proc. Roy. Soc. **A117**, 610.
 DM1 Collaboration (A. Quenzer, *et al.*), 1978, Phys. Lett. **B76**, 512.
 DM2 Collaboration (D. Bisello, *et al.*), 1989, Phys. Lett. **B220**, 321.
 Dominguez, C.A., and E. de Rafael, 1987, Ann. Phys. **174**, 372.

Dominguez, C.A, C. Van Gend, and N. Paver, 1991, Phys. Lett. **B253**, 241.

Dominguez, C.A, and K. Schilcher, 2004, Phys. Lett. **B581**, 193.

Donoghue, J.F., and E. Golowich, 1994, Phys. Rev. **D49**, 1513.

E143 Collaboration (K. Abe, *et al.*), 1995, Phys. Rev. Lett. **74**, 346.

Eidelman, S., and F. Jegerlehner, 1995, Z. Phys. **C67**, 585.

Ellis, J., and M. Karliner, 1995, Phys. Lett. **B341**, 397.

Erler, J., 1999, Phys. Rev. **D59**, 054008.

Farley, F.J.M., and E. Picasso, 1990, "The muon (g-2) Experiments", Advanced Series on Directions in High Energy Physics - Vol. 7 Quantum Electrodynamics, Ed. T. Kinoshita, World Scientific.

Finkemeier, M., and E. Mirkes, 1996, Z. Phys. **C72**, 619.

Floratos, E., S. Narison, and E. de Rafael, 1979, Nucl. Phys. **B155**, 115.

Friot, S., D. Greynat, and E. de Rafael, 2004, JHEP **0410**, 043.

Fuchs, N.H., H. Sazdjian, and J. Stern, 1990, Phys. Lett. **B238**, 380.

Fuchs, N.H., H. Sazdjian, and J. Stern, 1991, Phys. Lett. **B269**, 183.

Furmanski, W., and R. Petronzio, 1982, Z. Phys. **C11**, 293.

Gabrielse, G., and J. Tan, 1994, "Cavity Quantum Electrodynamics", Ed. P. Berman, Academic Press, San Diego, 267.

Gao, D.-N., 2004, [hep-ph/0411284].

Gámiz, E., *et al.*, 2003, JHEP **0301**, 060.

Gámiz, E., *et al.*, 2005, Phys. Rev. Lett. **94**, 011803.

Gasser, J., and H. Leutwyler, 1982, Phys. Rept. **87**, 77.

Gasser, J., and H. Leutwyler, 1984, Ann. Phys. **158**, 142.

Gasser, J., and H. Leutwyler, 1985, Nucl. Phys. **B250**, 465.

Gell-Mann, M., R.J. Oakes, and B. Renner, 1978, Phys. Rev. **175**, 2195.

Generalis, S.C., 1989, J. Phys. **G15**, L225.

Ghozzi, S., and F. Jegerlehner, 2004, Phys. Lett. **B583**, 222.

Goldstone, J., 1961, Nuovo Cim. **19**, 154.

Goldstone, J., A. Salam, and S. Weinberg, 1961, Phys. Rev. **127**, 965.

Golowich, E., and J. Kambor, 1995, Nucl. Phys. **B447**, 373.

Golowich, E., and J. Kambor, 1996, Phys. Rev. **D53**, 2651.

Golowich, E., and J. Kambor, 1997, Phys. Lett. **B421**, 319.

Golowich, E., and J. Kambor, 1998, Phys. Rev. **D58**, 036004.

Gómez Dumm, D., A. Pich, and J. Portolés, 2000, Phys. Rev. **62**, 054014.

Gorishnii, S.G., K.L. Kataev, and S.A. Larin, 1991, Phys. Lett. **B259**, 144.

Gounaris, G.J., and J.J. Sakurai, 1968, Phys. Rev. Lett. **21**, 244.

Gourdin, M., and E. de Rafael, 1969, Nucl. Phys. **B10**, 667.

Groote, S., J.G. Körner, K. Schilcher, and N.F. Nasrallah, 1998, Phys. Lett. **B440**, 375.

Gross, D., and C. Llewellyn-Smith, 1969, Nucl. Phys. **B14**, 337.

Grozin, A., and Y. Pinelis, 1986, Phys. Lett. **B166**, 429.

Grunberg, G., 1980, Phys. Lett. **B95**, 70.

Grunberg, G., 1984, Phys. Rev. **D29**, 2315.

Guerrero, F., and A. Pich, 1997, Phys. Lett. **B412**, 382.

Hagiwara, K., A.D. Martin, D. Nomura, and T. Teubner, 2004, Phys. Rev. **D69**, 093003.

Haidt, D., 1995, in "Direction in High Energy Physics" Vol 14, Precision Tests of the Standard Electroweak Model, Ed. P. Langacker, World Scientific.

Hayakawa, M., and T. Kinoshita, 1998, Phys. Rev. **D57**, 465; Erratum 2002, *ibid* **D66**, 019902.

Hayakawa, M., T. Kinoshita, and A.I. Sanda, 1996, Phys. Rev. **D54**, 3137.

Hertzog, D.W., 2005, [hep-ex/0501053].

Höcker, A., and V. Kartvelishvili, 1996, Nucl. Inst. Meth. **A372**, 469.

Höcker, A., 1997, Nucl. Phys. (Proc. Suppl.) **55C**, 379.

Höcker, A., 2004, To appear in the proceedings of the 32nd International Conference on High-Energy Physics (ICHEP'04), Beijing, China, August 2004, [hep-ph/0410081].

Holstein, B.R., 1990, Comm. Nucl. Part. Phys. **19**, 221.

t'Hooft, G., and M. Veltman, 1972, Nucl. Phys. **B44**, 189.

HRS Collaboration (B. Bylsma, *et al.*) 1987, Phys. Rev. **D35**, 2269.

Hughes, V.W., and T. Kinoshita, 1999, Rev. Mod. Phys. **71**, S133.

Ibrahim, T., and P. Nath, 1998, Phys. Rev. **D57**, 478.

Ioffe, B.L., and K.N. Zyablyuk, 2001, Nucl. Phys. **A687**, 437.

Ioffe, B.L., and K.N. Zyablyuk, 2003, Eur. Phys. J. **C27**, 229.

Isidori, G., 2005, CKM 2005 Workshop, March 15-18 2005, San Diego, California.

Jadach, S., B.F.L. Ward, and Z. Was, 1994, Comp. Phys. Comm. **79**, 503.

Jamin, M., and M. Münz, 1995, Z. Phys. **C66**, 633.

Jamin, M., 1998, Nucl. Phys. (Proc. Suppl.) **B64**, 250.

Jamin, M., 2002, Phys. Lett. **B538**, 71.

Jamin, M., J.A. Oller, and A. Pich, 2002, Eur. Phys. J. **C24**, 237.

Jegerlehner, F., 2003, [hep-ph/0312372].

Kambor, J., and K. Maltman, 2000, Nucl. Phys. **A680**, 155; 2001, Nucl. Phys. (Proc. Suppl.) **B98**, 314.

Kartvelishvili, V.G., and M.V. Margvelashvili, 1992, Z. Phys. **C55**, 83.

Kartvelishvili, V., M. Margvelashvili, and G. Shaw, 1997, Nucl. Phys. (Proc. Suppl.) **54A**, 309.

Kataev, A.L., N.V. Krasnikov, and A.A. Pivovarov, 1983, Nuovo Cim. **A76**, 723.

Kataev, A.L., and V.V. Starshenko, 1995, Mod. Phys. Lett. **A10**, 235.

Kawarabayashi, K., and M. Suzuki, 1966, Phys. Rev. Lett. **16**, 225.

Kinoshita, T., and M. Nio, 2004, Phys. Rev. **D70**, 113001.

KLOE Collaboration (A. Aloisio, *et al.*), (2005), Phys. Lett. **B606**, 12.

Knecht, M., and J. Stern, 1995, *The second DAΦNE Physics Handbook, Vol I*, Eds. L. Maiani, G. Pancheri and N. Paver, INFN, Frascati, 169.

Knecht, M., and A. Nyffeler, 2002, Phys. Rev. **D65**, 073034.

Knecht, M., *et al.*, 2002, Phys. Rev. Lett. **88**, 071802.

Körner, J.G., F. Krajewski, and A.A. Pivovarov, 2001a, Phys. Rev. **D63**, 036001.

Körner, J.G., F. Krajewski, and A.A. Pivovarov, 2001b, Eur. Phys. J. **C20**, 259.

Krause, B., 1997, Phys. Lett. **B390**, 392.

Kühn, J.H., and A. Santamaría, 1990, Z. Phys. **C48**, 445.

Kühn, J.H., and E. Mirkes, 1992, Z. Phys. **C56**, 661.

Kühn, J.H., and M. Steinhauser, 1998, Phys. Lett. **B437**, 425.

L3 Collaboration (M. Acciarri, *et al.*) 2001, Phys. Lett. **B507**, 47.

Lanin, L.V., V.P. Spiridonov and K.G. Chetyrkin, 1986, Yad. Fiz. **44**, 1372; Sov. J. Nucl. Phys. **44**, 892.

Larin, S.A., F.V. Tkachov, and J.A.M. Vermaseren 1991, Phys. Rev. Lett. **66**, 862.

Larin, S.A., and J.A.M. Vermaseren 1991, Phys. Lett. **B259**, 345.

Larin, S.A., T. van Ritbergen, and J.A.M. Vermaseren, 1997a, Phys. Lett. **B400**, 379.

Larin, S.A., T. van Ritbergen, and J.A.M. Vermaseren, 1997b, Phys. Lett. **B404**, 153.

Le Diberder, F., and A. Pich, 1992a, Phys. Lett. **B286**, 147.

Le Diberder, F., and A. Pich, 1992b, Phys. Lett. **B289**, 165.

Le Diberder, F., 1995, Nucl. Phys. (Proc. Suppl.) **B39**, 318.

The LEP Electroweak Working Group, 2002, LEPEWWG/2002-01.

The LEP Electroweak Working Group (D. Abbaneo, *et al.*), 2004, LEPEWWG/2004-01, CERN-PH-EP/2004-069, [hep-ex/0412015].

Lovett-Turner, C.N., and C.J. Maxwell, 1994, Nucl. Phys. **B432**, 147.

Maltman, K., 1998a, Phys. Rev. **D58**, 093015.

Maltman, K., 1998b, Phys. Lett. **B428**, 179.

Maltman, K., and J. Kambor, 2002, Phys. Rev. **D65**, 074013.

Maltman, K., 2005, [hep-ph/0504201].

Marciano, W., and A. Sirlin, 1988, Phys. Rev. Lett. **61**, 1815.

Marciano, W., 1996, “Particle Theory and Phenomenology”, Eds. K. Lassila, *et al.*, World Scientific, 22.

Marciano, W.J., 2005, CKM 2005 Workshop, March 15-18 2005, San Diego, California.

Margvelashvili, M.V., 1988, Phys. Lett. **B215**, 763.

Martin, A.D., and D. Zeppenfeld, 1995, Phys. Lett. **B345**, 558.

Maxwell, C.J., and D.G. Tonge, 1996, Nucl. Phys. **B481**, 681.

Maxwell, C.J., and D.G. Tonge, 1998, Nucl. Phys. **B535**, 19.

Maxwell, C.J., and A. Mirjalili, 2000, Nucl. Phys. **B577**, 209.

Melnikov, K., and A. Vainshtein, 2004, Phys. Rev. **D70**, 113006.

Menke, S., 1998, PhD Thesis [BONN-IR-98-13].

Menke, S., 1999, Nucl. Phys. (Proc. Suppl.) **76**, 299.

Menke, S., 2001, eConf C010430 M09 [hep-ex/0106011].

Moroi, T., 1996, Phys. Rev. **D53**, 6565; Erratum 1997, *ibid* **D56**, 4424;

Morse, W.M., 2004, [hep-ph/0410062].

Mueller, A.H., 2003, “The QCD Perturbation Series”, in “QCD – 20 Years Later”, Aachen 1992, Eds. P. Zerwas, and H.A. Kastrup, World Scientific, Singapore.

Muon ($g - 2$) Collaboration (R.M. Carey, *et al.*), 1999, Phys. Rev. Lett. **82**, 1632.

Muon ($g - 2$) Collaboration (H.N. Brown, *et al.*), 2000, Phys. Rev. **D62**, 091101.

Muon ($g - 2$) Collaboration (H.N. Brown, *et al.*), 2001, Phys. Rev. Lett. **86**, 2227.

Muon ($g - 2$) Collaboration (G.W. Bennett, *et al.*), 2004, Phys. Rev. Lett. **92**, 161802.

NA7 Collaboration (S.R. Amendolia, *et al.*), 1986, Nucl. Phys. **B277**, 168.

Nagle, J., R. Julian, and J. Zacharias, 1947a, Phys. Rev. **72**, 971.

Nagle, J., E. Nelson, and I. Rabi, 1947b, Phys. Rev. **71**, 914.

Nambu, Y., and G. Jona-Lasinio, 1961, Phys. Rev. **122**, 345.

Narison, S., 1982, Z. Phys. **C14**, 263.

Narison, S., and A. Pich, 1988, Phys. Lett. **B211**, 183.

Narison, S., 1989, Phys. Lett. **B216**, 191.

Narison, S., 1995, Phys. Lett. **B358**, 113.

Narison, S., 1999, Phys. Lett. **B466**, 345.

Neubert, M., 1996, Nucl. Phys. **B463**, 511.

OLYA Collaboration (I.B. Vasserman, *et al.*), 1979, Sov. J. Nucl. Phys. **30**, 519.

OLYA and CMD Collaborations (L.M. Barkov, *et al.*), 1985, Nucl. Phys. **B256**, 365.

OPAL Collaboration (R. Akers, *et al.*), 1995a, Z. Phys. **C67**, 45.

OPAL Collaboration (R. Akers, *et al.*), 1995b, Z. Phys. **C68**, 555.

OPAL Collaboration (R. Akers, *et al.*), 1997, Z. Phys. **C75**, 593.

OPAL Collaboration (K. Ackerstaff, *et al.*), 1998, Eur. Phys. J. **C4**, 193.

OPAL Collaboration (G. Abbiendi, *et al.*), 1999a, Phys. Lett. **B447**, 134.

OPAL Collaboration (K. Ackerstaff, *et al.*), 1999b, Eur. Phys. J. **C7**, 571.

OPAL Collaboration (K. Ackerstaff, *et al.*), 1999c, Eur. Phys. J. **C8**, 183.

OPAL Collaboration (G. Abbiendi, *et al.*), 2003, Phys. Lett. **B551**, 35.

OPAL Collaboration (G. Abbiendi, *et al.*), 2004, Eur. Phys. J. **C35**, 437.

Particle Data Group (S. Eidelman, *et al.*), 2004, Phys. Lett. **B592**, 1.

Pascual, P., and E. de Rafael, 1982, Z. Phys. **C12**, 127.

Peccei, R.D., and J. Solà, 1987, Nucl. Phys. **B281**, 1.

Pich, A., 1987, Phys. Lett. **B196**, 561.

Pich, A., and J. Prades, 1998, JHEP **06**, 013.

Pich, A., and J. Prades, 1999, JHEP **10**, 004; 2000, Nucl. Phys. (Proc. Suppl.) **86**, 236.

Penin, A.A., and A.A. Pivovarov, 1998, Phys. Lett. **B435**, 413.

Peris, S., B. Phily, and E. de Rafael, 2001, Phys. Rev. Lett. **86**, 14.

Pivovarov, A.A., 1991, Sov. J. Nucl. Phys. **54**, 676.

Pivovarov, A.A., 1992, Z. Phys. **C53**, 461.

Poggio, E., H. Quinn, and S. Weinberg, 1976, Phys. Rev. **D13**, 1958.

Prades, J., and A. Pich, 1999, Nucl. Phys. (Proc. Suppl.) **74**, 309.

Prades, J., 1999, Nucl. Phys. (Proc. Suppl.) **76**, 341.

Raczka, P.A., 1998, Phys. Rev. **D57**, 6862.

Riazzuddin, K., and M. Fayazuddin, 1966, Phys. Rev. **147**, 1071.

van Ritbergen, T., J.A.M. Vermaasen, and S.A. Larin, 1997a, Phys. Lett. **B400**, 379.

van Ritbergen, T., J.A.M. Vermaasen, and S.A. Larin, 1997b, Phys. Lett. **B405**, 327.

Roberts, B.L., 1999, “High Intensity Muon Sources”, Eds. Y. Kuno, and T. Yokoi, World Scientific, 69.

Rodrigo, G., A. Pich, and A. Santamaria, 1998, Phys. Lett. **B424**, 367.

Rojo, J., and J.I. Latorre, 2004, JHEP **0401**, 055.

Santiago, J., and F.J. Yndurain, 2001, Nucl. Phys. **B611**, 447.

Schwinger, J., 1948, Phys. Rev. **73**, 416.

Shifman, M.A., A.L. Vainshtein, and V.I. Zakharov, 1979, Nucl. Phys. **B147**, 385, 448, 519.

SND Collaboration (M.N. Achasov, *et al.*), 2005, [hep-ex/0506076].

Snow, S., 1993, Proceedings of the 2nd International Workshop on τ Lepton Physics, Columbus 1992, Ed. K.K. Gan, World Scientific.

Steinhauser, M., 1998, Phys. Lett. **B429**, 158.

Stevenson, P.M., 1981, Phys. Rev. **D23**, 2916.

Surguladze, L.R., and M.A. Samuel, 1991, Phys. Rev. Lett. **66**, 560.

Terent'ev, M.V., 1973, Sov. J. Nucl. Phys. **16**, 87.

TOF Collaboration (I.B. Vasserman, *et al.*), 1981, Sov. J. Nucl. Phys. **33**, 709.

de Troconiz, J.F., and F.J. Yndurain, 2004, [hep-ph/0402285].

UA1 Collaboration (C. Albajar, *et al.*), 1996, Phys. Lett. **B369**, 46.

UA6 Collaboration (M. Werlen, *et al.*), 1999, Phys. Lett. **B452**, 201.

Vainshtein, A., 2003, Phys. Lett. **B569**, 187.

Van Dyck, R.S., P.B. Schwinberg, and H.G. Dehmelt, 1987, Phys. Rev. Lett. **59**, 26.

Weinberg, S., 1967, Phys. Rev. Lett. **18**, 507.

Weinberg, S., 1977, “*A Festschrift for I.I. Rabi*”, Eds. L. Motz, New York Academy of Sciences, New York.

Weinberg, S., 1979, Physica **A96**, 327.

Weinstein, A., 2001, Proceedings of the 6th International Workshop on τ Lepton Physics, Victoria 2000, Eds. R.J. Sobie, and J.M. Roney, North Holland.

Wetzel, W., 1982, Nucl. Phys. **B196**, 259.

Wilson, K.G., 1969, Phys. Rev. **179**, 1499.

Withlow, L.W., *et al.* 1992, Phys. Lett. **B282**, 475.

Zielinski, M., 1984, Phys. Rev. Lett. **52**, 1195.
Zyablyuk, K.N., 2004, Eur. Phys. J. **C38**, 215.